Final Report

Real-world tire and brake wear emissions

Prepared for:

Dr. Qi Yao
Dr. Seungju Yoon
California Air Resources Board
1001 I street
Sacramento, CA 95812
(916) 327-7213

August 2020

Heejung Jung (PI), UC Riverside
Guoyuan Wu (Co-PI), UC Riverside
L.-W. Antony Chen (Co-PI), University of Nevada, Las Vegas
Xiaoliang Wang (Co-PI), Desert Research Institute
Ke Max Zhang (Consultant)
Brenda Lopez (Graduate student)
University of California
CE-CERT
Riverside, CA 92521
951-781-5799
951-781-5790 (fax)

Disclaimers

The statements and conclusions in this report are those of the contractor and not necessarily those of California Air Resources Board. The mention of commercial products, their source, or their use in connection with material reported herein is not to be construed as actual or implied endorsement of such products.

Acknowledgments

The authors acknowledge CARB for funding (18RD017) and lending instruments for this study. PIs would like to thank Drs. Sonya Collier, Qi Yao and Seungju Yoon for managing the project. Heejung Jung is indebted to Drs. Marko Princevac and Manabu Shraiwa for their in-kind contribution to the project regarding turbulence and toxicity measurement respectively. H.J. thanks Dr. Akula Venkatram for lending his sonic anemometer and tower. The authors are thankful to Drs. Kihong Park and Minhan Park for their in-kind chemical analysis of MOUDI samples. Organic speciation of filter samples was conducted by Dr. Steven Ho. Authors are grateful to CARB staff who attended monthly meetings and gave useful feedbacks. The project may have not been possible without enthusiastic and diligent work by students and staff at UCR/CE-CERT, UCI, DRI, and Cornell University. Heejung Jung would like to thank graduate students (Chas Frederickson, Brenda Lopez, Jerry Ma, Brian Hwang), a postdoc (Ting Fang), undergraduate students (David Mendez-Jimenez, Jesse Stuart) and staff (Chengguo Li, Ling Cobb, Steven Gronstal, and Steve Kohl). Project investigators are thankful to SCAQMD staff (Rene Bermudez, Albert Dietrich, Keith Brown, Loc Nguyen, Jeremy Graham, and Michael Koch) to provide access to their air quality monitoring sites. Heejung Jung gratefully acknowledges Horiba for providing us 4 units of PX-375. Hejung Jung especially is thankful to Yusuke Mizuno and Mitsuhiko Maeda for on-site advice and help on PX-375. Heejung Jung is grateful to Modi Chen and Patrick Roth at TSI for providing an instrument. Heejung Jung is indebted to Tyler Beck at Particle Instruments LLC for ELPI. The measurement would have not been possible without help from staff at the Majestic Garden Hotel and Coast Corvette in Anaheim and ATD in Compton. Heejung Jung is thankful to Jorn Herner and Seungju Yoon bearing with annoying calls asking for contingency fund. Fortunately, there was no damage of instruments/equipment, no theft, and no injury throughout the field test and so no need for contingency fund.

Table of Contents

List of Tables

List of Figures

Acronyms and Abbreviations

ALP .....automated license plate recognition
APS .....aerodynamic particle sizer
AQMD .....Air Quality Management District
ATD .....American Tire Distributors
BC .....black carbon
CalTrans.....California Department of Transportation
CARB .....California Air Resources Board
CBDC.....California brake dynamometer cycle
CC .....Coast Corvette
CE-CERT .....College of Engineering Center for Environmental Research and Technology
CMB .....chemical mass balance
CO .....carbon monoxide
CO2 .....carbon dioxide
CRPAQS .....California Regional Particulate Air Quality Study
CTAG .....Comprehensive Turbulent Aerosol Dynamics and Gas Chemistry
DRI .....Desert Research Institute
EC .....elemental carbon
EDX .....energy-dispersive X-ray
ELPI .....electrical low pressure impactor
EPA .....Environmental Protection Agency
EV-CMB .....effective chemical mass balance
HDV .....heavy duty vehicles
HRELPI+ .....high resolution electrical low pressure impactor plus
IC .....ion chromatography
ILD .....inductive loop detector
LDV .....light duty vehicles
LM .....low metallic
MDV .....medium duty vehicle
MGH/MH .....Majestic Garden Hotel

MMC .....metal matrix composite
MOUDI .....micro-orifice uniform deposit impactor
MPIN .....modified pseudo-inverse normalized
NAO .....non-asbestos organic
Nox .....nitrogen oxides
NR .....near road
OC .....organic carbon
OM .....organic matter
PAH .....polycyclic aromatic hydrocarbon
PeMS .....performance measurement system
PM .....particulate matter
$PM_{2.5}$ .....fine particles less than 2.5 µm
PM_{10} .....coarse particles less than 10 µm
PN .....particle number
PSD .....particle size distributions
QCM .....quartz crystal microbalance
RANS .....reynolds averaged navier-stokes
RMS .....Root Mean Square
SCAQMD .....South Coast Air Quality Management District
SCE .....source contribution estimates
SEM .....scanning electron microscopy
SMPS .....scanning mobility particle sizer
SOA .....secondary organic aerosols
TRWP .....tire and road wear particles
TSI .....Thermo-Systems Inc.
TSP .....total suspended particles
TTI .....travel time index
UCI .....University of California Irvine
UCR .....University of California Riverside
VDS .....vehicle detection station
VMT .....vehicle miles of travel
VOC .....volatile organic compounds
WIM .....weigh in motion

XRF...x-ray fluorescence

Abstract

Non-exhaust emissions, including brake, tire, and road wear particles, have become larger contributors to traffic-related emissions as exhaust PM emissions have been steadily decreasing thanks to legislative efforts and advancement in engine and control technology. This project aims to understand the chemical and physical nature as well as source contributions of non-exhaust PM in real-world near-road environment.

Gas and particle sampling was conducted over a two-week period in winter 2020 to reduce the contribution of secondary organic aerosol to the sample. Samples were taken at upwind and downwind locations near highway 5 in Anaheim and highway 710 in Long Beach/Compton, representing traffic of a typical mix of light and heavy-duty and a heavy-duty freight corridor in Southern California, respectively. Integrated $PM_{2.5}$ and PM_{10} filter samples were collected over 4-hour periods during morning and evening rush hours as well as middle-day hours for gravimetric mass measurement and chemical speciation. Gas and particle concentrations, particle elemental composition and size distribution, and wind data were measured in real time. In addition, traffic data were collected from the CalTrans PeMS, video footage processed by the ALPR system, and WIM stations.

Average concentrations $PM_{2.5}$ and PM_{10} at both near-road sites were 10-15 and ~30 µg/m3, respectively, with PM_{10} being 2–3 times of $PM_{2.5}$. For $PM_{2.5}$, the most abundant components were: organic matter (OM; ~30–40%), mineral dust (~25–30%), and elemental carbon (EC; ~10–15%). For PM_{10}, mineral dust (~40–45%) was the dominant composition, followed by OM (~25%), NO_3^- (~6-11%), and EC (6-8%). Likely due to more diesel vehicles on highway 710, EC concentrations near highway 710 were 19–26% higher than those near highway 5, and PAH concentrations near highway 710 were 47% higher than those near highway 5. High correlations were found for elements with common sources, such as markers for brake wear (e.g., Ba, Cu, and Zr) and road dust (e.g., Al and Si). Very high concentrations (up to 4 µg/m3) of phthalates were found during all sampling periods of 0600-1000 near highway 5, which were not found near highway 710, indicating that traffic was probably not the source of high concentrations of phthalates.

Source apportionment based on the EV-CMB was carried out for time-integrated $PM_{2.5}$ and PM_{10} samples. Seven sources and their respective influential markers were identified, including : 1) Al, Si, and Ca for road dust; 2) Fe, Cu, Ti, and Ba for brake wear; 3) Zn and OC3 for tire wear; 4) EC, OC1, and hopanes for diesel exhaust; 5) indeno[1,2,3,cd]pyrene, benzo[g,h,i]perylene, and coronene for gasoline engine exhaust; 6) NH_4NO_3 for secondary ammonium nitrate; and 7) $(NH_4)_2SO_4$ for secondary ammonium sulfate. The EV-CMB results indicate the dominance of road dust, which contributed significantly higher to PM_{10} than $PM_{2.5}$ samples. On average, contributions of the brake + tire wear to $PM_{2.5}$ exceeded those of exhaust fractions (diesel + gasoline) at Anaheim (29–30% vs. 19–21%) while they were comparable at Long Beach (15–17% vs. 15–19%). For PM_{10}, the brake + tire wear contributions were 2 – 3 times more than the exhaust contributions. Brake wear particles were generally more abundant than tire wear particles, though there was a higher uncertainty in the tire wear contribution estimates. Compared with Anaheim, the Long Beach samples showed brake wear with a higher

copper content, reflecting different fleet compositions. More unidentified PM mass found at Long Beach can partially be attributed to fresh and aged sea salt. The Long Beach site and the Anaheim site are approximately 8 miles and 11 miles away from seashore respectively. The upwind-downwind differences of the total PM mass were not significant at both locations due to large contribution of background PM mass, making determination of emission factors from traffic extremely difficult due to low signal to noise ratio. Determining non-tailpipe emissions from field study in crowded urban area is quite challenging and further study is required.

Computational Fluid Dynamic simulation was conducted to assess the impact of exhaust and non-exhaust emissions on the downwind communities. We developed a two-domain approach to take advantage of the field measurement data, including those from both the meteorological and particle measurements, to greatly reduce the uncertainties in modeling inputs while making the computational resources manageable. Focusing on the Highway 5 location, the two domains are referred to as the Highway domain and the Community domain. The goal of the simulations on the Highway domain is to generate velocity and concentration profiles as inputs to the simulations for the Community domain. The dispersion and deposition of exhaust and non-exhaust particles were simulated. Our modeling results suggest that the deposition can reduce particle mass concentrations by 1 to 2% for the size range pertain to brake PM and by 4-7% for the size range relevant to road dust in the downwind community (<400 m from the roadway). The implication is that near-road communities are likely exposed to non-exhaust particles coming from roadways, even though those particles have relatively higher deposition velocity than exhaust particles. Future studies that able to separate contributions from exhaust and non-exhaust sources to the overall particle size distributions can help elucidate the community exposure to non-exhaust particles.

Executive Summary

There is growing interest in non-exhaust particle emissions from vehicles as its contribution to $PM_{2.5}$ becomes more significant compared to exhaust particle emissions which have been steadily decreasing thanks to legislative efforts and advancement in engine and control technology. CARB's latest project (17RD016) conducted brake particle emission source testing using a brake dynamometer in the laboratory condition. The project contributed quantifying emission factors to update emission inventory. The current project aims to understand contribution of non-exhaust particle emissions (i.e. brake and tire wear particle emissions) in near-road environment.

Two near-road locations were identified for the study. For both locations, the downwind measurement sites were at AQMD NR sites to take advantage of existing measurement network. One location is in Anaheim near highway 5 where the traffic is a typical mix of light duty and heavy-duty vehicles in Southern California highways. Upwind location was at the parking lot of the Majestic Garden Hotel and the downwind location was AQMD NR site next to highway 5 in Anaheim. The other location was at highway 710 in Long Beach/Compton. The upwind location was at the parking lot of ATD in Compton and the downwind location was AQMD NR site next to highway 710 in Long Beach. Highway 710 site was chosen due to its known characteristics of heavy-duty vehicle freight corridor. Time resolved gravimetric sampling, real time PM, and gas measurement were conducted for physical and chemical characterization of sampled PM along with wind and turbulence measurement at the downwind locations.

To understand the influence of traffic on the near-road brake and tire wear emissions (in terms of PM concentrations) with background mobile sources, this study performed traffic data analysis based on various sources across Southern California, including: 1) CalTrans PeMS which collects, rectifies and archives real-world measurements of traffic count and occupancy from every loop detector; 2) Video footage processed by the ALPR and vehicle registration database to retrieve license plate information and vehicle/powertrain characteristics; and 3) WIM stations, which capture and record key features of trucks as they move over the measurement points. Although these data sources may provide a significant amount of traffic information from different perspectives, it is very challenging to conduct data fusion or information association due to the inconsistency in data collection sites (with respect to different data sources) and potential measurement noises. Therefore, the PeMS data is considered to be the primary traffic information source in this study to investigate the relationship with brake and tire wear emissions.

Average concentrations of $PM_{2.5}$ and PM_{10} at both near-road locations were 10-15 and ~30 $\mu g/m^3$, respectively, with PM_{10} being 2–3 times of $PM_{2.5}$ (Figure ES 1). The average $PM_{2.5}$ and PM_{10} concentrations at the nominal downwind sites were slightly higher than those at the nominal upwind sites, by approximately 1–4 $\mu g/ m^3$.

(a) I-5

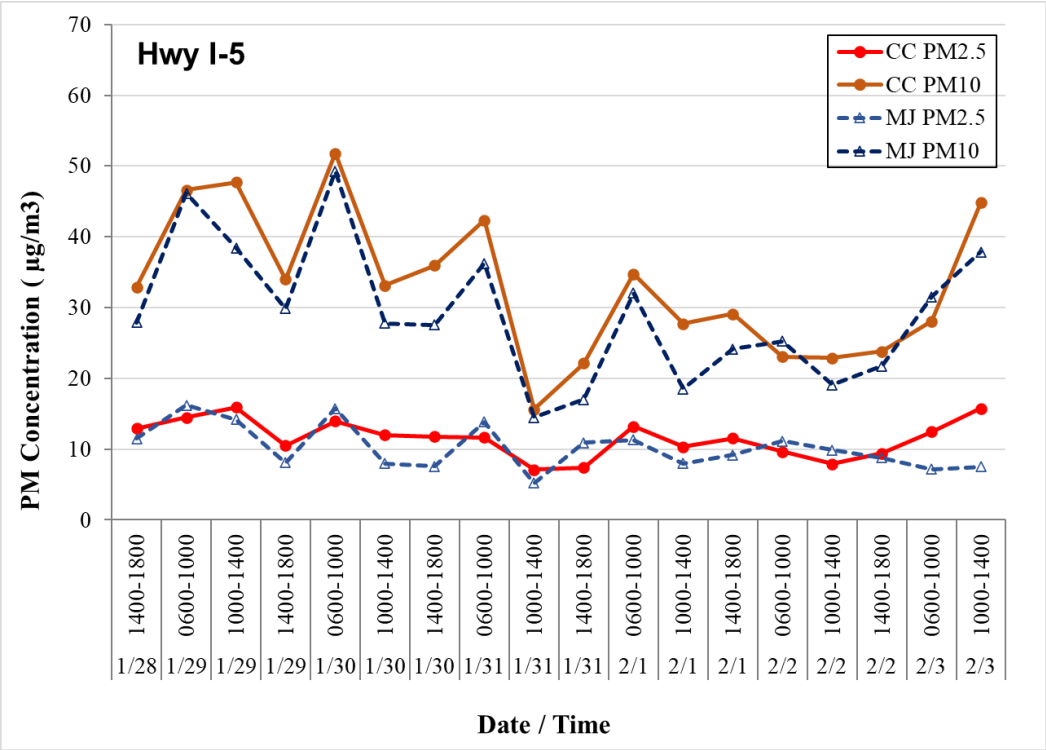
Hwy I-5
CC PM2.5
CC PM10
MJ PM2.5
MJ PM10
PM Concentration (µg/m3)
70
60
50
40
30
20
10
0
1400-1800 1/28
0600-1000 1/29
1000-1400 1/29
1400-1800 1/29
0600-1000 1/30
1000-1400 1/30
1400-1800 1/30
0600-1000 1/31
1000-1400 1/31
1400-1800 1/31
0600-1000 2/1
1000-1400 2/1
1400-1800 2/1
0600-1000 2/2
1000-1400 2/2
1400-1800 2/2
0600-1000 2/3
1000-1400 2/3
Date / Time

(b) Hwy-710

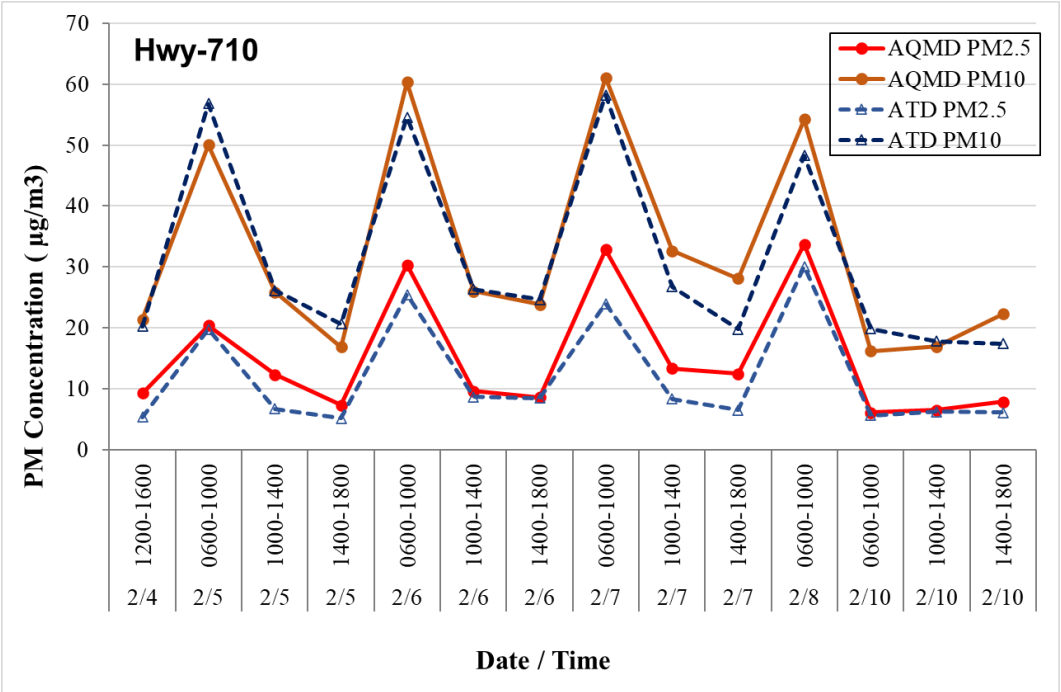

Figure ES 1: Gravimetric $PM_{2.5}$ and PM_{10} concentrations at: (a) I-5 and (b) Hwy-710 sites.

Detailed chemical analyses were conducted to study the nature of the near-road aerosols, seek source markers, and enable source apportionment. As shown in Figure ES 2, for $PM_{2.5}$, the most abundant compositions were: organic matter (OM; ~30–40%), mineral dust (~25–30%), and elemental carbon (EC; ~10–15%). For PM_{10}, mineral dust (~40–45%) was the dominant composition, followed by OM (~25%), NO_3^- (~6-11%), and EC (6-8%). EC concentrations at the Hwy-710 sites were ~20% higher than those at the I-5 sites, likely due to more diesel vehicles on Hwy-710. Compared to more diverse ion abundances at the I-5 sites, ammonium nitrate was the dominant inorganic salt, followed by sulfates at the Hwy-710 sites. Anion and cation ion balance analysis indicates that particles were slightly acidic during most sampling periods when ion concentrations were relatively low, while they were nearly neutral when ion concentrations were high. Sulfates are approximately the same, indicating that it is a regional air pollutant. However, nitrate and ammonium were much higher near Hwy-710 sites than near I-5. High correlations were found for elements with common sources, such

as markers for brake wear (e.g., Ba and Cu) and road dust (Al and Si), as shown in Figure ES 3. Pie chart of the relative abundance of PM2.5 at I-5 freeway. Organic matter is largest at 37.2 percent.

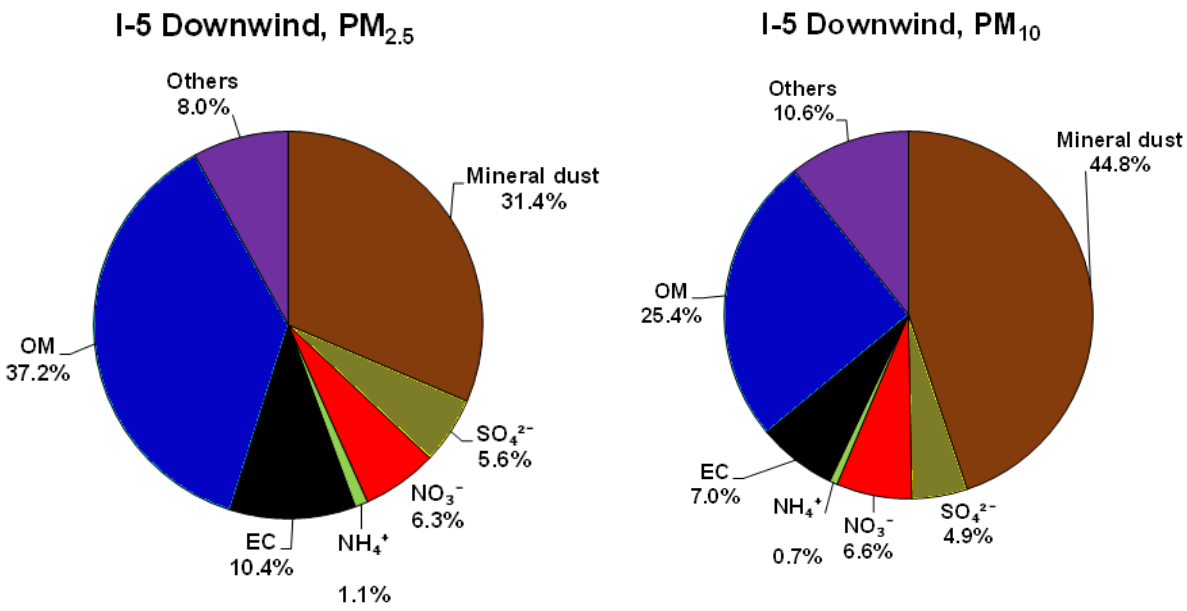

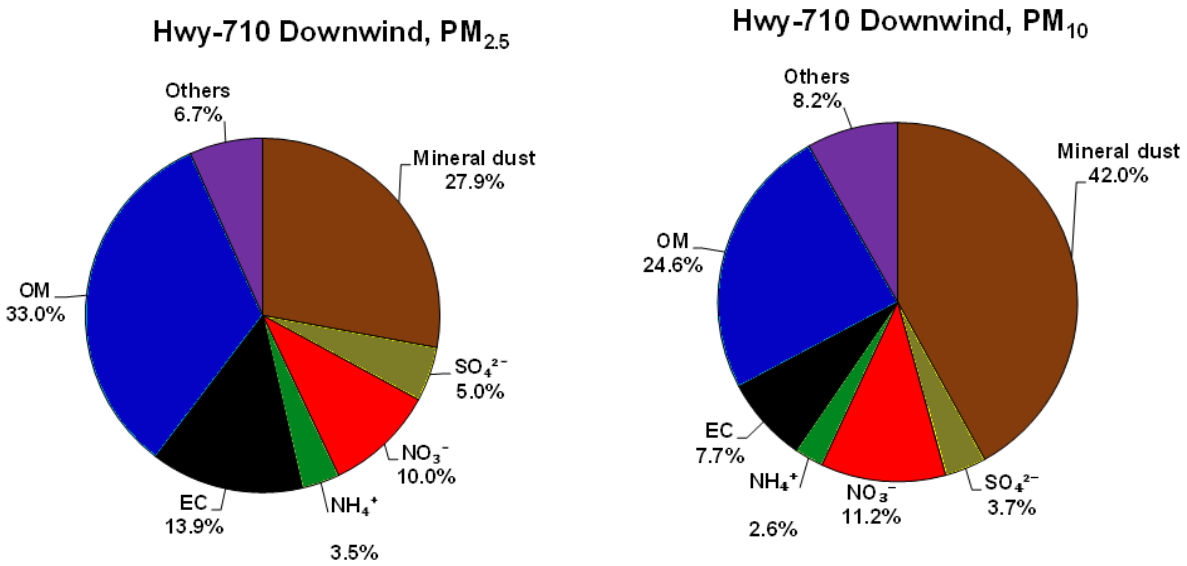

Figure ES 2: Relative abundance of major $PM_{2.5}$ and PM_{10} chemical compositions at the nominal downwind sampling sites.

Size-segregated elemental concentrations were compared between the two near-road sites and an urban background site in Irvine, CA. The concentrations of most elements were the highest near I-5 and the lowest at the Irvine site, indicating strong influence of traffic-related emissions near highways. For nominal resuspended road dust markers Al and Si in the 1-10 µm size range, the concentrations near I-5 were 2-3 times of those near I-710 and >4 times of those in Irvine. For brake wear markers Cu, Zr, and Ba, the concentrations near I-5 were 1.5–4 times of those near I-710 and 2–10 times of those in Irvine across all size ranges. For tire wear marker Zn, the concentrations near I-5 were 1.8 times of those near I-710 and 2 times of those in Irvine for the 1-10 µm size ranges. Therefore, non-exhaust exposures are higher in near road environment than urban background environment.

The I-5 sites had higher measured organic concentrations than the Hwy-710 sites except that PAH concentrations near Hwy-710 were 47% higher than those near I-5 (Figure ES 4: Average PAH concentrations near I-5 and Hwy-710.Figure ES 4). Both highways had similar PAH distributions: high abundances of 4-ring, 5-ring, and some 6-ring and 7-ring PAHs. Hwy-710 had much higher abundances of fluoranthene and pyrene than I-5 sites, probably due to higher diesel vehicle fractions. PM from both highways had abundant n-alkanes, with similar bimodal distributions peaking near C23 and C29, respectively, although the relative concentrations of these two modes are different near the two highways. Very high concentrations (up to 4 µg/m3) of phthalates were found during all sampling periods of 06:00-10:00 at the I-5 sites, about a factor of 10 higher than other sampling periods. These high concentration periods were

not found near Hwy-710, indicating that traffic was probably not the source of high concentrations of phthalates. The sources and potential exposure risks of phthalates warrant further studies as bis(2-ethylhexyl) phthalate is designated by the U.S. EPA as a probable human carcinogen.

(a) I-5 Downwind PM_{10}

Anaheim AQMD PM10 Filter XRF : Element vs Element Correlation R^2

	Fe	Si	Ca	Al	K	Zn	Ti	Cu	Ba	Sb	Sr	Cr	Mn	Zr
Fe														
Si	0.70													
Ca	0.77	0.94												
Al	0.66	0.98	0.91											
K	0.64	0.92	0.87	0.93										
Zn	0.47	0.36	0.42	0.31	0.42									
Ti	0.89	0.74	0.72	0.70	0.68	0.31								
Cu	0.43	0.08	0.09	0.06	0.07	0.09	0.50							
Ba	0.67	0.20	0.28	0.16	0.19	0.30	0.60	0.76						
Sb	0.00	0.03	0.04	0.05	0.05	0.02	0.00	0.07	0.02					
Sr	0.40	0.46	0.36	0.47	0.52	0.15	0.48	0.16	0.17	0.00				
Cr	0.25	0.09	0.17	0.10	0.07	0.01	0.22	0.22	0.24	0.01	0.01			
Mn	0.77	0.82	0.74	0.80	0.76	0.38	0.78	0.18	0.32	0.00	0.49	0.16		
Zr	0.39	0.05	0.07	0.03	0.05	0.08	0.44	0.95	0.75	0.14	0.13	0.24	0.17	
Mo	0.07	0.07	0.06	0.07	0.10	0.06	0.07	0.00	0.04	0.00	0.18	0.06	0.06	0.00

(b) Hwy-710 Downwind PM_{10}

Long Beach AQMD PM10 Filter XRF : Element vs Element Correlation R^2

	Fe	Si	Ca	Al	K	Zn	Ti	Cu	Ba	Sb	Sr	Cr	Mn	Zr
Fe														
Si	0.86													
Ca	0.88	0.98												
Al	0.88	0.98	0.98											
K	0.89	0.96	0.94	0.92										
Zn	0.85	0.71	0.78	0.74	0.79									
Ti	0.75	0.65	0.68	0.75	0.61	0.67								
Cu	0.88	0.58	0.61	0.61	0.67	0.78	0.66							
Ba	0.61	0.29	0.30	0.30	0.36	0.47	0.46	0.79						
Sb	0.17	0.19	0.17	0.16	0.27	0.13	0.02	0.15	0.04					
Sr	0.78	0.80	0.78	0.79	0.77	0.58	0.78	0.60	0.48	0.04				
Cr	0.67	0.54	0.61	0.61	0.58	0.88	0.58	0.61	0.32	0.13	0.38			
Mn	0.84	0.84	0.88	0.85	0.86	0.81	0.73	0.65	0.37	0.20	0.78	0.67		
Zr	0.86	0.59	0.61	0.62	0.69	0.80	0.62	0.97	0.72	0.23	0.57	0.67	0.68	
Mo	0.32	0.16	0.21	0.15	0.26	0.42	0.08	0.33	0.29	0.15	0.08	0.33	0.30	0.31

Figure ES 3: Squared Pearson correlation coefficient (R^2) among elements for PM_{10} collected at downwind sites. Light green shows $R^2>0.6$ while darker green shows $R^2\geq0.8$.

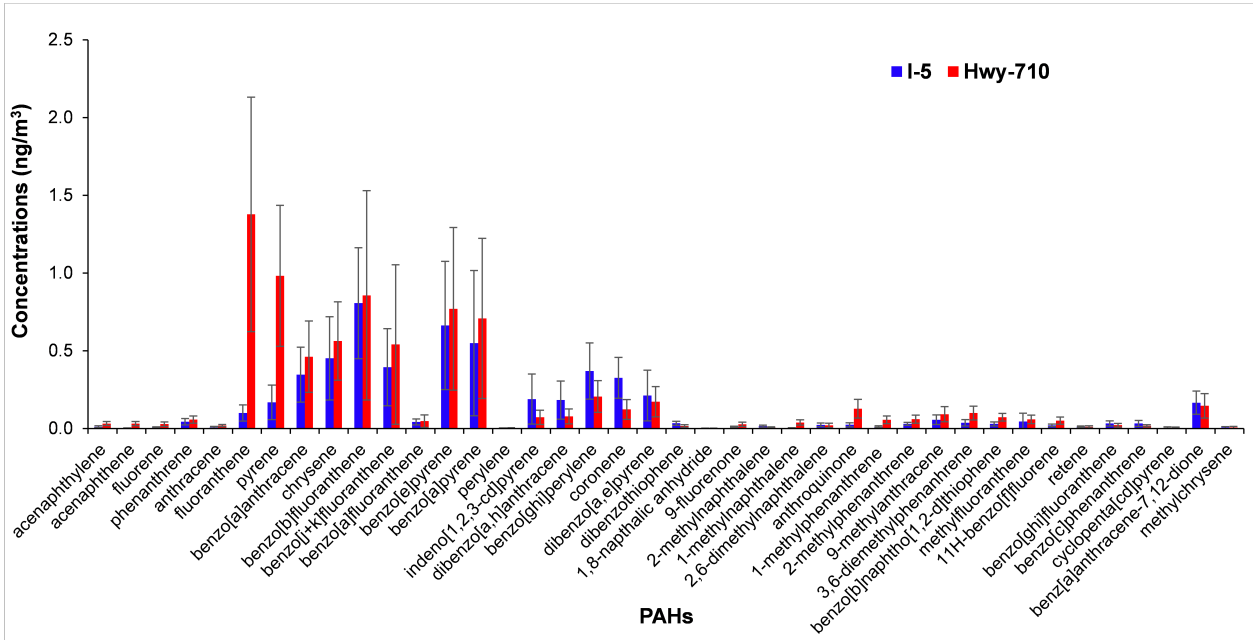

Figure ES 4: Average PAH concentrations near I-5 and Hwy-710.

Source apportionment based on the EV-CMB was carried out for time-integrated $PM_{2.5}$ and PM_{10} samples acquired at Anaheim (I-5) and Long Beach (Hwy-710). Source profiles tested include those for road dust collected near the monitoring sites, tire wear acquired from a dynamometer test, brake wear from the CRPAQS and recent CARB sponsored brake dynamometer study, as well as diesel and gasoline exhausts based on the National Renewable Energy Laboratory Gas/Diesel Split Study. Sensitivity tests using the difference in PM chemical composition between the average downwind and upwind samples from Anaheim (Figure ES 5) suggested a combination of road dust, brake wear, tire wear, and vehicle exhausts (diesel and gasoline) profiles that provide optimal model fits and explains 102% and 84% of $PM_{2.5}$ and PM_{10}, respectively, generated from the on-road traffic. Influential markers identified by EV-CMB include: 1) Al, Si, and Ca for road dust; 2) Fe, Cu, Ti, and Ba for brake wear; 3) Zn and OC3 for tire wear; 4) EC, OC1, and hopanes for diesel exhaust; and 5) indeno[1,2,3,cd]pyrene (incdpy), benzo[g,h,i]perylene (bghipe), and coronene for gasoline engine exhaust. Two brake wear profiles, one with high Cu and the other with low Cu fractions, were found necessary to achieve acceptable CMB fitting metrics. Additionally, substantial secondary ammonium nitrate and ammonium sulfate in the background air were accounted for by pure NH_4NO_3 and $(NH_4)_2SO_4$ profiles.

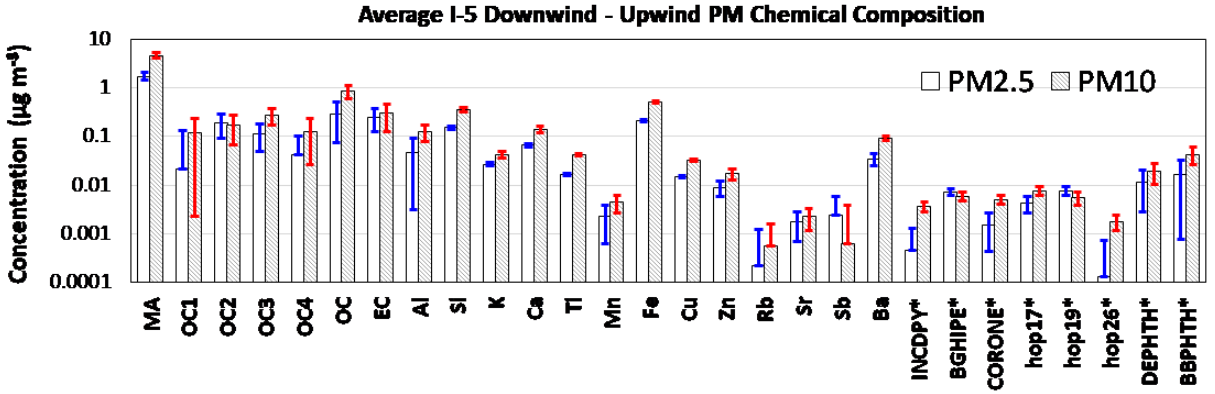

(a)

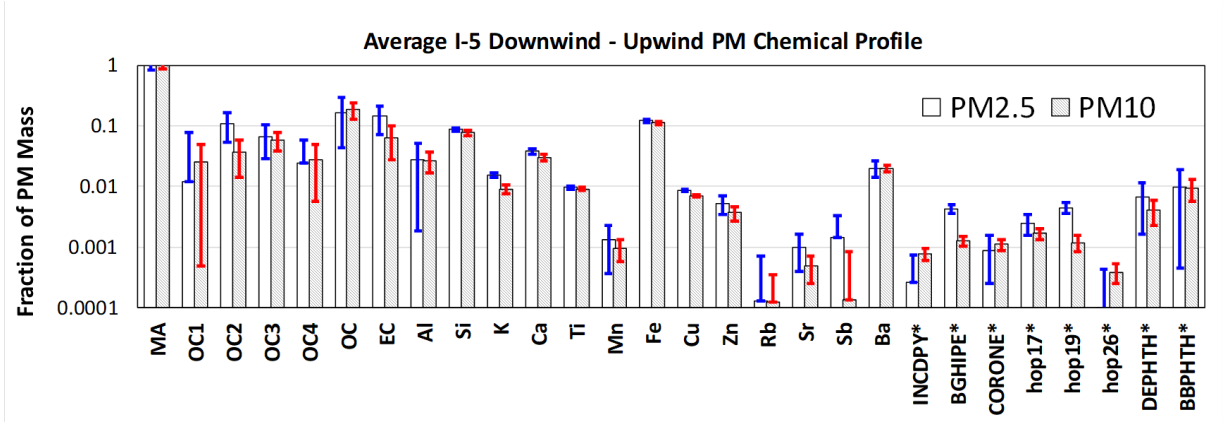

(b)

Figure ES 5: Average $PM_{2.5}$ and PM_{10} (a) chemical composition (b) chemical profiles derived from the difference of downwind and upwind measurements at the Anaheim (I-5) site.

Using the CMB model established by the sensitivity test, SCEs with uncertainties were calculated for $PM_{2.5}$ and PM_{10} at both the downwind and upwind sites for the I-5 and Hwy-710. The model fitting performances are about the same for individual $PM_{2.5}$ and PM_{10} samples except of a lower performance for PM_{10} at Long Beach. There are only moderate correlations between $PM_{2.5}$ and PM_{10} SCEs, with R^2 (Anaheim/Long Beach) of 0.59/0.59, 0.78/0.86, 0.35/0.33, 0.65/0.035, 0.29/0.68, 0.74/0.90, and 0.77/0.97 for road dust, brake

wear (high-Cu + low-Cu), tire wear, gasoline exhaust, diesel exhaust, secondary nitrate, and secondary sulfate, respectively. This signifies uncertainties particularly for tire wear and vehicle exhaust SCEs, as the current model may have difficulties separating them. When combing diesel exhaust, gasoline exhaust, and tire wear into one source, the SCE R^2 improves to ~0.7 between $PM_{2.5}$ and PM_{10} for both Anaheim and Long Beach.

The EV-CMB results indicate the dominance of road dust, which contributes significantly higher to PM_{10} than $PM_{2.5}$ mass despite of a large sample-to-sample variability. The contributions of brake wear and tire wear are also higher in PM_{10}, but the differences between $PM_{2.5}$ and PM_{10} are generally not significant considering the larger uncertainty in the CMB results. Low-copper brake wear exceeds high-copper brake wear at Anaheim, but vice versa at Long Beach, likely due to different fleet compositions. Overall, brake and tire wear levels in $PM_{2.5}$ are higher at Anaheim than at Long Beach. The downwind-upwind differences of non-exhaust particles (road dust, brake wear, tire wear) are small, although higher values are more often found at the downwind site, especially for Anaheim. For gasoline and diesel exhausts, there are little upwind-downwind differences. Their contributions to PM_{10} and $PM_{2.5}$ are also similar (except for gasoline exhaust at Long Beach), consistent with the dominance of fine particles in vehicle exhausts.

The insignificant upwind-downwind differences at both locations suggest contribution of on-road traffic emissions at either measurement site is much smaller compared to contribution of background PM. It should be noted that the designated downwind sites are not always downwind due to wind direction changes throughout a day. Averaged over the upwind and downwind SCEs (Table ES 1), contributions of the non-exhaust fractions (brake + tire) to $PM_{2.5}$ exceed those of exhaust fractions (diesel + gasoline) at Anaheim (29–30% vs. 19–21%) while they are comparable at Long Beach (15–17% vs. 15–19%). For PM_{10}, the non-exhaust contributions are 2 – 3 times the exhaust contributions. Brake wear particles are generally more abundant than tire wear particles, though there is a higher uncertainty in the tire wear contribution estimates. It is somewhat surprising for significantly higher contributions of secondary nitrate and secondary sulfate in PM_{10} than in $PM_{2.5}$ at both Anaheim and Long Beach. Secondary nitrate is higher at Long Beach, while secondary sulfate appears to be relatively uniform across the Los Angeles basin. More unidentified PM_{10} mass found at Long Beach can partially be attributed to fresh and aged sea salt.

Table ES 1: Average and standard error of source contribution estimates (SCEs in µg/m^3) for $PM_{2.5}$ and PM_{10} measured at Anaheim and Long Beach.

	Anaheim (I-5)	Anaheim (I-5)	Anaheim (I-5)	Anaheim (I-5)	Long Beach (Hwy-710)	Long Beach (Hwy-710)	Long Beach (Hwy-710)	Long Beach (Hwy-710)
	Downwind (CC)	Downwind (CC)	Upwind (Majestic)	Upwind (Majestic)	Downwind (AQMD)	Downwind (AQMD)	Upwind (ATD)	Upwind (ATD)
	$PM_{2.5}$	PM_{10}	$PM_{2.5}$	PM_{10}	$PM_{2.5}$	PM_{10}	$PM_{2.5}$	PM_{10}
# of Data	18	18	18	18	14	14	14	14

Total Mass	10.9	32.5	9.6	28.5	14.4	31.9	11.0	30.4
Road Dust	3.60±0.57	17.1±1.44	2.50±0.47	14.4±1.30	3.39±0.29	10.3±1.36	2.50±0.29	10.5±1.39
Brake I	1.44±0.96	2.10±1.26	1.21±0.90	1.76±1.29	0.40±0.22	1.23±1.17	0.34±0.19	0.93±1.10
Brake II	0.54±0.36	1.18±0.61	0.34±0.31	0.68±0.55	0.74±0.34	1.81±1.39	0.55±0.33	1.97±1.63
Tire Wear	1.28±0.73	2.01±1.10	1.21±0.70	1.60±0.99	1.05±0.42	1.84±1.56	0.96±0.42	1.25±1.53
Gasoline	0.77±0.47	0.65±0.41	0.61±0.36	0.62±0.36	0.26±0.13	0.73±0.72	0.31±0.15	0.47±0.46
Diesel	1.34±0.68	1.48±0.85	1.40±0.64	1.13±0.78	1.84±0.45	1.92±1.32	1.75±0.45	1.80±1.26
S. Nitrate	0.99±0.11	2.34±0.16	0.92±0.11	2.18±0.17	2.56±0.21	4.81±0.46	2.51±0.22	3.13±0.37
S. Sulfate	0.69±0.19	1.28±0.27	0.65±0.18	1.28±0.26	0.78±0.12	1.16±0.38	0.74±0.13	1.13±0.37
Others	0.23±1.88	4.37±3.11	0.72±1.74	4.83±2.88	3.33±1.43	8.08±3.74	1.34±1.52	9.23±3.76

Determining emission factors of non-tailpipe emissions in near-road environment turned out to be very challenging in crowded urban areas due to multiple aspects. First, contribution of background aerosol is very high and so signal to noise ratio is very low. Second, there is no ideal upwind location to subtract the contribution of the background aerosol. If the upwind location is too close to the road then vehicle induced turbulence transport emissions to the upwind location. If the upwind location is too far from the downwind location then background concentrations at upwind differ from that in downwind. Third, increasing number of battery electric vehicles causes error when dilution ratio or dispersion is determined based on co-pollutant (e.g. NO_x, CO or CO_2) concentrations. As there is much less chemical reaction or transformation of non-tailpipe emissions compared to tailpipe emissions after the wear particles are emitted, models should be able to predict both emission factors and characteristics very well. The reason tailpipe emissions have a lot more chemical transformation is due to semivolatile PM taking part into SOA formation. There is not much VOC coming from brake PM as evidenced by much lower OC fraction compared to exhaust PM. As such further study should investigate detailed dispersion characteristics of non-tailpipe emissions based on emission rates determined from the laboratory experiment.

The main objective of the simulation component of this project is to assess the impact of exhaust and non-exhaust emissions on the downwind communities. We developed a two-domain approach to take advantage of the field measurement data, including those from both the meteorological and particle measurements, to greatly reduce the uncertainties in modeling inputs while making the computational resources manageable. Focusing on the highway 5 locations, the two domains are referred to as the Highway domain and the Community domain as depicted in Figure ES 6.

(a) 

(b) 

Figure ES 6: Aerial images showing (a) the Highway domain and (b) the Community domain.

The goal of the simulations on the Highway domain is to generate velocity and concentration profiles as inputs to the simulations for the Community domain. The dispersion and deposition of exhaust and non-exhaust particles were simulated in the Community domain. Our modeling results suggest that the deposition can reduce particle mass concentrations by 1 to 2% for the size range pertain to brake PM and by 4-7% for the size range relevant to road dust in the downwind community (<400 m from the roadway). The implication is that near-road communities are likely exposed to non-exhaust particles coming from roadways, even though those particles have relatively higher deposition velocity than exhaust particles. Future studies that able to separate contributions from exhaust and non-exhaust sources to the overall particle size distributions can help elucidate the community exposure to non-exhaust particles.

Introduction

Background

Brake and tire wear PM present a large fraction of non-exhaust particle emissions from vehicles. The legislative effort by CARB and other agencies has resulted in much lower tailpipe PM emissions over the years but has not affected non-exhaust PM emissions. Thus, non-exhaust sources, including brake and tire wear PM, have become larger contributors to traffic-related emissions. When tailpipe achieves zero emissions, all traffic emissions will come from non-exhaust sources. Previously, CARB has funded a project to measure laboratory generated airborne brake wear PM emissions using a brake dynamometer. However, the laboratory results do not fully represent the diverse driving and road conditions in real world. There is still a need to evaluate the contributions of different types of non-exhaust emissions to near road PM concentrations. One of concerns is that non-exhaust PM has high metal content, which could result in higher toxicity and negative outcomes for impacted communities and therefore it is critical to improve our understanding of the impact of brake and tire wear PM emissions. The results of this study will support near-road air quality mitigation strategies as well as health effect analysis related to toxic PM constituents.

Project Objectives

The objective of this research is to measure the real-world impact of brake and tire wear emissions on PM concentrations near roadways. The size distribution, chemical composition, and emission rate of brake and tire wear PM will be characterized and their importance relative to tailpipe emissions and other regional background sources will be calculated. The results of this study will be used to quantify PM contributions from vehicular sources (tailpipe and non-tailpipe) near roadways. The results will also help provide exposure information to examine possible health impacts of these sources on nearby receptor populations. In particular, this study aims to address the following objectives.

- Survey relevant literature and identify knowledge gaps (task 1)
- Measure real-time $PM_{2.5}$ and PM_{10} at near road locations. (tasks 2 and 4)
- Measure real-time particle number and mass distribution along with semi-real time metal content analysis to distinguish brake and tire PM from background and exhaust particles. (tasks 2 and 4)
- Use traffic information to infer brake activities and their relationship with brake PM emissions. (task 3)
- Conduct source apportionment analysis to determine contribution of brake and tire particles to $PM_{2.5}$ and PM_{10}. (tasks 4 and 5)
- Determine unique tracers for brake and tire-wear emissions from source apportionment and the on-going CARB brake dyno study. (tasks 4 and 5)

- Conduct particle dispersion modeling to evaluate impact of brake and tire wear particles on nearby communities at downwind locations. (task 6)
- Determine fleet emission factors for brake and tire wear PM. (task 6)

1 Task 1: Identify prior methods and gaps in knowledge

1.1 Task 1: Brake wear literature survey

1.1.1 *Brake Particle Size Distribution*

Brake wear particles can exist in the range from a few hundred nanometers to a few tens of micrometers due to the mechanical abrasion between the brake pad and the rotor or disk, but these particles have been shown to be predominant in the coarse to fine size range [1-3]. In the following summary, particles are defined as coarse, fine, and ultrafine if their diameters fall between (2.5 μm < D < 10 μm), (0.1 μm < D < 2.5 μm), and (D < .1 μm) respectively.

The study by Garg et al. [4] used a brake dynamometer to test seven new brake pads at four different temperatures (100, 200, 300, and 400 ºC). The brake pads were selected to represent 88% of the brakes used by General Motors in 1998, and the ratio of car to truck brakes was 1.13. Semi-metallic brakes, potassium titanate fiber brakes, and aramid fiber brakes were used to conduct the experiment. Each brake test was performed from 50 to 0 km/h with a deceleration of 2.94 m/s^2. Within each temperature test, the system was allowed to cool to the desired temperature. After each complete test, brakes were removed, weighed, and had accumulated brake dust removed into Ziplock bags for elemental testing. Pallflex 47 mm diameter Tissue Quartz filters were also used to collect samples for carbon analysis at the 100 and 300 ºC tests while Nuclepore 47 mm diameter, 0.8 μm pore size polycarbonate filters were used at the 200 and 400 ºC test for mass and elemental analysis. Particle size distributions were obtained using a MOUDI and particle number distributions were measured using a Dekati ELPI. It was found that mass median diameters fell within the range of 0.62 and 2.49 μm with an average of 1.49 μm. The average percent mass of airborne particles had an average of 86%PM_{10}, 63% $PM_{2.5}$, and 33% $PM_{0.1}$.

A similar study by Hagino et al. [5] used brake dynamometer tests and found brake wear particles to be less than 10 μm with a unimodal shape mass size range of 0.68 – 3.5 μm. Their study consisted of two passenger car disc brake systems (Vehicle I and II) and one middle class truck drum brake system (Vehicle III). To mimic urban driving and braking patterns, Vehicle I and II were tested with an average deceleration of 0.28 m/s^2 while Vehicle III was tested at 1.6 m/s^2. To better quantify and track the whereabouts of the brake wear particles, they collected fallout from the bottom of the dynamometer test chamber using stainless steel trays, deposition on the surface of the brake pads and linings using a micro spoon-shaped spatula, and airborne PM using eight filter sampling systems. Real-time particle mass concentrations were measured by two DustTrakII, aerosol monitors based on light scattering. Although, their results showed there was no significant contribution from ultrafine particles, they found that Vehicles I and II had mass size distribution peaks at the 1.2-3.5 μm range while vehicle III showed peaks at 1.2-2μm. The difference between the size ranges show that particle size is a function of brake assembly structure (disc or drum).

Iijima et al. [1] also used brake dynamometer tests on three non-steel brake pads to produce brake particles at varying temperatures, driving conditions, and intensity of braking. They used a cast iron disk fixed on a rotating shaft which was set at constant speed then

decelerated constantly at 3.0m/s^2. Using an APS particle size distributions were measured at temperatures of 200, 300 and 400 ºC. Number concentrations showed peaks at 1-2 μm in diameter while calculated mass size distribution had peaks at 3 and 6 μm. This led to an estimation of $PM_{2.5}$ to fall between 74% and 92% of total particle number and 12-36% of particle mass. $PM_{2.5}$ was also found to be more abundant at the 200 ºC temperatures which simulated urban driving conditions. As suggested by the authors, data in this study differs from that of Garg et al. [4] because this study used an open system brake dynamometer and as a result particle aggregation or deposition due to the interaction between the particles and the chamber wall of a closed system is not a factor of particle size.

A study that closely resembles Iijima's results is by Sanders et al. [6], as they too used an open system brake dynamometer test on low metallic (mid-size car), semi-metallic (full-size truck), and non-asbestos organic (full size car) brakes. Sanders allowed the brakes to run for more than 1000 stops each to "break them in". Urban driving was modeled by conducting 24 stops at less than 1.6 m/s^2 with speeds of less than 90 km/h. Harsh braking conditions were modeled by running 10 consecutive 7.9 m/s^2 stops from 100 to 0 km/h. To compare between wear debris recorded using the dynamometer to the airborne debris measured behind a vehicle, a series of tests at 1.8 m/s^2 stops from 96km/h were performed in a wind tunnel. To collect particle samples, a hood was placed around the brake assembly along with a blower at constant flow of ~3.6 m^3/min. Particle size distributions were measured using a MOUDI and an ELPI. Using average wear densities of 5, 4, and 3 g/cm^3 for low metallic, semi-metallic, and NAO linings respectively, the number weighted distributions of the brake wear particles under urban driving conditions peaked in the range of 0.5-2 μm. The mass mean diameter brake wear debris for the urban driving condition was reported to be about 6 μm for all three brake material types. Although the size distributions were the similar for the three brakes, the low metallic linings generated 2-3 times the number of wear particles than the semi-metallic and NAO linings. This study also suggests that particle size is not only a function of material type, but temperature as well. Under the harsh braking conditions, the number-weighted size distributions were dominated by particles less than 0.3 μm in diameter which likely occurs due to chemical processes occurring while the brakes reach 500 - 600°C. In addition, the mass-weighted average of particles at the harsh braking conditions occurred at 10 μm.

Many studies have also used the results of laboratory tests using open and closed brake dynamometer systems, pin-on disk configurations, and disk brake assembly test stands to compare with real-world on road driving data. Wahlström et al. [7] tested the validity of results between a disk brake assembly test stand, a pin-on-disc machine, and field tests using a passenger car. All three test were controlled to simulate urban driving conditions on a passenger car with low metallic brake pads and cast-iron rotors. Testing on the disk brake assembly shown in

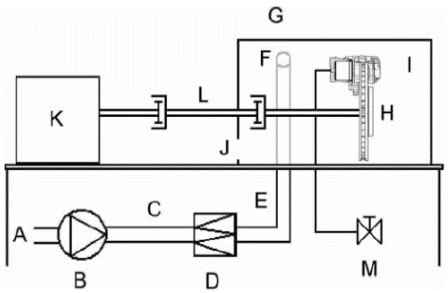

Figure 1-1 consisted of contact pressures of about 1.1 bar and speed of 55km/h. The pin on disc set up in

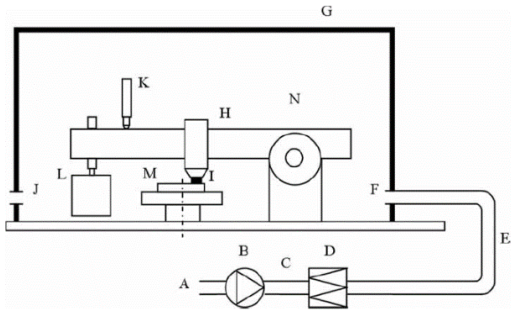

Figure 1-2 was controlled at 1.2 MPa with a speed of 7 km/h. Particles from both the disc brake assembly and pin-on-disk test were measured using a PTrack counter and a Grim 1.109 aerosol spectrometer. The vehicle field test shown in Figure 1-3 were performed on a test track in Stockholm, Sweden to simulate country roads at speeds of 30 km/h. To reduce the influence of resuspended traffic-generated particles, the vehicle tests were conducted on days when it rained. The car was fitted with two Grimm and two Dust Trak instruments to measure number and mass concentrations. An additional test was performed in heavy traffic to represent data from long tunnels, urban traffic and expressways. Results of this study showed that all test methods had peaks in number concentration of about 0.41 µm and volume-weighted mean diameters of 3, 2, and 1.7 µm for the brake, pin, and field tests respectively. As stated by the authors, regardless of the difference in load, load conditions, sliding velocity, and pad temperature, all three test methods showed similar number distributions.

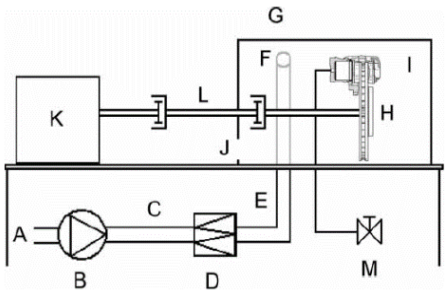

Figure 1-1: Schematic of the disc brake assembly test stand. A: room air; B: fan; C: flowrate measurement; D: filter; E: flexible tube; F: inlet for clean air, measurement point; G: chamber; H: disc brake assembly; I: air inside the chamber, well mixed; J: air outlet, measurement points; K: motor; L: drive shaft; M: hydraulic system [7].

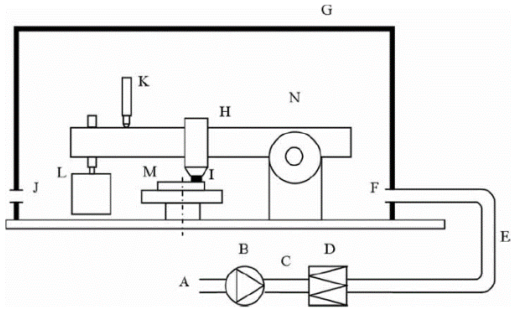

Figure 1-2: Schematic diagram of the pin-on-disc material test stand. A: room air; B: fan; C: flowrate measurement; D: filter; E: flexible tube; F: inlet for clean air, measurement point; G: closed chamber; H: pin-on-disc machine; I: pin sample, well mixed; J: air outlet, measurement points; K: displacement gauge; L: dead weight; M: rotating disc sample; N: air inside the chamber [7].

Figure 1-3: Test vehicle with sampling test tubes. Photo of the test tubes for particle measurements mounted directly behind the brake pad on the piston side (left), and test tubes mounted in front of the test car for measurement of background particle concentration (right) [7].

This study was continued further to investigate the size, shape, and elemental composition of brake wear particles using a disc brake assembly stand (

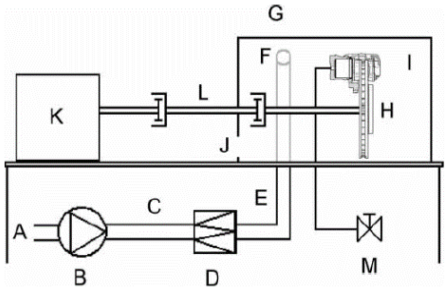

Figure 1-1) on low-metallic and non-asbestos brake pads [8]. The rotational speed was set to 600 rpm with a brake pressure of .22 MPa which corresponds to urban braking from a vehicle speed of 55 km/h. A Grimm 1.109 aerosol spectrometer, a PTrack counter, and a Dust Trak aerosol monitor were used to measure brake wear particle size distributions and concentrations. Both brake pad types showed peaks in airborne particle concentration of 280 nm for number size distribution and 350 nm for volume distribution. Mosleh et al. [9] used commercial truck disk brake pad material to slide against gray cast iron in laboratory conditions. A pin on disk configuration on where the pin was made of pad materials and had a square cross section. The tests were varied by using a minimum sliding speed of 0.275 m/s with contact pressures at 0.125, 0.375, and 0.625 MPa. The maximum sliding speed was 5 m/s with contact pressures at 0.75, 1.0, and 1.25 MPa. At the low-speed sliding, both continuous contact and discontinuous contact with 5 s contact and 3 s separation were used. Aluminum foil was used to make a cup around the disk and number size distribution of the wear particles were obtained using an LA-700 laser scattering analyzer capable of detecting particle sizes in the range of 0.04-262 μm. For the higher-speed sliding, only

continuous contacts were used. The results showed that the lower speed tests had a size distribution peak around 350 nm for all contact pressures. This data supports the findings of Wahlström et al. [7], as the second peaks were at 2, 7 and 15 μm for pressures of 0.125, 0.375, and 0.625 MPa respectively as shown in Figure 1-4a. For high-speed tests the first peak also occurred around 350 nm while the second peak showed to be at 3, 5, and 6 micrometers for 0.75, 1.0, and 1.25 MPa, respectively, as shown in Figure 1-4b. These results support Sanders et al. [6] as they suggest that higher pressures (harsh braking) leads to larger sizes of wear particles between different brake lining materials.

(a) (b)

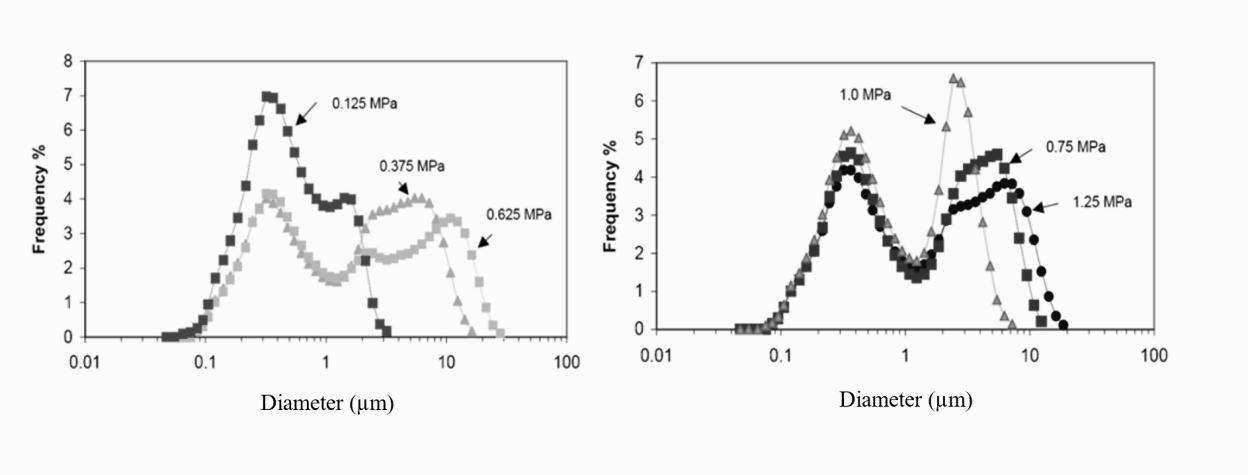

Figure 1-4: Size distribution of wear particles. Size distributions of wear particles generated during (a) low-speed tests (sliding speed=0.275 m/s) ; (b) high-speed tests (sliding speed = 5 m/s) [9].

Kwak et al. [10] also used on-road driving and in laboratory tests to investigate the physical and chemical properties of non-exhaust coarse and fine particles. Four vehicle speeds were used at 50, 80, 110, and 140 km/h for the constant speed driving test. On the other hand, "braking" conditions were set up for the vehicle to gradually accelerate from 0 to 150 km/h at a rate of 0.71 m/s^2 and stopped with a deceleration rate of 3.02 m/s^2. "Normal cornering" was conducted on a round track with a diameter of 50m at a constant velocity of 30 km/h, while "extreme cornering" was performed at 50 km/h. Two Dust Traks were simultaneously used to measure PM concentrations of the background and at the tire/road interface or brake pad. It was found that under braking conditions, the PM concentrations coming from road wear particles and tire wear particles were significantly less than those of brake wear particles. The brake wear particles had a broad size range from 1 μm to 10 μm, and there were no particles larger than 10 μm recorded during braking.

Studies reviewed by Grigoratos et al. [11] report that around urban environments, brake wear particles to non-exhaust traffic related PM_{10} contributes between 16 to 55 % by mass, while near highways that percentage is around 3% by mass. The tables below show an overview of important literature studies dealing with the characterization of brake wear particles in terms of particle mass distribution (Table 1-1) and particle number distribution (Table 1-2).

Table 1-1: Overview of literature studies investigating the mass distribution of airborne brake wear particles [11].

Reference	Type of study	Brake pads tested	Method	Mass size distribution
Cha et al. 1983	Brake dynamometer	Asbestos		Unimodal (2.1–3.3 μm)
Garg et al. 2000	Brake dynamometer	Semimetallic and NAO	MOUDI (>0.1 μm)	Unimodal (0.1–1.0 μm)
Sanders et al. 2003	Brake dynamometer	Low metallic, semimetallic and NAO	MOUDI–ELPI	Unimodal (4–5 μm)
von Uexküll et al. 2005	Brake dynamometer	Disc and drum (trucks)	Optical particle counter (>0.3 μm)	Unimodal (2–3 μm)
Iijima et al. 2007	Brake dynamometer	NAO	APS (>0.5 μm)	Unimodal (3–6 μm)
Iijima et al. 2008	Brake dynamometer	NAO	APS (>0.5 μm)	Unimodal (2.0 μm)
Kukutschová et al. 2011	Brake dynamometer	Low metallic	APS–SMPS–BLPI	Unimodal (2–4 μm)
Harrison et al. 2012	On-road measurement	Roadside PM	MOUDI	Unimodal (2–3 μm)
Kwak et al. 2013	On-road measurement	Roadside PM	APS (>0.5 μm)	Unimodal (1–10 μm)

Table 1-2:Overview of literature studies investigating the particle number distribution of airborne brake wear particles [11]

Reference	Type of study	Brake pads tested	Method	Particle number distribution
Sanders et al. 2003	Brake dynamometer	Low metallic, semimetallic and NA004F	ELPI	Unimodal (1.0 μm)
Mosleh et al. 2004	Brake dynamometer	Semimetallic (truck)	Laser scattering analyser	Bimodal (350 nm and 2.0 μm)
von Uexküll et al. 2005	Brake dynamometer	Disc and drum (trucks)	Optical particle counter (>0.3 μm)	Unimodal (0.5–1.0 μm)
Iijima et al. 2007	Brake dynamometer	NAO	APS (>0.5 μm)	Unimodal (1.0–2.0 μm)
Riediker et al. 2008	Brake dynamometer	Vehicles under different driving conditions	TEM	Bimodal (80 and 400 nm)
Iijima et al. 2008	Brake dynamometer	NAO	APS (>0.5 μm)	Unimodal (0.8–1.0 μm)
Wahlström et al. 2010a	Brake dynamometer	Low metallic and NAO	GRIMM (>0.25 μm)	Bimodal (280 and 350 nm)
Wahlström et al. 2010b	Brake dynamometer	Low metallic and NAO	GRIMM–SMPS	Multimodal (100–550 nm)
Mathissen et al. 2011	On-road direct measurement	Vehicle under different driving conditions	EEPS (<0.56 μm)	Bimodal (10 and 40 nm)
Kukutschová et al. 2011	Brake dynamometer	Low-metallic brake pads	APS–SMPS	Bimodal (100 and 300 nm)

1.1.2 *Brake pad components and types*

Modern brakes are composed of fibers, matrix binders, friction modifiers, abrasives, and fillers which vary in composition and amount depending on the manufacturer [3, 12]. Table 1-3 shows a breakdown of the different components seen in modern brakes along with the average percent by mass and their composition. Binders are used to provide mechanical strength, abrasives increase friction and maintain cleanliness between the contact surfaces, lubricants assist in stabilizing frictional properties at high temperatures, fillers improve manufacturability, and binders maintain structural integrity of the brakes under mechanical and thermal stress [3].

Table 1-3: Percent by mass and composition of brake components [11]; [12]

Component	Percent by Mass	Composition
Binders	20 – 40 %	Modified phenol-formaldehyde resins
Fibers	6 – 35 %	Metallic, mineral, ceramic or organic, aramid, glass, potassium titanate
Fillers	15 – 70 %	Barium and antimony sulphate, magnesium and chromium oxides, silicates, ground slag, stone and metal powders, calcium carbonate
Lubricants	5 - 29 %	Inorganic metallic, ground rubber, metallic particles, antimony trisulphide
Abrasives	10 %	Aluminum oxide, iron oxides, quartz, zircon, graphite

A review of automotive brake friction materials by Chan et al. [12] shows that the complete composition of brake friction material is rarely disclosed because it is treated as proprietary and manufacturers are not obligated to release that information. The composition of brakes is obtained from academic research and patents. Overall, there are four main classifications of brake pads. NAO are most common, although as the vehicle age increases, semi-metallic and low-metallic brake pads become cost-effective replacements for light duty vehicles [13]

- Metallic: which are made of steel fibers, and copper fibers,

- Semi-Metallic: which is a mixture of metallic and organic ingredients. These brake pads are usually noisier than others and have low wear.
- Low-Metallic: which have a relatively high abrasive content, high friction, and good braking capacity at high temperatures [8].
- Non-asbestos organic (NAO): Predominantly organic, such as mineral fibers, rubber, graphite, etc. This type of brake pads exhibit relatively low brake noise and low wear rates, but are hindered at higher temperatures [6]. These type of brake linings are descendants of asbestos formulations but substitute potassium titanate fibers [6].

1.1.3 *Chemical composition: Brake wear elemental composition*

Compositions of brake wear particles vary depending on brake friction material parameters, brake assembly type, and vehicle operating conditions [5]. Overall, iron (Fe), copper (Cu), lead (Pb), and zinc (Zn) have been reported to be the highest in concentrations by many studies [3]. Figure 1-5 shows a summary of metal concentrations in mg/kg which were reported to be present in brake linings and emitted brake dust from studies reviewed by Thorpe et al. [3].

Metal	Car brake linings (mg/kg, unless indicated otherwise)	Car brake dust (mg/kg, unless indicated otherwise)
Al	3765	330–2500
As	<2–18	<2–11
Ba	2638	5900–74,400
Ca	14,300	920–8600
Cd	<1–41.4	<0.06–2.6
Co	6.4–45.8	12–42.4
Cr	<10–411	135–1320
Cu	11–234,000	70–39,400
Fe (%)	1.2–63.7	1.1–53.7
K	857	190–5100
Li	55.6	Not reported
Mg	6140	83,000
Mn	181–3220	620–5640
Mo	0.4–215	5–740
Na	15,400	80
Ni	3.6–660	80–730
Pb	1.3–119,000	4–1290
Sb	0.07–201	4–16,900
Se	<1–15	4.5–115
Sr	81.4	300–990
Zn	25–188,000	120–27,300

Figure 1-5: Summary of metal concentrations present in brake linings and emitted brake dust [3].

Additionally, Wahlström et al. [8] found that most of the coarse particles formed from a laboratory brake disc assembly consists mainly of iron and iron oxide. There were also traces of titanium, copper, and aluminum, which are predicted to originate from the low-metallic and non-asbestos organic brake pad material. These results have been confirmed by Kwak et al. [10] as they found that Fe, Ca, and Zn contained the highest concentrations in the coarse fraction particles generated under constant speed driving and cornering conditions. On the other hand, Fe, Ca, Ti, Ba, and Sb were highest in concentrations for the fine fraction particles generated under regular braking conditions. The concentrations of elements found during braking events from highest to lowest showed as Fe > Ba > Ti > Sb.

Österle et al. [14] showed the original composition of the brake pad prior to being tested. The brake pad used had a composition of 20% vol of mineral fibers, 8.5 % vol metallic fibers and 12% vol of solid lubricants, plus more. The purpose of their paper was to study third body formation at the interference between a brake pad and brake disc using a simple pin-on-disc test with a cylindrical pin cut from an original brake pad and a commercial cast iron disk. As defined by the authors, in the course of a gradual build up in the rotors, a fine-grained wear debris comprising a mix of pad and disc constituents is produced and trapped in trough at the surface. The trapped material differs with respect to the overall composition of the original material as a friction film formed which is defined as a third body. The test used a constant rotation speed of 900 rpm (10 m/s) and normal load of 230 N with a time interval of 225 s. Dust particles were collected with a brush and analyzed using Transmission Electron Microscopy. The results of the Energy filter transmission electron microscopy showed three main constituents being iron oxide, carbon and copper. The chemical composition of the original brake pad material was obtained by x-ray fluorescence analysis shown in the Figure 1-6. The smaller signals from Pb, Cr, Mn, Ti, Sn and K correspond to the brake pad composition but their masses were minor compared to iron, copper, and zinc.

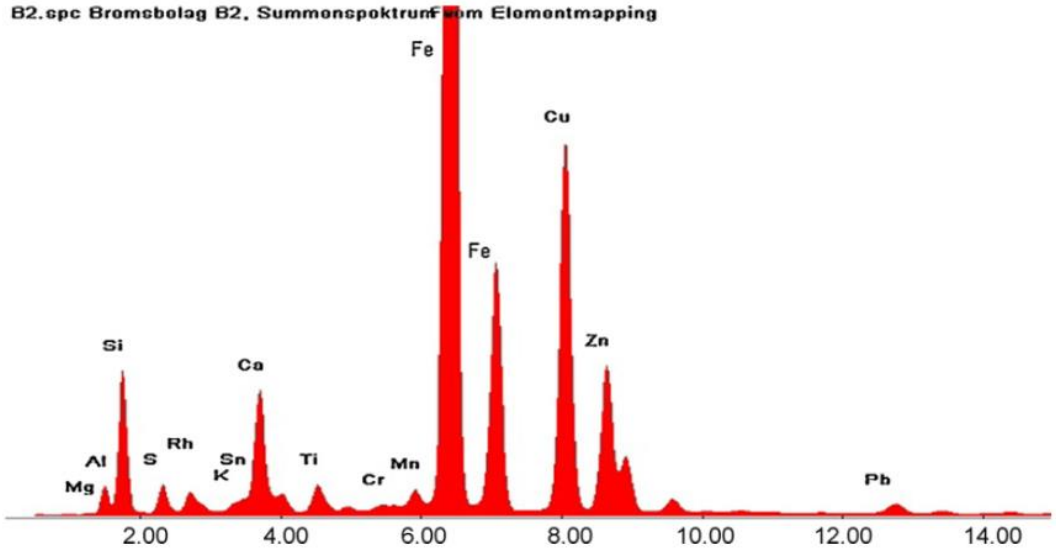

Figure 1-6: XRF analysis sum spectrum of a representative pad area prior to braking [14]. Much like particle size, the shape and chemical composition of emitted brake dust is a factor of driving conditions, frequency of braking, intensity of braking, and composition of the brake system [10]. Many studies have shown microscopy images of particles that are emitted from various disk and brake pad sources to study their morphology and microstructures [15];[9];[16].

Blau and Meyer [17] collected disk wear particles from grey cast iron , carbon / silicon carbide ceramic composite, Al-based MMC, and Fe3Al disks using a sub-scale disc brake testing system. The testing phase was composed of using a sliding speed of 10.96 m/s, normal force of 161 N, and contact time of 30 s. An adhesive extraction method with Scotch tape type 666 was used to collect loose wear particles from the surfaces of each test disk.

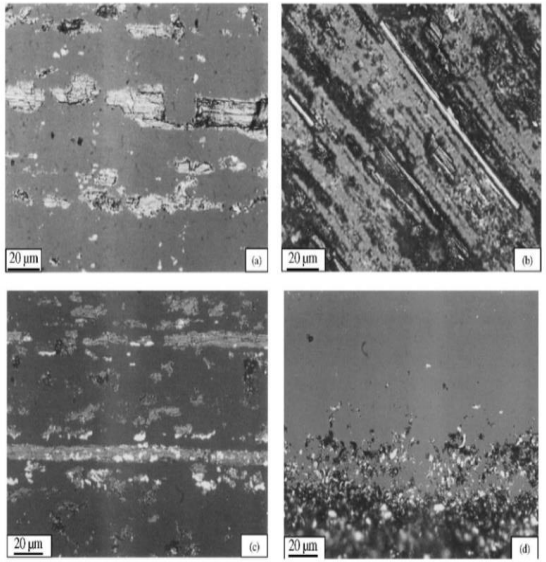

Figure 1-7 shows optical microscope images of particles on the adhesive tape used at a magnification of 420x.

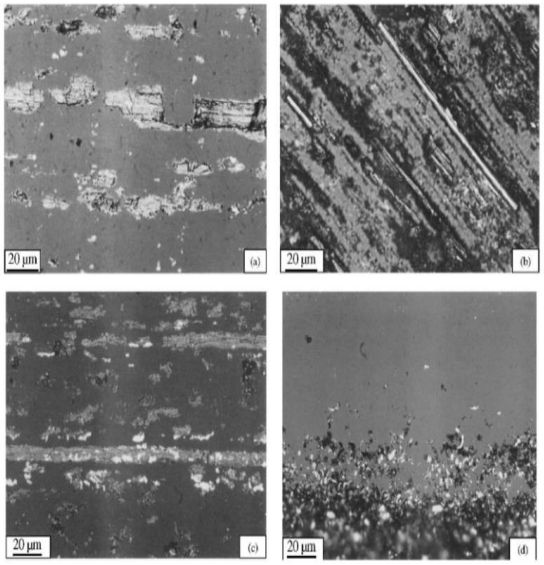

Figure 1-7a shows an image of the cast iron disk particles after testing. The particles are appear as thin, brittle and flat where most of th material was not highly reflective. As compared to the other disk types, the cast iron particles were the largest and widest of all.

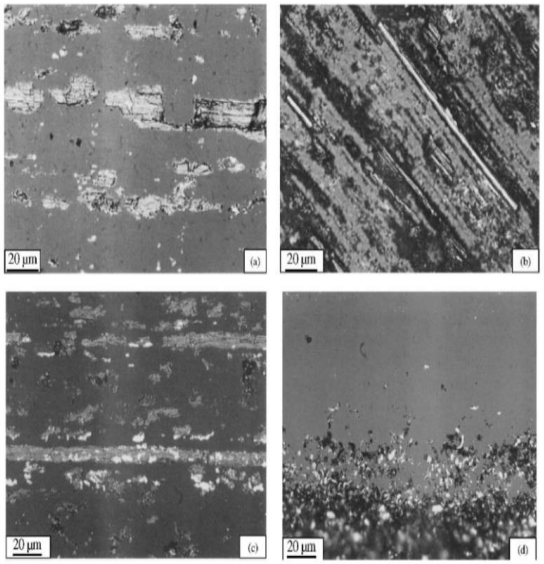

Figure 1-7b shows that some particlces from the Carbon / Silicon carbide ceramic disk appear as fine submicrometer dust while other particles are thin, long fiber fragments.

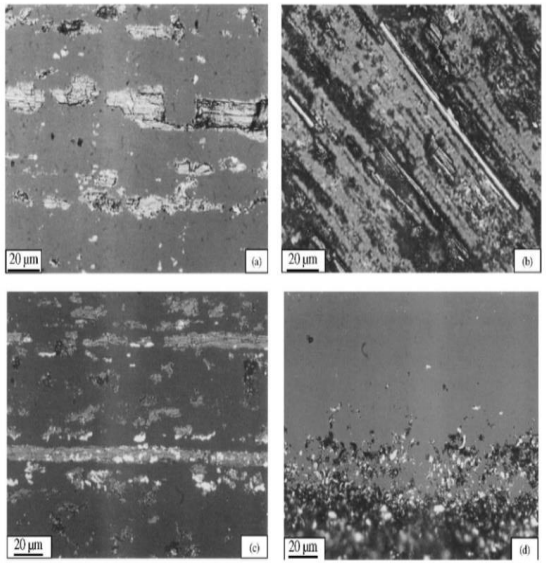

Figure 1-7c shows flake-like long metallic particles from the MMC disk, while

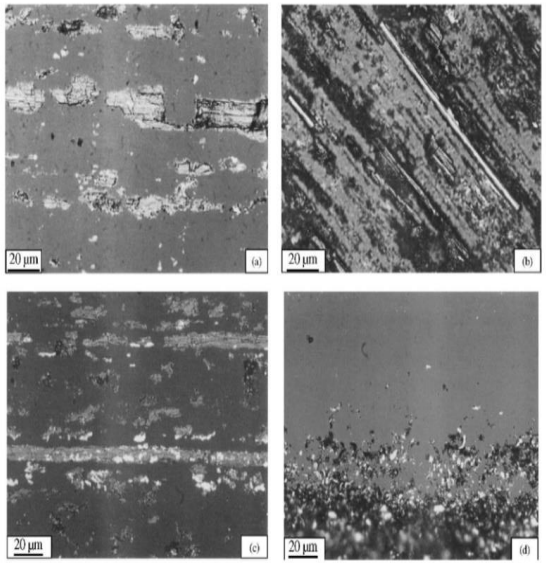

Figure 1-7d had iron aluminide particles show up as a combination of culrs and flakes.

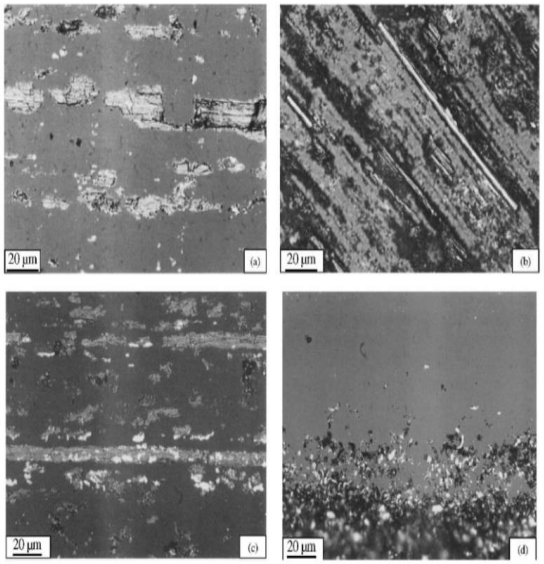

Figure 1-7: Light optical images of particles extracted from the surfaces of tested discs.
(a) Cast Iron Disk (b) C/SiC disc (c) MMC disc which contained flake-like long metallic particles. (d) Fe3Al disk [17].

von Uexküll et al. [18] sampled brake dust from 15 different trucks and three trailers from Swedish brake repair garages. 45 different brake pads and disc wear samples were acquired from exhaust air filters of brake dynamometer tests. SEM images of particles collected

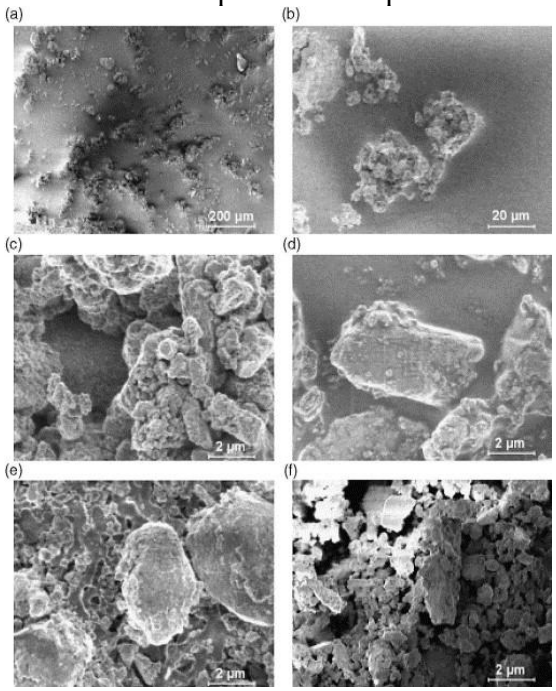

are shown in

Figure 1-8, where the most frequent shape appeared as semi-spherical agglomerates. Other shaped showed up as semi-spherical and non-agglomerated flat shapes.

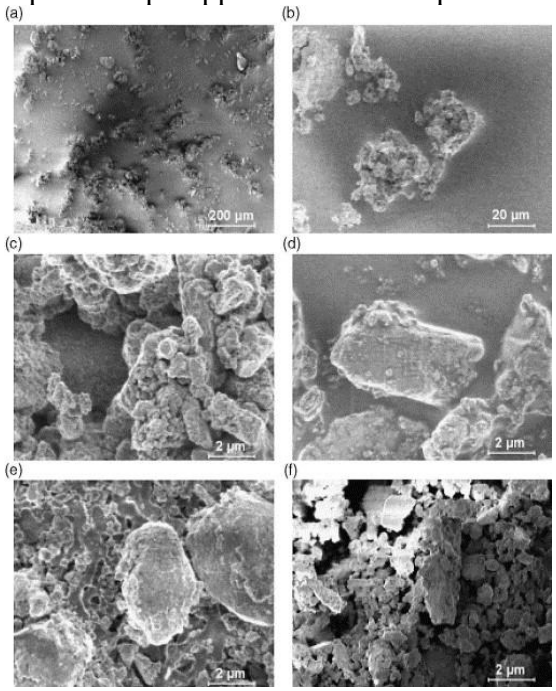

Figure 1-8 is a good representation of what shape and size brake wear particles can look like.

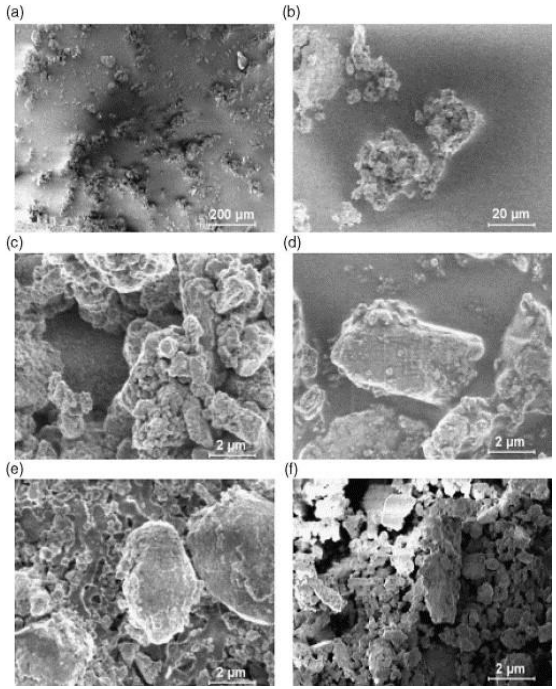

Figure 1-8: Scanning electron microscopy pictures of brake dust.
(a) 100_ microscope magnification of typical semi-spherical agglomerates; (b) 1000_ magnification of the same sample; (c) 10,000_ magnification of the same sample; (d) 10,000_ magnification of non-agglomerated flat particles from other sample (rectangles on particle originate from microscope electron beam); (e) 10,000_ magnification of non-agglomerated semi-spherical particles attached on a cellulose acetate filter (seen in the background); (f) 10,000_ magnification on layer structures in still another sample [18].

When braking occurs, the kinetic energy from the rotating discs is converted into heat which consequently results in the brake system to reach high temperatures. The heat generation can lead to the alteration of the brake lining material surface chemistry and the released debris may differ from the matter of the bulk [19]; [20]; [21].

Kukutschová et al. [22] used a series of brake dynamometer test on "low-metallic brake linings with grey cast iron rotors found in mid-size passage cars. The testing process consisted of three steps: increasing speed to 73 km/h, braking for 30s and reducing speed to 67 km/h, and finally allowing the brake to cool back down by allowing the system to run for 120s. Debris samples were collected for 11 cycles using a SMPS for 5 minutes and an APS for 1 minute. Following this, the SMPS and APS were disconnected, and a Berner Low Pressure Impactor was connected for the next 24 tests. Figure 1-9 shows the samples taken from the impactor which concluded that the

particles were formed by combined abrasive and oxidative mechanisms since there are fractured edges and pits along the main surface areas. As explained by the authors, when organic matter oxidizes, numerous pittings are observed due to material removal. In addition, a transmission electron microscopy diffraction analysis on the samples showed the presence of maghemite (γ-Fe_2O_3) and magnetite ($FeO \cdot Fe_2O_3$).

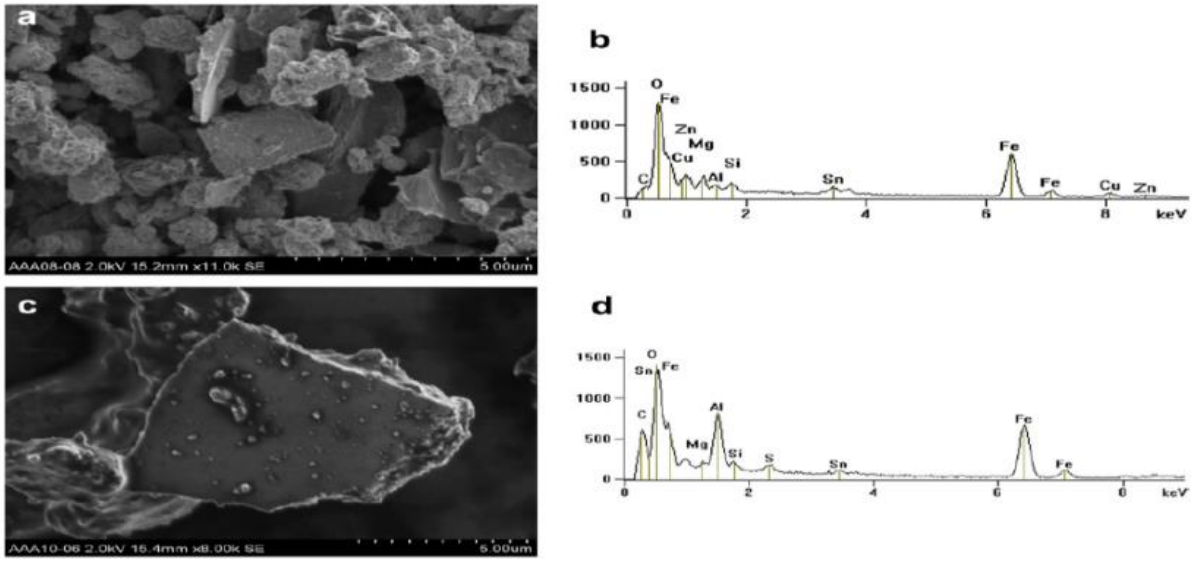

Figure 1-9: SEM images with EDX spectra of total area of the fine < 2.5 mm (a) and the coarse > 2.5 mm (b) fractions. (Kukutschová et al. 2011).

Similar results in terms of shape and composition were obtained by Kukutschová et al. [19], where semimetalic brakes were tested using brake dynamometer tests followed with a ball milling technique. Randomly selected brake samples were repeatedly ball-milled for 10 min until sample particles with major fraction below 200 micro meters were obtained. As a result, the morphology of the ball-milled samples are shown in Figure 1-10.

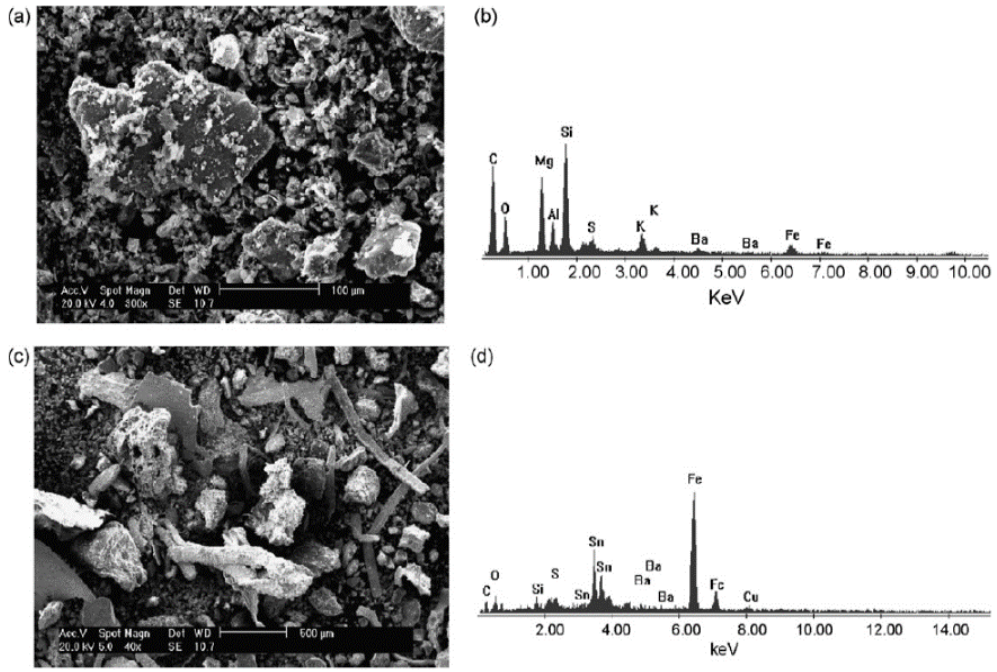

Figure 1-10: SEM images with EDX analysis of debris collected after ball-milling (a and b) and brake dynamometer test (c and d) [19].

1.1.4 *Key Tracers*

As reported by Grigoratos et al. [11] the trace elements most widely used in the past by other researches contain Ba, Cu, Fe, Zn, and Sb. For example, Sanders et al. [6] reported that Fe, Cu, Si, Ba, K and Ti were highest in concentrations from low-metallic, semi-metallic, and non-asbestos organic brake pads [23]. These findings are similar to those of Johansson et al. [24] with Zn included on the list. Han et al. [25] also characterized PM_{10} and $PM_{2.5}$ source profiles of re-suspended road dust with a focus on metal contents. They collected re-suspended road dust behind the front wheel of the test vehicle, and used Cu/Sb ratio and Zn as markers for brake wear PM. Thorpe and Harrison [3] reviewed sources and properties of non-exhaust PM and suggested Cu/Sb ratio as a good marker for brake PM. The element Ti could also be an important tracer for brake wear particles of NAO brake pads as they are descendant of asbestos formulations but substituted with potassium titanate fibers [2]. The magnitude of concentrations that contribute to wear debris from highest to lowest is Fe, Ba, Ti, and Sb [10]. Beddows et al. [26] used Aerosol Time-of-Flight Mass Spectrometer to characterize brake wear particles in the size range of 0.3 to 3.0 micrometers. This instrument provides an aerodynamic diameter and a positive and negative mass spectrum

for each particle ionized by a pulse UV laser. Collection of particles were obtained from both a laboratory setting and different road site testing. For the laboratory setting, brake dust from the ten best selling cars for 2001 in the United Kingdom were sampled into the spectrometer nozzle orifice inlet. An enclosed automotive brake and caliper system was used as a secondary test with the spectrometer aerodynamic focusing lens inlet. The disc was rotated at 1500 rmp with variations in pressures between 1-4 bar to mimic light, medium, and heavy braking conditions. The field studies were performed at six different locations, three used the aerodynamic lens inlet and the other three used the nozzle inlet. In both [^{56}Fe] and [$^{-88}FeO_2$] were detected in high percentages of the particles with aerodynamic diameter greater than ~0.7 and ~0.9 micrometers respectively. This concludes that they are more reliable markers for brake wear particles than [^{138}Ba] since there was only a 40% detection of this ion in both devices, but it can also be a strong indicator of brake dust particles. [^{138}Ba] can be used as a tracer since there are few other sources of barium in the atmosphere but they appeared in the mass spectra only at higher laser energies. The study also notes that [$^{-88}FeO_2$] appears in small quantities in other types of dust such as soil and tire dust which is confirmed by Dall'Osto et al. [23]. In addition, Gietl et al. [27] collected particle samples at both a road side and background sites in London and conducted metal and ion analysis. Their study concluded that barium can be used as a marker for brake dust in urban air since iron (Fe) can have possible contributions from tire wear and resuspended particles, leading to an over estimation. Dall'Osto et al. [23] sampled aerosol mass concentrations of seventeen elements by time (1h) and size ($PM_{2.5}$) at urban background and road sites using particle induced x-ray emission measurements. Their results showed higher concentration of Ca (17%), Fe (27%) and Cu (20%) at the roadside location than that of the urban location. This showed that Fe and Cu together can also be used as a tracer of brake wear because both elements periodically showed up in higher concentrations as two peaks in the data during traffic rush hours. Their findings also showed that Fe and Cu are primarily emitted into the atmosphere and not resuspended particles from the road. Birmili et al. [28] also confirmed that iron in coarse particles could be used as a tracer of non-exhaust particle, because calcium is primarily a tracer of particles from soils. Table 1-4 below shows a summary of key tracers that have been repeatedly used by important literature surveyed by Pant and Harrison [29]

Table 1-4: Key tracers used for non-exhaust PM [29]

Reference	Brake wear
Adachi and Tainosho (2004)	Fe, Ba, Cu, Sb, Zr
Schauer et al. (2006)	Fe, Cu, Ba
Grieshop et al. (2006)	Cu, Sb, Ba and Ga
Wahlin et al. (2006)	Cr, Fe, Cu, Zn, Zr, Mo, Sn, Sb, Ba and Pb
Tanner et al. (2008)	Cu, Cd
Canepari et al. (2008)	Ba, Fe, Sb, Sr
Harrison (2009)	Ba, Cu
Dongarra et al. (2009)	Cu, Mo, Sb
Fabretti et al. (2009)	Cu, Zn, Sb, Sn (vehicular abrasion)
Keuken et al. (2010)	Cu
Bukowiecki et al. (2010)	Fe, Cu, Zn, Zr, Mo, Sn, Sb and Ba
Pey et al. (2010)	–
Perez et al. (2010)	Sb, Cu, Ni, Sn (wear of brake, tire and other parts)
Amato et al. (2011a)	Fe, Cu, Zn, Cr, Sn, Sb
Apeagyei et al. (2011)	Fe, Ti, Cu, Ba
Duong and Lee (2011)	Ni, Cu
Ondráček et al. (2011)	Cu, Ba, Fe, Zn
Song and Gao (2011)	Sb, Cu, Fe, Pb
Sahu et al. (2011)	Zn (brake and tyre wear)
Peltier et al. (2011)	–
Harrison et al. (2012b)	Ba, Cu, Fe, Sb

1.1.5 *Emission Factors*

Abu-Allaban et al. [30] determined emission factors for tailpipe, brake and tire wear, and re-entrained road dust by performing testing at four locations. Two locations were by city roads that accounted for low-speed, light duty traffic and the other for high-speed light duty traffic. The other two sites were near highways to account for heavy- duty traffic, and for brake-wear impact. The study used CMB receptor modeling and SEM to characterize the source material. $PM_{2.5}$ and PM_{10} were collected on a 6-8-hour basis and two medium volume samples for chemical analysis on samples. Teflon-impregnated glass fiber filters were weighed before and after sample collection to determine mass concentrations of polycyclic aromatic hydrocarbons (PAHs). The study found that brake-wear contributed the most on highway exit testing sites than other locations due to high amounts of stopping. $PM_{2.5}$ rates varied from 10 to 50 mg/km and 60 to 480 mg/km for light -duty and heavy-duty vehicles respectively. While PM_{10} emission rates ranged from 40 to 780 mg/km and 230 to 7800mg/km for light-duty and heavy-duty vehicles, respectively.

1.1.6 *Testing Methods*

Overall, most of the studies in this review used one or more of the following methods shown below to obtain brake wear and/ or disc wear data:

Kukutschová et al. [22] used a brake dynamometer to generate brake wear particles while the front wheel was enclosed in a variable controlled chamber shown in Figure 1-11. Brake wear particles were produced from recreating sub-urban driving by 1) increasing vehicle speed to 73 km/h 2) braking for 30 seconds followed by a speed slowdown to 67 km/h and 3) an idle run for 120 s allowing for the brake and rotor to cool in temperature. The previous three steps were repeated multiple times, but testing was always done after the system was completely cooled to room temperature.

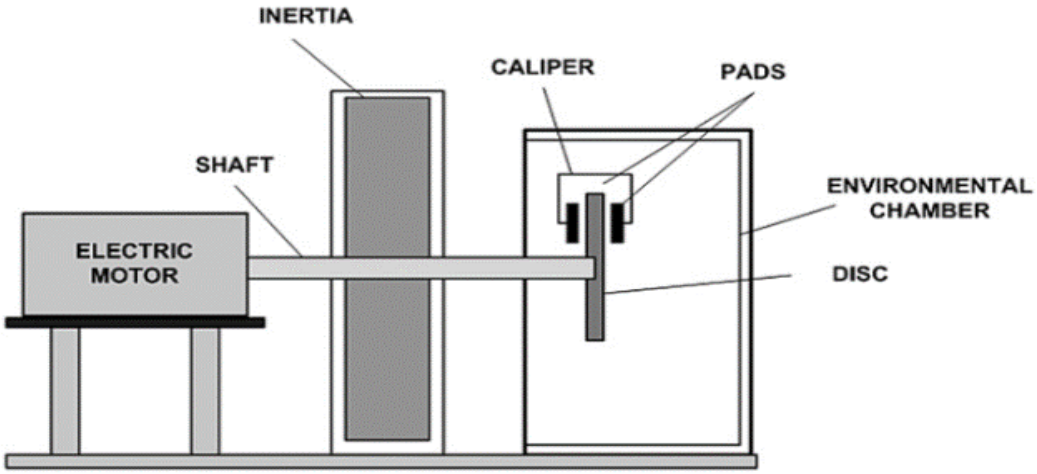

Figure 1-11: Schematic of the closed system brake dynamometer with environmental chamber [22].

Österle et al. [14] performed a pin on disk test shown in Figure 1-12 with constant rotation of 900 rpms and a normal load of 230 N. The cylindrical pin has a diameter of 20 mm and a height of 14 mm which was machined from a real brake pad.

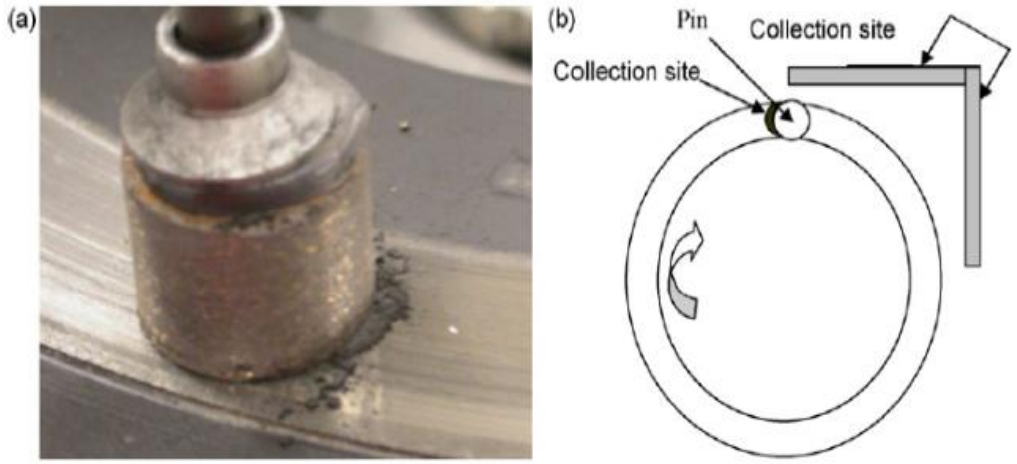

Figure 1-12: (a) Test device pin actuating against disc, (b) and schematic of test [14]

Sanders et al. [6] used test tubes to collected real time brake wear particles from a series of driving conditions shown in Figure 1-13. As the authors state, this method has some disadvantages because of the losses in particle collection due to the bending angle of the tubes and due to non-isokinetic (constant) sampling.

Figure 1-13: Image of test vehicle showing location of sampling tubes [6].

Figure 1-14 shows a sub-scale disc brake testing system which can test small brake pads and discs of candidate brake materials under flat-on-flat sliding conditions. The system uses 10 hp and a three-phase motor to simulate highway diving speeds on the brakes. The friction force and disc temperature are measured by the load cell and actuator respectfully, and recorded using a data acquisition system at a sampling rate of 128 samples/s.

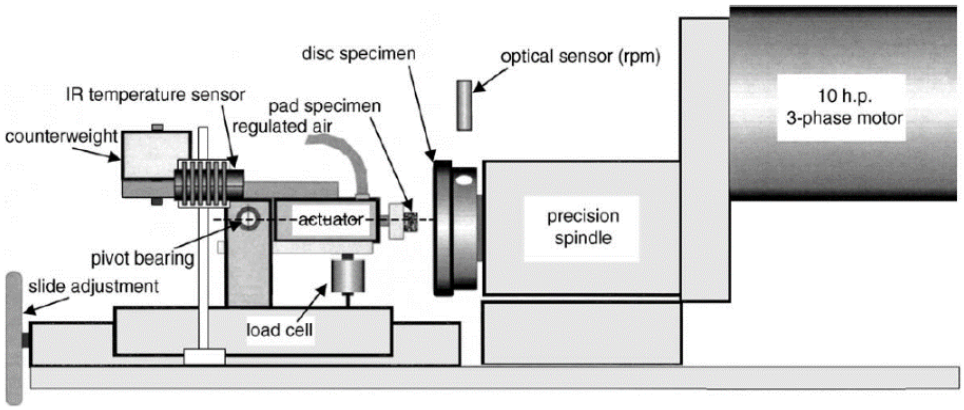

[17].

Figure 1-14: Schematic diagram of the sub-scale disc braketesting system used in [17].

A study by Koupal et al.[31], used a heavy-duty brake dynamometer to measure the PM concentrations that are representative of a range of heavy-duty trucks in California, and from one light duty electric vehicle with regenerative braking. Vehicles used included one tractor trailer with drum brakes, one tractor trailer with disc brakes, one bus with disc brakes, one municipal work truck with hydraulic disc brakes, a refuse truck simulation (class 8 all-Disc tractor with actuators), and bus coach. Each vehicle was equipped with new brake pads and instrumented with thermocouples to obtain realistic temperatures on a test track and used for implementation to dynamometer tests. A brake temperature model was obtained from the University of Michigan Transportation Research Institute (UMTRI) which assessed brake activity temperatures under varying loads. To calculate braking horsepower, the product of braking kinetic energy and vehicle speed was used. A test matrix was developed to address different speed ranges, to facilitate modeling of PM emissions as a function of speed in the EMFAC model, and to cover a range of vocation cycle brake power densities. A dynamometer was modified to enclose the brake assembly with a ducting system for PM sampling, see Figure 1-15. It included the use of a QCM MDOUDI for continuous, real-time $PM_{2.5}$ measurements, a Condensation Particle Counter, Aerodynamic Particle Sizer (0.5-20 μm), Electrodynamic Particle Sizer, and Gravimetric sampler shown in Figure 1-16. Key elements of the dyno include low background noise, minimal aerodynamic losses, Isokinetic sampling within a 10% maximum deviation, and particle transport time below 5 seconds. These factors are relevant to have proper measurements for particle mass and particle number [32].

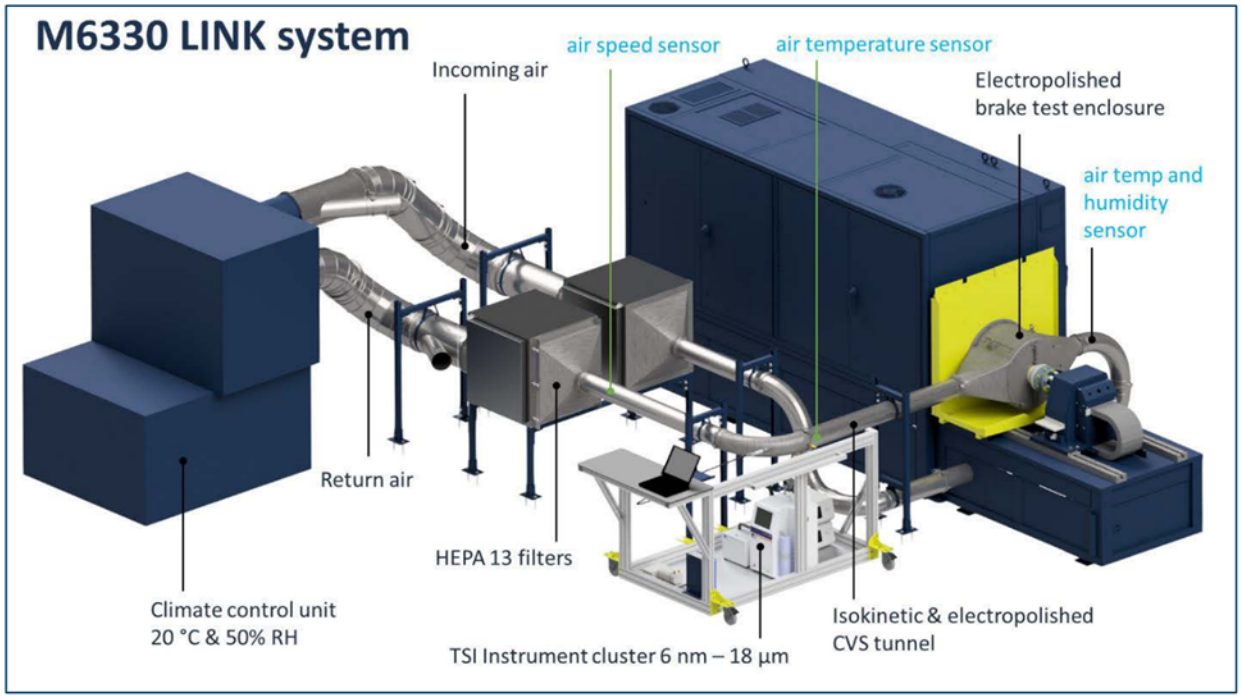

Figure 1-15: LINK Brake PM Test Setup [31]

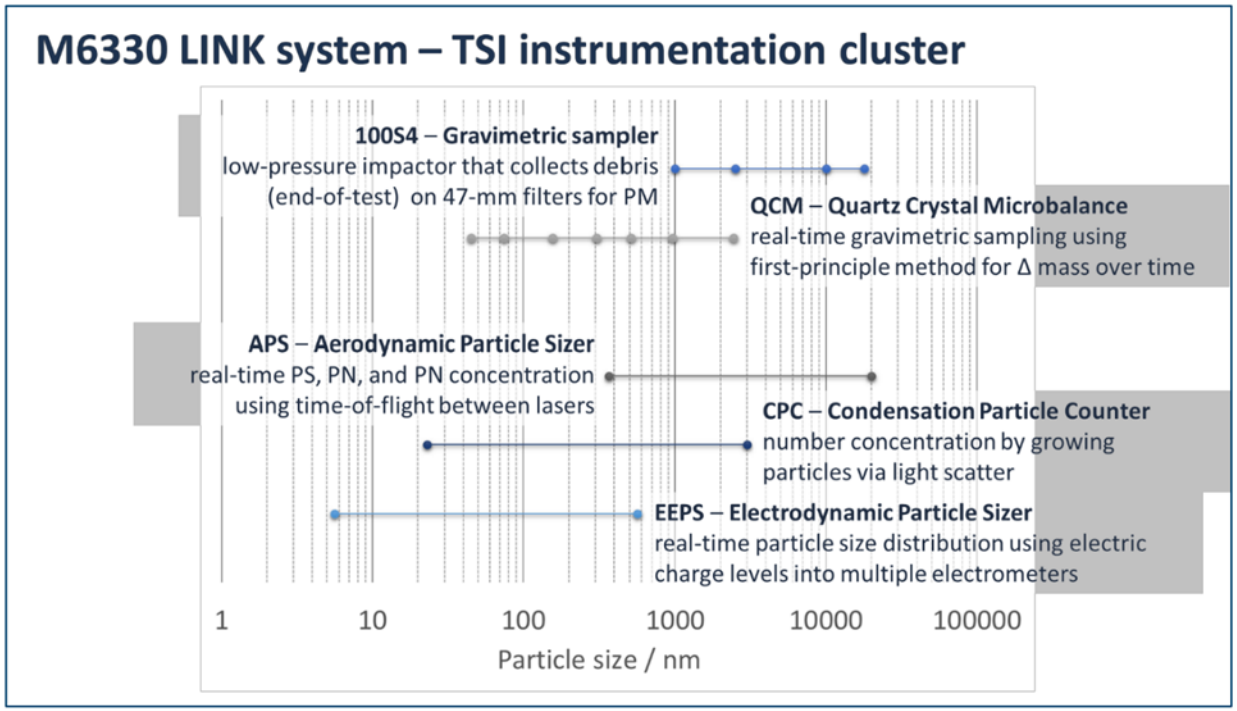

Figure 1-16: TSI Inc. Particulate Sampling Equipment Ranges [31]

For the class 8 truck individual-wheel with disc brakes tests showed total PM_{10} emissions near 50 mg/mi for Drayage vocation cycle which is representative of fully loaded, short distance trip parameters. The same truck with drum brakes also showed PM_{10} emissions at the highest value near 44 mg/mi. The refuse truck PM_{10} emissions occurred the highest around 37 mg/mi for the Refuse Drive cycle. The general trend showed on average the unloaded test produced 50 % less emissions than loaded tests.

Regarding the light duty vehicle testing, the research team used a fully electric vehicle in order to understand how regenerative braking behaves under realistic braking activity whilst being representative of the growing market of electric vehicles. The Tesla test showed higher brake torques between 5 to 10 N-m compared to a Toyota Prius tested by Standard et. al 2020 under the same CBDC cycle. The Tesla produced an estimate of 1.42 mg/mi PM_{10} emission rate which is lower than the Prius, see Figure 1-17. Although, based on filter data collected, the $PM_{2.5}$ emission fraction was instead higher at 70%.

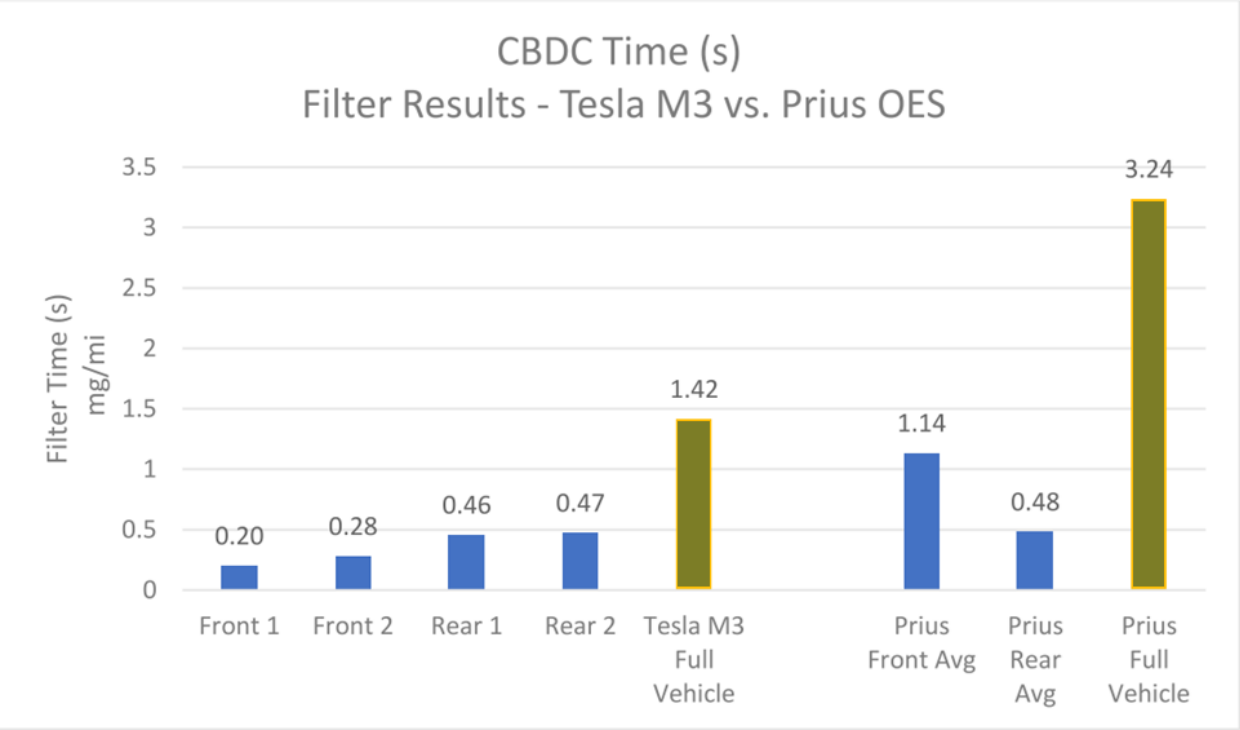

Figure 1-17: Tesla Model 3 PM_{10} Emissions [31]

Stanard et al. [13], conducted a study to measure and analyze particulate matter from light duty vehicles and understand how brake PM emissions are associated with varying operational conditions. The conditions involved parameters such as vehicle speed, deceleration rate, brake temperature, and braking event time. The brake dynamometer shown in Figure 1-15 is the same laboratory setup for this study. Using test track temperature data from six light duty vehicles, air flow rate was adjusted on the dyno chamber to mimic real-world cooling during on and off braking. They developed a driving test cycle (CBDC) with a duration of approximately 4.3 hours that covers medium, high, and low trip average speeds. A mix of metallic versus NAO brake pad were used for the six vehicles selected with consideration of aftermarket replacements. Figure 1-18 shows the total average composed of the two front and two rear single-wheel emission rates based on friction material type. The Toyota Prius is representative of regenerative braking with the lowest emission rates which is comparable to Tesla model 3 results in Koupal et al.[31]. The Ford F-150 was suggested to be a top in the list for large pick up trucks by industry experts and shows highest emissions at 31 mg/mi. In addition, particle size distributions were measured for two size

ranges, 5.6 to 560 nm, and 0.5 to 18 µm. Figure 1-19 shows the normalized particle count in the larger size range for the front axle test of the Camry vehicle. This figure is representative of most test results as all tests showed multimodal behavior. This study also evaluated the accuracy of the regenerative system on the Prius during brake dynamometer testing. Due to similar class weights, the Camry was used as a non-regenerative brake system comparison. With similar deceleration events, the Prius showed to have lower brake pressures overall. Moreover, brake heating rates for the Prius between the test track test and dynamometer test are comparable. This comparison gives insight into emission testing that reflect the changes caused by new technologies, materials, and speed-dependent vehicle usage [33].

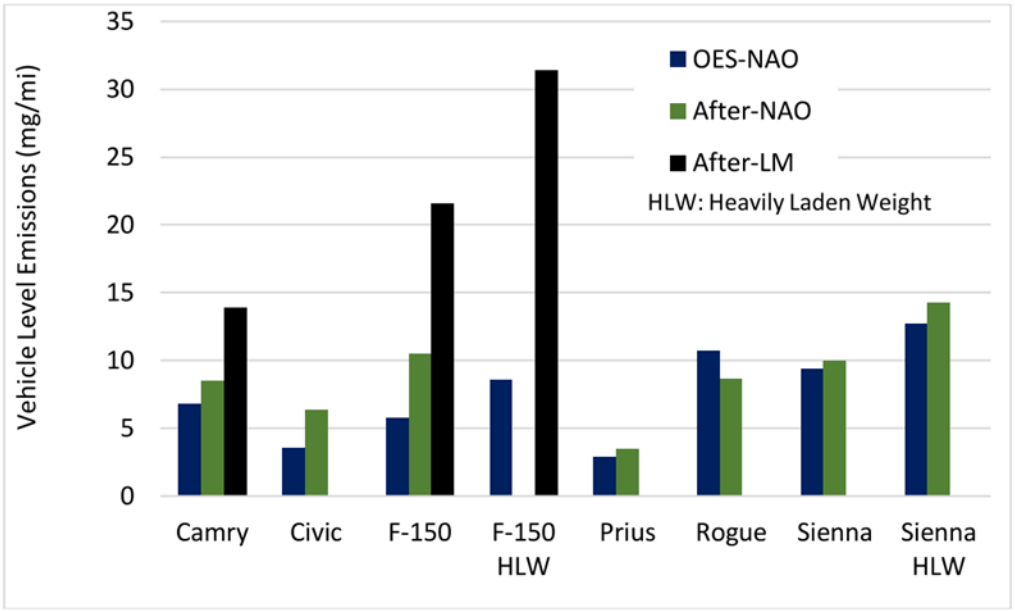

Figure 1-18: Vehicle level braking emissions by model and friction material [13]

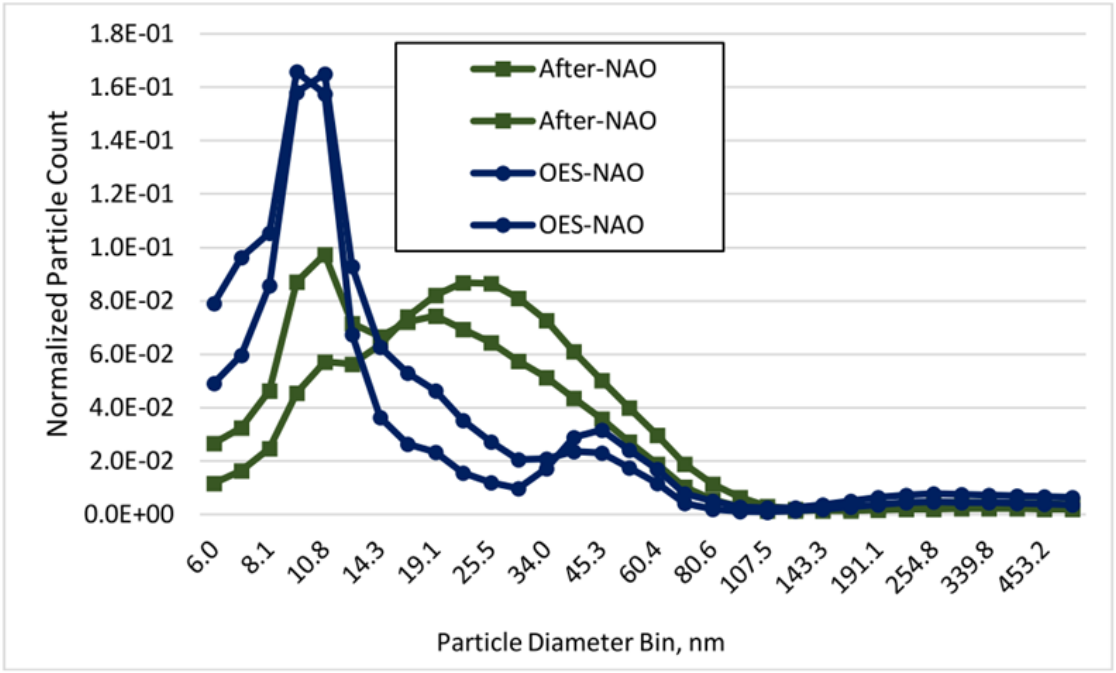

Figure 1-19: Particle size distribution for the Camry Front axle tests [13]

1.2 Tire Wear literature Survey

1.2.1 *Tire wear particle chemical composition*

Tire tread contains natural rubber copolymers such as styreneebutadiene rubber and polyisoprene rubber. Zinc (Zn) is added as zinc oxide and organozinc compounds to facilitate the vulcanization process [29]. Zn is also present within brass coatings that are sometimes applied to the steel wires that reinforce the tire structure [3]. Passenger car tyres in EU are known to contain ~1% zinc oxide, 47% rubber, 16.5% metals, 21.5% carbon black, and 7.5% additives [34]. Similar tire composition are reported by Thorpe and Harrison [3] as shown in Table 1-5.

Table 1-5: Percentage by weight of the main components used in passenger car tire manufacture [3].

Component	Percentage by weight
Rubber hydrocarbons	47–55%

Carbon black	22–30%
Hydrocarbon oils	5%
Resins	5%
Curing agents and activators	3–5%
Other additives — e.g. anti-degradants, accelerators	2–10%

The key tracer components of tire wear include trace metals, n-alkanes, n-alkanoic acids, PAHs, and benzothiazoles [29].

Zn is ~1% by weight in rubber tires and its concentrations in tires are higher than that in brakes [35]. However, Zn cannot be used as the only tracer for tire wear because other sources, such as brake wear and motor oil, also emit Zn [36]. Table 1-6 summarizes metal concentrations observed in passenger car tire tread [3]. Among the PAHs, pyrene, benzo(ghi)perylene, fluoranthene, phenanthrene, and dibenzopyrenes are known to be emitted from tires [29, 37]. Benzothiazole and its derivates are commonly used in rubber products to accelerate the vulcanization of rubbers and to enhance mechanical strength and abrasion resistance [38]. Therefore, benzothiazoles can be used as markers for tire wear, particularly benzothiazole (BT), 2-hydroxy benzothiazole (HOBT), 2-(4-morpholinyl)benzothiazole (24MoBT) and Ncyclohexyl-2-benzothiazolamine (NCBA) [29]. Pierson and Brachaczek [39] used styrene butadiene rubber (SBR) as a marker for tire wear particles.

Table 1-6: Summary of metal concentrations observed in passenger car tire thread (mg/kg) [3].

Metal	Hildemann et al. (1991)	Legret and Pagotto (1999)	Kennedy and Gadd (2003)
Al	470	–	7–129
Ba	370	–	10.4–166
Ca	2000	–	100–1680
Cd	–	2.6	<0.05–0.34
Co	–	–	0.5–4.1
Cr	30	–	<1–2
Cu	490	1.8	<1–2
Fe	4600	–	40–220
K	380	–	110–410
Mg	–	–	<4–37
Mn	100	–	0.8–2.5
Na	–	–	120–530
Ni	50	–	<1–3
Pb	160	6.3	1–5.7
Sb	–	–	<0.2–0.9
Sr	40	–	<0.5–2.6
Ti	560	–	–
Zn	430	10,250	5650–9640

1.2.2 *Tire wear particle size distribution*

Kreider et al. [40] measured tire wear particle distributions using transmission optical microscopy and found that the number distribution was bimodal, with a range from 4 μm to 350 μm with peaks at approximately 5 μm and 25 μm. The volume distribution is unimodal, ranging from 4 μm to 350 μm, with a mode at 100 μm.

Gustafsson et al. [41] sampled particles through a PM_{10} inlet and measured size distributions with an APS and SMPS from a road simulator with different combinations of pavem-6ent, tire, and vehicle speed. While the dense asphalt with granite (Figure 1-21a) have higher concentrations than pavement with quartzite (ABS; Figure 1-21b) for studded tires, the particle size distribution shapes are very similar, with a mass distribution ode at 4-5 μm and a peak at 7-8 μm. The friction tires generate much lower concentrations than the studded tires (Figure 1-21c). For particle number concentration, the studded tire generates unimodal particle distribution with a mode at ~40 nm, while studded particles peaks at < 20 nm. Particle concentration increases with speed. Mathissen et al. [42] measured particle size distribution behind wheel of an instrumented Sport Utility Vehicle equipped with summer tires while driving on a regular asphalt

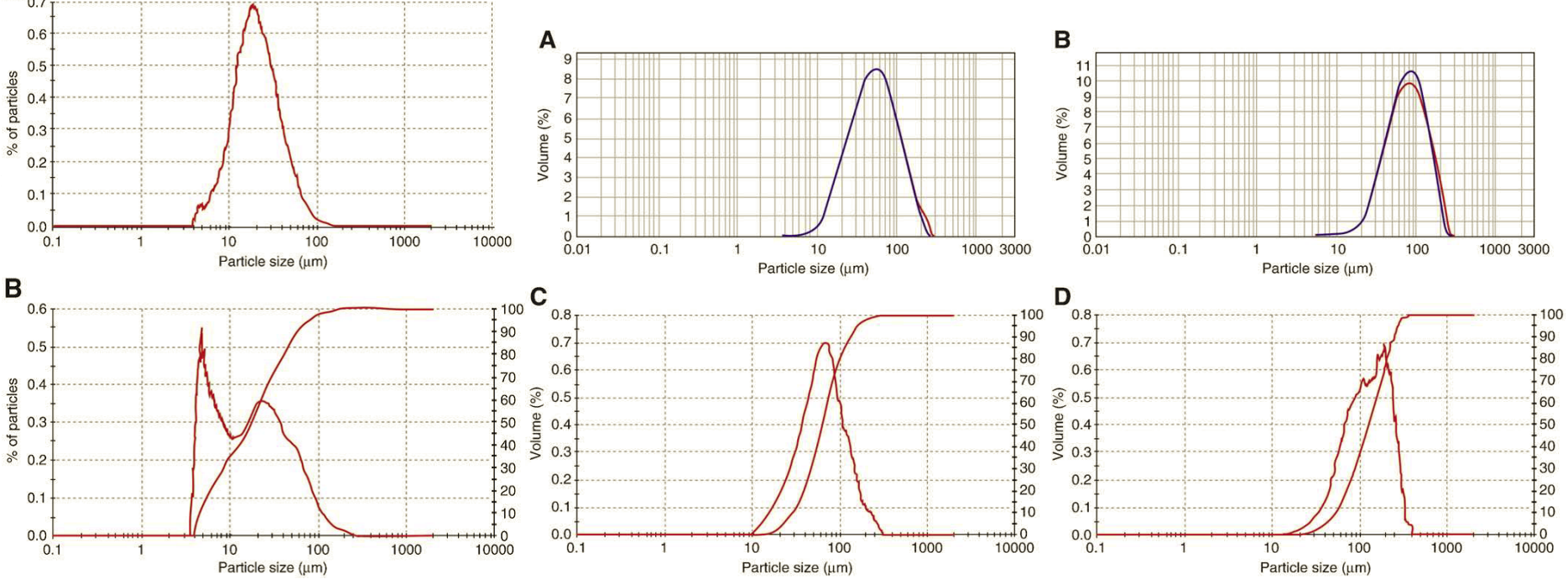

Figure 1-20:Tire wear particle number and volume distribution measured by transmission optical microscopy [40].

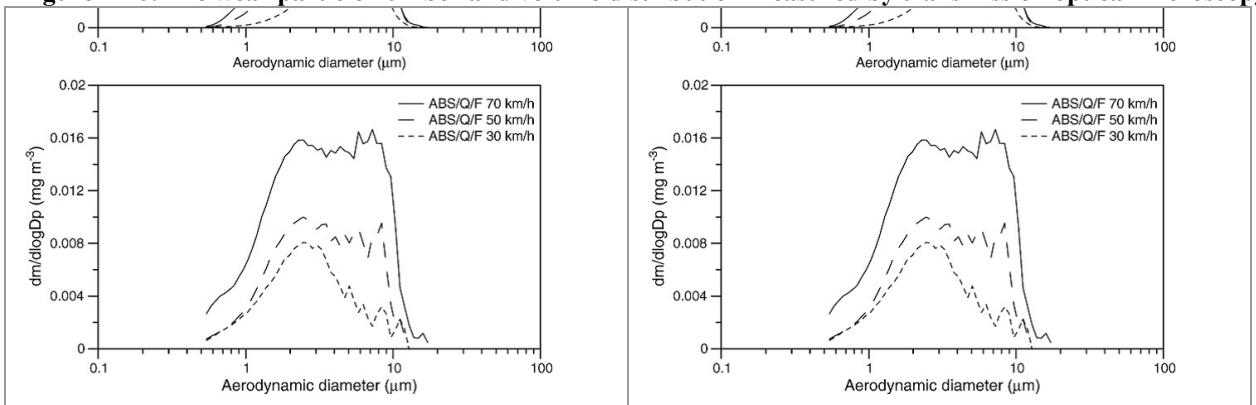

(c) (d)

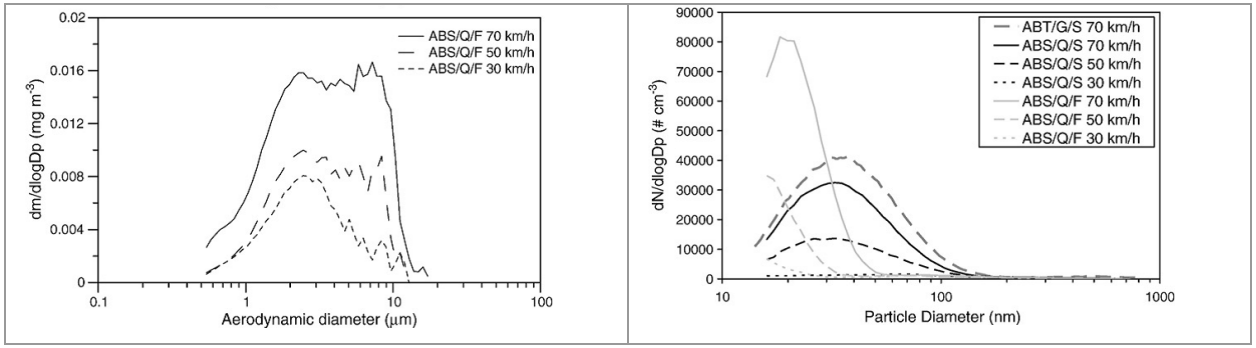

Figure 1-21.Tire wear particle mass size distributions from the road simulator for: (a) dense asphalt concrete (ABT) with granite (G) and studded tire (S); (b) stone mastic asphalt (ABS) with quartzite (Q) and studded tire (S); and (c) stone mastic asphalt (ABS) with quartzite (Q) and friction tire (F) measured by APS. (d) Number size distributions of particles 16–723 nm for the ABS/Q/S and ABS/Q/F at different speeds measured by SMPS [41].

Thorpe and Harrison [3] point out that tire rubber particles tend to carry electrical charges, causing a fraction to be lost when transporting to measurement device. Particle size distribution measurement could be affected by these losses. It should also be noted that only a small fraction (~10% by mass) of tire wear particles become airborne [39]. The larger particles will deposit to the road surface near the point of emission.

1.2.3 *Tire wear particle morphology*

Tire wear particles usually show elongated shape with rough surfaces resulting from abrasion [40, 44, 45]. They may contain incrustations of minerals from the road surface. EDX spectrum shows that they contain Zn. Kreider et al. [40] found that it is difficult to differentiate road dust and tire wear particles based on morphology.

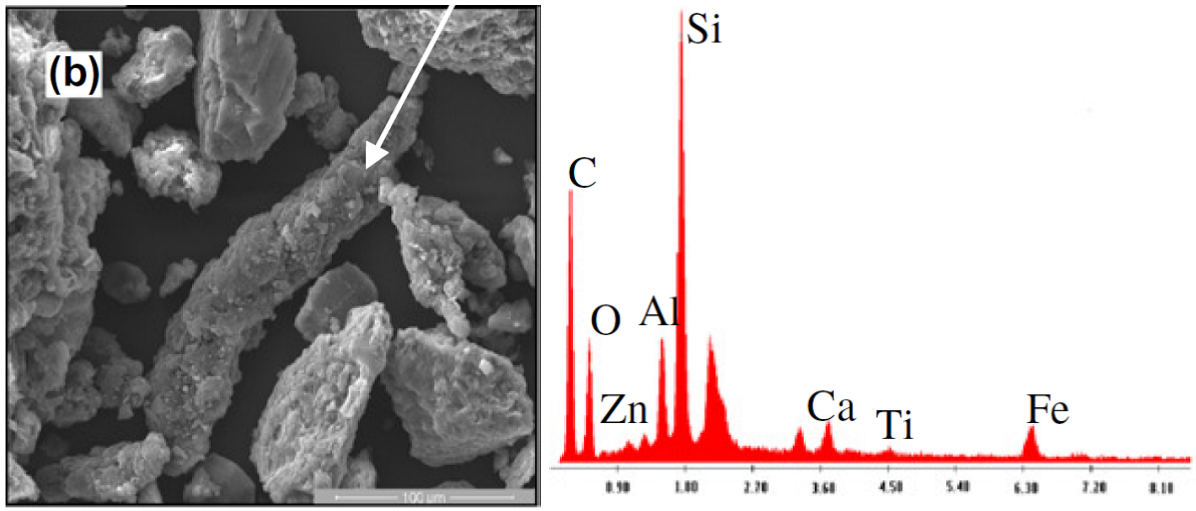

Figure 1-22:SEM image and EDX spectrum of a tire wear particle [44].

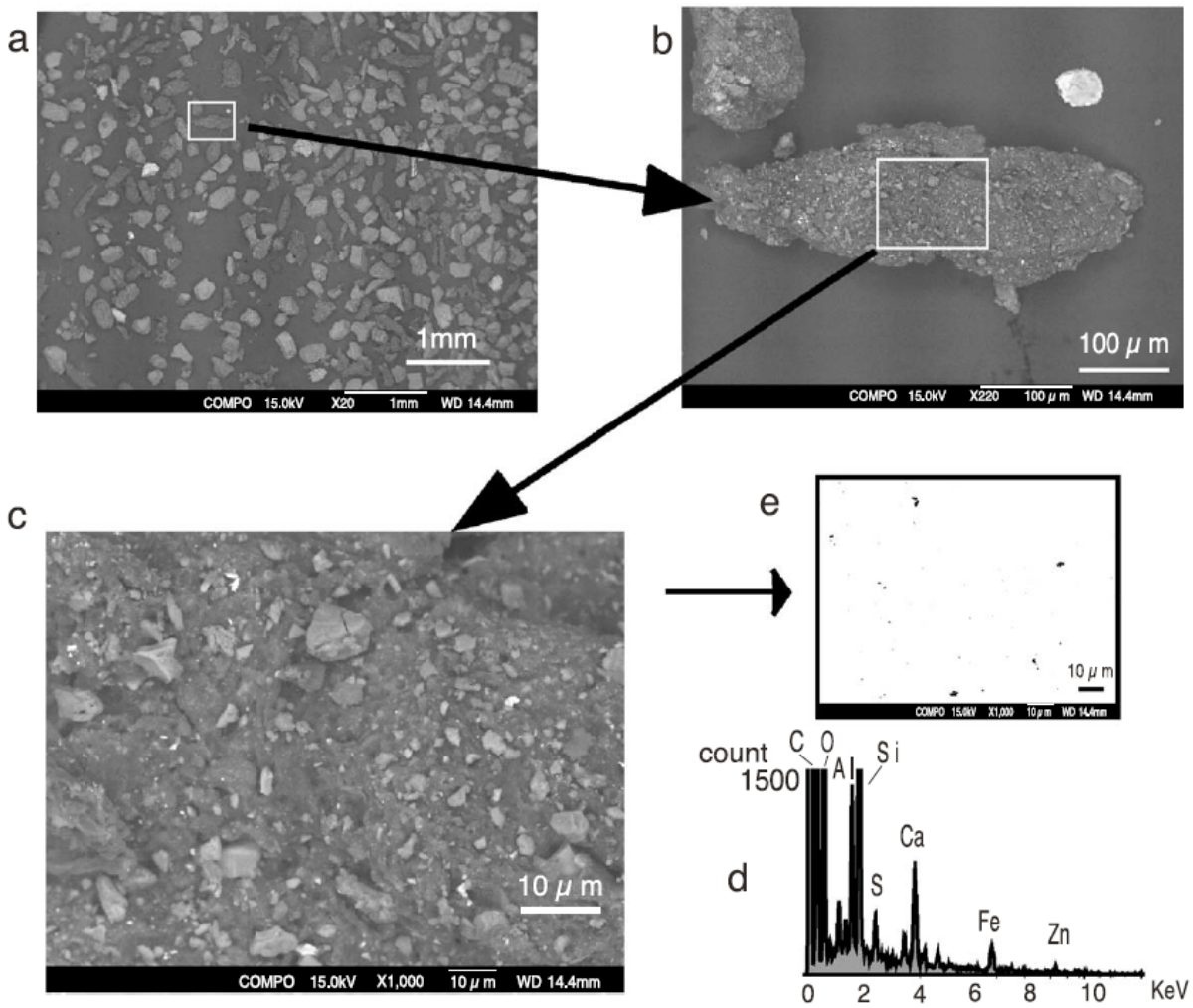

Figure 1-23: Detection method of heavy metal particles from tire dust surface. (a) Selection of tire dust particle in street dust, (b) tire dust particle, (c) analytical area (0.01 mm^2), (d) EDX spectra in the analytical area, (e) high contrast and negative image of the analytical area [45].

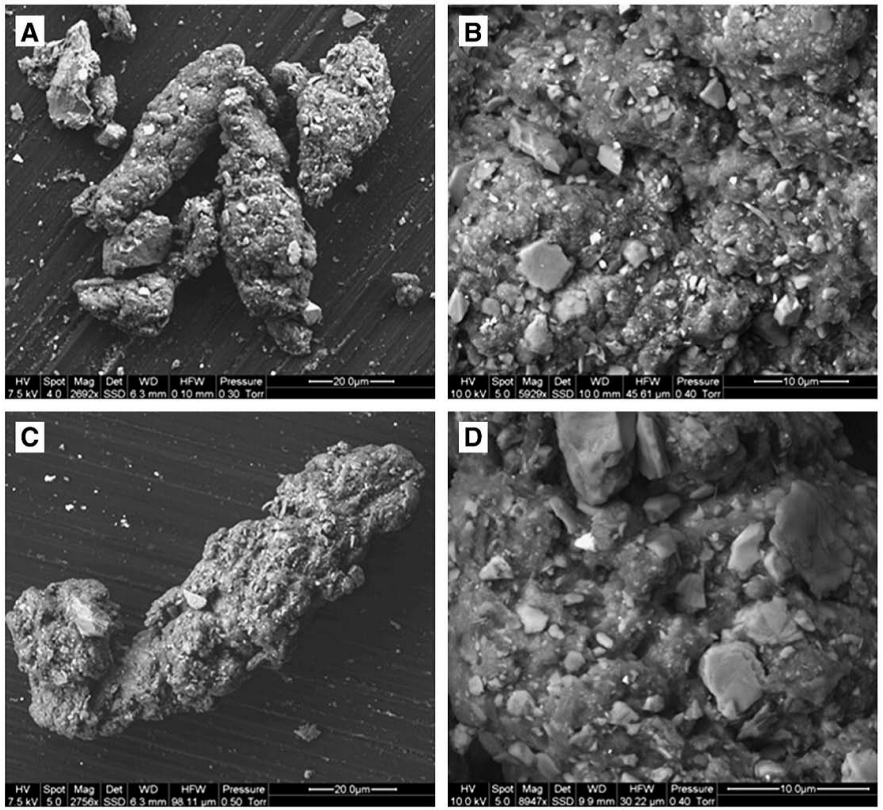

Figure 1-24: Scanning electron microscope images of road dust (A, B) and tire wear particle (C, D). Mineral incrustations are evident in the photos of greater magnification (B, D) [40].

1.2.4 *Tire wear particle emission factor and influencing factors*

Tire wear particles are generated by: (1) the shear force between the tire tread and the road surface or (2) volatilization. Average tire tread wear is 0.006-0.009 g/kg, depending on road, tire, and vehicle conditions [37].

1.2.5 *Tire wear particle measurement methods: On road collection*

Kreider et al. [40] used an aspiration system, Figure 1-25, attached to the rear tire hub of a car and a truck and collected tire wear particles (0.3-100 μm) in two vacuum cleaners. A similar system was used by Mathissen et al. [42] to study particle size distribution under different driving conditions.

(a) 

(b) 

Figure 1-25: Photographs of on-road systems (a)BMW 535i equipped with the collecting device on the rear axle wheel (back view) and (b) MAN10 truck equipped with collecting device on rear axle wheels (side view) [40].

1.2.6 *Tire wear particle measurement methods: Road simulator laboratory collection*

Road simulator laboratories, Figure 1-26, allow collection of tire wear particles from specific tire types without interference from other road surface contaminants such as brake dust, vehicle exhaust, oil/grease, salts, soil, vegetation, etc. The test can mimic a variety of driving conditions by varying speed, temperature, acceleration, braking, and steering. Combinations of road surfaces and tires can be tested [40, 41].

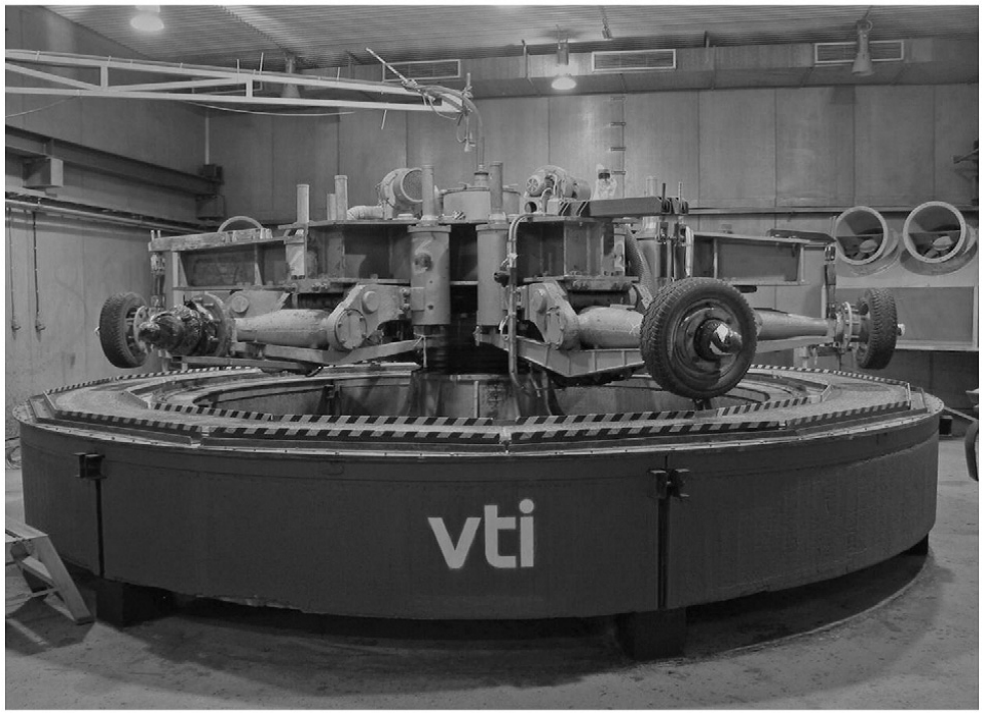

Figure 1-26:The road simulator at the Swedish National Road and Transport Research Institute (VTI) [41].

1.2.7 *Source apportionment studies related specifically to non-exhaust traffic emissions*

Table 1-7: Source apportionment studies review

LOCATION/YEAR/ REFERENCE	MEASUREMENT METHODS	SA METHODS AND MARKERS	MAIN FINDINGS
LONDON, UK, 2007-2011 [46]	Curbside sampling using a MOUDI with 10 size fractions 0.21 – 21.4 µm. PM mass, major ions, and elements quantified at 1–4 day time resolution.	Tracer methods using Zn, Ba, and Si as surrogate for tire wear, brake wear, and road dust.	Coarse particles (0.9–11.5 µm) consisting of 10.7±2.3% tire dust, 55.3±7.0% brake dust, and 38.1±9.7% resuspended road dust. Larger particle sizes found for road dust.

ZÜRICH, SWITZERLAND, BARCELONA AND GIRONA, SPAIN, 2007-2008 [47]	Road dust sampling with a vacuum/resuspension chamber. Particles < 10 μm from 1 m^2 surface area were deposited onto Teflon and quartz-fiber filters.	Positive matrix factorization receptor modeling with 4 factors: Road wear (Al, Ca, Fe), Tailpipe exhausts (OC, EC), Brake wear (Fe, Cu, Sb), and Tire wear (OC, S, Zn)	Road wear is the dominating source in Spanish cities (~60%), but represents only 30% of road dust loading in Zürich where contributions are more equally distributed among the four sources of road dust.
HATFIELD, UK, NOVEMBER-DECEMBER, 2006 [48]	PM_{10} sampling at the entrance and exit of the Hatfield Tunnel using HiVol (quartz-fiber filter) and Partisol (Teflon filter) samplers. PM mass, elements, and PAHs quantified at 12-hour time resolution.	PCA to identify 5 factors: Brake wear (Cu, Sb), Gasoline exhaust (BaP, BeP), Diesel exhaust (pyrene, fluoranthene), Resuspension (Na, Ti, V), and Road surface wear (Ca), to which PM_{10} was apportioned by MLRA.	The 5 sources explained 82% of the PM_{10} mass generated in the tunnel (i.e., increased from the entrance to the exit), including Resuspension (27%), Diesel exhaust (21%), Gasoline exhaust (12%), Brake wear (11%) and Road surface wear (11%).
NICE, FRANCE, 2006-2007 [49]	$PM_{2.5}$ sampling inside the Malraux tunnel using both low and high volume samplers equipped with quartz-fiber filters. Target elements and isotopes were quantified at 48-hour (low volume) and 9-hour (high volume) time resolution.	Positive matrix factorization receptor modeling with 3 factors: Vehicle abrasion (Cu, Zn and Sb), Resuspension (Mn, Fe, As, Rb, Sr), and Fuel combustion (V, Ni, Co). Vehicle abrasion include both brake and tire wear.	The positive matrix factorization model attribute 36%, 43%, and 21% of metals in $PM_{2.5}$ to Vehicle abrasion, Resuspension, and Fuel combustion, respectively. Sn may be a good marker for Vehicle abrasion as >60% of Sn was apportioned to that source.
MONTERREY, MEXICO, JUNE 2009 [50]	$PM_{2.5}$ sampling at the entrance and exit of the tunnel with MiniVol samplers. $PM_{2.5}$ mass, ions, OC, EC, and trace elements were quantified at 2.5-hour resolution for different traffic volumes (97% gasoline).	Four sources resolved by a factor analysis method: Dust resuspension (Si, Ca, K, Fe), Tailpipe exhaust (OC, EC), Petroleum combustion (V, sulfate), and Brake wear (Sb).	The contribution of dust resuspension to $PM_{2.5}$ mass was 20-25%. OC and EC accounted for 71.5% of the total $PM_{2.5}$ mass corrected by dust resuspension. Downhill $PM_{2.5}$ EFs tended to be higher than the uphill ones due to the brake-wear contribution.
PRAGUE, CZECH REPUBLIC, SEPTEMBER 2008 – MAY 2009 [51]	Near-road sampling at a freeway and urban street. Particle number, size distribution, and OC-EC were quantified in real-time, while size-segregated PM were collected with a Berner Low Pressure Impactor for analysis of ions, elements, and total carbon. PM_{10} and gases were also measured.	Tracer methods using Fe, Cu, Mn, and Zn for Brake and Tire wear, Si, Al, and Ca for Resuspension road dust, and K for Long-range transport.	Most of major elements were found in coarse fraction of mass size distribution (1 – 10 μm) and it can be attributed to three different sources: abrasion of different vehicle parts (Fe, Cu, Mn and Zn), resuspension of the road dust (Si, Al, Ca), and long range transport or regional background (Ca

			and K).
CARLSTADT, NJ, USA, DEC. 2007 – FEB. 2008 [52]	Near-road sampler at the New Jersey Turnpike. Size-segregated PM were collected using a MOUDI for analysis of PM mass and trace elements. The sampling duration ranged 72-96 hours.	Cluster analysis to separate coarse (Al, Fe, Sc, Mn, Sb, Cu, etc.) and fine PM elements (Cd, Pb, Ni, V, and Co). Three factors resolved by FA: brake wear + fuel combustion (Pb, sb, Fe, and Cd), fuel combustion (Cu, V, and Cr), and tire abrasion (Zn, Co).	Brake wear, fuel combustion, and tire wear explained ~35%, ~28.3%, and ~23.7% of variations of trace metals, respectively. Weather factors, in particular temperature, wind speed and precipitation, were found to significantly influence the concentrations of trace metals and their size distributions.
RURAL AREAS IN FRANCE, JAPAN, AND UNITED STATES, 2011 [53]	PM_{10} sampled in rural areas using Federal Reference Method. All samples were collected for 24-48 hours and analyzed with pyrolysis-GC/MS method for rubber polymer as surrogates for Tread and Tire and road wear particles (TRWP).	Both Tread and TRWP were used to estimate tire wear fraction in PM_{10}.	TRWP concentrations in the PM_{10} fraction were low with averages ranging from 0.05 to 0.70 µg m^{-3}, representing an average PM_{10} contribution of 0.84%. TRWP concentration in air was associated with traffic load and population density.

2 Task 2: Define study location and season

We proposed to take samples at three locations in Southern California most likely in South Coast Air Basin during winter season. Winter season is known to have reduced contribution from SOA. Shirmohammadi et al. [54] suggested that SOA has the lowest contribution to ambient PM from October to February in Southern California. The sampling location was determined in consultation with CARB scientists. SCAQMD operates 4 near-road monitoring stations (Highway 710, Highway 60, Anaheim, and Ontario) where $PM_{2.5}$, NO_2, wind speed and wind directions are monitored. These data are publicly accessible. We proposed to conduct sampling next to the existing SCAQMD near-road monitoring site at Highway 710 location as one possibility to take advantage of existing infrastructure. This location represents a heavy-duty vehicle corridor and is upwind of environmental justice communities. A second location representing a light duty vehicle corridor with minimum heavy-duty traffic and a third location potentially with an equal mix of light and heavy-duty vehicles would be identified in consultation with CARB scientists. We also looked into daily traffic patterns and braking activities to decide sampling locations as we were interested to take samples at different traffic conditions such as well-flowing, congested, off-ramp, and busy intersections. We proposed to take four-day (two weekdays and two weekend days) sampling at each location to cover weekday and weekend traffic variations. Contributions of background PM will be accounted for in sampling and data analysis.

In case we take measurements at a near highway location (e.g. highway 710), we would measure PM at both upwind and downwind locations (see Figure 2-1a). In case an urban street canyon is chosen for light duty traffic, we plan to use PM_{10} and $PM_{2.5}$ data from a nearby AQMD monitoring station to correct for background PM mass and chemical composition as shown in Figure 2-1b [55]. Prior to sampling, PM concentrations during hours with low traffic (early morning) will be compared between the proposed street canyon site and the AQMD monitoring station to ensure that the concentrations at the AQMD station represent that of the street canyon site.

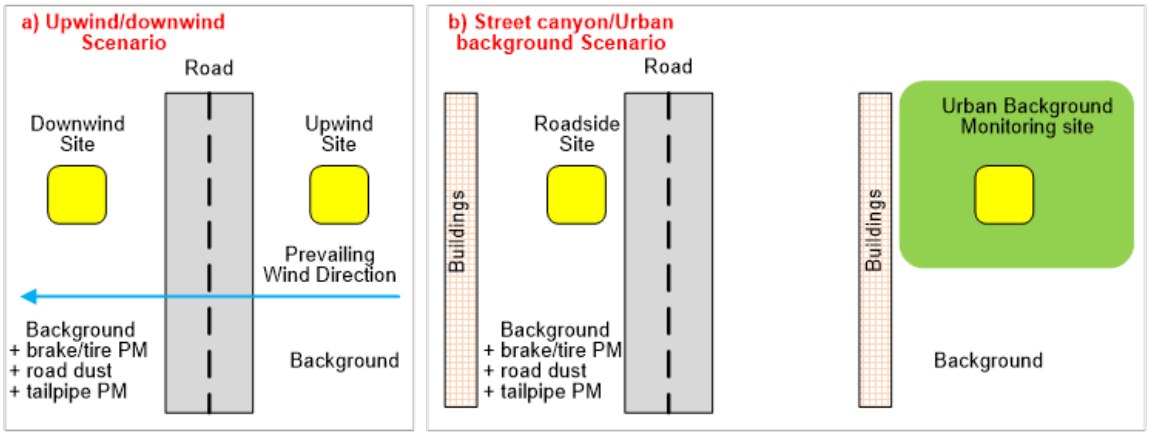

Figure 2-1: Measurement site plan for a) Upwind/Downwind scenario b) Urban street canyon scenario.

2.1 Investigation on candidate measurement sites

During this period, the team focused identifying sites for measurements. SCAQMD currently operates 4 near road measurement sites in So. Cal. We investigated locations and traffic patterns. Near road sites are located in Ontario near the 60 and 10 freeways, Anaheim near the 5, and in Long Beach adjacent to the 710 freeway. Following pages show locations and general aspect of the 4 NR sites.

Last updated: May, 2018

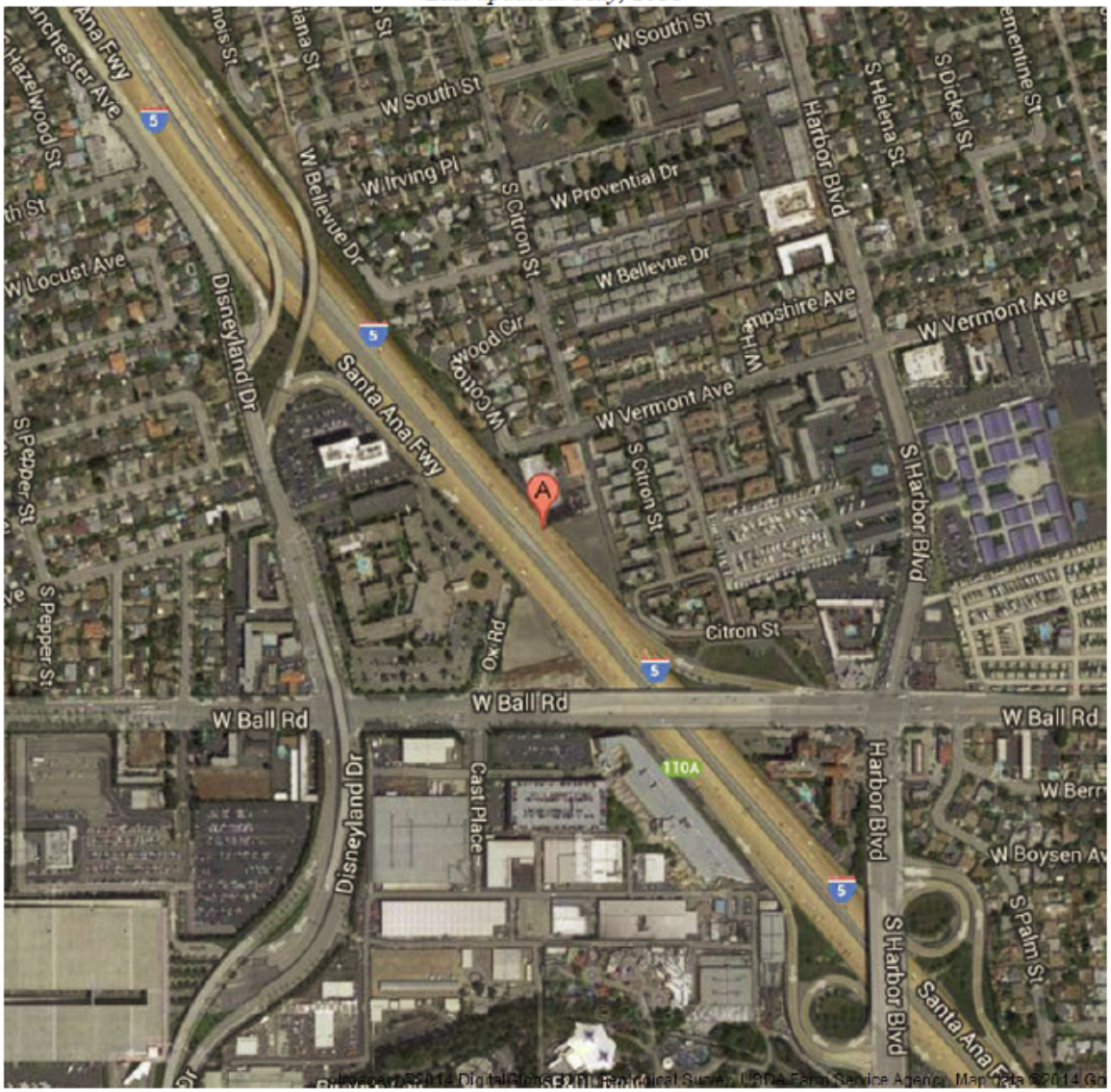

Site Address	County	Air Basin	Latitude	Longitude	Elevation
812 W. Vermont St.	Orange	South Coast	33.819305	-117.918759	43.6m

AIRS Number	ARB Number	Site Start Date	Reporting Agency and Agency Code
060590008	30031	01/14	South Coast AQMD (061)

Figure 2-2: South Coast AQMD Site Survey Report for Anaheim Route 5-Near Road.

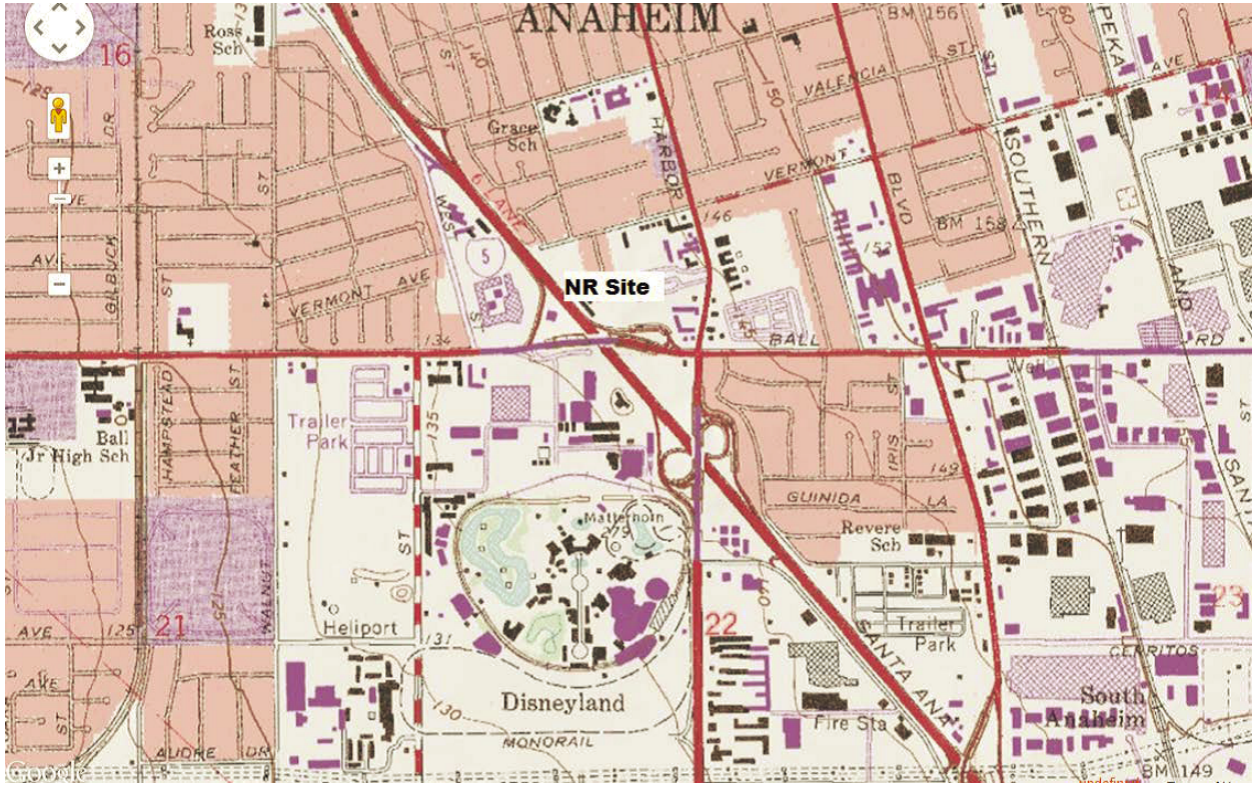

Figure 2-3: Anaheim City Site Survey

Detailed Site Information

Local site name	Anaheim Near Road
AQS ID	060590008
GPS coordinates (decimal degrees)	Latitude: 33.819305 Longitude: -117.918759
Street Address	812 W. Vermont Street, Anaheim, CA 92802
County	Orange
Distance to roadways (meters)	9.0 meters
Traffic count (AADT, year)	695776 (FEAADT)
Groundcover (e.g. asphalt, dirt, sand)	Asphalt
Representative statistical area name (i.e. MSA, CBSA, other)	31080-Los Angeles-Long Beach-Anaheim, MSA

Pollutant, POC	Nitrogen Dioxide, 1	Carbon Monoxide, 1		
Primary / QA Collocated / Other	N/A	N/A		
Parameter code	42602	42101		
Basic monitoring objective(s)	NAAQS	NAAQS		
Site type(s)	Population Exposure	Population Exposure		
Monitor (type)	SLAMS	SLAMS\Near Road		
Network Affiliation	Near Road	Near Road		
Instrument manufacturer and model	Thermo 42i	Thermo 48i-TLE		
Method code	074	554		
FRM/FEM/ARM/ other	FRM	FRM		
Collecting Agency	SCAQMD	SCAQMD		
Analytical Lab (i.e.weigh lab, toxics lab, other)	N/A	N/A		
Reporting Agency	SCAQMD	SCAQMD		
Spatial scale (e.g. micro, neighborhood)	Micro	Micro		
Monitoring start date (MM/DD/YYYY)	01/2014	12/2014		
Current sampling frequency (e.g.1:3, continuous)	1:1	1:1		
Calculated sampling frequency (e.g. 1:3/1:1)	N/A	N/A		
Sampling season (MM/DD-MM/DD)	01/01-12/31	01/01-12/31		
Probe height (meters)	4.5	4.5		
Distance from supporting structure (meters)	2.0	2.0		
Distance from obstructions on roof (meters)	N/A	N/A		

Distance from obstructions not on roof (meters)	N/A	N/A		
Distance from trees (meters)	N/A	N/A		
Distance to furnace or incinerator flue (meters)	N/A	N/A		
Distance between collocated monitors (meters)	N/A	N/A		
Unrestricted airflow (degrees)	360°	360°		
Probe material for reactive gases (e.g. Pyrex, stainless steel, Teflon)	Teflon	Teflon		
Residence time for reactive gases (seconds)	6.8	6.8		
Will there be changes within the next 18 months? (Y/N)	No	No		
Is it suitable for comparison against the annual PM2.5? (Y/N)	N/A	N/A		
Frequency of flow rate verification for manual PM samplers	N/A	N/A		
Frequency of flow rate verification for automated PM analyzers	N/A	N/A		
Frequency of one-point QC check for gaseous instruments	Nightly	Nightly		
Last Annual Performance Evaluation for gaseous parameters (MM/DD/YYYY)	06/02/2016, 06/23/2017	06/02/2016, 06/23/2017		
Last two semi-annual flow rate audits for PM monitors (MM/DD/YYYY, MM/DD/YYYY)	N/A	N/A		

Figure 2-4: Anaheim NR Det

Anaheim-Near Road
Site Photos

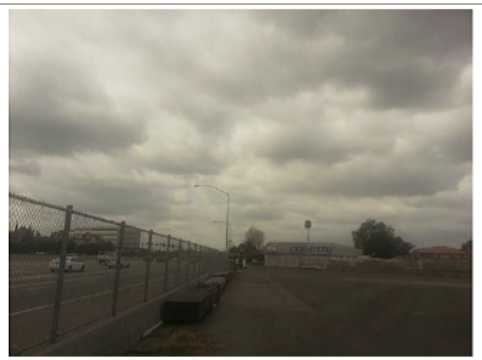

Looking North from the probe.

Looking East from the probe.

Looking South from the probe.

Looking West from the probe.

Figure 2-5: Anaheim Near Road Site Photos

Anaheim-Near Road
Site Photos (Cont.)

Looking at the probe from the North.

Looking at the probe from the East.

Looking at the probe from the South.

Unavailable due to freeway

Looking at the probe from the West.

Figure 2-6: Anaheim Near Road Site Photos (Cont.)

Quality Assurance
Site Survey Report for Long Beach Route 710 Near Road

Last updated: May, 2018

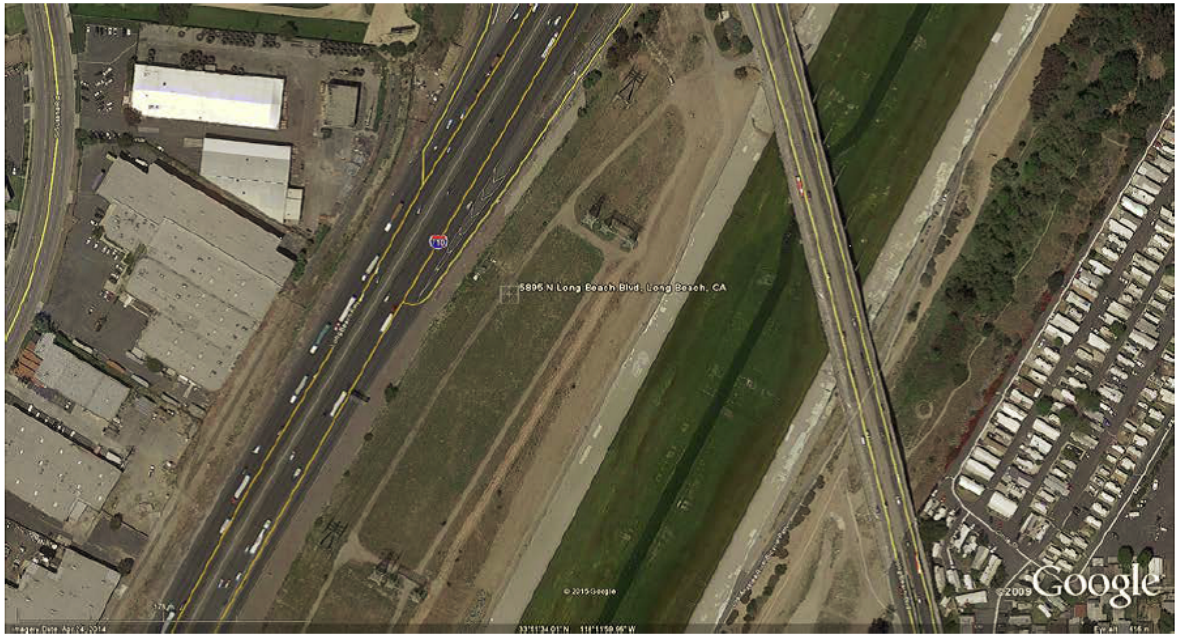

AQS ID	ARB Number	Site Start Date	Reporting Agency and Agency Code
060374008	70032	1/1/2015	South Coast AQMD (061)

Site Address	County	Air Basin	Latitude	Longitude	Elevation
5895 Long Beach Blvd	Los Angeles	South Coast	33° 51' 34"N	118° 12' 01"W	12 m

Figure 2-7: Quality Assurance Site Survey Report for Long Beach Route 710 Near Road

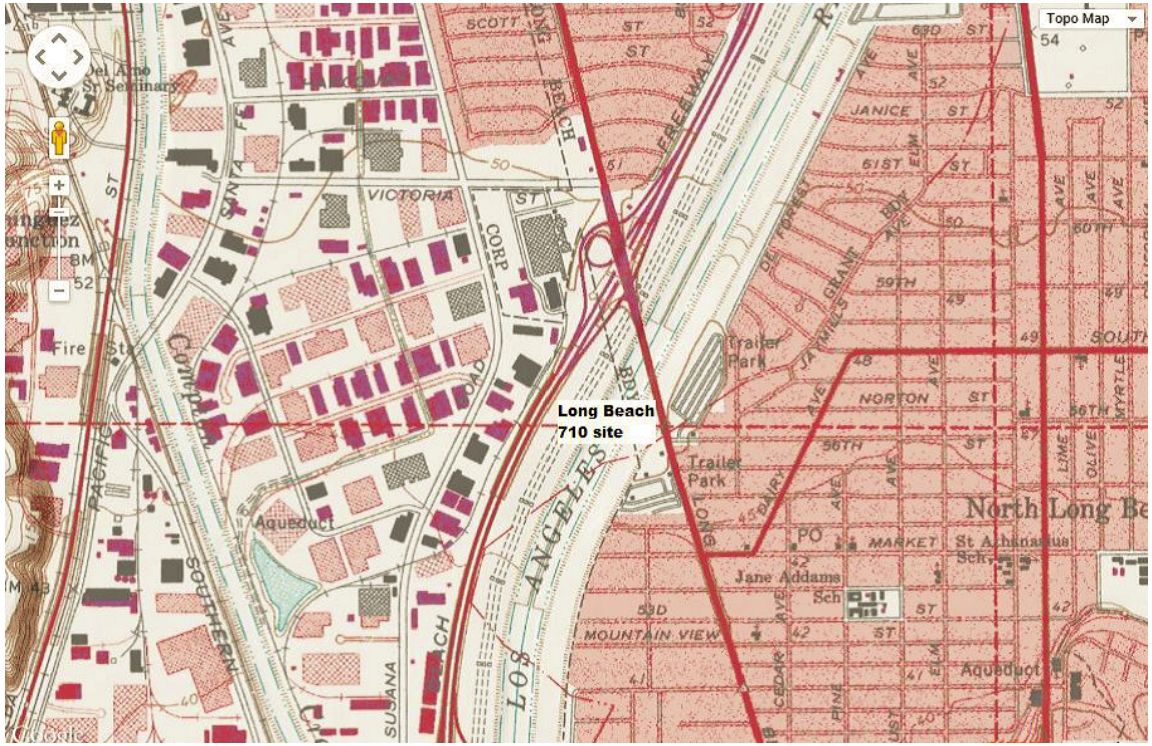

Figure 2-8: Long Beach City Site Survey

Detailed Site Information

Local site name	710 Near Road
AQS ID	060374008
GPS coordinates (decimal degrees)	Latitude: 33° 51' 34"N Longitude: 118° 12' 01"W
Street Address	5895 Long Beach Blvd., Long Beach, CA 90806
County	Los Angeles
Distance to roadways (meters)	20
Traffic count (AADT, year)	192,000 / 2012
Groundcover (e.g. asphalt, dirt, sand)	Concrete/dry vegetation
Representative statistical area name (i.e. MSA, CBSA, other)	31080-Los Angeles-Long Beach-Anaheim MSA

Pollutant, POC	Nitrogen Dioxide, 1	24 Hour PM2.5, 1	Continuous PM2.5, 3	
Primary / QA Collocated / Other	N/A	Primary	Other	
Parameter code	42602	See Table 26	88101	
Basic monitoring objective(s)	NAAQS	NAAQS	NAAQS	
Site type(s)	Population Exposure	Population Exposure	Population Exposure	
Monitor (type)	SLAMS\Near Road	SLAMS\Near Road	SLAMS\Near Road	
Network Affiliation	Near Road	Near Road	Near Road	
Instrument manufacturer and model	Thermo 42i	Partisol 2025i	Thermo 5014	
Method code	074	118,145	183	
FRM/FEM/ARM/ other	FRM	FRM	FEM	
Collecting Agency	SCAQMD	SCAQMD	SCAQMD	
Analytical Lab (i.e.weigh lab, toxics lab, other)	N/A	SCAQMD	N/A	
Reporting Agency	SCAQMD	SCAQMD	SCAQMD	
Spatial scale (e.g. micro, neighborhood)	Micro	Micro	Micro	
Monitoring start date (MM/DD/YYYY)	01/2015	1/2015	1/2016	
Current sampling frequency (e.g.1:3, continuous)	1:1	1:1	1:1	
Calculated sampling frequency (e.g. 1:3/1:1)	N/A	1:1	1:1	
Sampling season (MM/DD-MM/DD)	01/01-12/31	01/01-12/31	01/01-12/31	
Probe height (meters)	4.5	4.5	4.5	
Distance from supporting structure (meters)	2.0	2.0	2.0	
Distance from obstructions on roof (meters)	N/A	N/A	N/A	

Distance from obstructions not on roof (meters)	N/A	N/A	N/A	
Distance from trees (meters)	N/A	N/A	N/A	
Distance to furnace or incinerator flue (meters)	N/A	N/A	N/A	
Distance between collocated monitors (meters)	N/A	N/A	N/A	
Unrestricted airflow (degrees)	360°	360°	360°	
Probe material for reactive gases (e.g. Pyrex, stainless steel, Teflon)	Teflon	NA	NA	
Residence time for reactive gases (seconds)	6.8	NA	NA	
Will there be changes within the next 18 months? (Y/N)	No	No	No	
Is it suitable for comparison against the annual PM2.5? (Y/N)	N/A	Yes	Yes	
Frequency of flow rate verification for manual PM samplers	N/A	Monthly	N/A	
Frequency of flow rate verification for automated PM analyzers	N/A	N/A	Monthly	
Frequency of one-point QC check for gaseous instruments	Nightly	N/A	N/A	
Last Annual Performance Evaluation for gaseous parameters (MM/DD/YYYY)	05/30/2017	N/A	N/A	
Last two semi-annual flow rate audits for PM monitors (MM/DD/YYYY, MM/DD/YYYY)	N/A	05/19/2016, 11/19/2016, 05/20/2017, 11/02/2017	07/27/2016, 12/28/2016, 05/30/2017, 12/14/2017	

Figure 2-9 Long Beach NR Detail

Long Beach Route 710 Near Road
Site Photos

Looking North from the probe.

Looking East from the probe.

Looking South from the probe.

Looking West from the probe.

Figure 2-10: Long Beach Route 710 Near Road Site Photos

Long Beach Route 710 Near Road

Site Photos (Cont.)

Looking at the probe from the North.

Looking at the probe from the East.

Looking at the probe from the South.

Looking at the probe from the West.

Figure 2-11: Long Beach Route 710 Near Road Site Photos (Cont.)

South Coast AQMD
Site Survey Report for Ontario Etiwanda-Near Road

Last updated: May, 2018

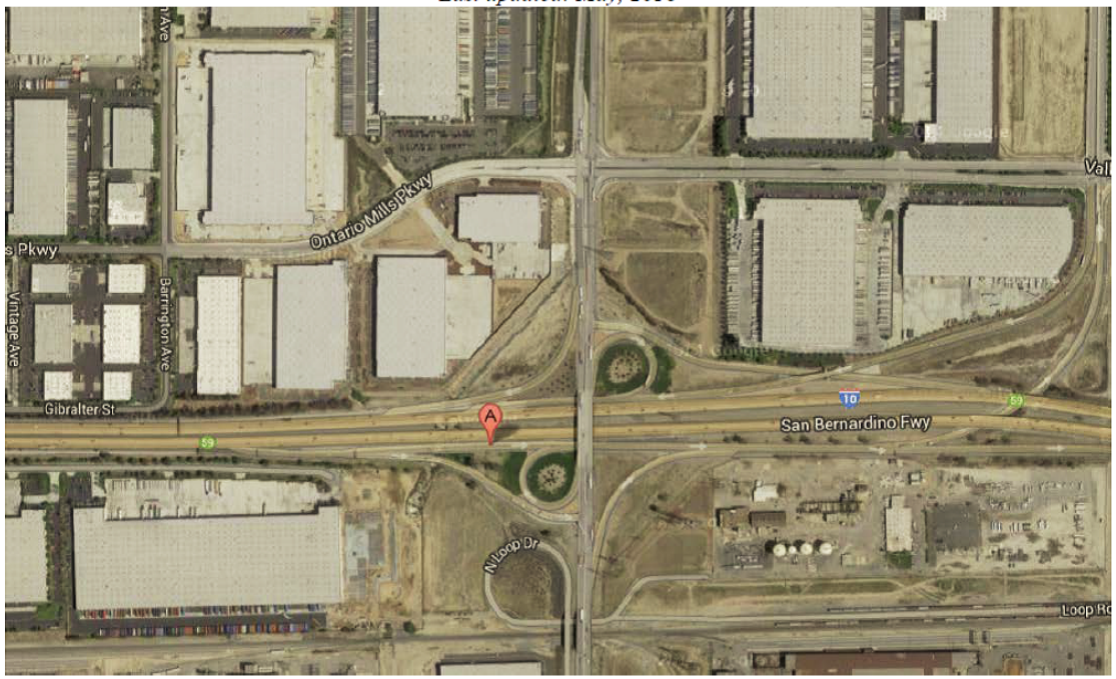

Site Address	County	Air Basin	Latitude	Longitude	Elevation
NW Corner Interstate 10 & Etiwanda Ontario, CA	San Bernardino	South Coast	34° 04' 04"N	117° 31' 33"W	300m

AIRS Number	ARB Number	Site Start Date	Reporting Agency and Agency Code
060710026	36035	07/14	South Coast AQMD (061)

Figure 2-12: South Coast AQMD Site Survey Report for Ontario Etiwanda-Near Road

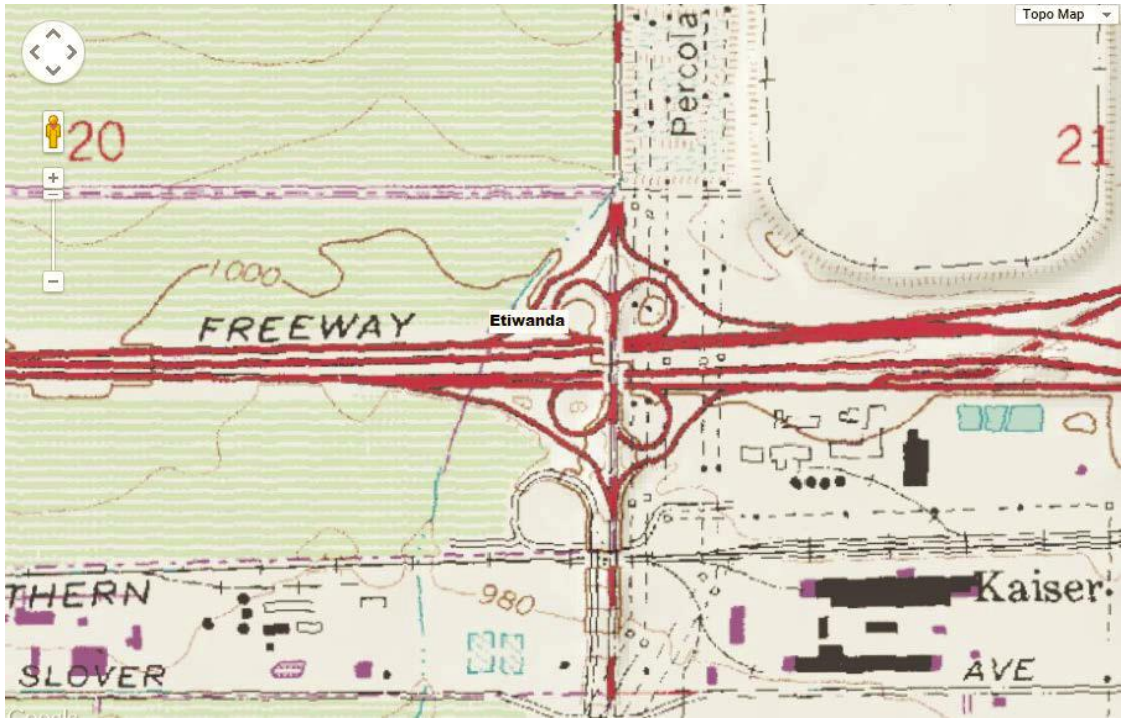

Figure 2-13: Ontario Etiwanda-Near Road Site Survey

Detailed Site Information

Local site name	Ontario Etiwanda – Near Road
AQS ID	060710026
GPS coordinates (decimal degrees)	Latitude: 34° 04' 04"N Longitude: 117° 31' 33"W
Street Address	NW CORNER INTERSTATE 10 & ETIWANDA Ontario, CA
County	San Bernardino
Distance to roadways (meters)	49.0 meters
Traffic count (AADT, year)	646804 (FEAADT)
Groundcover (e.g. asphalt, dirt, sand)	Gravel, sand
Representative statistical area name (i.e. MSA, CBSA, other)	40140-Riverside-San Bernardino-Ontario, MSA

Pollutant, POC	Nitrogen Dioxide, 5	Carbon Monoxide, 1		
Primary / QA Collocated / Other	N/A	N/A		
Parameter code	42603	42101		
Basic monitoring objective(s)	NAAQS	NAAQS		
Site type(s)	Population Exposure	Population Exposure		
Monitor (type)	SLAMS	SLAMS		
Network Affiliation	Near Road	Near Road		
Instrument manufacturer and model	Thermo 42i	Thermo 48i-TLE		
Method code	074	554		
FRM/FEM/ARM/ other	FRM	FRM		
Collecting Agency	SCAQMD	SCAQMD		
Analytical Lab (i.e.weigh lab, toxics lab, other)	N/A	N/A		
Reporting Agency	SCAQMD	SCAQMD		
Spatial scale (e.g. micro, neighborhood)	Microscale	Microscale		
Monitoring start date (MM/DD/YYYY)	07/2014	12/2014		
Current sampling frequency (e.g.1:3, continuous)	1:1	1:1		
Calculated sampling frequency (e.g. 1:3/1:1)	N/A	N/A		
Sampling season (MM/DD-MM/DD)	01/01-12/31	01/01-12/31		
Probe height (meters)	4.2	4.5		
Distance from supporting structure (meters)	2.0	2.0		
Distance from obstructions on roof (meters)	N/A	N/A		

Distance from obstructions not on roof (meters)	N/A	N/A		
Distance from trees (meters)	N/A	N/A		
Distance to furnace or incinerator flue (meters)	N/A	N/A		
Distance between collocated monitors (meters)	N/A	N/A		
Unrestricted airflow (degrees)	360°	360°		
Probe material for reactive gases (e.g. Pyrex, stainless steel, Teflon)	Teflon	Teflon		
Residence time for reactive gases (seconds)	6.8	6.8		
Will there be changes within the next 18 months? (Y/N)	No	No		
Is it suitable for comparison against the annual PM2.5? (Y/N)	N/A	N/A		
Frequency of flow rate verification for manual PM samplers	N/A	N/A		
Frequency of flow rate verification for automated PM analyzers	N/A	N/A		
Frequency of one-point QC check for gaseous instruments	Nightly	Nightly		
Last Annual Performance Evaluation for gaseous parameters (MM/DD/YYYY)	11/09/2016, 12/12/2017	11/09/2016, 12/12/2017		
Last two semi-annual flow rate audits for PM monitors (MM/DD/YYYY, MM/DD/YYYY)	N/A	N/A		

Figure 2-14: Ontario Etiwand

Ontario Etiwanda-Near Road
Site Photos

Looking North from the probe.

Looking East from the probe.

Looking South from the probe.

Looking West from the probe.

Figure 2-15: Ontario Etiwanda-Near Road Site Photos

Ontario Etiwanda-Near Road
Site Photos (Cont.)

Looking at the probe from the North.

Looking at the probe from the East.

Looking at the probe from the South.

Looking at the probe from the West.

Figure 2-16: Ontario Etiwanda-Near Road Site Photos (Cont.)

Quality Assurance
Site Survey Report for Ontario-Route 60 Near Road

Last updated, 2018

AQS ID	ARB Number	Site Start Date	Reporting Agency and Agency Code
060710027	36036	1/1/2015	South Coast AQMD (061)

Site Address	County	Air Basin	Latitude	Longitude	Elevation
2330 S. Castle Harbour	San Bernardino	South Coast	34° 01' 51" N	117° 37' 02" N	258m

Figure 2-17: Quality Assurance Site Survey Report for Ontario-Route 60 Near Road

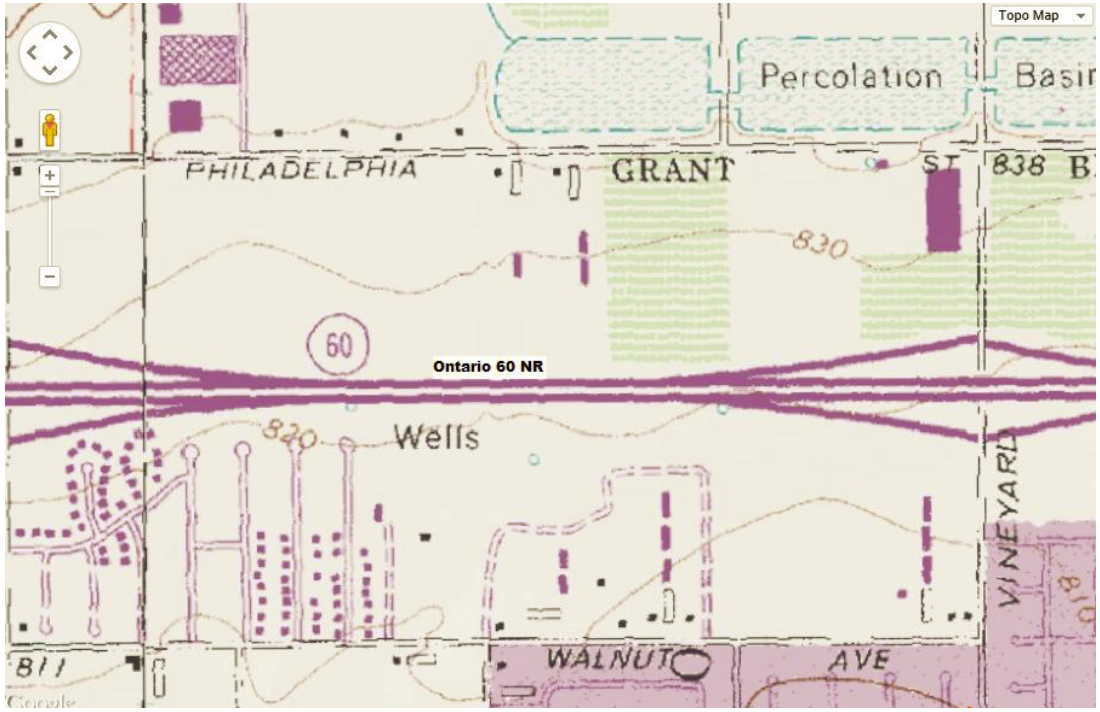

Figure 2-18: Ontario-Route 60 Near Road Site Survey

Detailed Site Information

Local site name	Ontario-Route 60 Near Road
AQS ID	060710027
GPS coordinates (decimal degrees)	Latitude: 34° 01' 51" N Longitude: 117° 37' 02" N
Street Address	2330 S. Castle Harbour Ontario, CA 91761
County	San Bernardino
Distance to roadways (meters)	10 m
Traffic count (AADT, year)	215,000 / 2012
Groundcover (e.g. asphalt, dirt, sand)	Gravel/Grass
Representative statistical area name (i.e. MSA, CBSA, other)	40140-Riverside-San Bernardino-Ontario, CA MSA

Pollutant, POC	Nitrogen Dioxide, 1	24 Hour PM2.5, 1	Continuous PM2.5, 3	
Primary / QA Collocated / Other	N/A	Primary	Other	
Parameter code	42602	See Table 26	88101	
Basic monitoring objective(s)	NAAQS	NAAQS	NAAQS	
Site type(s)	Population Exposure	Population Exposure	Population Exposure	
Monitor (type)	SLAMS	SLAMS	SLAMS	
Network Affiliation	Near Road	Near Road	Near Road	
Instrument manufacturer and model	Horiba APNA 370 NOx	Thermo 2025i	Thermo 5014	
Method code	157	118,145	183	
FRM/FEM/ARM/ other	FRM	FRM	FEM	
Collecting Agency	SCAQMD	SCAQMD	SCAQMD	
Analytical Lab (i.e.weigh lab, toxics lab, other)	N/A	SCAQMD	N/A	
Reporting Agency	SCAQMD	SCAQMD	SCAQMD	
Spatial scale (e.g. micro, neighborhood)	Micro	Micro	Micro	
Monitoring start date (MM/DD/YYYY)	01/2015	1/2015	1/2015	
Current sampling frequency (e.g.1:3, continuous)	1:1	1:1	1:1	
Calculated sampling frequency (e.g. 1:3/1:1)	N/A	1:1	1:1	
Sampling season (MM/DD-MM/DD)	01/01-12/31	01/01-12/31	01/01-12/31	
Probe height (meters)	4.5	4.5	4.5	
Distance from supporting structure (meters)	2.0	2.0	2.0	
Distance from obstructions on roof (meters)	N/A	N/A	N/A	

Distance from obstructions not on roof (meters)	N/A	N/A	N/A	
Distance from trees (meters)	N/A	N/A	N/A	
Distance to furnace or incinerator flue (meters)	N/A	N/A	N/A	
Distance between collocated monitors (meters)	N/A	N/A	N/A	
Unrestricted airflow (degrees)	360°	360°	360°	
Probe material for reactive gases (e.g. Pyrex, stainless steel, Teflon)	Teflon	NA	NA	
Residence time for reactive gases (seconds)	6.8	NA	NA	
Will there be changes within the next 18 months? (Y/N)	No	No	No	
Is it suitable for comparison against the annual PM2.5? (Y/N)	N/A	Yes	Yes	
Frequency of flow rate verification for manual PM samplers	N/A	Monthly	N/A	
Frequency of flow rate verification for automated PM analyzers	N/A	N/A	Monthly	
Frequency of one-point QC check for gaseous instruments	Nightly	N/A	N/A	
Last Annual Performance Evaluation for gaseous parameters (MM/DD/YYYY)	11/04/2016	N/A	N/A	
Last two semi-annual flow rate audits for PM monitors (MM/DD/YYYY, MM/DD/YYYY)	11/16/2017	04/21/2016, 11/10/2016, 05/16/2017, 10/20/2017	07/26/2016, 12/28/2016, 06/01/2017, 12/15/2017	

Figure 2-19: Ontario-Route 60 Nea

Ontario-Route 60 Near Road
Site Photos

Looking North from the probe.

Looking East from the probe.

Looking South from the probe.

Looking West from the probe.

Figure 2-20: Ontario-Route 60 Near Road site photos

Ontario-Route 60 Near Road
Site Photos (Cont.)

Looking at the probe from the North.

Looking at the probe from the East.

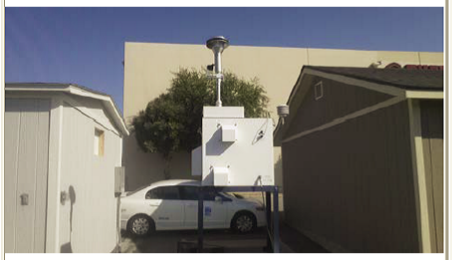

Looking at the probe from the South.

Looking at the probe from the West.

Figure 2-21: Ontario-Route 60 Near Road site photos (Cont.)

2.2 VMT at four AQMD NR sites for Jan 2018 and July 2018

Figure 2-22 shows VMT (Veh-Miles), Truck-VMT (Veh-Miles), and Truck VMT/VMT (%) at the 4 NR sites for Jan 2018 and July 2018. Figures on the left are for Jan and on the right are for July. Traffic patterns are repeatable regardless or measurement period except at the highway 710 location. Highway 710 had construction in Jan 2018 and so the data in July is more representative.

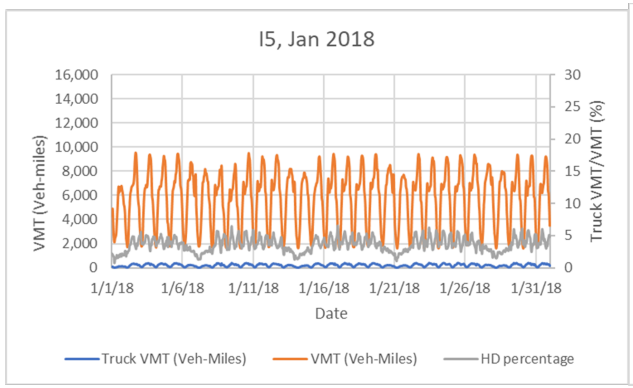
I5, Jan 2018
VMT (Veh-miles)
Truck VMT/VMT (%)
Date
Truck VMT (Veh-Miles)
VMT (Veh-Miles)
HD percentage

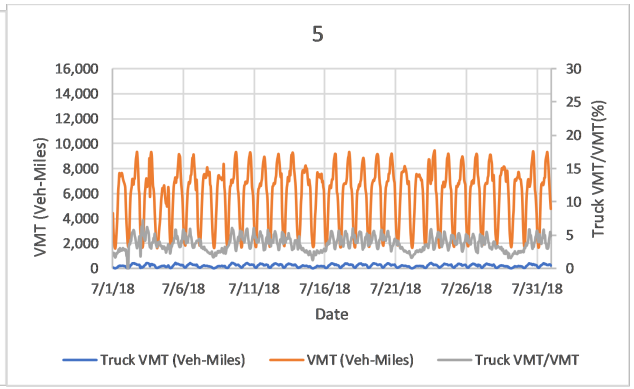
5
VMT (Veh-Miles)
Truck VMT/VMT(%)
Date
Truck VMT (Veh-Miles)
VMT (Veh-Miles)
Truck VMT/VMT

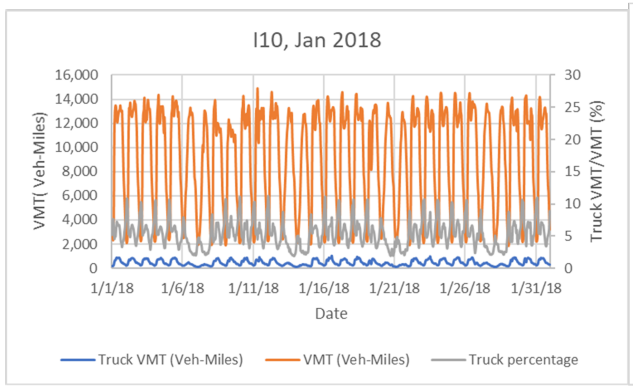
I10, Jan 2018
VMT(Veh-Miles)
Truck VMT/VMT (%)
Date
Truck VMT (Veh-Miles)
VMT (Veh-Miles)
Truck percentage

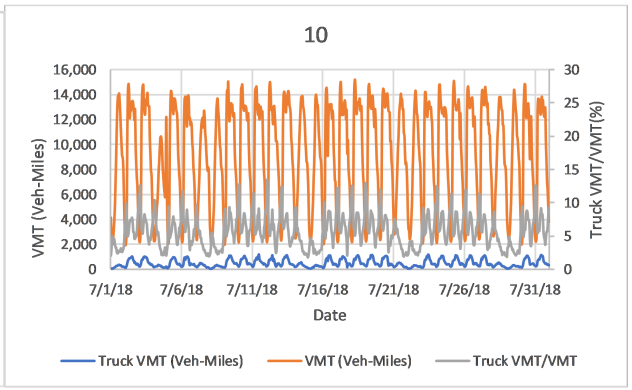
10
VMT (Veh-Miles)
Truck VMT/VMT(%)
Date
Truck VMT (Veh-Miles)
VMT (Veh-Miles)
Truck VMT/VMT

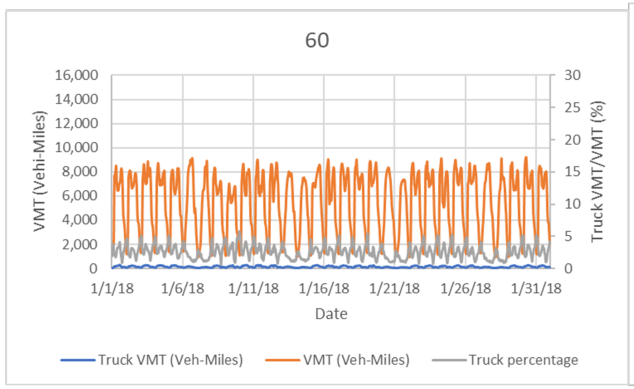
60
VMT (Vehi-Miles)
Truck VMT/VMT (%)
Date
Truck VMT (Veh-Miles)
VMT (Veh-Miles)
Truck percentage

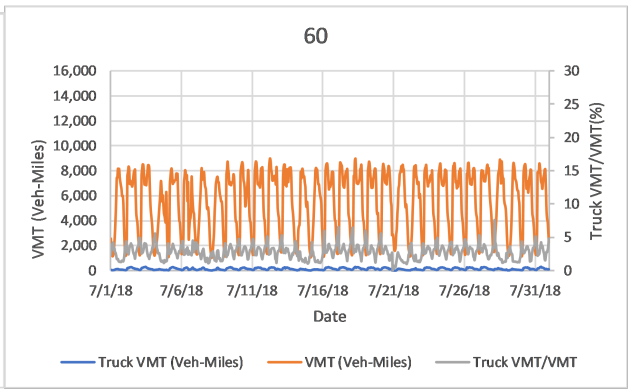
60
VMT (Veh-Miles)
Truck VMT/VMT(%)
Date
Truck VMT (Veh-Miles)
VMT (Veh-Miles)
Truck VMT/VMT

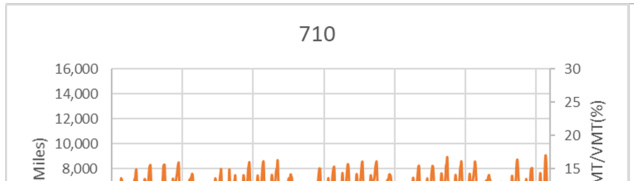
710

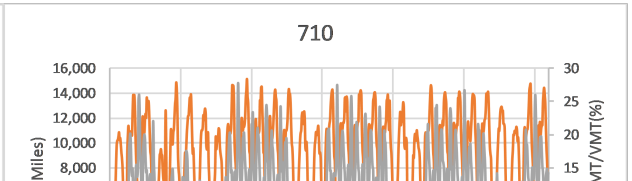
710

Figure 2-22: VMT analysis at the 4 NR sites.

Highway 10 and 710 show the highest VMTs while I5 and SRT60 shows the lowest VMTs. Highway 710 has the highest truck percentage while SRT60 shows the lowest truck percentage.

The traffic flow (vehicle-mile-traveled, VMT) itself may not be an effective indicator for the traffic condition (i.e., congested or not). Therefore, we output the Q (equivalently average speed) values and TTI for July 2018 at the 4 NR sites as shown in Figure 2-22. The higher Q value is, the faster the traffic flow on average. If TTI is high, then the road segment is under congestion. For some TTI higher than 2, there might be some accident on that specific date and time. Highway 710 and 60 showed most congested conditions followed by I10 and I5.

We first identified 3 candidate sites as following:

- AQMD NR site at 710: Heavy-duty corridor, most congested
- AQMD NR site at SRT60: Light-duty corridor, 2nd most congested
- AQMD NR site at 10: Mixed traffic corridor, 3rd most congested

Then visited local business and owners of empty lots or building owners to get access for upwind measurement locations. After lots of effort we could not get permission from owners of the land or building in SRT60 and I10 locations. In addition SRT60 location is expected to have lots of road repair planned in 2020 winter. As such the team decided in consultation with CARB scientists the following two locations for longer measurement period. In addition, co-PI (Dr. Antony Chen) asserted that it is a lot more advantageous to have one-week measurement at each measurement location than 4 day measurement at each location because more sample numbers will ensure better constrain the results for the source apportionment analysis.

2.3 Wind Data

Historic wind data were obtained from AQMD and analyzed to predict wind pattern during sampling period (Jan and Feb of 2020) of this study. Wind direction changes around 10 am and the downwind location (the AQMD NR site) is receiving wind from upwind location (across highway 5) at the Anaheim location as shown in Figure 2-23 and Figure 2-25 over two previous year periods (2018 and 2019 Jan). Wind speed peaked near midday as shown in Figure 2-24 and Figure 2-26.

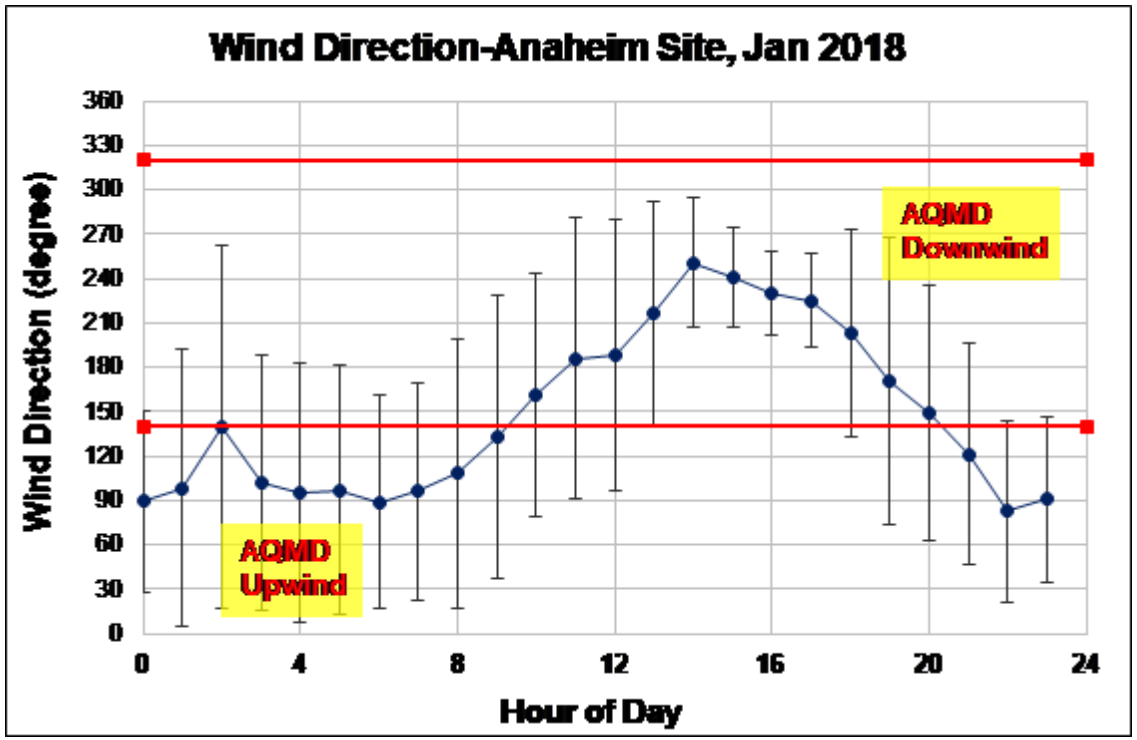

Figure 2-23: Wind Direction – Anaheim Site January 2018

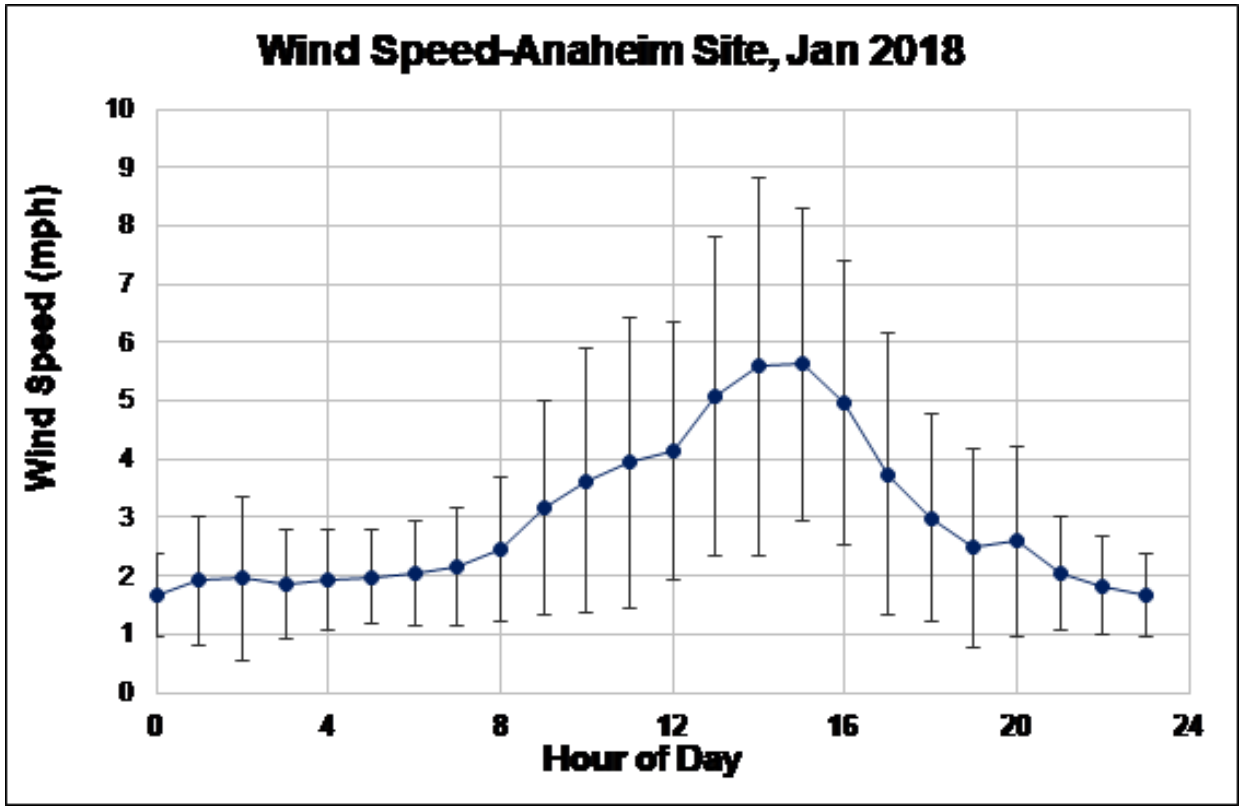

Figure 2-24: Wind Speed – Anaheim Site January 2018

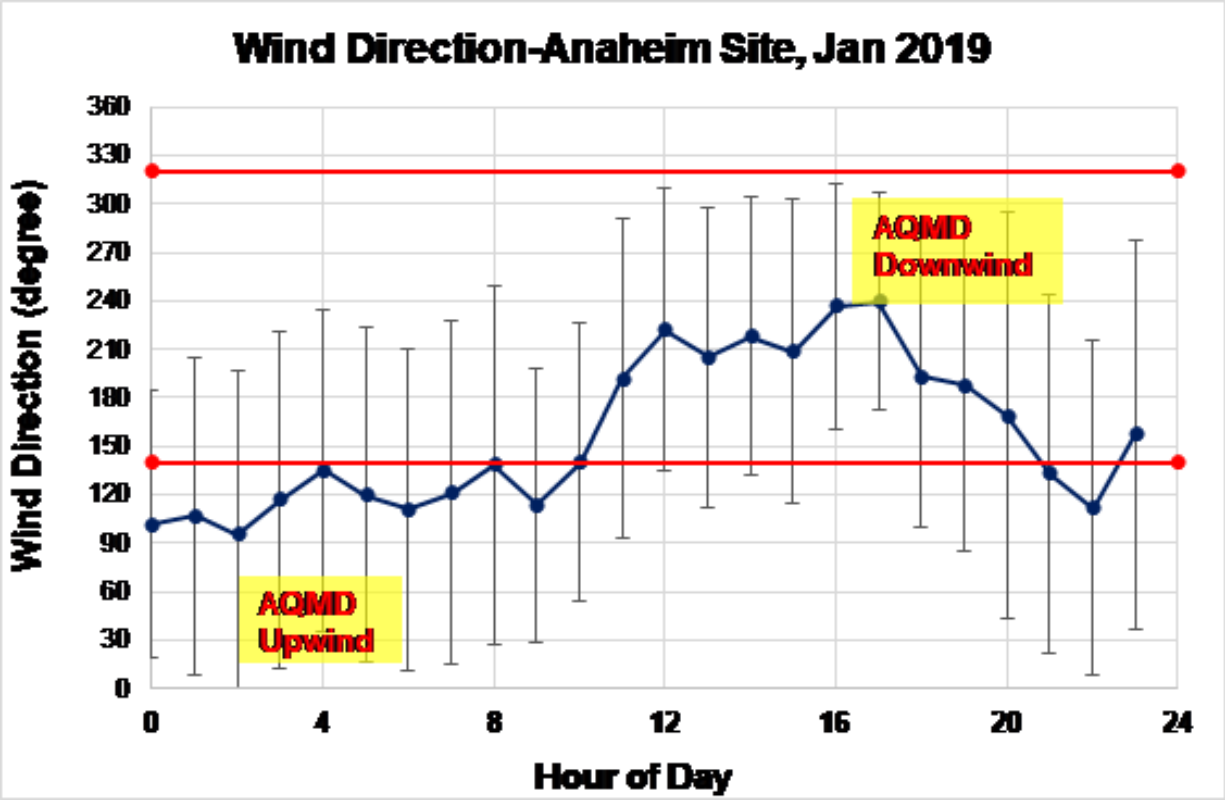

Figure 2-25: Wind Direction – Anaheim Site January 2019

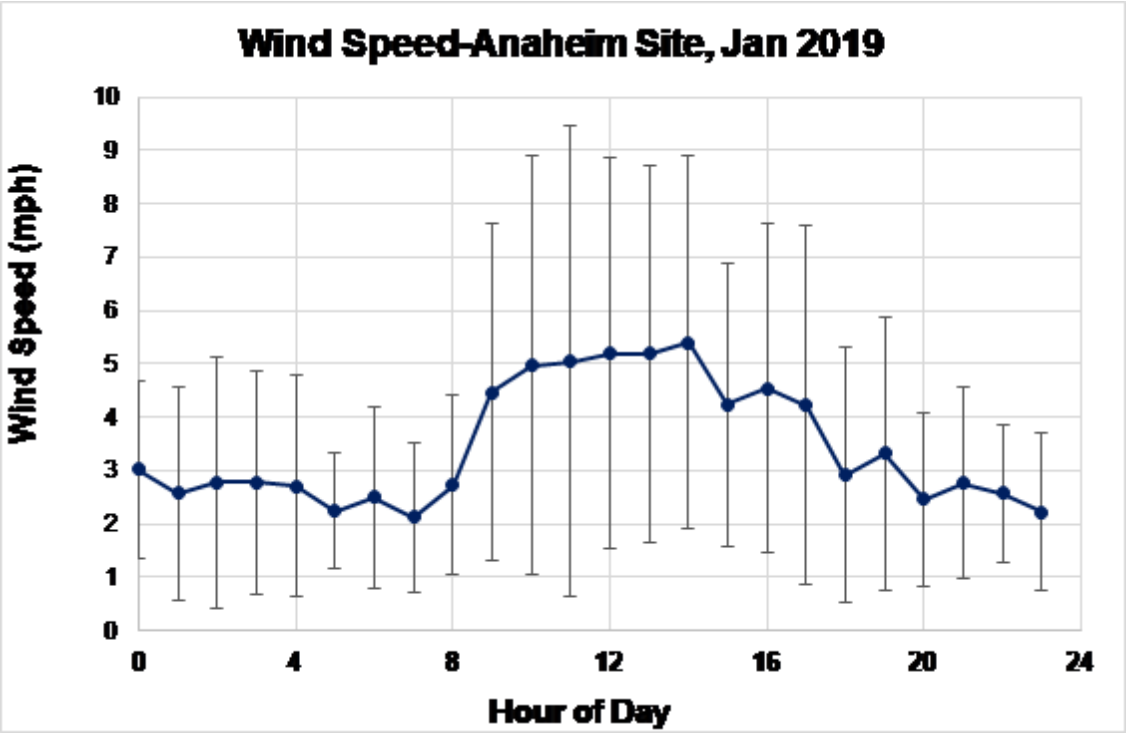

Figure 2-26: Wind Speed – Anaheim Site January 2019

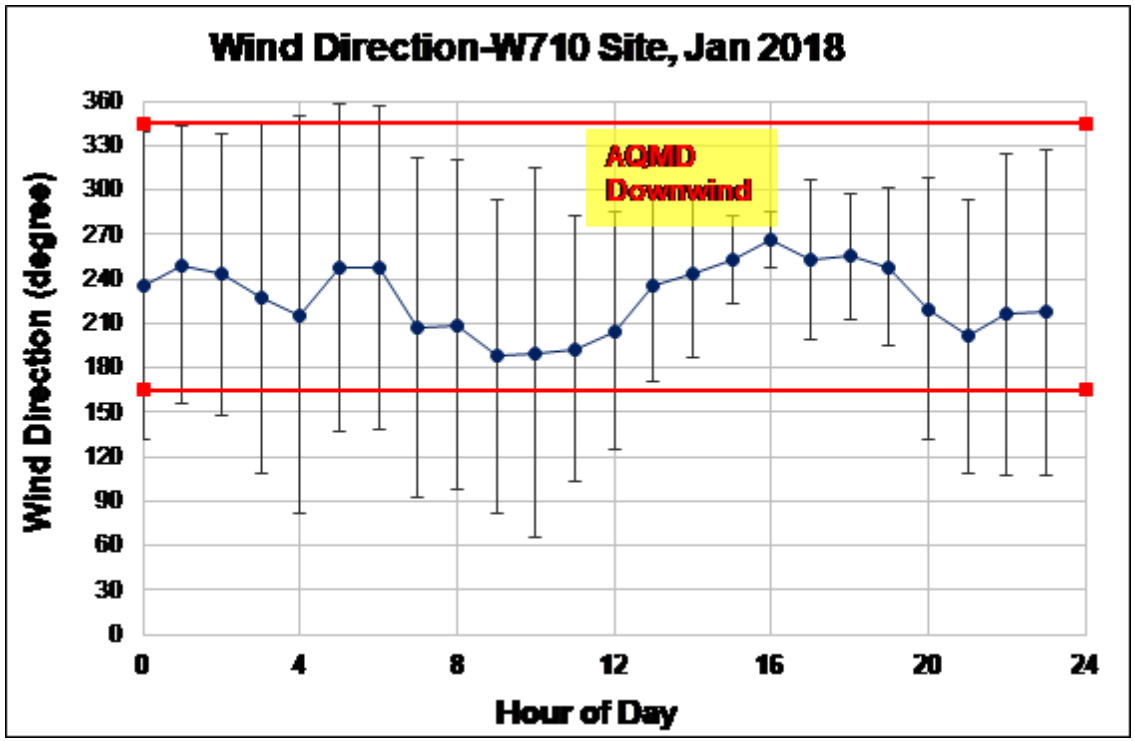

Figure 2-27: Wind Direction – W710 Site January 2018

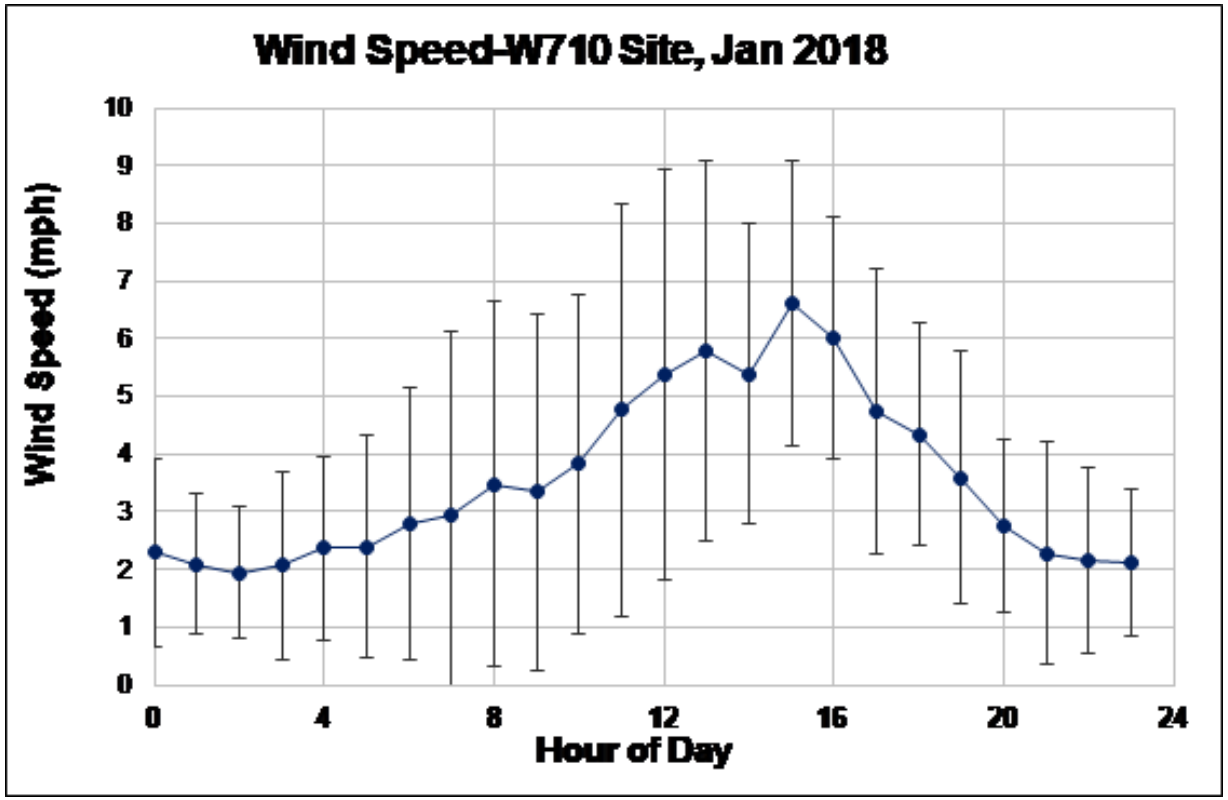

Figure 2-28: Wind Speed W710 Site January 2018

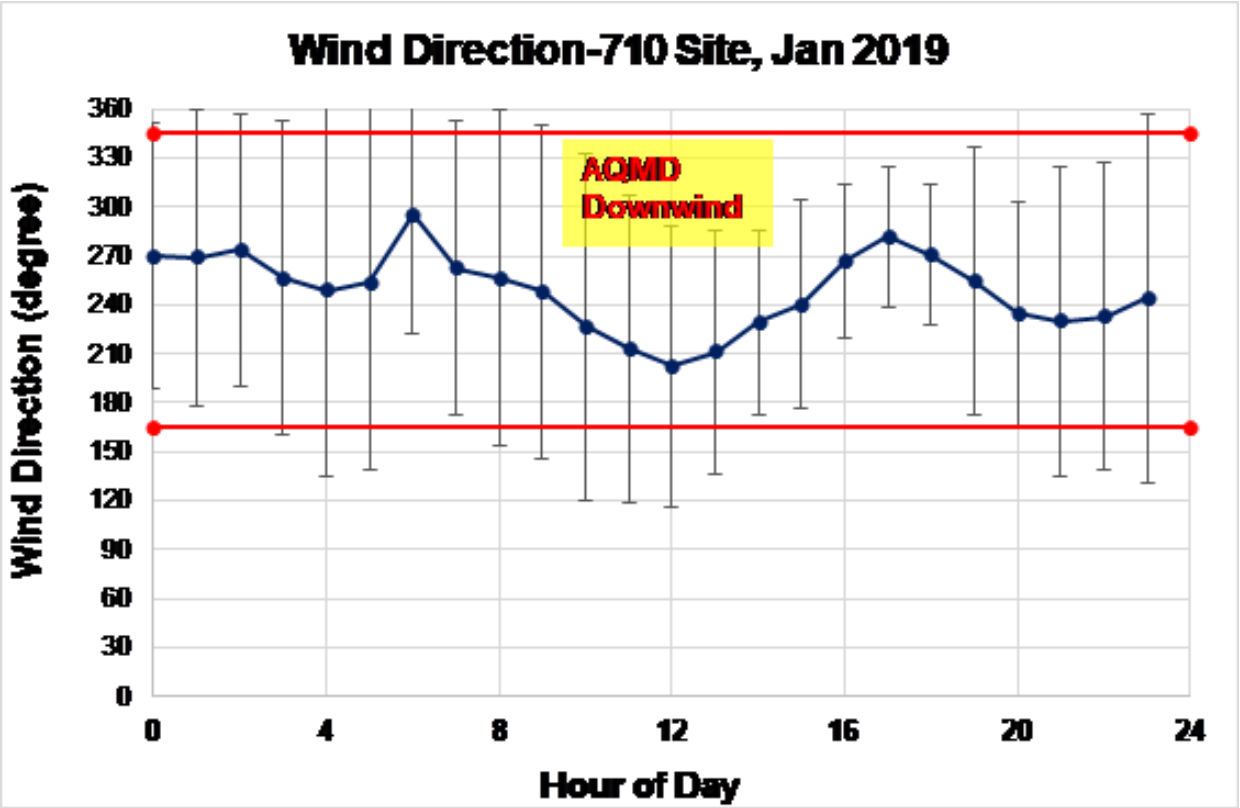

Figure 2-29: Wind Direction W710 Site January 2019

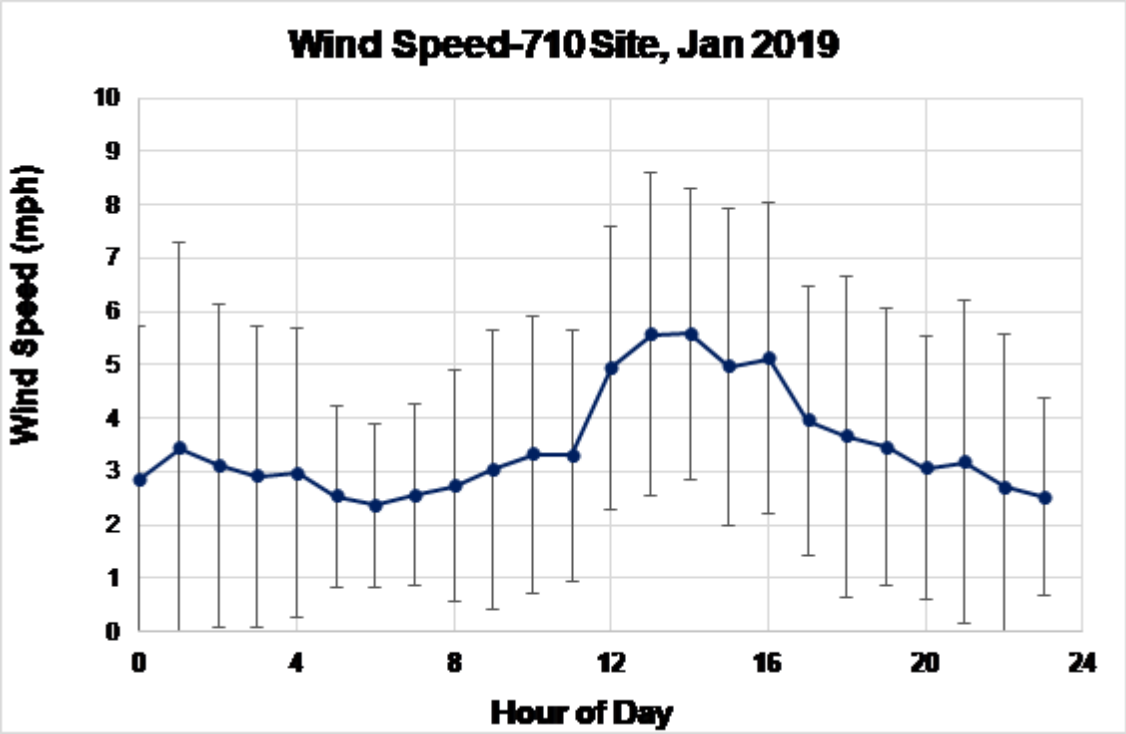

Figure 2-30: Wind Speed W710 site January 2019

Wind data in Long Beach location showed the downwind location remains the same throughout the day while the wind speed peaked in the midday as shown in Figure 2-27 to Figure 2-30. These analyses ensured that the designation of upwind and downwind sites at two measurement locations are appropriate based on previous two years' wind data.

3 Task 3: Collect and Analyze Traffic Data

3.1 Traffic Data Collection

Regarding the real-world traffic along freeways in California, one of the major data sources is PeMS [56]. This comprehensive system receives real-time 30-second raw measurements of traffic count and occupancy on a lane basis from each ILD, detects the invalid or missing data samples, and rectifies them or fills the "holes" in an efficient manner. Based on the rectified traffic flow and occupancy data for each lane, aggregate traffic speed at each single loop detector can be estimated using the g-factor algorithm [57]. The truck volume is estimated in PeMS based on the algorithm proposed by Kwon et al. [58]. In addition, all these raw data can be aggregated at

various temporal levels (e.g., 5 minutes, 1 hour or even 1 day), for different purposes of analyses. It is noted that PeMS also archives the geographic information of each ILD or cluster of ILDs, i.e., VDS, including the latitude and longitude as well as the associated post-mile. With such information, we can easily identify the most related VDS.

In addition, to obtain a reliable estimate of the truck volume and vehicle weight distribution, we will select the study site and VDS location to be near a WIM station. A candidate study site along I-710 is around the ramp of Long Beach Blvd. (see Figure 3-1), where a WIM station (Site #60 at CA postmile 11.5 of I-710 NB) and a mainline VDS (ID #717966 at CA postmile 12.13) are close to each other. More ideally, a SCAQMD NO_2 monitoring station is bracketed by the aforementioned WIM station and VDS. License plate reader cameras may be used to help identify vehicle fleet mix at other stations/locations that may not have WIM/VDS.

Figure 3-1: Google Maps illustrating the locations of WIM station, VDS, and NO2 monitoring station, respectively, along I-710N around Long Beach Blvd.

3.2 Traffic Analysis

This chapter documents the work performed on traffic data analysis, based on the following major data sources:

1. PeMS [56], which receives real-time 30-second measurements of traffic count and occupancy from every loop detector (per lane) throughout the California freeway system, detects the invalid or missing data, and rectifies them or fills those "holes". Based on the flow and occupancy data for each lane, speed is estimated using the well-known g-factor algorithm for single loop detector [57]. In addition, all these raw data are aggregated at various temporal levels, e.g., 5 minutes, for different purposes of analysis.
2. Video footage processed by the ALPR, which relies on: 1) collection of footage for on-road traffic (via camcorders); 2) recognition of vehicle license plate information using the ALPR software; and 3) linkage with DMV registration records and other database to access vehicle/powertrain characteristics [59]
3. WIM stations, which capture and record key features of vehicles (in particular trucks) such as axle weights and gross vehicle weights, as vehicles move over the measurement points.

The data collection effort on the Caltrans PeMS dataset is presented in section 3.3. The work performed on the video footage (along with ALPR) is described in Section 3.4. Section 3.5 illustrates the information obtained from WIMs, and the last section summarizes the key findings from these data sources.

3.3 Caltrans Performance System (PeMS) Data Analysis

3.3.1 *Anaheim NR Site (I-5 North)*

At the Anaheim NR site, we selected two vehicle detection stations (VDSs) that bracket the monitoring location, whose IDs are #1205452 (upstream) and #1205473 (downstream), respectively. The data collection period spans from 01/28/2020 to 02/03/2020.

3.3.1.1 VDS #1205452 (upstream)

Figure 3-2 indicates the location of this VDS with respect to the monitoring location. Figure 3-3 and Figure 3-4 present the time series of four key traffic states over the data collection period, i.e., total flow per 5 minutes (veh/5-min), average speed (mph), total truck flow per 5 minutes (veh/5-min), and truck proportion (%).

As can be observed from Figure 3-3, the 5-min traffic flows (red line) show a periodic daily pattern over the entire week. In particular, the peak hours (in terms of flow) initiated at around 3 pm during weekdays (01/28/2020 – 01/31/2020, and 02/03/2020) and the average speeds (green line) could drop to 40 mph. During weekends (02/01/2020 and 02/02/2020), the peak of traffic volumes shifted to noon and the speeds were relatively smoothed. Figure 3-4 indicates that absolute truck volumes (red line) varied significantly and reached peaks in the late afternoon (at around 6 pm) on 01/28/2020 and 01/29/2020.

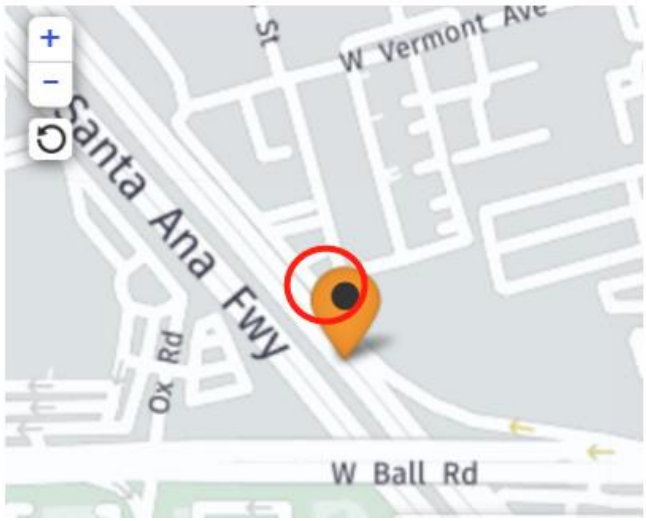

Figure 3-2: Location of VDS #1205452 (orange pin) with respect to the monitoring site (red circle).

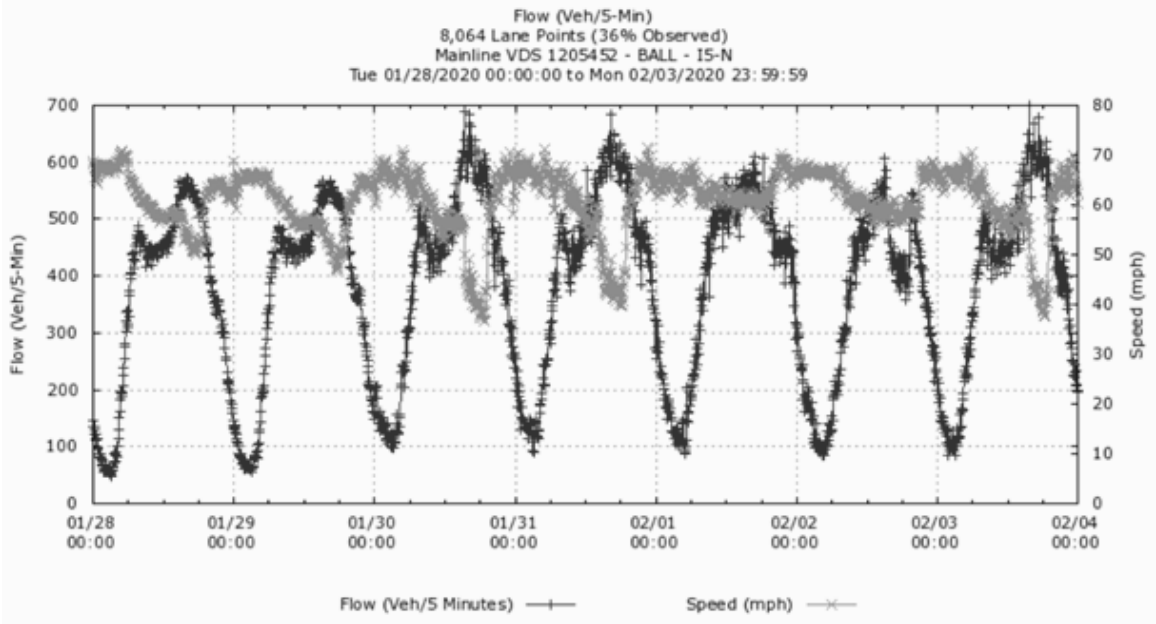

Figure 3-3: Time series of 5-min traffic flow and 5-min traffic speed for VDS #1205452 over the period.

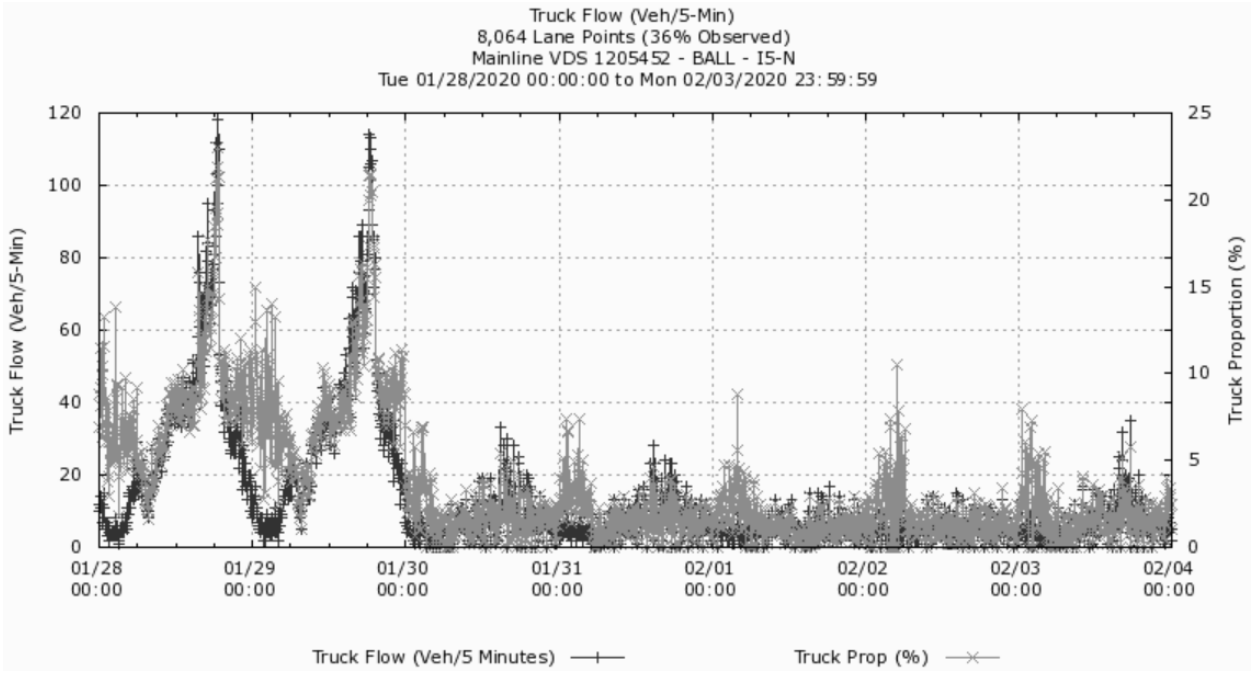

Figure 3-4: Time series of 5-min truck flow and 5-min truck proportion for VDS #1205452 over the period.

3.3.1.2 VDS #1205473 (downstream)

Figure 3-5 indicates the location of this VDS and the monitoring location as well. Similarly, Figure 3-6 and Figure 3-7 present the time series of the key traffic states. Due to the strong correlation with the upstream VDS (i.e., #1205452), the traffic patterns in terms of traffic flow, average speed and truck proportion, are aligned with the upstream measurements, except for truck traffic.

3.3.2 *Anaheim NR Site (I-5 South)*

Considering the potential impacts of traffic along the opposite direction (i.e., I-5 South), we also analyzed traffic data from two closest VDSs (with respect to the monitoring location), whose IDs are #1205463 (upstream) and #1205440 (downstream), respectively, during the same period.

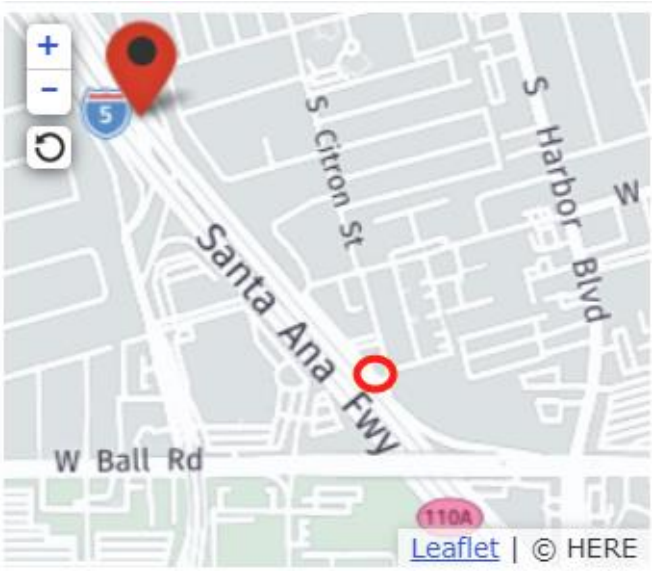

Figure 3-5: Illustration for the locations of VDS #1205473 (red pin) and the monitoring site (red circle).

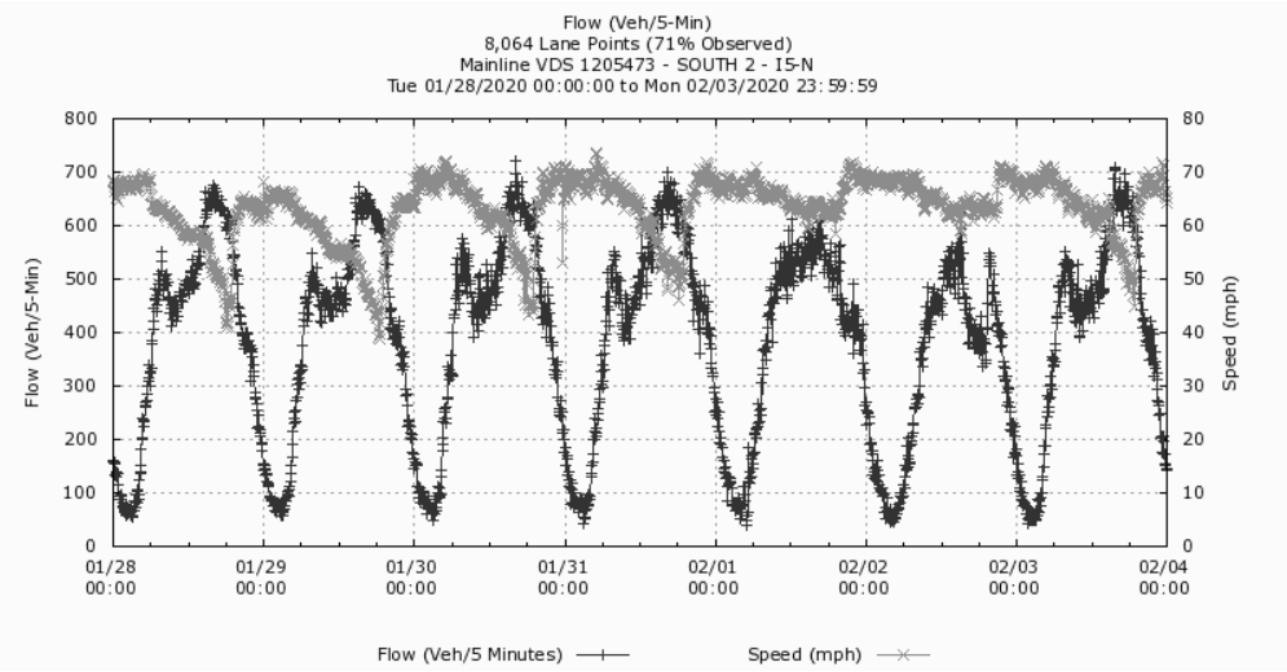

Figure 3-6: Time series of 5-min traffic flow and 5-min traffic speed for VDS #1205473 over the period.

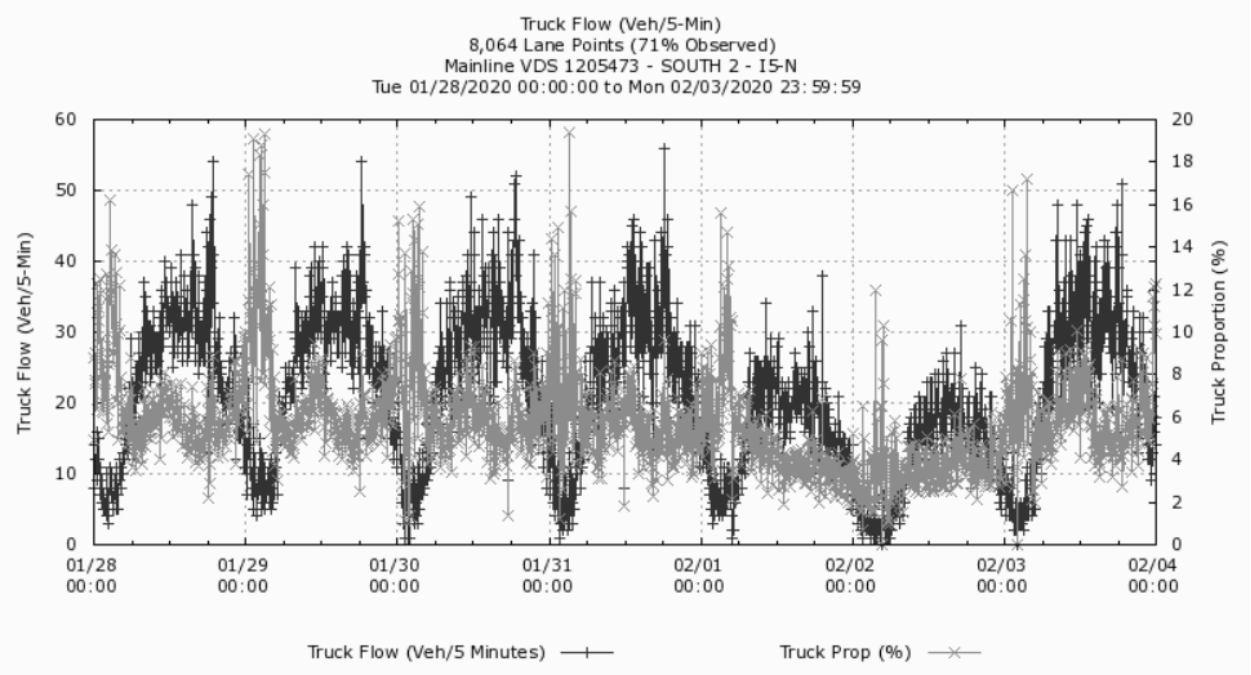

Figure 3-7: Time series of 5-min truck flow and 5-min truck proportion for VDS #1205473 over the period.

3.3.2.1 VDS #1205463 (upstream)

Figure 3-8 indicates the location of this VDS and the monitoring location. Figure 3-9 and Figure 3-10 present the time series of key traffic states.

Unlike the traffic states along I-5N, the 5-min traffic flows (red line) show a periodic daily pattern with two peak hours (see Figure 3-9) in weekdays, one in the mornings (starting at around 6 am) and the other in the afternoons (starting at around 3 pm). The average speeds (green line) could reduce to around 45 mph. During weekends, the traffic might get less congested and free-flow speed (at around 65 mph) could maintain at most of the time. Figure 3-10 shows some daily pattern for the absolute truck volumes (red line) where there are not apparent peak demands. The truck volumes are relatively higher in the period of 01/30/2020 – 02/03/2020, compared to those within the time 01/28/2020 – 01/29/2020.

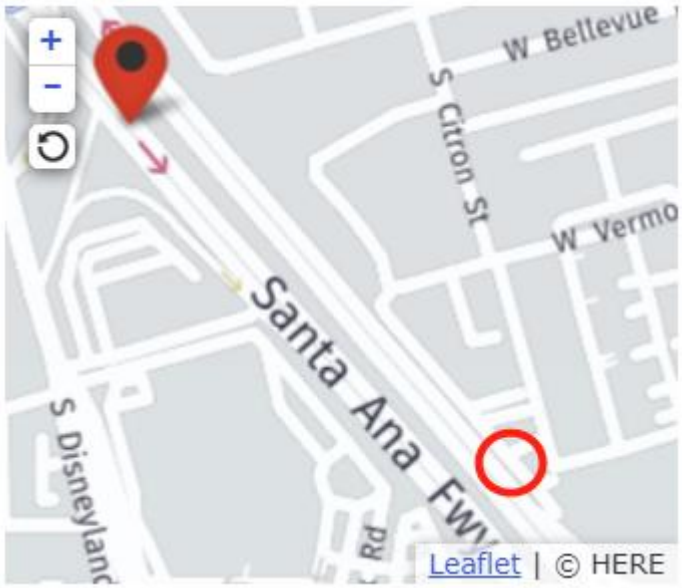

Figure 3-8: Illustration for the locations of VDS #1205463 (red pin) and the monitoring site (red circle).

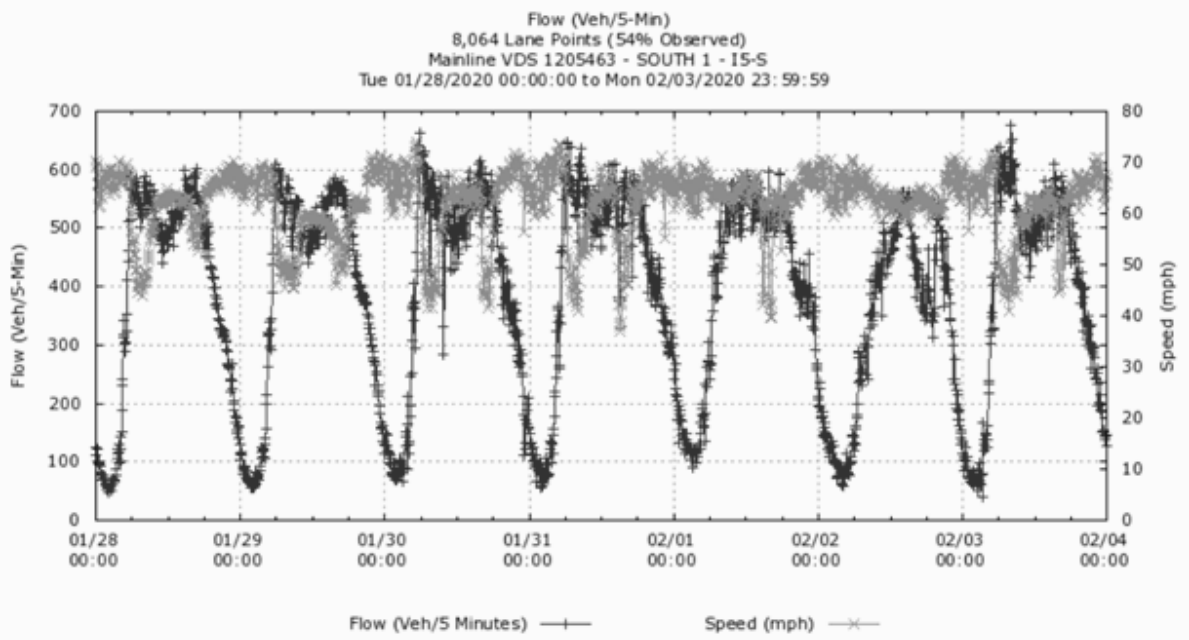

Figure 3-9: Time series of 5-min traffic flow and 5-min traffic speed for VDS #1205463 over the period.

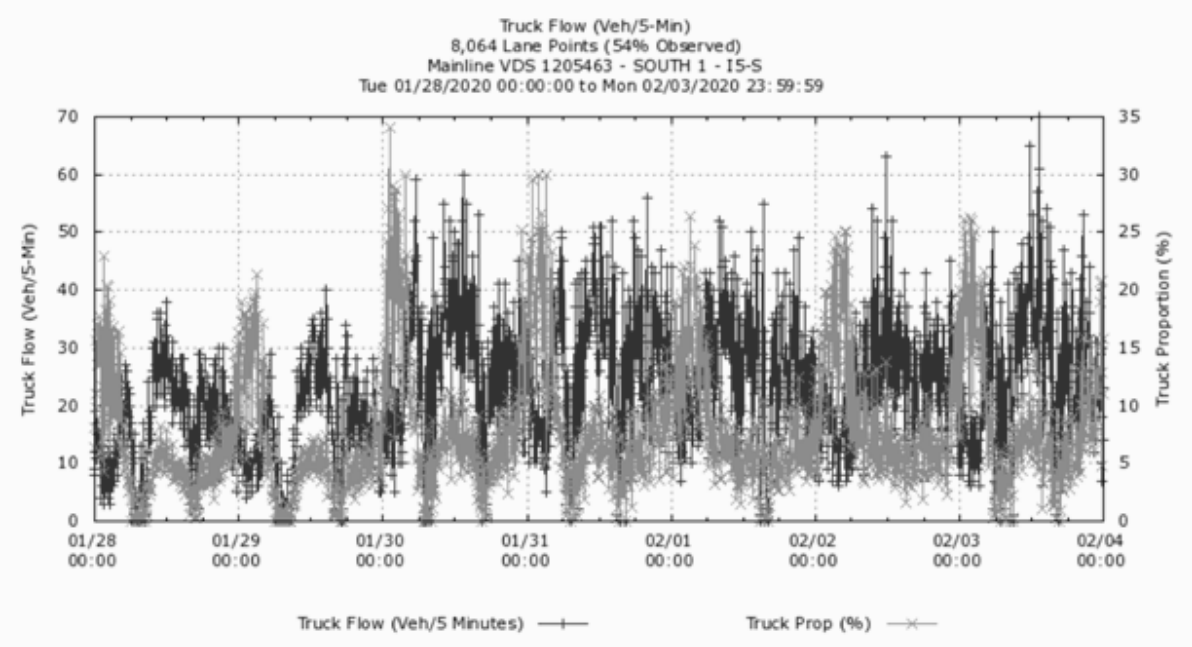

Figure 3-10: Time series of 5-min truck flow and 5-min truck proportion for VDS #1205463 over the period.

3.3.2.2 VDS #1205440 (downstream)

Figure 3-11 indicates the location of this VDS and the monitoring location. Figure 3-12 and Figure 3-13 present the time series of four key traffic states.

Due to the strong correlation with the upstream VDS (i.e., #1205463), the traffic patterns measured in this VDS in terms of traffic flow and average speed are similar to its upstream counterpart. However, the truck volumes are significantly lower. A hypothesis is that a large portion of truck traffic gets off the freeway and heads to the Harbor Blvd.

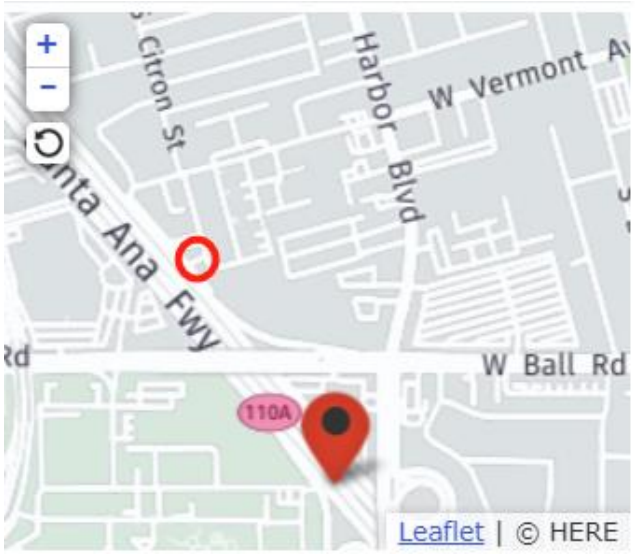

Figure 3-11: Illustration for the locations of VDS #1205440 (red pin) and the monitoring site (red circle).

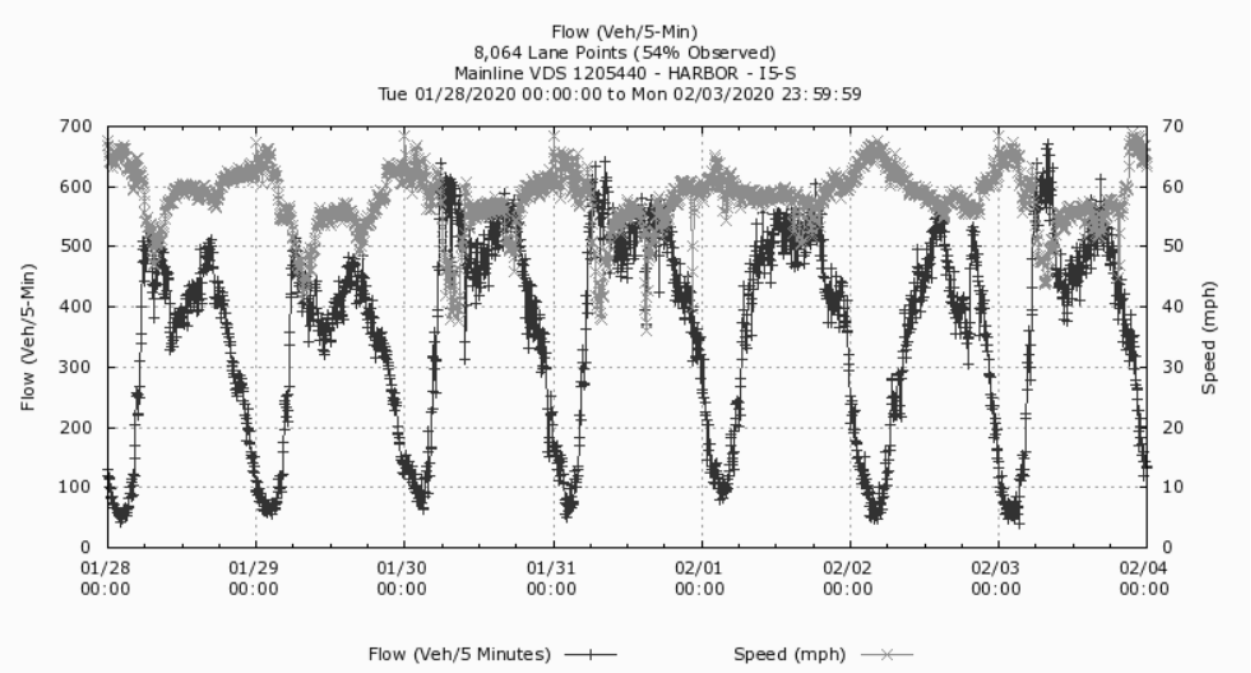

Figure 3-12: Time series of 5-min traffic flow and 5-min traffic speed for VDS #1205440 over the period.

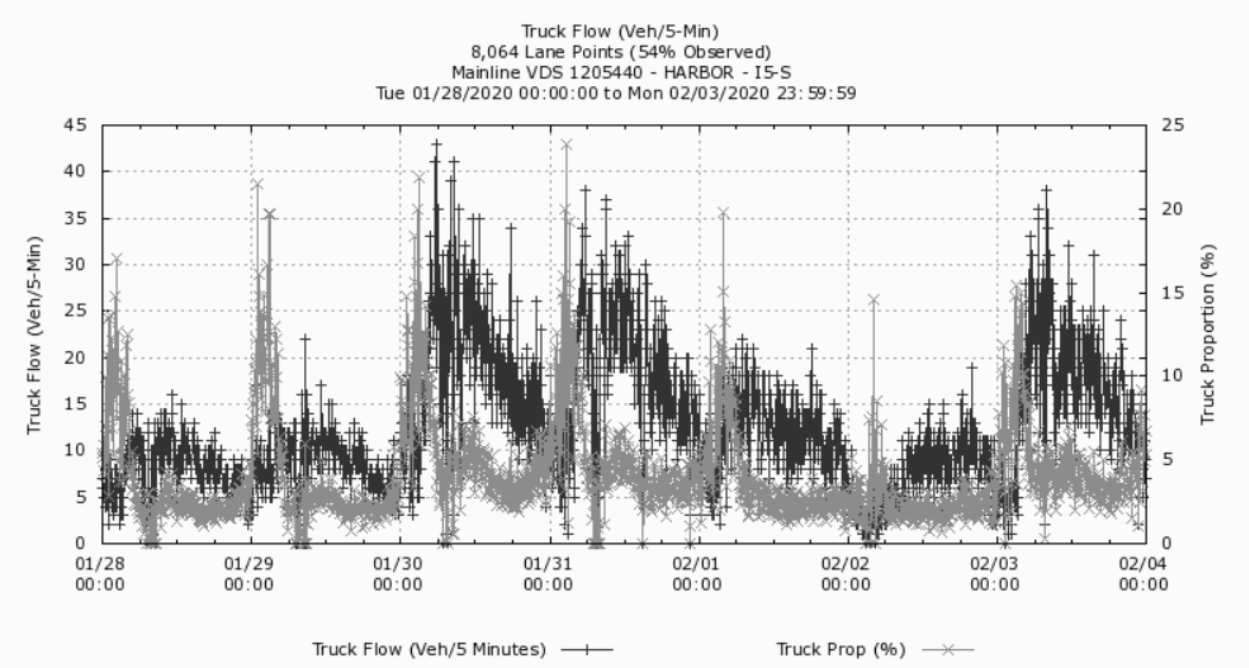

Figure 3-13: Time series of 5-min truck flow and 5-min truck proportion for VDS #1205440 over the period.

3.3.3 *I-710 NR Site (I-710 North)*

For the I-710 NR site, the IDs of two bracketed VDSs (with respect to the monitoring location) along I-710 N are #717962 (upstream) and #717966 (downstream).

3.3.3.1 VDS #717962 (upstream)

Figure 3-14 indicates the location of this VDS (red pin) and the monitoring location (red circle). Figure 3-15 and Figure 3-16 present the time series of four key traffic states.

A too much clear dual-mode pattern can be observed from Figure 3-15 regarding traffic volume and average speed during weekdays. Single peak periods occurred at noon in weekends. The truck traffic (shown in Figure 3-16) presents the same trends as in total traffic volumes. A double check of data quality was performed and it turned out the VDS exhibited “Ctrl Down” for the entire week.

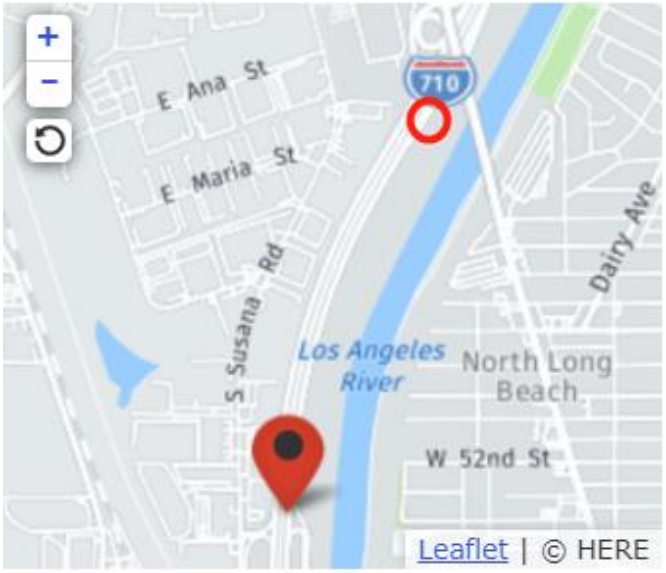

Figure 3-14: Illustration for the locations of VDS #717962 (red pin) and the monitoring site (red circle).

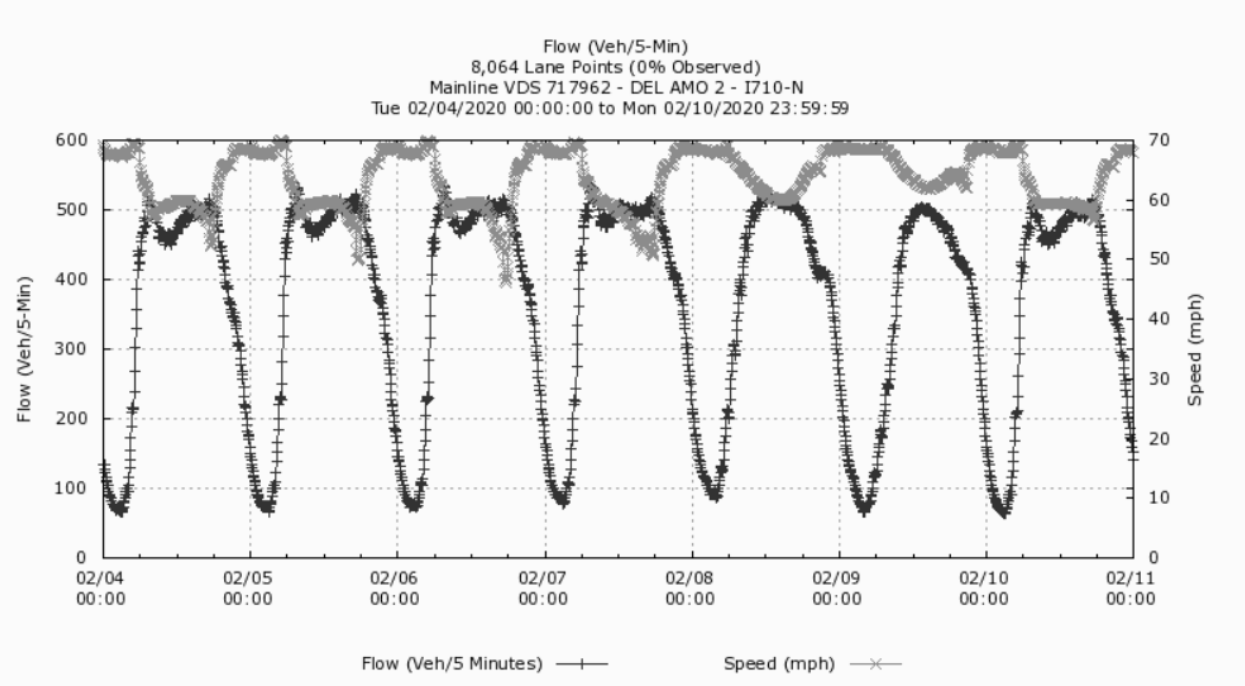

Figure 3-15: Time series of 5-min traffic flow and 5-min traffic speed for VDS #717962 over the period.

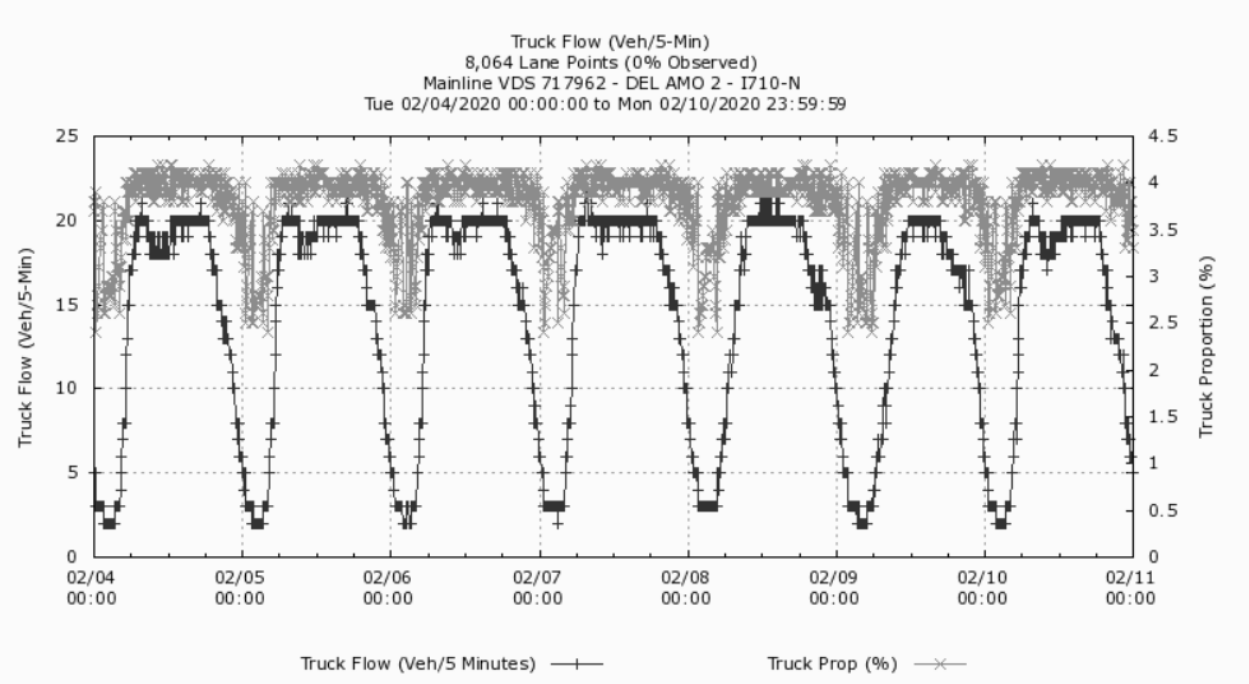

Figure 3-16: Time series of 5-min truck flow and 5-min truck proportion for VDS #717962 over the period.

3.3.3.2 VDS #717966 (downstream)

Figure 3-17 indicates the location of this VDS (red pin) and the monitoring location (red circle). Again, Figure 3-18 and Figure 3-19 present the time series of four key traffic states.

As shown in these figures, the patterns are quite different from the upstream VDS. An examination of data quality indicates that the VDS did not function properly (also "Ctrl Down") during the experiment period.

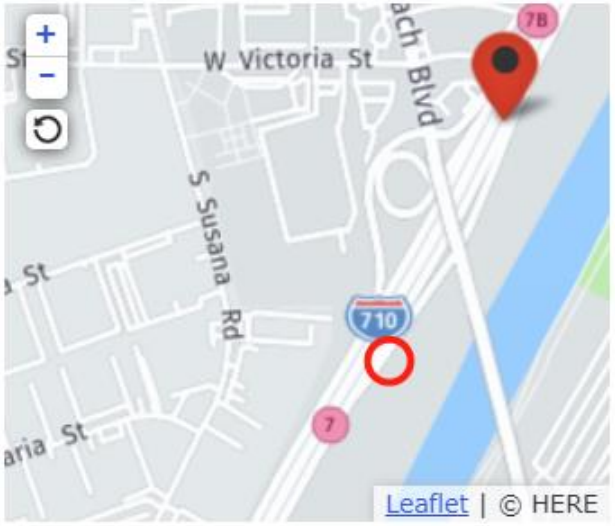

Figure 3-17: Illustration for the locations of VDS #717966 (red pin) and the monitoring site (red circle).

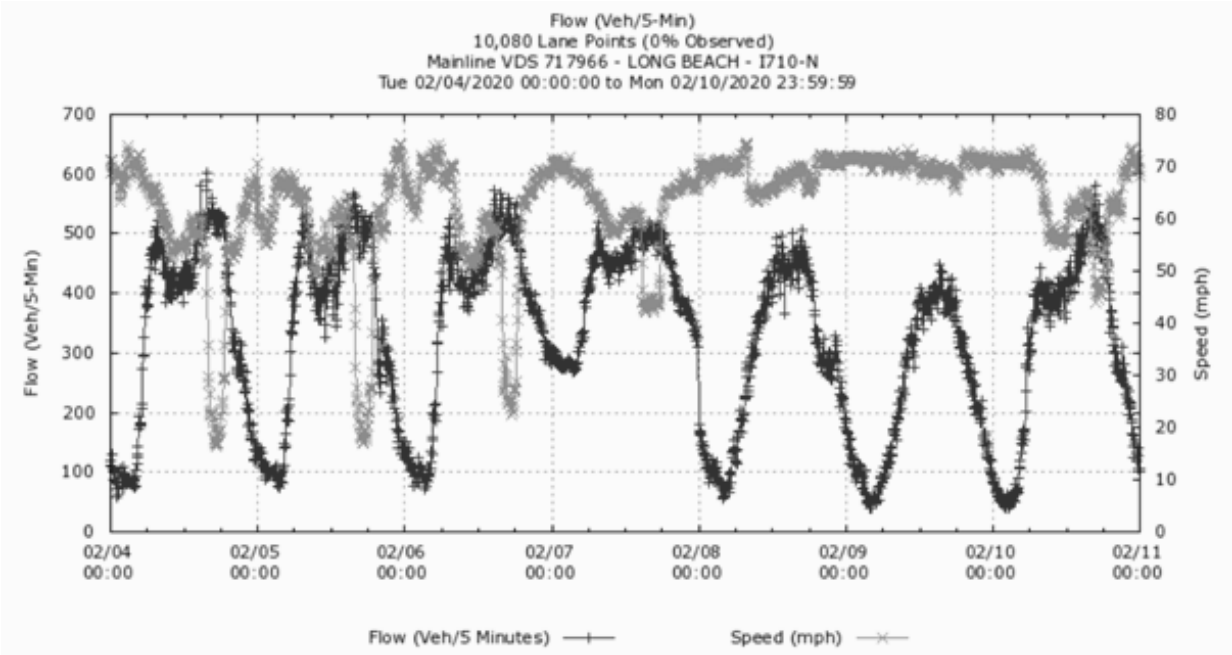

Figure 3-18: Time series of 5-min traffic flow and 5-min traffic speed for VDS #717966 over the period.

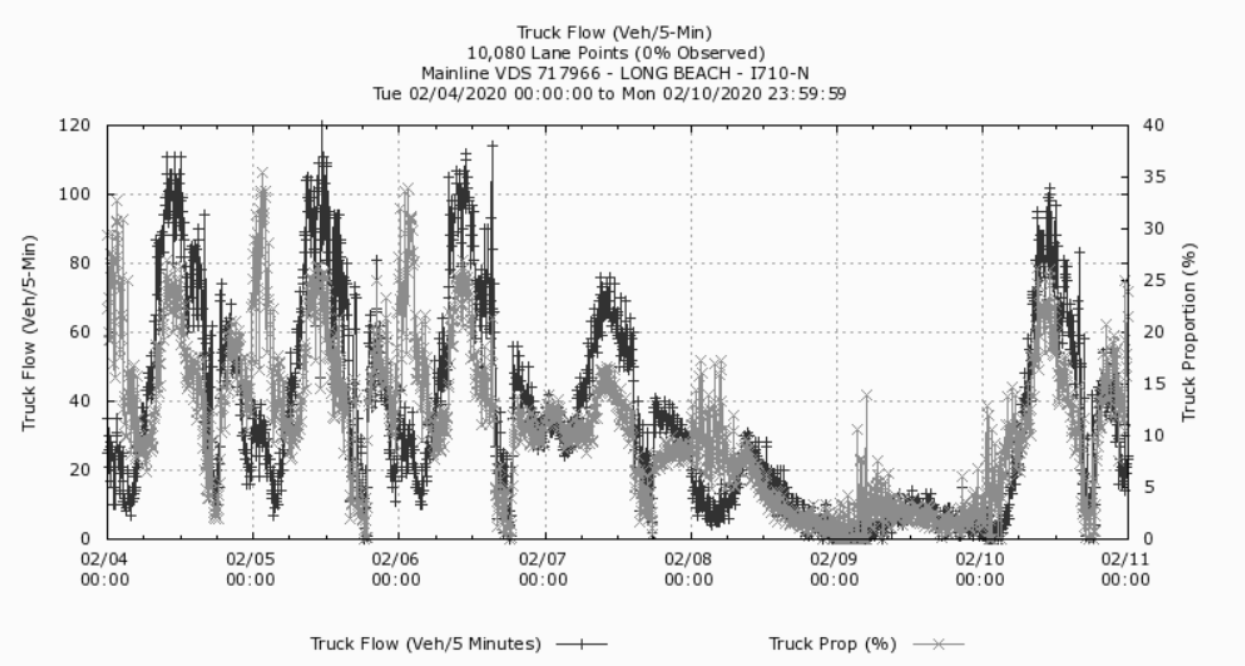

Figure 3-19: Time series of 5-min truck flow and 5-min truck proportion for VDS #717966 over the period.

3.3.4 *I-710 NR Site (I-710 South)*

The IDs of two bracketed VDSs along I-710 S are #717963 (upstream) and #717960 (downstream).

3.3.4.1 VDS #717963 (upstream)

Figure 3-20 indicates the location of this VDS and the monitoring location. Figure 3-21 and Figure 3-22 present the time series of four key traffic states.

Figure 3-21 exhibits daily pattern over the weekdays (01/28/2020 – 01/31/2020, and 02/03/2020), where peak hours (in terms of 5-min flow) initiated at around 6 am and the average speeds (green line) could drop to 20 mph. During weekends (02/01/2020 and 02/02/2020), the peak of traffic volumes shifted to noon and the speeds were much higher. Figure 3-22 presents that absolute truck volumes (red line) reached peaks in the middle of weekdays (between 8 am and 4 pm). This might correlate the speed drops in the middle of weekdays as shown in Figure 3-21.

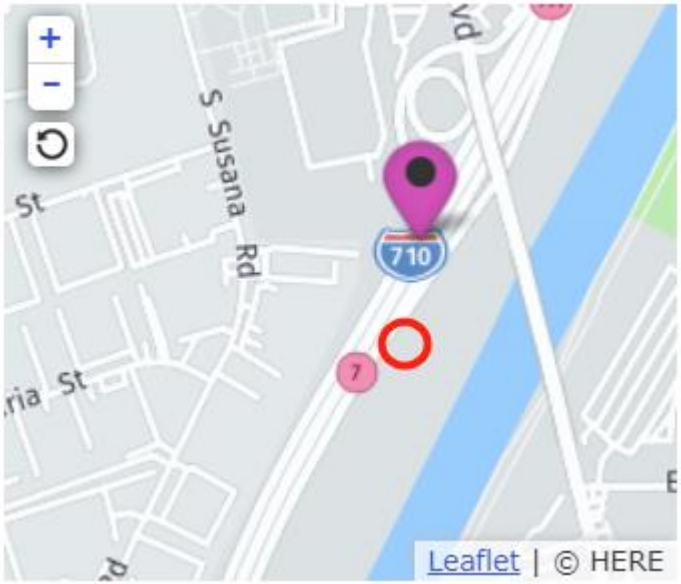

Figure 3-20: Illustration for the locations of VDS #717963 (purple pin) and the monitoring site (red circle).

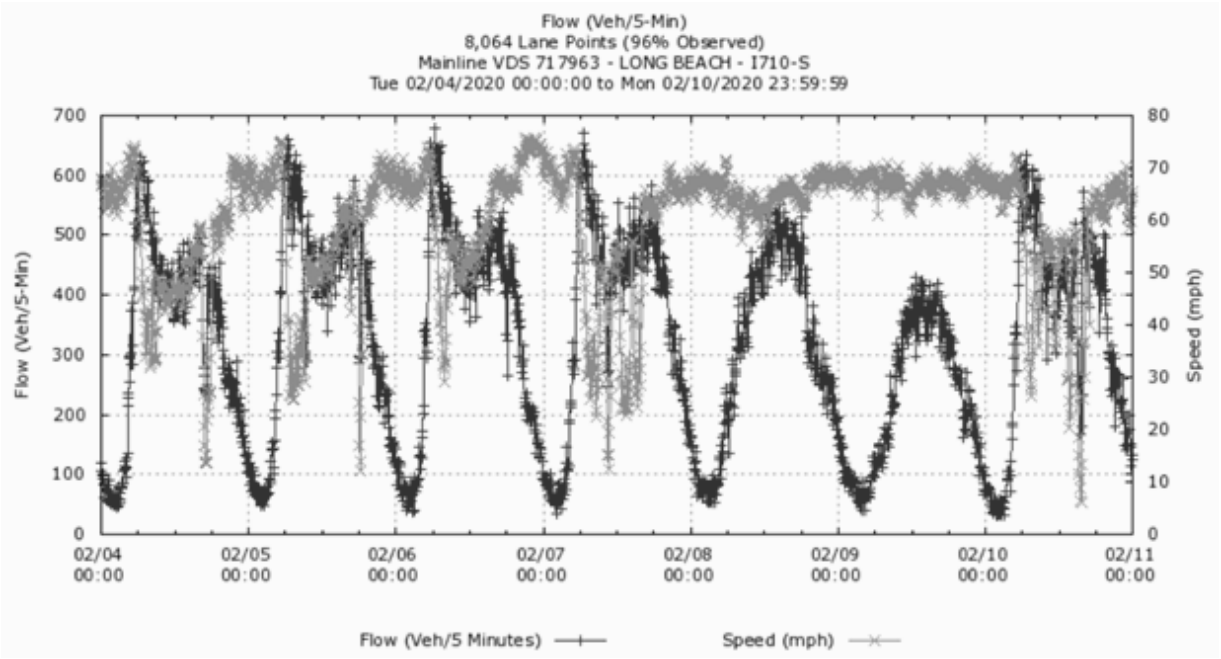

Figure 3-21: Time series of 5-min traffic flow and 5-min traffic speed for VDS #717963 over the period.

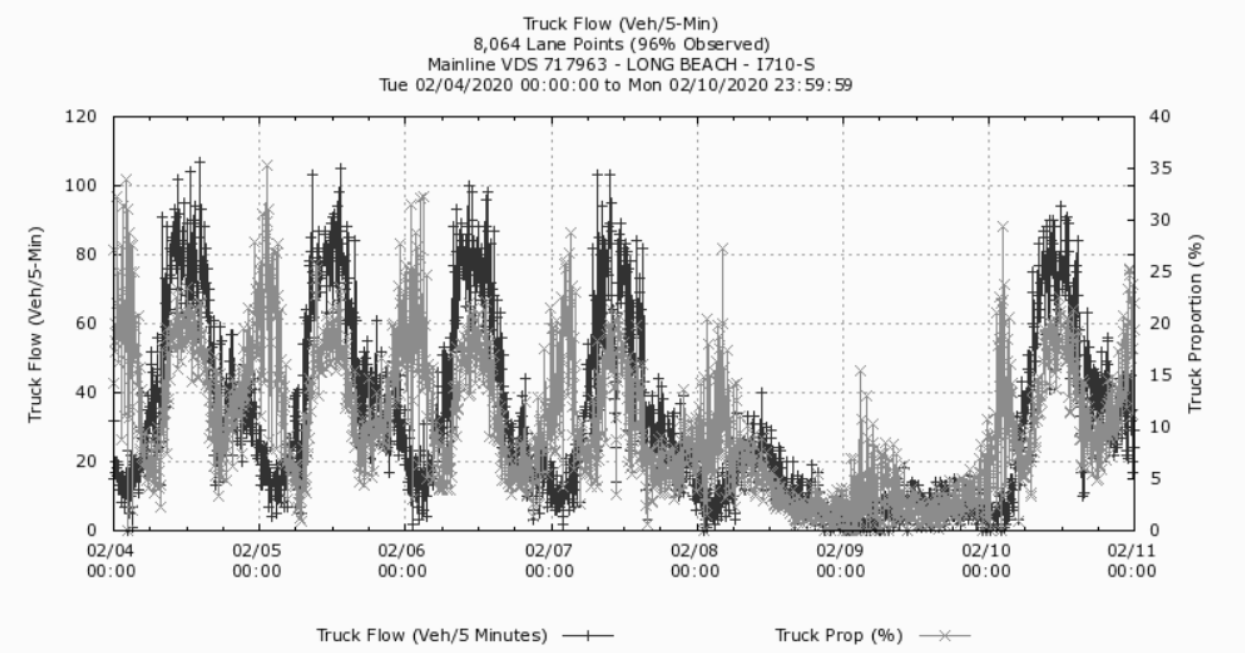

Figure 3-22: Time series of 5-min truck flow and 5-min truck proportion for VDS #717963 over the period.

3.3.4.2 VDS #717960 (downstream)

Figure 3-23 indicates the location of this VDS and the monitoring location. Figure 3-24 and Figure 3-25 present the time series of four key traffic states.

Because of the strong correlation between downstream and upstream locations, traffic volume and speed measured in VDS #717960 show the similar patterns as in VDS #717963. However, due to the downstream bottleneck (lane drops from 4 to 3), portion of traffic stream (including truck stream) get off the freeway or re-route right before this VDS.

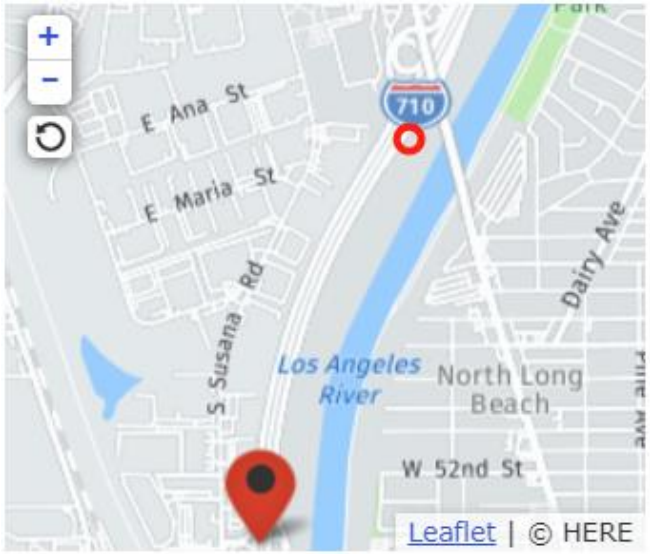

Figure 3-23: Illustration for the locations of VDS #717960 (red pin) and the monitoring site (red circle).

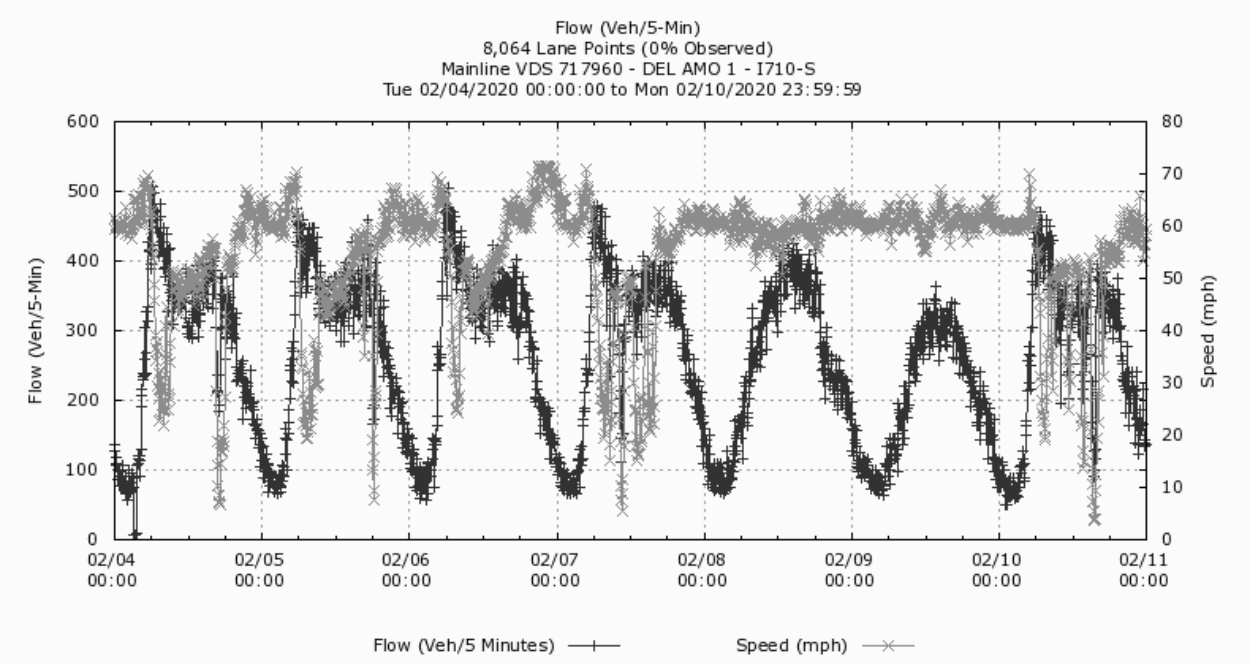

Figure 3-24: Time series of 5-min traffic flow and 5-min traffic speed for VDS #717960 over the period.

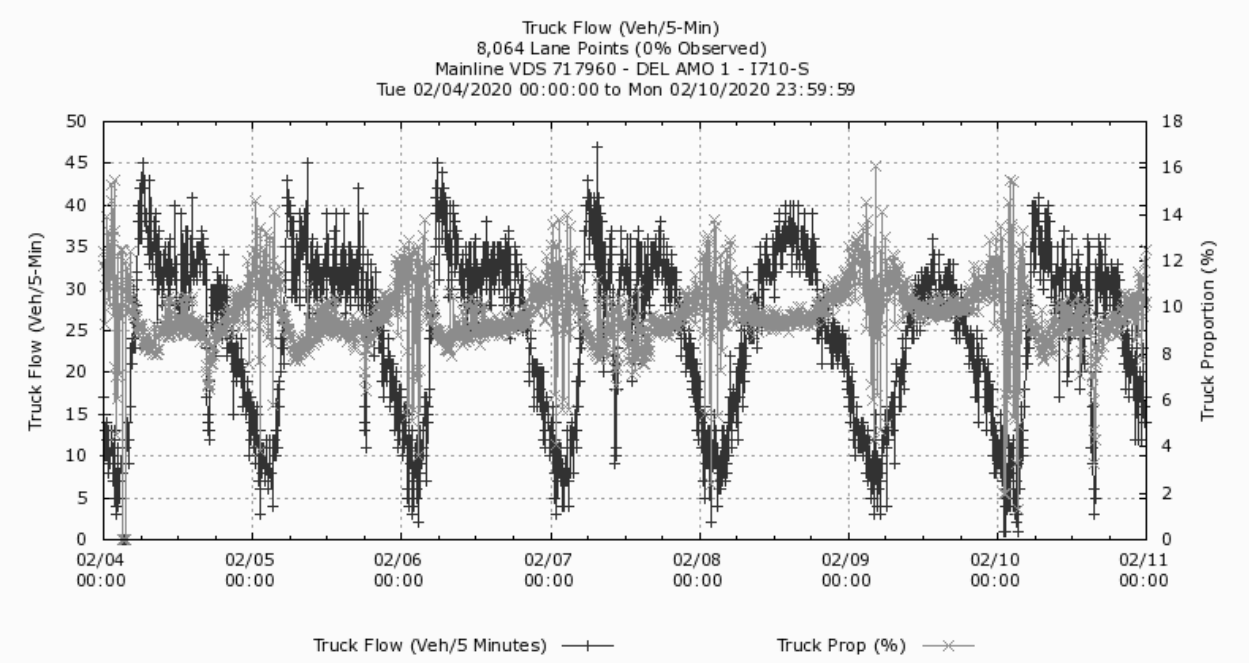

Figure 3-25: Time series of 5-min truck flow and 5-min truck proportion for VDS #717960 over the period.

Appendix A: Chemical Mass Balance Source Profiles

PNO	Mnemonic	SIZE	K+	K+U	NO3-	NO3-U	OC1	OC1U	OC2	OC2U	OC3	OC3U	OC4	OC4U	EC1	EC1U	EC2	EC2U	EC3	EC3U	POC	POCU	OC	OCU	EC
20013	Brake_1	PM2.5	0.00033	0.00005	0.00000	0.00046	0.05398	0.00478	0.02276	0.00287	0.06414	0.00600	0.02512	0.00361	0.00938	0.00338	0.01445	0.00207	0.00869	0.00265	0.00006	0.00067	0.16607	0.01139	0.03246
20014	Brake_2	PM2.5	0.00027	0.00003	0.00062	0.00019	0.01963	0.00174	0.02509	0.00307	0.07567	0.00657	0.02036	0.00285	0.01171	0.00090	0.01697	0.00233	0.01302	0.00396	0.00005	0.00027	0.14080	0.00978	0.04166
20015	Brake_3	PM2.5	0.00314	0.00023	0.00110	0.00016	0.01773	0.00157	0.01540	0.00189	0.06072	0.00527	0.06211	0.00863	0.07991	0.00597	0.02827	0.00386	0.00564	0.00171	0.00000	0.00021	0.15596	0.01220	0.11382
20016	Brake_C	PM2.5	0.00125	0.00164	0.00057	0.00055	0.03045	0.02041	0.02108	0.00506	0.06684	0.00783	0.03587	0.02285	0.03366	0.04007	0.01990	0.00736	0.00912	0.00371	0.00004	0.00043	0.15427	0.01272	0.06264
ARB1	Brake_D	PM10																							
ARB2	Brake_E	PM10																							
ARB3	Brake_F	PM10																							
ARB4	Brake_G	PM10																							
20017	Tire_1	PM2.5	0.00271	0.00027	0.01643	0.00212	0.12925	0.01181	0.08657	0.01105	0.20442	0.02013	0.07980	0.01173	0.06504	0.02329	0.04330	0.00643	0.01378	0.00427	0.00034	0.00252	0.50038	0.03659	0.12177
20018	Tire_2	PM2.5	0.00366	0.00049	0.02234	0.00425	0.14834	0.01527	0.22169	0.02970	0.61421	0.06371	0.14819	0.02308	0.12465	0.04507	0.14962	0.02228	0.00000	0.00173	0.00030	0.00557	1.13274	0.09850	0.27397
25346	WS-L	PM2.5	0.00110	0.00073	0.03212	0.01702	0.19522	0.19406	0.16631	0.03654	0.23437	0.09011	0.11142	0.03673	0.14665	0.06558	0.18015	0.16097	0.00792	0.00494	0.00853	0.00849	0.71584	0.26229	0.32621
25347	CS-L	PM2.5	0.00098	0.00063	0.01857	0.01172	0.15857	0.14201	0.16649	0.03150	0.16480	0.04900	0.08066	0.01817	0.15386	0.03912	0.11874	0.08489	0.00551	0.00303	0.00219	0.00266	0.57270	0.13559	0.27590
25348	WS-H	PM2.5	0.00098	0.00131	0.00759	0.00929	0.48691	0.27152	0.12247	0.06331	0.13346	0.08451	0.06879	0.03980	0.07915	0.05612	0.11183	0.11882	0.00561	0.00429	0.02787	0.05211	0.83949	0.32462	0.16867
25349	CS-H	PM2.5	0.00038	0.00035	0.00485	0.00405	0.40785	0.22825	0.13453	0.07484	0.08876	0.02678	0.05879	0.02050	0.08976	0.05237	0.06491	0.05147	0.00397	0.00305	0.01081	0.01710	0.70074	0.21502	0.14784
25350	WS-BC	PM2.5	0.00036	0.00009	0.02207	0.01611	0.07793	0.08474	0.08486	0.04795	0.11353	0.03081	0.07871	0.03388	0.20774	0.08889	0.18095	0.17329	0.00334	0.00339	0.00205	0.00488	0.35709	0.18291	0.38997
25351	CS-BC	PM2.5	0.00040	0.00020	0.01407	0.00955	0.13575	0.08841	0.07380	0.02629	0.06317	0.01312	0.04134	0.00667	0.15490	0.05497	0.27477	0.14642	0.00209	0.00146	0.02639	0.02864	0.34045	0.08704	0.40532
25352	MDD-MIX	PM2.5	0.00185	0.00078	0.00362	0.00705	0.25566	0.09574	0.21996	0.10517	0.26885	0.11163	0.17548	0.09093	0.23664	0.07531	0.51141	0.07351	0.00835	0.00634	0.00062	0.00176	0.92056	0.39516	0.75573
25353	HHDD-HW	PM2.5	0.00154	0.00015	0.00119	0.00238	0.21570	0.09525	0.11314	0.03852	0.19881	0.06746	0.08482	0.03434	0.28968	0.06091	0.48064	0.19344	0.00457	0.00304	0.00022	0.00148	0.61268	0.23565	0.77466
25354	HHDD-HCS	PM2.5	0.00136	0.00058	0.00000	0.00080	0.16895	0.01907	0.08068	0.00891	0.12333	0.02153	0.05370	0.00660	0.24723	0.05227	0.56250	0.05625	0.00023	0.00038	0.00022	0.00121	0.42687	0.05128	0.80989
25355	HHDD-MIX	PM2.5	0.00145	0.00040	0.00059	0.00168	0.19233	0.06782	0.09691	0.03116	0.16107	0.06146	0.06926	0.02830	0.26846	0.04750	0.52157	0.13573	0.00240	0.00306	0.00022	0.00095	0.51978	0.18652	0.79228
25356	DIESEL	PM2.5	0.00155	0.00053	0.00135	0.00383	0.20816	0.07616	0.12767	0.06294	0.18801	0.07289	0.09581	0.05461	0.26050	0.05994	0.51903	0.12689	0.00389	0.00384	0.00032	0.00138	0.61997	0.21715	0.78314
25357	GAS	PM2.5	0.00070	0.00068	0.01655	0.01211	0.24370	0.18195	0.12474	0.04988	0.13301	0.06082	0.07328	0.02851	0.13868	0.06143	0.15522	0.12997	0.00474	0.00353	0.01297	0.02560	0.58772	0.20124	0.28565
Copper1	COTIRE1	TSP					0.00007	0.00000	0.04876	0.00001	0.42867	0.00002	0.02743	0.00001	0.05600	0.00001	0.18831	0.00002	0.00067	0.00000	0.00916	0.00001	0.51409	0.00003	0.23582
Copper2	COTIRE2	TSP					0.00008	0.00000	0.04647	0.00001	0.35330	0.00002	0.01278	0.00002	0.06665	0.00001	0.12773	0.00003	0.00000	0.00000	0.18948	0.00001	0.60211	0.00004	0.19438
Michelin1	MITIRE1	TSP	0.00002	0.00001	0.00025	0.00009	0.00000	0.00000	0.07890	0.00001	0.49254	0.00002	0.03634	0.00002	0.10956	0.00001	0.29825	0.00003	0.00000	0.00000	0.00000	0.00002	0.60779	0.00004	0.40782
Michelin2	MITIRE2	TSP	0.00002	0.00001	0.00019	0.00007	0.00004	0.00000	0.07881	0.00001	0.47160	0.00003	0.01553	0.00002	0.11335	0.00001	0.26122	0.00003	0.00000	0.00000	0.00000	0.00002	0.56598	0.00004	0.37457
Copper	COTIRE	TSP					0.00008	0.00000	0.04762	0.00162	0.39099	0.05329	0.02010	0.01036	0.06133	0.00754	0.15802	0.04284	0.00033	0.00047	0.09932	0.12751	0.55810	0.06224	0.21510
Michelin	MITIRE	TSP	0.00002	0.00001	0.00022	0.00008	0.00002	0.00002	0.07886	0.00007	0.48207	0.01480	0.02593	0.01471	0.11145	0.00267	0.27974	0.02619	0.00000	0.00000	0.00000	0.00002	0.58688	0.02956	0.39119
MiCo	TIRE	TSP					0.00005	0.00004	0.06324	0.01806	0.43653	0.06153	0.02302	0.01092	0.08639	0.02931	0.21888	0.07602	0.00017	0.00033	0.04966	0.09331	0.57249	0.04311	0.30315
RESQ2485	AQ Dust	PM2.5	0.00198	0.00017	0.00295	0.00033	0.00608	0.00046	0.02961	0.00230	0.09156	0.01155	0.06946	0.01171	0.01860	0.01174	0.02062	0.00898	0.00000	0.00002	0.00755	0.00062	0.20425	0.01536	0.03168
RESQ2489	MA Dust	PM2.5	0.00103	0.00012	0.00283	0.00055	0.00932	0.00083	0.02811	0.00255	0.11300	0.01519	0.03743	0.00657	0.04906	0.03105	0.03838	0.01682	0.00000	0.00005	0.01269	0.00126	0.20056	0.01772	0.07475
RESQ2493	CC Dust	PM2.5	0.00088	0.00008	0.00165	0.00028	0.00570	0.00043	0.01209	0.00096	0.06238	0.00792	0.03033	0.00514	0.01662	0.01049	0.01413	0.00617	0.00000	0.00003	0.00151	0.00032	0.11201	0.00856	0.02923
RESQ2497	AT Dust	PM2.5	0.00044	0.00006	0.00179	0.00036	0.00044	0.00011	0.00981	0.00083	0.06726	0.00869	0.03141	0.00538	0.02540	0.01605	0.02077	0.00908	0.00000	0.00004	0.00000	0.00041	0.10892	0.00874	0.04618
RESQ2520	Dust	PM2.5	0.00108	0.00065	0.00231	0.00068	0.00539	0.00367	0.01990	0.01040	0.08355	0.02342	0.04216	0.01847	0.02742	0.01917	0.02348	0.01100	0.00000	0.00004	0.00544	0.00583	0.15644	0.05312	0.04546
RESQ2540	MCDust	PM2.5	0.00095	0.00011	0.00224	0.00083	0.00751	0.00256	0.02010	0.01133	0.08769	0.03579	0.03388	0.00590	0.03284	0.02318	0.02625	0.01715	0.00000	0.00004	0.00710	0.00791	0.15628	0.06262	0.05199
RESQ2560	AADust	PM2.5	0.00121	0.00110	0.00237	0.00082	0.00326	0.00398	0.01971	0.01401	0.07941	0.01718	0.05043	0.02691	0.02200	0.01406	0.02070	0.00903	0.00000	0.00003	0.00377	0.00534	0.15659	0.06741	0.03893
RESQ2487	AQDust	PM10	0.00217	0.00018	0.00281	0.00031	0.00270	0.00021	0.02627	0.00200	0.08212	0.01030	0.04713	0.00792	0.02320	0.01464	0.00809	0.00354	0.00000	0.00002	0.01302	0.00098	0.17124	0.01264	0.01827
RESQ2491	MADust	PM10	0.00102	0.00011	0.00162	0.00044	0.00488	0.00041	0.01081	0.00094	0.04587	0.00602	0.02364	0.00409	0.01531	0.00968	0.01327	0.00587	0.00000	0.00005	0.02166	0.00182	0.10686	0.00881	0.00691
RESQ2495	CCDust	PM10	0.00110	0.00010	0.00094	0.00025	0.00135	0.00013	0.01322	0.00103	0.07830	0.00987	0.05167	0.00871	0.02279	0.01439	0.01059	0.00464	0.00000	0.00003	0.01340	0.00103	0.15793	0.01185	0.01999
RESQ2499	ATDust	PM10	0.00034	0.00005	0.00268	0.00035	0.00312	0.00025	0.01461	0.00115	0.08350	0.01056	0.04929	0.00832	0.02875	0.01815	0.03423	0.01490	0.00000	0.00003	0.02258	0.00172	0.17311	0.01309	0.04040
RESQ2510	Dust	PM10	0.00116	0.00076	0.00201	0.00089	0.00302	0.00145	0.01623	0.00688	0.07245	0.01785	0.04293	0.01299	0.02251	0.01453	0.01654	0.01198	0.00000	0.00003	0.01766	0.00516	0.15229	0.03103	0.02139
RESQ2530	MCDust	PM10	0.00106	0.00010	0.00128	0.00048	0.00312	0.00249	0.01201	0.00170	0.06208	0.02293	0.03765	0.01982	0.01905	0.01226	0.01193	0.00529	0.00000	0.00004	0.01753	0.00584	0.13239	0.03611	0.01345
RESQ2550	AADust	PM10	0.00126	0.00130	0.00275	0.00033	0.00291	0.00030	0.02044	0.00824	0.08281	0.01043	0.04821	0.00812	0.02598	0.01649	0.02116	0.01848	0.00000	0.00003	0.01780	0.00676	0.17218	0.01287	0.02933

PNO	Mnemonic	SIZE	ECU	Al	AlU	Si	SiU	S	SU	Cl	ClU	K	KU	Ca	CaU	Ti	TiU	V	VU	Mn	MnU	Fe	FeU	Co	CoU
20013	Brake_1	PM2.5	0.00499	0.00050	0.00010	0.00432	0.00033	0.00761	0.00055	0.00020	0.00021	0.00041	0.00005	0.00140	0.00012	0.00012	0.00402	0.00000	0.00170	0.00467	0.00045	0.65766	0.04666	0.00000	0.00973
20014	Brake_2	PM2.5	0.00498	0.00060	0.00007	0.00434	0.00032	0.00539	0.00039	0.00032	0.00005	0.00052	0.00005	0.00129	0.00010	0.00001	0.00340	0.00000	0.00144	0.00579	0.00049	0.59290	0.04195	0.00064	0.00877
20015	Brake_3	PM2.5	0.00823	0.00667	0.00049	0.01937	0.00138	0.02352	0.00167	0.00000	0.00052	0.00455	0.00034	0.03420	0.00242	0.00000	0.01556	0.00000	0.00614	0.00181	0.00020	0.19954	0.01412	0.00018	0.00295
20016	Brake_C	PM2.5	0.04456	0.00259	0.00354	0.00934	0.00868	0.01217	0.00989	0.00017	0.00033	0.00182	0.00236	0.01230	0.01897	0.00004	0.00948	0.00117	0.00377	0.00409	0.00205	0.48337	0.24792	0.00027	0.00775
ARB1	Brake_D	PM10		0.00000	0.00734	0.01127	0.00238	0.02326	0.00980			0.01369	0.00463	0.00936	0.00445	0.04820	0.02245	0.00000	0.00009	0.00744	0.00997	0.15062	0.02798	0.00026	0.00023
ARB2	Brake_E	PM10		0.00749	0.00734	0.01106	0.00425	0.02786	0.00664			0.00912	0.00942	0.01328	0.00613	0.04121	0.03952	0.00020	0.00019	0.00187	0.00012	0.20914	0.01997	0.00023	0.00020
ARB3	Brake_F	PM10		0.00000	0.00734	0.00942	0.00807	0.02263	0.01048			0.01290	0.00178	0.02218	0.02766	0.06098	0.00324	0.00000	0.00100	0.00077	0.00009	0.11414	0.01052	0.00022	0.00002
ARB4	Brake_G	PM10		0.00000	0.00734	0.00521	0.00006	0.00330	0.00003			0.00000	0.00100	0.00000	0.00100	0.00078	0.00001	0.00011	0.00015	0.00422	0.00075	0.46595	0.02513	0.00138	0.00020
20017	Tire_1	PM2.5	0.02517	0.02721	0.00212	0.02993	0.00232	0.01907	0.00144	0.00133	0.00027	0.00557	0.00046	0.01600	0.00122	0.00206	0.00059	0.00000	0.00072	0.00106	0.00013	0.18321	0.01355	0.00000	0.00273
20018	Tire_2	PM2.5	0.05237	0.02380	0.00226	0.02904	0.00270	0.01939	0.00172	0.00063	0.00120	0.00632	0.00073	0.01745	0.00159	0.00241	0.00396	0.00002	0.00162	0.00090	0.00018	0.22076	0.01898	0.00031	0.00331
25346	WS-L	PM2.5	0.18850	0.00183	0.00059	0.04276	0.01121	0.04319	0.03678	0.00297	0.00317	0.00106	0.00069	0.00765	0.00403	0.00005	0.00076	0.00000	0.00500	0.00010	0.00006	0.00681	0.00433	0.00000	0.01000
25347	CS-L	PM2.5	0.12170	0.00162	0.00081	0.03697	0.00980	0.03833	0.02871	0.00467	0.00550	0.00096	0.00072	0.00736	0.00397	0.00005	0.00038	0.00000	0.00500	0.00004	0.00003	0.00630	0.00551	0.00000	0.01000
25348	WS-H	PM2.5	0.12452	0.00094	0.00124	0.05087	0.07358	0.00926	0.00929	0.00061	0.00042	0.00034	0.00036	0.00742	0.00553	0.00002	0.00078	0.00000	0.00500	0.00003	0.00005	0.00307	0.00265	0.00000	0.01000
25349	CS-H	PM2.5	0.07321	0.00049	0.00026	0.03556	0.04536	0.01403	0.02035	0.00183	0.00283	0.00042	0.00043	0.00583	0.00384	0.00002	0.00036	0.00000	0.00500	0.00003	0.00003	0.00290	0.00289	0.00000	0.01000
25350	WS-BC	PM2.5	0.15073	0.00082	0.00073	0.07576	0.04460	0.02037	0.01381	0.00126	0.00033	0.00042	0.00017	0.01625	0.03319	0.00000	0.00064	0.00000	0.00500	0.00002	0.00004	0.00435	0.00237	0.00000	0.01000
25351	CS-BC	PM2.5	0.14315	0.00074	0.00031	0.04534	0.02149	0.03484	0.02859	0.00361	0.00215	0.00028	0.00015	0.00270	0.00130	0.00005	0.00028	0.00000	0.00500	0.00003	0.00002	0.00193	0.00056	0.00000	0.01000
25352	MDD-MIX	PM2.5	0.08315	0.00265	0.00302	0.01202	0.00696	0.03274	0.02017	0.00151	0.00060	0.00142	0.00161	0.00764	0.00491	0.00016	0.00127	0.00000	0.00500	0.00000	0.00009	0.00646	0.00574	0.00000	0.01000
25353	HHDD-HW	PM2.5	0.25732	0.00140	0.00122	0.01198	0.00120	0.01011	0.00483	0.00027	0.00025	0.00084	0.00069	0.00737	0.00219	0.00021	0.00090	0.00000	0.00500	0.00003	0.00006	0.00454	0.00064	0.00000	0.01000
25354	HHDD-HCS	PM2.5	0.08099	0.00141	0.00062	0.01209	0.00136	0.00765	0.00165	0.00078	0.00038	0.00114	0.00012	0.00632	0.00063	0.00009	0.00076	0.00000	0.00500	0.00001	0.00006	0.00868	0.00449	0.00000	0.01000
25355	HHDD-MIX	PM2.5	0.17285	0.00140	0.00089	0.01203	0.00120	0.00888	0.00359	0.00052	0.00039	0.00099	0.00049	0.00685	0.00158	0.00015	0.00059	0.00000	0.00500	0.00002	0.00004	0.00661	0.00370	0.00000	0.01000
25356	DIESEL	PM2.5	0.14858	0.00172	0.00171	0.01203	0.00365	0.01484	0.01197	0.00077	0.00053	0.00110	0.00091	0.00705	0.00282	0.00015	0.00091	0.00000	0.00500	0.00001	0.00007	0.00657	0.00410	0.00000	0.01000
25357	GAS	PM2.5	0.13364	0.00107	0.00074	0.04788	0.04112	0.02667	0.02478	0.00249	0.00298	0.00058	0.00047	0.00787	0.01403	0.00003	0.00057	0.00000	0.00500	0.00004	0.00004	0.00423	0.00342	0.00000	0.01000
Copper1	COTIRE1	TSP	0.00002	0.00171	0.00012	0.06113	0.00177	0.00000	0.01000	0.00000	0.00100	0.00038	0.00007	0.00111	0.00015	0.00010	0.00001	0.00000	0.00000	0.00002	0.00000	0.00122	0.00003	0.00000	0.00000
Copper2	COTIRE2	TSP	0.00003	0.00177	0.00012	0.06016	0.00174	0.00000	0.01000	0.00000	0.00100	0.00043	0.00008	0.00122	0.00016	0.00011	0.00001	0.00000	0.00000	0.00001	0.00000	0.00118	0.00003	0.00000	0.00000
Michelin1	MITIRE1	TSP	0.00003	0.00044	0.00004	0.00590	0.00019	0.00000	0.01000	0.00000	0.00100	0.00034	0.00006	0.00070	0.00013	0.00006	0.00000	0.00000	0.00000	0.00001	0.00000	0.00206	0.00005	0.00000	0.00000
Michelin2	MITIRE2	TSP	0.00003	0.00045	0.00004	0.00615	0.00020	0.00000	0.01000	0.00000	0.00100	0.00042	0.00007	0.00077	0.00013	0.00006	0.00000	0.00000	0.00000	0.00001	0.00000	0.00208	0.00005	0.00000	0.00000
Copper	COTIRE	TSP	0.02930	0.00174	0.00012	0.06065	0.00175	0.00000	0.01000	0.00000	0.00100	0.00040	0.00007	0.00116	0.00016	0.00010	0.00001	0.00000	0.00000	0.00001	0.00000	0.00120	0.00003	0.00000	0.00000
Michelin	MITIRE	TSP	0.02351	0.00044	0.00004	0.00603	0.00019	0.00000	0.01000	0.00000	0.00100	0.00038	0.00007	0.00074	0.00013	0.00006	0.00000	0.00000	0.00000	0.00001	0.00000	0.00207	0.00005	0.00000	0.00000
MiCo	TIRE	TSP	0.10396	0.00109	0.00075	0.03334	0.03154	0.00000	0.01000	0.00000	0.00100	0.00039	0.00007	0.00095	0.00025	0.00008	0.00003	0.00000	0.00000	0.00001	0.00000	0.00164	0.00050	0.00000	0.00000
RESQ2485	AQ Dust	PM2.5	0.00247	0.01441	0.00196	0.05643	0.00419	0.00125	0.00010	0.00045	0.00005	0.00481	0.00036	0.02861	0.00213	0.00238	0.00018	0.00000	0.00000	0.00050	0.00007	0.02176	0.00163	0.00014	0.00002
RESQ2489	MA Dust	PM2.5	0.00676	0.01197	0.00384	0.04723	0.00413	0.00134	0.00014	0.00022	0.00008	0.00419	0.00037	0.00940	0.00086	0.00129	0.00013	0.00007	0.00001	0.00026	0.00014	0.01642	0.00150	0.00013	0.00004
RESQ2493	CC Dust	PM2.5	0.00234	0.02285	0.00254	0.07361	0.00554	0.00427	0.00032	0.00073	0.00007	0.00864	0.00065	0.02706	0.00204	0.00244	0.00019	0.00001	0.00000	0.00034	0.00007	0.02353	0.00178	0.00014	0.00002
RESQ2497	AT Dust	PM2.5	0.00381	0.01889	0.00293	0.05270	0.00416	0.00286	0.00023	0.00024	0.00005	0.00563	0.00045	0.00843	0.00069	0.00279	0.00022	0.00000	0.00000	0.00034	0.00010	0.02324	0.00186	0.00008	0.00003
RESQ2520	Dust	PM2.5	0.02091	0.01703	0.00483	0.05749	0.01139	0.00243	0.00143	0.00041	0.00024	0.00582	0.00197	0.01837	0.01095	0.00223	0.00065	0.00002	0.00003	0.00036	0.00010	0.02124	0.00330	0.00012	0.00003
RESQ2540	MCDust	PM2.5	0.03218	0.01741	0.00770	0.06042	0.01865	0.00280	0.00207	0.00047	0.00036	0.00642	0.00315	0.01823	0.01249	0.00187	0.00081	0.00004	0.00004	0.00030	0.00011	0.01997	0.00503	0.00013	0.00004
RESQ2560	AADust	PM2.5	0.01026	0.01665	0.00317	0.05456	0.00417	0.00206	0.00113	0.00034	0.00015	0.00522	0.00058	0.01852	0.01427	0.00258	0.00029	0.00000	0.00000	0.00042	0.00011	0.02250	0.00174	0.00011	0.00004
RESQ2487	AQDust	PM10	0.00145	0.02658	0.00232	0.08825	0.00643	0.00248	0.00018	0.00077	0.00006	0.00790	0.00058	0.05478	0.00399	0.00341	0.00025	0.00003	0.00000	0.00086	0.00008	0.03848	0.00281	0.00017	0.00002
RESQ2491	MADust	PM10	0.00122	0.02595	0.00350	0.09186	0.00740	0.00294	0.00024	0.00044	0.00007	0.00852	0.00069	0.02262	0.00184	0.00410	0.00033	0.00000	0.00001	0.00069	0.00012	0.03469	0.00282	0.00011	0.00003
RESQ2495	CCDust	PM10	0.00163	0.04383	0.00363	0.13467	0.00996	0.00775	0.00058	0.00122	0.00010	0.01555	0.00115	0.04851	0.00359	0.00412	0.00031	0.00000	0.00000	0.00087	0.00009	0.04148	0.00307	0.00023	0.00003
RESQ2499	ATDust	PM10	0.00316	0.04575	0.00385	0.12319	0.00919	0.00646	0.00048	0.00043	0.00005	0.01346	0.00100	0.01659	0.00125	0.00479	0.00036	0.00012	0.00001	0.00083	0.00009	0.05022	0.00375	0.00022	0.00003
RESQ2510	Dust	PM10	0.01393	0.03553	0.01072	0.10949	0.02298	0.00491	0.00260	0.00071	0.00038	0.01136	0.00374	0.03562	0.01883	0.00410	0.00056	0.00004	0.00005	0.00081	0.00009	0.04122	0.00661	0.00018	0.00005
RESQ2530	MCDust	PM10	0.00924	0.03489	0.01264	0.11327	0.03028	0.00535	0.00340	0.00083	0.00056	0.01204	0.00497	0.03557	0.01830	0.00411	0.00032	0.00000	0.00000	0.00078	0.00012	0.03809	0.00480	0.00017	0.00009
RESQ2550	AADust	PM10	0.01565	0.03617	0.01355	0.10572	0.02471	0.00447	0.00281	0.00060	0.00024	0.01068	0.00393	0.03568	0.02700	0.00410	0.00097	0.00007	0.00006	0.00085	0.00008	0.04435	0.00831	0.00019	0.00003

PNO	Mnemonic	SIZE	Ni	NiU	Cu	CuU	Zn	ZnU	As	AsU	Se	SeU	Br	BrU	Rb	RbU	Sr	SrU	Sb	SbU	Ba	BaU	Pb	PbU	FLUORA
20013	Brake_1	PM2.5	0.00000	0.00021	0.00078	0.00006	0.00017	0.00002	0.00000	0.00009	0.00000	0.00002	0.00000	0.00003	0.00007	0.00001	0.00182	0.00013	0.00010	0.00041	0.03393	0.00249	0.00047	0.00004	0.00001
20014	Brake_2	PM2.5	0.00000	0.00019	0.00049	0.00004	0.00019	0.00001	0.00000	0.00014	0.00001	0.00000	0.00001	0.00002	0.00015	0.00001	0.00088	0.00006	0.00000	0.00022	0.02897	0.00208	0.00091	0.00007	0.00001
20015	Brake_3	PM2.5	0.00000	0.00007	0.00042	0.00003	0.01389	0.00098	0.00000	0.00003	0.00002	0.00000	0.00001	0.00002	0.00007	0.00001	0.00202	0.00014	0.00004	0.00017	0.13481	0.00955	0.00016	0.00002	0.00001
20016	Brake_C	PM2.5	0.00000	0.00017	0.00057	0.00019	0.00475	0.00792	0.00000	0.00010	0.00001	0.00001	0.00000	0.00002	0.00010	0.00004	0.00157	0.00060	0.00005	0.00029	0.06590	0.05973	0.00051	0.00038	0.00001
ARB1	Brake_D	PM10	0.00014	0.00015	0.04888	0.05071	0.00000	0.00100																	
ARB2	Brake_E	PM10	0.00005	0.00004	0.00060	0.00025	0.00293	0.00472																	
ARB3	Brake_F	PM10	0.00012	0.00005	0.01717	0.01402	0.00000	0.00100																	
ARB4	Brake_G	PM10	0.00004	0.00005	0.00035	0.00003	0.00000	0.00100																	
20017	Tire_1	PM2.5	0.00000	0.00011	0.01034	0.00077	0.03363	0.00249	0.00000	0.00016	0.00000	0.00008	0.00015	0.00003	0.00001	0.00007	0.01075	0.00080	0.00090	0.00122	0.00000	0.00430	0.00026	0.00008	0.00019
20018	Tire_2	PM2.5	0.00000	0.00018	0.01889	0.00163	0.01829	0.00158	0.00000	0.00036	0.00000	0.00019	0.00023	0.00008	0.00000	0.00016	0.01511	0.00131	0.00000	0.00279	0.00000	0.01005	0.00031	0.00055	0.00037
25346	WS-L	PM2.5	0.00019	0.00008	0.00053	0.00018	0.00432	0.00212	0.00000	0.00007	0.00000	0.00004	0.00064	0.00048	0.00003	0.00003	0.00002	0.00003	0.00000	0.01000	0.00362	0.00346	0.00039	0.00029	0.00353
25347	CS-L	PM2.5	0.00017	0.00012	0.00054	0.00029	0.00475	0.00278	0.00000	0.00003	0.00001	0.00002	0.00076	0.00066	0.00000	0.00002	0.00001	0.00002	0.00000	0.01000	0.00151	0.00130	0.00030	0.00027	0.00180
25348	WS-H	PM2.5	0.00004	0.00003	0.00063	0.00094	0.00462	0.00343	0.00001	0.00007	0.00000	0.00004	0.00005	0.00008	0.00000	0.00003	0.00001	0.00003	0.00000	0.01000	0.00263	0.00471	0.00035	0.00036	0.00531
25349	CS-H	PM2.5	0.00003	0.00002	0.00052	0.00059	0.00434	0.00367	0.00000	0.00003	0.00000	0.00002	0.00010	0.00016	0.00000	0.00001	0.00001	0.00002	0.00000	0.01000	0.00047	0.00091	0.00025	0.00024	0.00116
25350	WS-BC	PM2.5	0.00005	0.00003	0.00065	0.00059	0.00522	0.00704	0.00000	0.00006	0.00000	0.00003	0.00024	0.00018	0.00000	0.00003	0.00001	0.00003	0.00000	0.01000	0.00240	0.00187	0.00013	0.00009	0.00212
25351	CS-BC	PM2.5	0.00004	0.00002	0.00026	0.00014	0.00276	0.00341	0.00000	0.00003	0.00000	0.00001	0.00046	0.00039	0.00000	0.00002	0.00001	0.00001	0.00000	0.01000	0.00040	0.00072	0.00013	0.00004	0.00126
25352	MDD-MIX	PM2.5	0.00000	0.00005	0.00004	0.00006	0.00314	0.00124	0.00001	0.00011	0.00003	0.00006	0.00175	0.00142	0.00001	0.00006	0.00003	0.00006	0.00000	0.01000	0.00576	0.00432	0.00001	0.00017	0.00062
25353	HHDD-HW	PM2.5	0.00000	0.00004	0.00017	0.00003	0.00373	0.00037	0.00001	0.00008	0.00003	0.00004	0.00001	0.00004	0.00001	0.00003	0.00002	0.00004	0.00000	0.01000	0.00072	0.00230	0.00007	0.00012	0.00166
25354	HHDD-HCS	PM2.5	0.00002	0.00003	0.00022	0.00009	0.00424	0.00093	0.00000	0.00006	0.00001	0.00003	0.00003	0.00003	0.00000	0.00003	0.00004	0.00003	0.00000	0.01000	0.00280	0.00188	0.00015	0.00010	0.00154
25355	HHDD-MIX	PM2.5	0.00001	0.00002	0.00020	0.00007	0.00398	0.00070	0.00000	0.00005	0.00002	0.00003	0.00002	0.00003	0.00001	0.00002	0.00003	0.00003	0.00000	0.01000	0.00176	0.00149	0.00011	0.00008	0.00160
25356	DIESEL	PM2.5	0.00001	0.00004	0.00016	0.00008	0.00377	0.00087	0.00000	0.00008	0.00002	0.00004	0.00045	0.00086	0.00001	0.00004	0.00003	0.00004	0.00000	0.01000	0.00276	0.00272	0.00009	0.00012	0.00135
25357	GAS	PM2.5	0.00009	0.00007	0.00052	0.00054	0.00433	0.00406	0.00000	0.00005	0.00000	0.00003	0.00038	0.00038	0.00001	0.00002	0.00001	0.00002	0.00000	0.01000	0.00184	0.00260	0.00026	0.00024	0.00253
Copper1	COTIRE1	TSP	0.00000	0.00000	0.00003	0.00000	0.00975	0.00015	0.00000	0.00000	0.00000	0.00000	0.00000	0.00100	0.00000	0.00000	0.00001	0.00000	0.00001	0.00000	0.00006	0.00000	0.00001	0.00000	0.00000
Copper2	COTIRE2	TSP	0.00000	0.00000	0.00003	0.00000	0.00949	0.00014	0.00000	0.00000	0.00000	0.00000	0.00000	0.00100	0.00000	0.00000	0.00001	0.00000	0.00001	0.00000	0.00006	0.00000	0.00001	0.00000	0.00000
Michelin1	MITIRE1	TSP	0.00000	0.00000	0.00004	0.00000	0.00497	0.00007	0.00000	0.00000	0.00000	0.00000	0.00000	0.00100	0.00000	0.00000	0.00000	0.00000	0.00001	0.00000	0.00004	0.00000	0.00000	0.00000	0.00000
Michelin2	MITIRE2	TSP	0.00000	0.00000	0.00004	0.00000	0.00496	0.00007	0.00000	0.00000	0.00000	0.00000	0.00000	0.00100	0.00000	0.00000	0.00000	0.00000	0.00001	0.00000	0.00004	0.00000	0.00000	0.00000	0.00000
Copper	COTIRE	TSP	0.00000	0.00000	0.00003	0.00000	0.00962	0.00018	0.00000	0.00000	0.00000	0.00000	0.00000	0.00100	0.00000	0.00000	0.00001	0.00000	0.00001	0.00000	0.00006	0.00000	0.00001	0.00000	0.00000
Michelin	MITIRE	TSP	0.00000	0.00000	0.00004	0.00000	0.00496	0.00007	0.00000	0.00000	0.00000	0.00000	0.00000	0.00100	0.00000	0.00000	0.00000	0.00000	0.00001	0.00000	0.00004	0.00000	0.00000	0.00000	0.00000
MiCo	TIRE	TSP	0.00000	0.00000	0.00003	0.00000	0.00729	0.00269	0.00000	0.00000	0.00000	0.00000	0.00000	0.00100	0.00000	0.00000	0.00000	0.00000	0.00001	0.00000	0.00005	0.00001	0.00000	0.00000	0.00000
RESQ2485	AQ Dust	PM2.5	0.00008	0.00001	0.00028	0.00003	0.00447	0.00033	0.00000	0.00003	0.00000	0.00004	0.00006	0.00004	0.00002	0.00004	0.00015	0.00003	0.00005	0.00012	0.00019	0.00038	0.00000	0.00008	0.00000
RESQ2489	MA Dust	PM2.5	0.00011	0.00002	0.00072	0.00008	0.00128	0.00013	0.00006	0.00006	0.00008	0.00009	0.00000	0.00010	0.00013	0.00009	0.00028	0.00008	0.00055	0.00028	0.00041	0.00086	0.00008	0.00018	0.00000
RESQ2493	CC Dust	PM2.5	0.00011	0.00001	0.00102	0.00008	0.00140	0.00011	0.00000	0.00003	0.00007	0.00004	0.00006	0.00005	0.00007	0.00004	0.00033	0.00004	0.00044	0.00014	0.00123	0.00044	0.00022	0.00009	0.00003
RESQ2497	AT Dust	PM2.5	0.00014	0.00002	0.00011	0.00003	0.00116	0.00011	0.00007	0.00004	0.00010	0.00006	0.00008	0.00007	0.00004	0.00006	0.00004	0.00005	0.00018	0.00019	0.00000	0.00058	0.00021	0.00012	0.00000
RESQ2520	Dust	PM2.5	0.00011	0.00002	0.00053	0.00042	0.00208	0.00160	0.00003	0.00004	0.00006	0.00006	0.00005	0.00007	0.00006	0.00006	0.00020	0.00013	0.00031	0.00023	0.00046	0.00060	0.00013	0.00013	0.00001
RESQ2540	MCDust	PM2.5	0.00011	0.00002	0.00087	0.00022	0.00134	0.00012	0.00003	0.00005	0.00008	0.00007	0.00003	0.00008	0.00010	0.00007	0.00030	0.00006	0.00050	0.00022	0.00082	0.00069	0.00015	0.00014	0.00002
RESQ2560	AADust	PM2.5	0.00011	0.00004	0.00020	0.00012	0.00282	0.00234	0.00004	0.00005	0.00005	0.00007	0.00007	0.00006	0.00003	0.00005	0.00010	0.00008	0.00012	0.00016	0.00009	0.00049	0.00010	0.00015	0.00000
RESQ2487	AQDust	PM10	0.00005	0.00001	0.00066	0.00005	0.00724	0.00053	0.00000	0.00002	0.00000	0.00003	0.00000	0.00003	0.00006	0.00003	0.00032	0.00003	0.00001	0.00009	0.00045	0.00029	0.00022	0.00006	0.00000
RESQ2491	MADust	PM10	0.00015	0.00002	0.00169	0.00014	0.00260	0.00022	0.00042	0.00006	0.00003	0.00007	0.00000	0.00008	0.00000	0.00007	0.00059	0.00007	0.00089	0.00022	0.00038	0.00065	0.00028	0.00014	0.00004
RESQ2495	CCDust	PM10	0.00008	0.00001	0.00190	0.00014	0.00224	0.00017	0.00002	0.00002	0.00000	0.00004	0.00004	0.00004	0.00005	0.00004	0.00066	0.00006	0.00034	0.00012	0.00323	0.00044	0.00018	0.00008	0.00000
RESQ2499	ATDust	PM10	0.00004	0.00001	0.00048	0.00004	0.00229	0.00017	0.00000	0.00003	0.00012	0.00004	0.00005	0.00005	0.00003	0.00004	0.00022	0.00004	0.00000	0.00013	0.00172	0.00042	0.00036	0.00009	0.00000
RESQ2510	Dust	PM10	0.00008	0.00005	0.00118	0.00072	0.00359	0.00244	0.00011	0.00021	0.00004	0.00005	0.00002	0.00005	0.00003	0.00005	0.00045	0.00021	0.00031	0.00042	0.00145	0.00134	0.00026	0.00010	0.00001
RESQ2530	MCDust	PM10	0.00012	0.00006	0.00180	0.00015	0.00242	0.00025	0.00022	0.00029	0.00002	0.00005	0.00002	0.00006	0.00002	0.00005	0.00063	0.00007	0.00062	0.00039	0.00180	0.00201	0.00023	0.00011	0.00002
RESQ2550	AADust	PM10	0.00005	0.00001	0.00057	0.00013	0.00477	0.00350	0.00000	0.00002	0.00006	0.00008	0.00002	0.00004	0.00004	0.00004	0.00027	0.00007	0.00001	0.00011	0.00109	0.00090	0.00029	0.00010	0.00000

PNO	Mnemonic	SIZE	FLUORAU	PYRENE	PYRENEU	BAPYRN	BAPYRNU	BEPYRN	BEPYRNU	INCDPY	INCDPYU	BGHIPE	BGHIPEU	CORONE	CORONEU	RETENE	RETENEU	hop17	hop17U	hop19	hop19U	hop25	hop25U	hop26	hop26U
20013	Brake_1	PM2.5	0.00001	0.00002	0.00001	0.00001	0.00002	0.00000	0.00001	0.00000	0.00002	0.00000	0.00002	0.00000	0.00001	0.00000	0.00001	0.00007	0.00004	0.00001	0.00001	0.00000	0.00001	0.00000	0.00001
20014	Brake_2	PM2.5	0.00001	0.00001	0.00000	0.00000	0.00001	0.00000	0.00000	0.00000	0.00001	0.00000	0.00001	0.00000	0.00000	0.00000	0.00000	0.00020	0.00011	0.00003	0.00001	0.00000	0.00000	0.00000	0.00000
20015	Brake_3	PM2.5	0.00000	0.00001	0.00000	0.00000	0.00001	0.00001	0.00000	0.00001	0.00001	0.00000	0.00001	0.00000	0.00000	0.00000	0.00000	0.00005	0.00003	0.00002	0.00001	0.00000	0.00000	0.00000	0.00000
20016	Brake_C	PM2.5	0.00001	0.00001	0.00000	0.00000	0.00001	0.00000	0.00000	0.00001	0.00001	0.00000	0.00002	0.00000	0.00000	0.00000	0.00001	0.00010	0.00008	0.00002	0.00001	0.00000	0.00000	0.00000	0.00000
ARB1	Brake_D	PM10																							
ARB2	Brake_E	PM10																							
ARB3	Brake_F	PM10																							
ARB4	Brake_G	PM10																							
20017	Tire_1	PM2.5	0.00006	0.00047	0.00005	0.00000	0.00010	0.00000	0.00003	0.00000	0.00008	0.00014	0.00011	#######	0.00010	0.00000	0.00004	0.00299	0.00162	0.00037	0.00013	0.00000	0.00006	0.00000	0.00006
20018	Tire_2	PM2.5	0.00012	0.00129	0.00013	0.00000	0.00019	0.00000	0.00006	0.00004	0.00016	0.00026	0.00021	0.00000	0.00006	0.00000	0.00008	0.00678	0.00368	0.00231	0.00072	0.00000	0.00006	0.00027	0.00033
25346	WS-L	PM2.5	0.00424	0.00420	0.00547	0.00006	0.00008	0.00019	0.00005	0.00056	0.00046	0.00144	0.00099	0.00119	0.00089	0.00007	0.00011	0.00002	0.00006	0.00000	0.00000	0.00000	0.00001	0.00000	0.00002
25347	CS-L	PM2.5	0.00206	0.00226	0.00301	0.00011	0.00011	0.00020	0.00011	0.00050	0.00031	0.00134	0.00078	0.00102	0.00066	0.00004	0.00004	0.00003	0.00005	0.00000	0.00000	0.00001	0.00001	0.00001	0.00002
25348	WS-H	PM2.5	0.00563	0.00612	0.00633	0.00010	0.00011	0.00013	0.00009	0.00009	0.00009	0.00022	0.00025	0.00029	0.00023	0.00001	0.00002	0.00031	0.00055	0.00132	0.00150	0.00003	0.00008	0.00004	0.00010
25349	CS-H	PM2.5	0.00209	0.00121	0.00216	0.00013	0.00012	0.00014	0.00012	0.00016	0.00010	0.00045	0.00031	0.00045	0.00049	0.00000	0.00000	0.00042	0.00032	0.00069	0.00087	0.00005	0.00005	0.00008	0.00007
25350	WS-BC	PM2.5	0.00047	0.00237	0.00181	0.00017	0.00025	0.00016	0.00017	0.00037	0.00035	0.00128	0.00153	0.00130	0.00188	0.00013	0.00030	0.00007	0.00006	0.00045	0.00078	0.00000	0.00001	0.00001	0.00002
25351	CS-BC	PM2.5	0.00053	0.00106	0.00032	0.00023	0.00013	0.00020	0.00007	0.00037	0.00012	0.00093	0.00013	0.00076	0.00020	0.00000	0.00001	0.00003	0.00005	0.00021	0.00037	0.00000	0.00000	0.00001	0.00001
25352	MDD-MIX	PM2.5	0.00010	0.00093	0.00024	0.00000	0.00002	0.00000	0.00001	0.00000	0.00002	0.00000	0.00002	0.00000	0.00001	0.00000	0.00001	0.00002	0.00002	0.00005	0.00006	0.00000	0.00002	0.00000	0.00002
25353	HHDD-HW	PM2.5	0.00110	0.00177	0.00114	0.00001	0.00002	0.00001	0.00002	0.00000	0.00001	0.00000	0.00002	0.00000	0.00001	0.00000	0.00001	0.00013	0.00008	0.00006	0.00003	0.00000	0.00001	0.00000	0.00001
25354	HHDD-HCS	PM2.5	0.00103	0.00179	0.00108	0.00002	0.00004	0.00001	0.00001	0.00000	0.00001	0.00000	0.00001	0.00000	0.00000	0.00001	0.00001	0.00017	0.00009	0.00008	0.00004	0.00000	0.00000	0.00000	0.00000
25355	HHDD-MIX	PM2.5	0.00099	0.00178	0.00103	0.00002	0.00003	0.00001	0.00001	0.00000	0.00001	0.00000	0.00001	0.00000	0.00000	0.00000	0.00001	0.00015	0.00008	0.00007	0.00004	0.00000	0.00000	0.00000	0.00000
25356	DIESEL	PM2.5	0.00090	0.00157	0.00095	0.00001	0.00003	0.00001	0.00001	0.00000	0.00001	0.00000	0.00002	0.00000	0.00000	0.00000	0.00001	0.00012	0.00008	0.00006	0.00005	0.00000	0.00001	0.00000	0.00001
25357	GAS	PM2.5	0.00313	0.00287	0.00381	0.00013	0.00014	0.00017	0.00011	0.00034	0.00028	0.00094	0.00083	0.00084	0.00092	0.00004	0.00013	0.00015	0.00026	0.00045	0.00079	0.00002	0.00004	0.00002	0.00005
Copper1	COTIRE1	TSP	0.00000	0.00000	0.00000	0.00000	0.00000	0.00000	0.00000	0.00000	0.00000	0.00000	0.00000	0.00000	0.00000	0.00000	0.00000	0.00000	0.00000	0.00000	0.00000	0.00000	0.00000	0.00000	0.00000
Copper2	COTIRE2	TSP	0.00000	0.00000	0.00000	0.00000	0.00000	0.00000	0.00000	0.00000	0.00000	0.00000	0.00000	0.00000	0.00000	0.00000	0.00000	0.00000	0.00000	0.00000	0.00000	0.00000	0.00000	0.00000	0.00000
Michelin1	MITIRE1	TSP	0.00000	0.00000	0.00000	0.00000	0.00000	0.00000	0.00000	0.00000	0.00000	0.00000	0.00000	0.00000	0.00000	0.00000	0.00000	0.00000	0.00000	0.00000	0.00000	0.00000	0.00000	0.00000	0.00000
Michelin2	MITIRE2	TSP	0.00000	0.00000	0.00000	0.00000	0.00000	0.00000	0.00000	0.00000	0.00000	0.00000	0.00000	0.00000	0.00000	0.00000	0.00000	0.00000	0.00000	0.00000	0.00000	0.00000	0.00000	0.00000	0.00000
Copper	COTIRE	TSP	0.00000	0.00000	0.00000	0.00000	0.00000	0.00000	0.00000	0.00000	0.00000	0.00000	0.00000	0.00000	0.00000	0.00000	0.00000	0.00000	0.00000	0.00000	0.00000	0.00000	0.00000	0.00000	0.00000
Michelin	MITIRE	TSP	0.00000	0.00000	0.00000	0.00000	0.00000	0.00000	0.00000	0.00000	0.00000	0.00000	0.00000	0.00000	0.00000	0.00000	0.00000	0.00000	0.00000	0.00000	0.00000	0.00000	0.00000	0.00000	0.00000
MiCo	TIRE	TSP	0.00000	0.00000	0.00000	0.00000	0.00000	0.00000	0.00000	0.00000	0.00000	0.00000	0.00000	0.00000	0.00000	0.00000	0.00000	0.00000	0.00000	0.00000	0.00000	0.00000	0.00000	0.00000	0.00000
RESQ2485	AQ Dust	PM2.5	0.00000	0.00000	0.00000	0.00000	0.00000	0.00000	0.00000	0.00000	0.00000	0.00000	0.00000	0.00000	0.00000	0.00000	0.00000	0.00000	0.00000	0.00000	0.00000	0.00000	0.00000	0.00000	0.00000
RESQ2489	MA Dust	PM2.5	0.00000	0.00000	0.00000	0.00000	0.00000	0.00000	0.00000	0.00000	0.00000	0.00000	0.00000	0.00000	0.00000	0.00000	0.00000	0.00000	0.00000	0.00000	0.00000	0.00000	0.00000	0.00000	0.00000
RESQ2493	CC Dust	PM2.5	0.00000	0.00001	0.00000	0.00000	0.00000	0.00000	0.00000	0.00000	0.00000	0.00000	0.00000	0.00000	0.00000	0.00000	0.00000	0.00000	0.00000	0.00001	0.00000	0.00000	0.00000	0.00000	0.00000
RESQ2497	AT Dust	PM2.5	0.00000	0.00000	0.00000	0.00000	0.00000	0.00000	0.00000	0.00000	0.00000	0.00000	0.00000	0.00000	0.00000	0.00000	0.00000	0.00001	0.00000	0.00000	0.00000	0.00000	0.00000	0.00000	0.00000
RESQ2520	Dust	PM2.5	0.00002	0.00000	0.00001	0.00000	0.00000	0.00000	0.00000	0.00000	0.00000	0.00000	0.00000	0.00000	0.00000	0.00000	0.00000	0.00000	0.00000	0.00000	0.00000	0.00000	0.00000	0.00000	0.00000
RESQ2540	MCDust	PM2.5	0.00002	0.00001	0.00001	0.00000	0.00000	0.00000	0.00000	0.00000	0.00000	0.00000	0.00000	0.00000	0.00000	0.00000	0.00000	0.00000	0.00000	0.00000	0.00000	0.00000	0.00000	0.00000	0.00000
RESQ2560	AADust	PM2.5	0.00000	0.00000	0.00000	0.00000	0.00000	0.00000	0.00000	0.00000	0.00000	0.00000	0.00000	0.00000	0.00000	0.00000	0.00000	0.00000	0.00001	0.00000	0.00000	0.00000	0.00000	0.00000	0.00000
RESQ2487	AQDust	PM10	0.00000	0.00000	0.00000	0.00000	0.00000	0.00000	0.00000	0.00000	0.00000	0.00000	0.00000	0.00000	0.00000	0.00000	0.00000	0.00000	0.00000	0.00000	0.00000	0.00000	0.00000	0.00000	0.00000
RESQ2491	MADust	PM10	0.00000	0.00002	0.00000	0.00000	0.00000	0.00001	0.00000	0.00000	0.00000	0.00000	0.00000	0.00000	0.00000	0.00000	0.00000	0.00000	0.00000	0.00001	0.00000	0.00000	0.00000	0.00000	0.00000
RESQ2495	CCDust	PM10	0.00000	0.00000	0.00000	0.00000	0.00000	0.00000	0.00000	0.00000	0.00000	0.00000	0.00000	0.00000	0.00000	0.00000	0.00000	0.00000	0.00000	0.00000	0.00000	0.00000	0.00000	0.00000	0.00000
RESQ2499	ATDust	PM10	0.00000	0.00000	0.00000	0.00001	0.00000	0.00000	0.00000	0.00000	0.00000	0.00000	0.00000	0.00000	0.00000	0.00000	0.00000	0.00001	0.00000	0.00000	0.00000	0.00000	0.00000	0.00000	0.00000
RESQ2510	Dust	PM10	0.00002	0.00000	0.00001	0.00000	0.00000	0.00000	0.00000	0.00000	0.00000	0.00000	0.00000	0.00000	0.00000	0.00000	0.00000	0.00000	0.00000	0.00000	0.00000	0.00000	0.00000	0.00000	0.00000
RESQ2530	MCDust	PM10	0.00003	0.00001	0.00001	0.00000	0.00000	0.00001	0.00000	0.00000	0.00000	0.00000	0.00000	0.00000	0.00000	0.00000	0.00000	0.00000	0.00000	0.00000	0.00000	0.00000	0.00000	0.00000	0.00000
RESQ2550	AADust	PM10	0.00000	0.00000	0.00000	0.00001	0.00001	0.00000	0.00000	0.00000	0.00000	0.00000	0.00000	0.00000	0.00000	0.00000	0.00000	0.00000	0.00001	0.00000	0.00000	0.00000	0.00000	0.00000	0.00000

PNO	Mnemonic	SIZE	prist	pristU	phytan	phytanU	DMPHTH	DMPHTHU	DEPHTH	DEPHTHU	DBPHTH	DBPHTHU	BBPHTH	BBPHTHU	BEPHTH	BEPHTHU	DOPHTH	DOPHTHU	BT	BTU	VLCYHE	VLCYHEU	DPTE	DPTEU	STYR	STYRU	ISOP	ISOPU	BUTD	BUTDU
20013	Brake_1	PM2.5	0.00190	0.00037	0.00053	0.00008	0.00000	0.00010	0.00000	0.00010	0.00000	0.00010	0.00000	0.00010	0.00000	0.00010	0.00000	0.00010	0.00000	0.00010	0.00000	0.00010	0.00000	0.00010	0.00000	0.00010	0.00000	0.00010	0.00000	0.00010
20014	Brake_2	PM2.5	0.00076	0.00015	0.00020	0.00003	0.00000	0.00010	0.00000	0.00010	0.00000	0.00010	0.00000	0.00010	0.00000	0.00010	0.00000	0.00010	0.00000	0.00010	0.00000	0.00010	0.00000	0.00010	0.00000	0.00010	0.00000	0.00010	0.00000	0.00010
20015	Brake_3	PM2.5	0.00068	0.00013	0.00014	0.00002	0.00000	0.00010	0.00000	0.00010	0.00000	0.00010	0.00000	0.00010	0.00000	0.00010	0.00000	0.00010	0.00000	0.00010	0.00000	0.00010	0.00000	0.00010	0.00000	0.00010	0.00000	0.00010	0.00000	0.00010
20016	Brake_C	PM2.5	0.00111	0.00068	0.00029	0.00021	0.00000	0.00010	0.00000	0.00010	0.00000	0.00010	0.00000	0.00010	0.00000	0.00010	0.00000	0.00010	0.00000	0.00010	0.00000	0.00010	0.00000	0.00010	0.00000	0.00010	0.00000	0.00010	0.00000	0.00010
ARB1	Brake_D	PM10																												
ARB2	Brake_E	PM10																												
ARB3	Brake_F	PM10																												
ARB4	Brake_G	PM10																												
20017	Tire_1	PM2.5	0.00618	0.00122	0.00395	0.00059	0.00000	0.00010	0.00000	0.00010	0.00000	0.00010	0.00000	0.00010	0.00000	0.00010	0.00000	0.00010	0.00000	0.00010	0.00000	0.00010	0.00000	0.00010	0.00000	0.00010	0.00000	0.00010	0.00000	0.00010
20018	Tire_2	PM2.5	0.01278	0.00257	0.00441	0.00072	0.00000	0.00010	0.00000	0.00010	0.00000	0.00010	0.00000	0.00010	0.00000	0.00010	0.00000	0.00010	0.00000	0.00010	0.00000	0.00010	0.00000	0.00010	0.00000	0.00010	0.00000	0.00010	0.00000	0.00010
25346	WS-L	PM2.5	0.00000	0.00010	0.00000	0.00010	0.00000	0.00010	0.00000	0.00010	0.00000	0.00010	0.00000	0.00010	0.00000	0.00010	0.00000	0.00010	0.00000	0.00010	0.00000	0.00010	0.00000	0.00010	0.00000	0.00010	0.00000	0.00010	0.00000	0.00010
25347	CS-L	PM2.5	0.00000	0.00010	0.00000	0.00010	0.00000	0.00010	0.00000	0.00010	0.00000	0.00010	0.00000	0.00010	0.00000	0.00010	0.00000	0.00010	0.00000	0.00010	0.00000	0.00010	0.00000	0.00010	0.00000	0.00010	0.00000	0.00010	0.00000	0.00010
25348	WS-H	PM2.5	0.00002	0.00002	0.00078	0.00081	0.00000	0.00010	0.00000	0.00010	0.00000	0.00010	0.00000	0.00010	0.00000	0.00010	0.00000	0.00010	0.00000	0.00010	0.00000	0.00010	0.00000	0.00010	0.00000	0.00010	0.00000	0.00010	0.00000	0.00010
25349	CS-H	PM2.5	0.00001	0.00002	0.00001	0.00003	0.00000	0.00010	0.00000	0.00010	0.00000	0.00010	0.00000	0.00010	0.00000	0.00010	0.00000	0.00010	0.00000	0.00010	0.00000	0.00010	0.00000	0.00010	0.00000	0.00010	0.00000	0.00010	0.00000	0.00010
25350	WS-BC	PM2.5	0.00008	0.00011	0.00000	0.00004	0.00000	0.00010	0.00000	0.00010	0.00000	0.00010	0.00000	0.00010	0.00000	0.00010	0.00000	0.00010	0.00000	0.00010	0.00000	0.00010	0.00000	0.00010	0.00000	0.00010	0.00000	0.00010	0.00000	0.00010
25351	CS-BC	PM2.5	0.00008	0.00002	0.00004	0.00006	0.00000	0.00010	0.00000	0.00010	0.00000	0.00010	0.00000	0.00010	0.00000	0.00010	0.00000	0.00010	0.00000	0.00010	0.00000	0.00010	0.00000	0.00010	0.00000	0.00010	0.00000	0.00010	0.00000	0.00010
25352	MDD-MIX	PM2.5	0.00002	0.00005	0.00244	0.00130	0.00000	0.00010	0.00000	0.00010	0.00000	0.00010	0.00000	0.00010	0.00000	0.00010	0.00000	0.00010	0.00000	0.00010	0.00000	0.00010	0.00000	0.00010	0.00000	0.00010	0.00000	0.00010	0.00000	0.00010
25353	HHDD-HW	PM2.5	0.00000	0.00001	0.00056	0.00010	0.00000	0.00010	0.00000	0.00010	0.00000	0.00010	0.00000	0.00010	0.00000	0.00010	0.00000	0.00010	0.00000	0.00010	0.00000	0.00010	0.00000	0.00010	0.00000	0.00010	0.00000	0.00010	0.00000	0.00010
25354	HHDD-HCS	PM2.5	0.00030	0.00020	0.00041	0.00008	0.00000	0.00010	0.00000	0.00010	0.00000	0.00010	0.00000	0.00010	0.00000	0.00010	0.00000	0.00010	0.00000	0.00010	0.00000	0.00010	0.00000	0.00010	0.00000	0.00010	0.00000	0.00010	0.00000	0.00010
25355	HHDD-MIX	PM2.5	0.00015	0.00021	0.00049	0.00009	0.00000	0.00010	0.00000	0.00010	0.00000	0.00010	0.00000	0.00010	0.00000	0.00010	0.00000	0.00010	0.00000	0.00010	0.00000	0.00010	0.00000	0.00010	0.00000	0.00010	0.00000	0.00010	0.00000	0.00010
25356	DIESEL	PM2.5	0.00012	0.00015	0.00097	0.00098	0.00000	0.00010	0.00000	0.00010	0.00000	0.00010	0.00000	0.00010	0.00000	0.00010	0.00000	0.00010	0.00000	0.00010	0.00000	0.00010	0.00000	0.00010	0.00000	0.00010	0.00000	0.00010	0.00000	0.00010
25357	GAS	PM2.5	0.00003	0.00008	0.00014	0.00034	0.00000	0.00010	0.00000	0.00010	0.00000	0.00010	0.00000	0.00010	0.00000	0.00010	0.00000	0.00010	0.00000	0.00010	0.00000	0.00010	0.00000	0.00010	0.00000	0.00010	0.00000	0.00010	0.00000	0.00010
Copper1	COTIRE1	TSP	0.00000	0.00000	0.00000	0.00000	0.00001	0.00000	0.00001	0.00000	0.00005	0.00000	0.00005	0.00000	0.00141	0.00007	0.00032	0.00002	0.00000	0.00000	0.00000	0.00000	0.00001	0.00000	0.00001	0.00000	0.00000	0.00000	0.00000	0.00000
Copper2	COTIRE2	TSP	0.00000	0.00000	0.00000	0.00000	0.00010	0.00001	0.00017	0.00001	0.00061	0.00003	0.00058	0.00003	0.00631	0.00032	0.00430	0.00022	0.00000	0.00000	0.00002	0.00000	0.00002	0.00000	0.00003	0.00000	0.00001	0.00000	0.00001	0.00000
Michelin1	MITIRE1	TSP	0.00000	0.00000	0.00000	0.00000	0.00001	0.00000	0.00002	0.00000	0.00007	0.00000	0.00006	0.00000	0.00083	0.00004	0.00057	0.00003	0.00000	0.00000	0.00000	0.00000	0.00000	0.00000	0.00000	0.00000	0.00000	0.00000	0.00000	0.00000
Michelin2	MITIRE2	TSP	0.00000	0.00000	0.00000	0.00000	0.00002	0.00000	0.00002	0.00000	0.00009	0.00000	0.00007	0.00000	0.01863	0.00093	0.00847	0.00042	0.00000	0.00000	0.00001	0.00000	0.00000	0.00000	0.00001	0.00000	0.00000	0.00000	0.00000	0.00000
Copper	COTIRE	TSP	0.00000	0.00000	0.00000	0.00000	0.00006	0.00007	0.00009	0.00011	0.00033	0.00039	0.00031	0.00037	0.00386	0.00346	0.00231	0.00282	0.00000	0.00000	0.00001	0.00002	0.00001	0.00001	0.00002	0.00002	0.00000	0.00000	0.00000	0.00000
Michelin	MITIRE	TSP	0.00000	0.00000	0.00000	0.00000	0.00002	0.00000	0.00002	0.00000	0.00008	0.00002	0.00006	0.00001	0.00973	0.01259	0.00452	0.00559	0.00000	0.00000	0.00000	0.00000	0.00000	0.00000	0.00001	0.00000	0.00000	0.00000	0.00000	0.00000
MiCo	TIRE	TSP	0.00000	0.00000	0.00000	0.00000	0.00004	0.00004	0.00005	0.00008	0.00020	0.00027	0.00019	0.00026	0.00679	0.00827	0.00342	0.00383	0.00000	0.00000	0.00001	0.00001	0.00001	0.00001	0.00001	0.00001	0.00000	0.00000	0.00000	0.00000
RESQ2485	AQ Dust	PM2.5	0.00000	0.00000	0.00000	0.00000	0.00105	0.00006	0.00081	0.00005	0.00579	0.00032	0.00478	0.00026	1.43721	0.07876	0.81168	0.04448	0.00008	0.00000	0.00049	0.00003	0.00023	0.00001	0.00053	0.00003	0.00026	0.00001	0.00016	0.00001
RESQ2489	MA Dust	PM2.5	0.00000	0.00000	0.00000	0.00000	0.00138	0.00011	0.00145	0.00011	0.00602	0.00043	0.00474	0.00034	1.34834	0.09634	0.76478	0.05464	0.00007	0.00001	0.00028	0.00002	0.00012	0.00001	0.00034	0.00002	0.00012	0.00001	0.00009	0.00001
RESQ2493	CC Dust	PM2.5	0.00001	0.00000	0.00000	0.00000	0.00003	0.00001	0.00002	0.00000	0.00009	0.00001	0.00011	0.00001	0.00180	0.00010	0.00070	0.00004	0.00001	0.00000	0.00001	0.00000	0.00001	0.00000	0.00001	0.00000	0.00000	0.00000	0.00001	0.00000
RESQ2497	AT Dust	PM2.5	0.00001	0.00000	0.00002	0.00000	0.00001	0.00001	0.00002	0.00001	0.00008	0.00001	0.00005	0.00001	0.00150	0.00009	0.00041	0.00003	0.00000	0.00000	0.00000	0.00000	0.00001	0.00000	0.00001	0.00000	0.00000	0.00000	0.00000	0.00000
RESQ2520	Dust	PM2.5	0.00001	0.00001	0.00000	0.00001	0.00062	0.00070	0.00058	0.00069	0.00299	0.00336	0.00242	0.00270	0.69721	0.80398	0.39439	0.45517	0.00004	0.00004	0.00020	0.00023	0.00009	0.00011	0.00022	0.00026	0.00010	0.00012	0.00007	0.00008
RESQ2540	MCDust	PM2.5	0.00001	0.00001	0.00000	0.00000	0.00070	0.00096	0.00074	0.00101	0.00305	0.00419	0.00242	0.00328	0.67507	0.95215	0.38274	0.54029	0.00004	0.00005	0.00015	0.00019	0.00006	0.00008	0.00018	0.00023	0.00006	0.00008	0.00005	0.00006
RESQ2560	AADust	PM2.5	0.00000	0.00001	0.00001	0.00001	0.00053	0.00073	0.00042	0.00056	0.00293	0.00403	0.00241	0.00334	0.71936	1.01520	0.40605	0.57366	0.00004	0.00005	0.00025	0.00034	0.00012	0.00016	0.00027	0.00037	0.00013	0.00018	0.00008	0.00011
RESQ2487	AQDust	PM10	0.00000	0.00000	0.00000	0.00000	0.00069	0.00004	0.00045	0.00003	0.00238	0.00013	0.00196	0.00011	0.39849	0.02108	0.24653	0.01304	0.00002	0.00000	0.00011	0.00001	0.00005	0.00000	0.00011	0.00001	0.00004	0.00000	0.00002	0.00000
RESQ2491	MADust	PM10	0.00002	0.00000	0.00000	0.00000	0.00003	0.00001	0.00003	0.00001	0.00010	0.00001	0.00013	0.00001	0.00316	0.00020	0.00088	0.00006	0.00001	0.00000	0.00002	0.00000	0.00002	0.00000	0.00003	0.00000	0.00001	0.00000	0.00001	0.00000
RESQ2495	CCDust	PM10	0.00001	0.00000	0.00000	0.00000	0.00001	0.00000	0.00001	0.00000	0.00004	0.00000	0.00003	0.00000	0.00093	0.00005	0.00019	0.00001	0.00000	0.00000	0.00000	0.00000	0.00000	0.00000	0.00000	0.00000	0.00000	0.00000	0.00000	0.00000
RESQ2499	ATDust	PM10	0.00001	0.00000	0.00001	0.00000	0.00001	0.00001	0.00001	0.00000	0.00003	0.00000	0.00003	0.00000	0.00127	0.00007	0.00017	0.00001	0.00000	0.00000	0.00000	0.00000	0.00000	0.00000	0.00001	0.00000	0.00000	0.00000	0.00000	0.00000
RESQ2510	Dust	PM10	0.00001	0.00001	0.00000	0.00001	0.00018	0.00034	0.00012	0.00022	0.00064	0.00116	0.00054	0.00095	0.10096	0.19836	0.06194	0.12306	0.00001	0.00001	0.00003	0.00005	0.00002	0.00002	0.00004	0.00005	0.00001	0.00002	0.00001	0.00001
RESQ2530	MCDust	PM10	0.00001	0.00001	0.00000	0.00000	0.00002	0.00002	0.00002	0.00001	0.00007	0.00004	0.00008	0.00007	0.00205	0.00158	0.00054	0.00048	0.00000	0.00000	0.00001	0.00001	0.00001	0.00001	0.00001	0.00002	0.00000	0.00000	0.00001	0.00001
RESQ2550	AADust	PM10	0.00000	0.00000	0.00001	0.00001	0.00035	0.00048	0.00023	0.00031	0.00121	0.00166	0.00099	0.00136	0.19988	0.28088	0.12335	0.17420	0.00001	0.00001	0.00006	0.00008	0.00003	0.00003	0.00006	0.00007	0.00002	0.00002	0.00001	0.00001

Appendix B: Data Samples from California PeMS presents some examples of traffic data files downloaded from PeMS at the target VDS and included in Appendix A. It should be pointed out that truck related data in PeMS is not directly measured from the inductive loop detectors but estimated from the algorithm by Kwon et al. [58].

3.4 Video Footage with Automated License Plate Reader

With the help from CARB's engineers, the project team was able to collect video footage data with HD camera at two monitoring sites, i.e., within the fenced area at Coast Corvette dealership along I-5N (see Figure 3-26) and at the North corner of the site along I-710N (see Figure 3-27). Specifically, two cameras (one for the front license plate and the other for the rear license plate) were set up for the I-5N site but only vehicles traveling along the two outermost lanes (of five lanes in total) were captured. For the I-710N site, only one camera was configured to capture traffic along all the lanes. It is also noted that both sites for video taping have the meteorological data collection equipment.

Figure 3-26: Video-taping site along I-5N.

Figure 3-27: Video-taping site along I-710N.

Once camera data was collected, CARB's engineers applied open-source image processing software to perform license plate recognition (see Figure 3-28 as an example). With the recognized license plate information, an association process was conducted to identify the matched records in either California Department of Motor Vehicle registration database (for those CA licenses registered by October 2019) or International Registration Plan, Inc database

(for those other state licenses registered by 2019). Based on the matched records, individual vehicle information can be retrieved, including vehicle type based on gross vehicle weight (e.g., LDV, MDV, HDV, and trailer), model year, and fuel type (e.g., gasoline, diesel, CNG, butane, and electricity).

Figure 3-29 shows some preliminary results on the license plate matching with the software. It turned out that the results varied significantly with different sites. Higher percentage of samples captured by the software at the I-5N location can be matched with the databases, compared to those collected at the I-710 N. A hypothesis is that more cameras were set up to capture less lanes (potentially less occlusions) at the I-5N location.

Figure 3-30 presents the fleet mix results based on license plate matching. It can be observed that the proportions of LDVs and MDVs were comparable between the I-5N site and the I-710N site. However, there were much more trailers detected at the I-710N site, compared to those at the I-5N site.

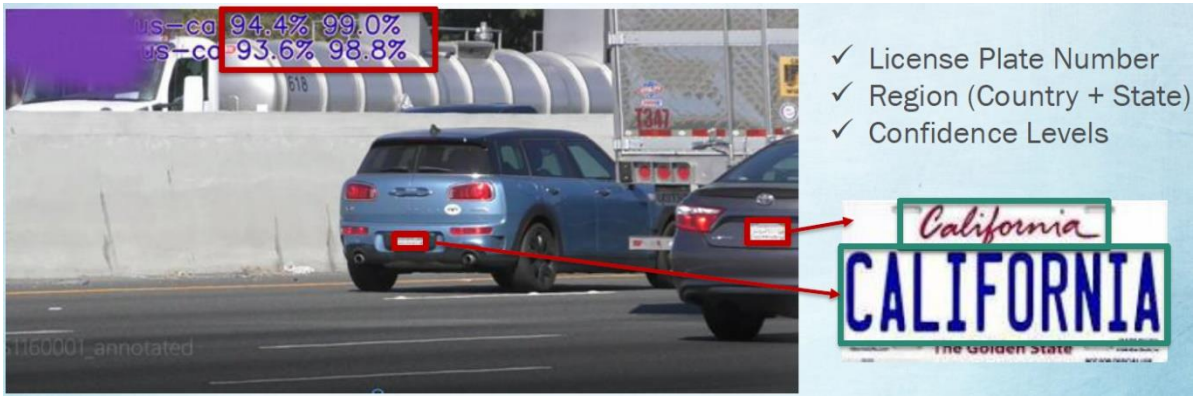

Figure 3-28 An example of license plate recognition.

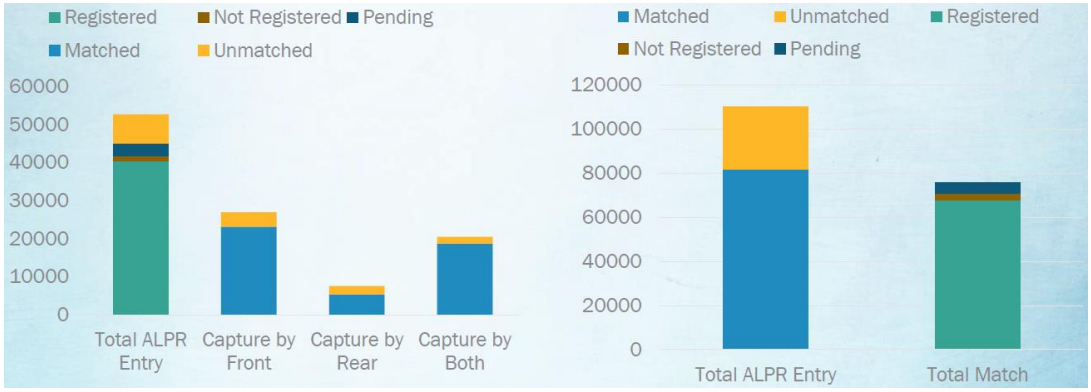

(a) I-5N location **(b) I-710 N location**

Figure 3-29: Preliminary results of license plate matching.

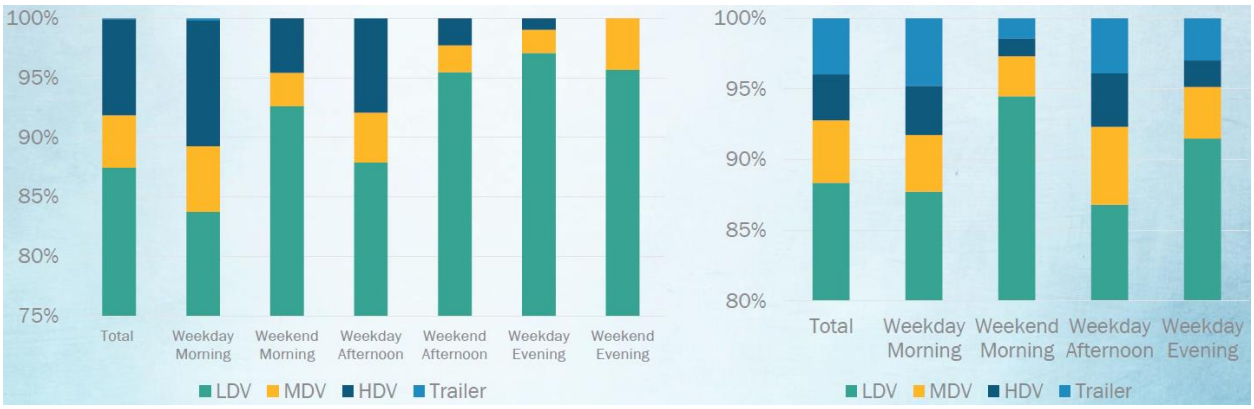

(a) I-5N location **(b) I-710 N location**

Figure 3-30: Preliminary results of fleet mix based on license plate matching.

3.5 Weight-in-Motion Data Records

With the help from CARB's engineers, the project team was able to access some limited WIM data on the stations that are close to the study sites. Figure 3-31 presents the WIM data sites in both Caltrans District 7 and Caltrans District 12.

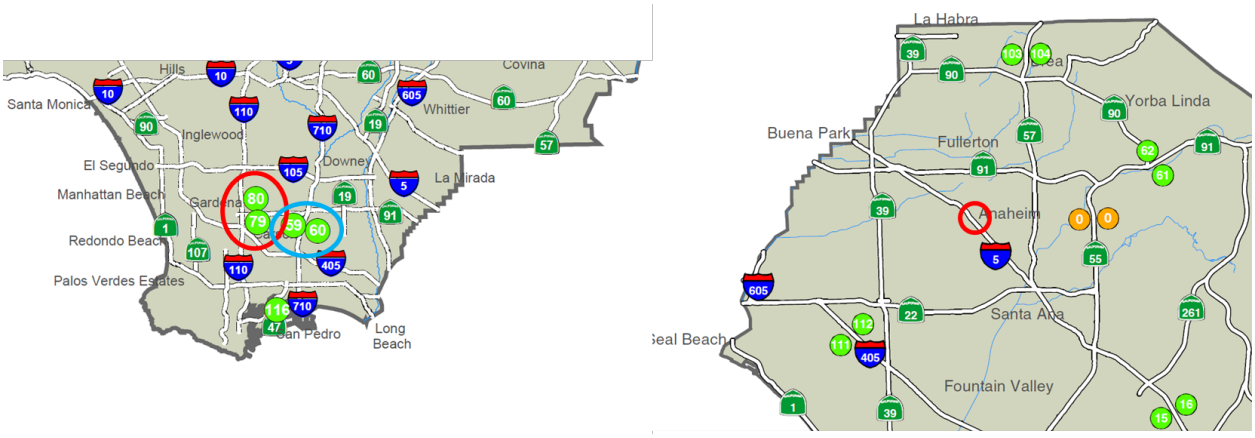

(a) In Caltrans District 7 **(b) In Caltrans District 12**

Figure 3-31: Weigh-in-motion data sites near the study sites.

According to the WIM data site map, Stations #59 and #60 are the closest (in terms of route distance) to the I-710 N study site, while Stations #79 and #80 are the closest to the I-5N study site. However, no data was available on Stations #59 and #60 during the experiment period (as can be seen in Appendix C), and Stations #79 and #80 are still a bit far away from the I-5N location (the red circle in Figure 3-31b).

3.6 Key Findings

Here is a summary of potential issues and findings of different traffic data sources used in this study:

- California Performance Measurement Systems (PeMS): As aforementioned, the truck volumes/proportions are "estimated" rather than "measured". In addition, such estimation is based on the effective vehicle length and some predefined threshold. There is no clear definition/mapping to more detailed vehicle classification.
- Vehicle footage with ALPR: Based on the QAQC process, the results are not accurate (missing rate ranges from 37 – 99% for I-5, and 8 – 29% for I-710). The vehicle classification mainly relies on gross vehicle weight to differentiate LDVs, MDVs, HDVs, and Trailers. Although model year and powertrain technology are available, this information has not been fully tapped in this project. Also, the lane-level traffic information is not available from the processed data.
- WIM stations: Those stations are sparsely located and are far from the measurement location for I-5. The data are not complete for I-710, although the stations are quite close. In addition, the data resolution is on a daily basis across entire segment, which might be too coarse.

4 Task 4: Conduct Near-Road Measurement

4.1 Near-road Measurement

Figure 4-1 shows a schematic diagram of the experimental setup at each downwind sampling site; key specifications of instruments used in this study are listed in Table 4-1. The upwind or background site used a subset of these instruments to measure background concentrations.

4.1.1 *Gas Concentrations*

CO_2 and CO concentrations were measured at both upwind and downwind sites. Because of they are major combustion products, we originally planned to use them to calculate fuel-based emission factors of PM using carbon balance principle [60, 61]. The fuel-based emission factors can be converted to distance-based emission factors by assuming fuel economy for different vehicle classes obtained from traffic data. However, the CO_2 data did not have sufficient differences between downwind and upwind sites to reliably attribute the concentration changes to traffic emissions, and the CO analyzers had drift during the study. As a result the fuel-based emission factors could not be calculated. NO_x is also a good tracer for traffic emissions, and it was used to correct for atmospheric dilution of traffic emissions [55, 62].

4.1.2 *Particle Size Distributions*

Particle size distributions at near road locations are very dynamic. Particles originating from individual vehicles mix rapidly with turbulence generated by the wake of vehicles along with atmospheric turbulence and wind. Two instruments were used to report real-time size distributions; both instruments were used at the downwind sampling sites only.

Dekati ELPI measures aerodynamic particle size distributions ranging from 6 nm to 10 μm at 10 Hz sampling rate [63]. This instrument also reports real-time particle mass distribution. The inversion algorithm is inherently complex and there is some level of uncertainty due to underlying assumption of particle charging as a function of particle size [64-66]. Furthermore, knowledge or assumptions of the effective density is required to reconcile differences between mobility diameter-dependent charging efficiency and aerodynamic diameter-dependent impaction separation [67]. Regardless, Dekati ELPI is one of the best performing instruments to

measure wide range of particle size distributions in number and mass with respect to aerodynamic diameter [68].

The TSI QCM-MOUDI determines real-time mass concentrations from the vibration frequency change of the quartz crystals [69]. This instrument overcomes the particle bouncing and poor particle coupling weaknesses of previous QCM instruments by controlling relative humidity inside the impactor. It measures $PM_{2.5}$ mass in six stages (45, 74, 156, 305, 510, 960, and 2440 nm) every second.

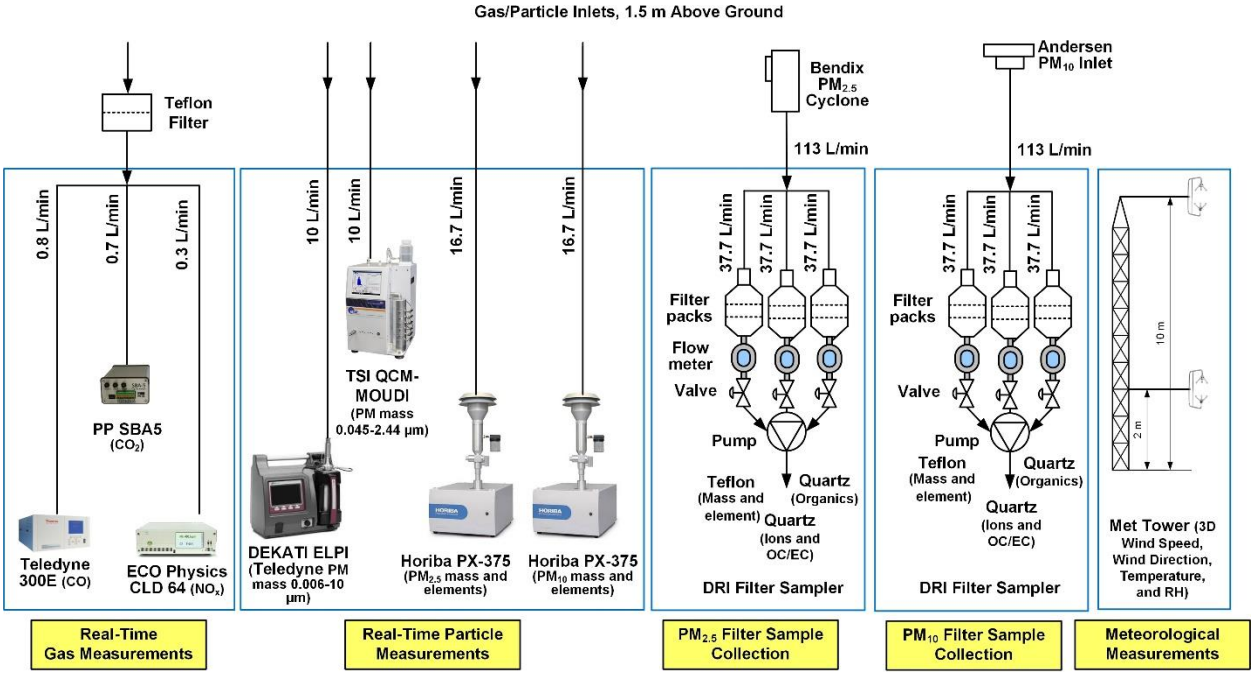

Figure 4-1: Schematic diagram of roadside sampling setup.

Table 4-1. List of instruments to be used for roadside sampling.

Make/Model	Equipment Type and Operating Principle	Measurement Range	Averaging Time
Teledyne Model 300E (2 units)	CO analyzer by gas filter correlation infrared absorbance	0.04-1,000 ppm	1 min
PP Systems SBA5 (2 units)	CO_2 analyzer by non-dispersive infrared (NDIR)	15-5000 ppm	1.5 s
ECO Physics CLD 64	NO, NO_2, and NOx by chemiluminescence	0-0.5 ppm to 0-100 ppm	1 min
DEKATI ELPI (1 unit)	Aerodynamic size and mass distribution by impaction and charge detection. It reports sizes in 14 channels: 10, 5.3, 3.6, 2.5, 1.6, 0.94, 0.60, 0.38, 0.25, 0.15, 0.094, 0.054, 0.030, 0.016, and 0.006 µm	~>0.01-20 $\mu g/m^3$ depending on particle size	0.1 s
TSI Quartz Crystal Microbalance (QCM)-MOUDI (1 unit)	Aerodynamic mass distribution by impaction and mass measurement. It reports mass in 6 channels: 2.44, 0.96, 0.51, 0.305, 0.156, 0.074, and 0.045 µm	Concentration × Sampling time > 150 $\mu g/m^3$ min	1 s
Horiba PX-375 (4 units)	$PM_{2.5}$ and PM_{10} mass by beta ray attenuation and elements by X-ray fluorescence	0-200 $\mu g/m^3$ for $PM_{2.5}$ and 0-500 $\mu g/m^3$ for PM_{10}	30 min

DRI 13-Channel $PM_{2.5}$ Medium- volume Filter Sampling System (2 units)	Two channels are activated at each sampling period to collect filter samples for laboratory analysis	NA	4 h integrated
DRI 13-Channel PM_{10} Medium- volume Filter Sampling System (2 units)	Two channels are activated at each sampling period to collect filter samples for laboratory analysis	NA	4 h integrated
R.M. Young Model 81000 Ultrasonic Anemometer (2 units)	3D wind speed (& turbulence), wind direction, temperature, and relative humidity by anemometer and hygrometer	0-40 m/s 0 to 360 degrees -40–65 °C 0–100% RH	4-32 Hz

4.1.3 *Semi-continuous Measurement of $PM_{2.5}$ and PM_{10} Mass Concentrations and Elemental Composition*

A pair of Horiba PX-375 Continuous Particulate Monitor with XRF with $PM_{2.5}$ or PM_{10} cyclones were used to measure PM mass concentration and elemental composition in real time at both upwind and downwind sites [70, 71]. The $PM_{2.5}$ or PM_{10} mass concentrations were measured using the beta-ray attenuation technology. Elemental concentrations were measured by XRF spectroscopy.

Figure 4-2: (a) Detectable elements shows elements that can be detected by PX-375. This instrument can report a reading as fast as every 100 s. However, its limit of detection (LOD) depends on particle mass loading. Asano et al. [70] showed diurnal trend of elements using PX-375 for background ambient aerosols with time interval of 1000 s. We conducted preliminary sampling near I5 prior to the field campaign and determined that 30-minute sampling time near highways was able to achieve a balance between time resolution and signal-to-noise ratio. LODs of some elements are provided in Figure 4-2b.

(a)

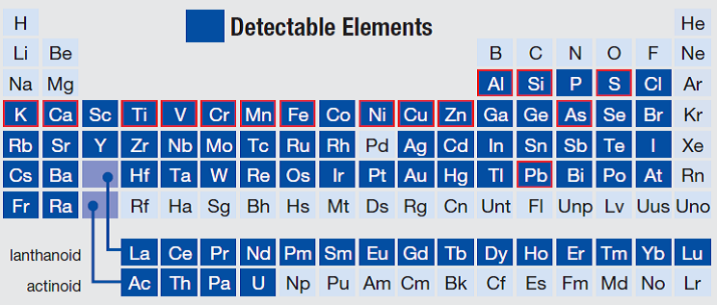

(b)

Element	Analysis time (sec.)		
	100	1000	10000
Ti	26.5	8.4	2.6
Cr	4.5	1.4	0.4
Mn	5.8	1.8	0.6
Cu	5.7	1.8	0.6
Zn	3.0	1.0	0.3
Se	3.4	1.1	0.3
Ag	15.8	5.0	1.6
Cd	35.9	11.3	3.6
Sn	38.4	12.2	3.8
Hg	7.7	2.4	0.8
Pb	5.3	1.7	0.5

Figure 4-2: (a) Detectable elements and (b) LOD (2σ) of selected elements by Horiba PX-375 (in ng/m^3).

4.1.4 *Integrated $PM_{2.5}$ and PM_{10} Filter Sample Collection*

As shown in Figure 4-1, integrated $PM_{2.5}$ and PM_{10} samples were collected using DRI medium-volume (medvol) PM samplers with a Bendix Model 240 $PM_{2.5}$ cyclone and a Sierra-Andersen

(SA) 254 PM_{10} inlet, respectively, similar to those used in previous roadside and tunnel studies [30, 72]. Each sampler has a conical plenum that can host up to 13 filter channels. One set of samplers were placed at both upwind and downwind sites. During each sampling period, three parallel channels were activated for each sampler, including a Teflon-membrane filter and two quartz-fiber filters. A timer and valve system automatically advanced the sampling channels and four sets of samples ($PM_{2.5}$ and PM_{10} at both upwind and downwind sites) were collected without operator intervention.

Most filter samples were collected at four-hour intervals during the following periods at both sites: 0600-1000 local daylight time (LDT; morning rush hours), 1000-1400 (middle day hours), and 1400-1800 (evening rush hours) as shown in Table 4-2. These sampling periods covered different traffic composition (i.e., different light and heavy-duty vehicle mixes) and vehicle operating conditions (e.g., free flow and more stop-and-go), representing different amount of tire and brake wear emissions. The medvol sampling flow rates were 37.7 L/min for each filter channel.

Table 4-2: Schedule of filter sample collection.

Location	Date	Time	Upwind						Downwind						Sample Sets #	Note
			$PM_{2.5}$			PM_{10}			$PM_{2.5}$			PM_{10}				
			T1	Q1	Q2	T2	Q3	Q4	T3	Q5	Q6	T4	Q7	Q8		
I-5	1/28/2020	8-12														Set up
	1/28/2020	14-18	x	x	x	x	x	x	x	x	x	x	x	x	1	
	1/29/2020	6-10	x	x	x	x	x	x	x	x	x	x	x	x	2	
	1/29/2020	10-14	x	x	x	x	x	x	x	x	x	x	x	x	3	
	1/29/2020	14-18	x	x	x	x	x	x	x	x	x	x	x	x	4	
	1/30/2020	6-10	x	x	x	x	x	x	x	x	x	x	x	x	5	
	1/30/2020	10-14	x	x	x	x	x	x	x	x	x	x	x	x	6	
	1/30/2020	14-18	x	x	x	x	x	x	x	x	x	x	x	x	7	
	1/31/2020	6-10	x	x	x	x	x	x	x	x	x	x	x	x	8	
	1/31/2020	10-14	x	x	x	x	x	x	x	x	x	x	x	x	9	
	1/31/2020	14-18	x	x	x	x	x	x	x	x	x	x	x	x	10	
	2/1/2020	6-10	x	x	x	x	x	x	x	x	x	x	x	x	11	
	2/1/2020	10-14	x	x	x	x	x	x	x	x	x	x	x	x	12	
	2/1/2020	14-18	x	x	x	x	x	x	x	x	x	x	x	x	13	

	2/2/2020	6-10	x	x	x	x	x	x	x	x	x	x	x	x	14	
	2/2/2020	10-14	x	x	x	x	x	x	x	x	x	x	x	x	15	
	2/2/2020	14-18	x	x	x	x	x	x	x	x	x	x	x	x	16	
	2/3/2020	6-10	x	x	x	x	x	x	x	x	x	x	x	x	17	
	2/3/2020	10-14	x	x	x	x	x	x	x	x	x	x	x	x	18	
																Tear down
I-710	2/4/2020	10-14														Set up
	2/4/2020	14-18	x	x	x	x	x	x	x	x	x	x	x	x	19	Upwind 14-16
	2/5/2020	6-10	x	x	x	x	x	x	x	x	x	x	x	x	20	
	2/5/2020	10-14	x	x	x	x	x	x	x	x	x	x	x	x	21	
	2/5/2020	14-18	x	x	x	x	x	x	x	x	x	x	x	x	22	Upwind 14-16
	2/6/2020	6-10	x	x	x	x	x	x	x	x	x	x	x	x	23	
	2/6/2020	10-14	x	x	x	x	x	x	x	x	x	x	x	x	24	
	2/6/2020	14-18	x	x	x	x	x	x	x	x	x	x	x	x	25	Upwind 14-16
	2/7/2020	6-10	x	x	x	x	x	x	x	x	x	x	x	x	26	
	2/7/2020	10-14	x	x	x	x	x	x	x	x	x	x	x	x	27	
	2/7/2020	14-18	x	x	x	x	x	x	x	x	x	x	x	x	28	Upwind 14-16
	2/8/2020	6-10	x	x	x	x	x	x	x	x	x	x	x	x	29	
	2/10/2020	6-10	x	x	x	x	x	x	x	x	x	x	x	x	30	
	2/10/2020	10-14	x	x	x	x	x	x	x	x	x	x	x	x	31	
	2/10/2020	14-18	x	x	x	x	x	x	x	x	x	x	x	x	32	Upwind 14-16; Tear down

4.1.5 *Source Sample Collection*

Source samples of road dust and tire particles were collected to develop relevant source profiles. One road dust sample was collected by sweeping the road surfaces near the highway at each sampling site, resulting in a total of four dust samples. These dust samples were aerosolized in a resuspension chamber and the $PM_{2.5}$ and PM_{10} size fractions were collected on filters for chemical analysis to establish the road dust source profiles [73].

Tire particles were collected from a CARB engine dynamometer laboratory. A light duty pickup truck ran through test cycles on rollers with a rough surface. Tire wear particles were collected behind the wheel without size classification. Therefore, the tire particles represent total suspended particles. Tire particles from two tire brands were analyzed: Michelin LTX A/T2 and Cooper Discoverer A/T3. The tire particles turned out to be very difficult to resuspend or nebulize and collect on filters. As such, tire particles were mixed with 80% ethanol and 20% deionized water to create a suspension. Pre-baked quartz-fiber filter punches were first weighed,

then spiked with the tire particle suspension, vacuum dried at 90 °C for 24 hours to evaporate the solution, and then weighed again to obtain the total mass of tire particles.

4.1.6 *Meteorological measurement*

A meteorological tower was set up at the prevailing downwind site to measure 3 dimensional (3D) wind speed, turbulence, wind direction, ambient temperature, and relative humidity (RH) at near ground (~2 m) and 10 m above ground locations. The wind speed, turbulence and direction were used as inputs to dispersion modeling. Additionally, wind speed, wind direction, and RH were measured at the AQMD near road sites, which are collocated with our downwind sampling sites. The AQMD wind data were used to determine time periods with valid downwind/upwind assumption.

4.2 Laboratory Chemical Analysis

Figure 4-3 shows detailed laboratory analysis of the three $PM_{2.5}$ and PM_{10} filter channels [74], including mass, elements, ions, carbon fractions, and organic compounds to identify potential source markers (Table 4-3) and to perform source apportionment [75].

Teflon-membrane filters were equilibrated in a clean room with controlled temperature (T; 21.5 ± 1.5 °C) and relative humidity (RH; 35 ± 5%) before gravimetric analysis [76]. Nominal values of 35% RH and 21.5 °C minimize particle volatilization and aerosol liquid water bias, as required by the U.S. EPA federal reference method [77, 78]. Filters were weighted before and after sampling using a XP6 microbalance (Mettler Toledo Inc., Columbus, OH) with a sensitivity of ±1 µg. To eliminate static charge on the filter, the equilibrated filter was placed over a low-level radioactive source (500 picocuries of polonium^{210}) and through an electrostatic charge neutralizer prior to sample weighing. Unexposed and sampled filters were re-weighed at 100% and 30% rates, respectively, by a second technician to ensure the accuracy and precision of all the weights.

As summarized in Table 4-3, elemental markers, such as Al, Si, Ca, Cu, Fe, Sb, Ba, Zn, and S, along with other elements (a total of 51 elements) were quantified on Teflon-membrane filters using a Panalytical XRF (Model Epsilon 5, Almelo, The Netherlands). This instrument uses secondary targets to generate excitation energies close to the absorption edges of four or five elements for elemental analysis. A side window X-ray tube with dual scandium (Sc)/tungsten (W) anodes excites secondary X-rays from up to 11 secondary targets (i.e., Al, Ca, Ti, Fe, Ge, Zr, Mo, Ag, Cs, Ba, and Ce), or an aluminum oxide (Al_2O_3) Barkla target, which in turn emits polarized X-rays that excite elements in the sample. The fluoresced photons are detected by a solid-state germanium (Ge) X-ray detector. Each photon that enters the detector generates an electrical charge, the magnitude of which is proportional to the photon's energy. Electrical signals from the detector are sorted into energy channels, counted, and displayed [79]. Analysis times, primary X-ray voltage and currents, and secondary targets are selected to minimize background and overlaps.

Half of the first quartz-fiber filters were extracted in distilled deionized water and analyzed for eight water-soluble ions, including: chloride (Cl^-), nitrate (NO_3^-), sulfate (SO_4^{2-}), ammonium (NH_4^+), sodium (Na^+), magnesium (Mg^{2+}), potassium (K^+), and calcium (Ca^{2+}) by ion chromatography [IC; 80]. Analyses were performed using Dionex ICS 5000$^+$ IC systems (Thermo Scientific, Sunnyvale, CA). For each type of analysis (i.e., anions and cations), calibration curves are constructed daily or the start of every run using standard solution mixtures

at seven concentration levels spanning expected levels in the extracts. Ions are identified by matching each peak with the retention times in the chromatograms of the standards. A DDW blank and a calibration standard are analyzed after every 10 samples in order to verify the baseline and span levels, respectively. Dionex and Environmental Research Associates (ERA) ion standards, traceable to National Institute of Standards and Technology (NIST), are used daily as an independent QC check.

OC, EC, and eight thermal fractions (OC1-OC4, pyrolyzed carbon [OP], EC1-EC3) were quantified following the IMPROVE_A thermal/optical protocol using the DRI Model 2015 Multiwavelength Carbon Analyzer (Magee Scientific, Berkeley, CA) [81-83]. A 0.5 cm^2 punch is taken from the first quartz-fiber filter and heated in pure helium environment at 140 ℃ (OC1), 280℃ (OC2), 480℃ (OC3), and 580℃ (OC4) temperature steps. Next, the gas is changed to 98% He/2% O_2, and the filter is continued to be heated at 580℃ (EC1), 740℃ (EC2), and 840℃ (EC3). Seven lasers with wavelength ranging from 405 nm to 980 nm are used to monitor light reflectance (R) and transmittance (T), which are used to calculate wavelength dependent light absorption and char correction.

Non-polar organic compounds, including PAHs, alkanes, cycloalkanes, hopanes, steranes, phthalates, and other organics were analyzed by in-injection port-thermal desorption-gas chromatography mass spectrometry (TD-GC/MS) [84-86]. Aliquots (1.0–1.5 cm^2) of the second quartz-fiber filters are for cut into small pieces, spiked with internal standards, and inserted into TD tubes for analyses. The sample tube is directly loaded into a GC injection port (GC7890, Agilent Technology, Santa Clara, CA), at an initial temperature of 50 °C. The temperature of injector is then ramped to 275 °C for desorption in a splitless mode, while the GC oven temperature is kept at 30 °C. The desorbed analytes are refocused at the column head. After the injector temperature reaches the set point, the oven program starts. The analytes are speared by an DB-5ms capillary column (30 m × 0.25 mm i.d. × 0.25 μm film thickness; J&W Scientific, Folsom, CA). The carrier gas is ultra-high purity (99.9999%) helium (He) at a constant flow of 1.0 cm^3 min^{-1}. The MSD (5975, Agilent Technology) is full scanned from 50 to 550 amu under electron impact ionization (EI) at a voltage of 70 eV and an ion source temperature of 230 °C. Identification is achieved by characteristic ion and retention times of the chromatographic peaks with those of authentic standards.

Thermal decomposition fragments of rubber were analyzed by pyrolysis(pyr)-GC/MS [53, 87, 88]. An aliquot (0.5 cm^2) of the second quartz-fiber filter is folded with ferromagnetic pyrofoil and loaded onto a Curie-point pyrolyzer coupled with a GC/MS system, and is rapidly heated to 670 °C in 5 s. The pyrolyzed compounds are separated with a DB-5ms capillary column. Peaks are identified based on the known fragmentation, mass spectra and retention time for the target pyrolysis products of rubber products. Previous studies have identified the most abundant pyrolysis products for natural rubber (NR), styrene-butadiene rubber (SBR) and butadiene rubber (BR) are: styrene (SBR), isoprene (NR), dipentene (NR), butadiene (SBR, BR), and vinylcyclohexene (SBR, BR) [87]. These five compounds are quantified for all filters in this study.

Benzothiazole is a marker for tire vulcanization accelerator and tire wear [29, 87]. An aliquot (5 cm^2) of the second quartz-fiber filter is extracted and concentrated. The separation of benzothiazole and its derivatives is accomplished by ultra-performance liquid chromatography (UPLC), and both identification and quantification are accomplished using a triple quadrupole

mass spectrometer [38]. Benzothiazole (BT) and eight derivatives are quantified, including 2-aminobenzothiazole (2-NH2-BT), 2-hydroxy benzothiazole (HOBT), 2-Mercaptobenzothiazole (MBT), 2-(Methylthio)benzothiazole (MTBT), 2-(4-morpholinyl)benzothiazole (24MoBT), N-cyclohexyl-2-benzothiazolamine (NCBA), 2-Benzothiazolyl-N-morpholinosulfide (OBS), and N-Cyclohexyl-2-benzothiazolesulfenamide (CBS).

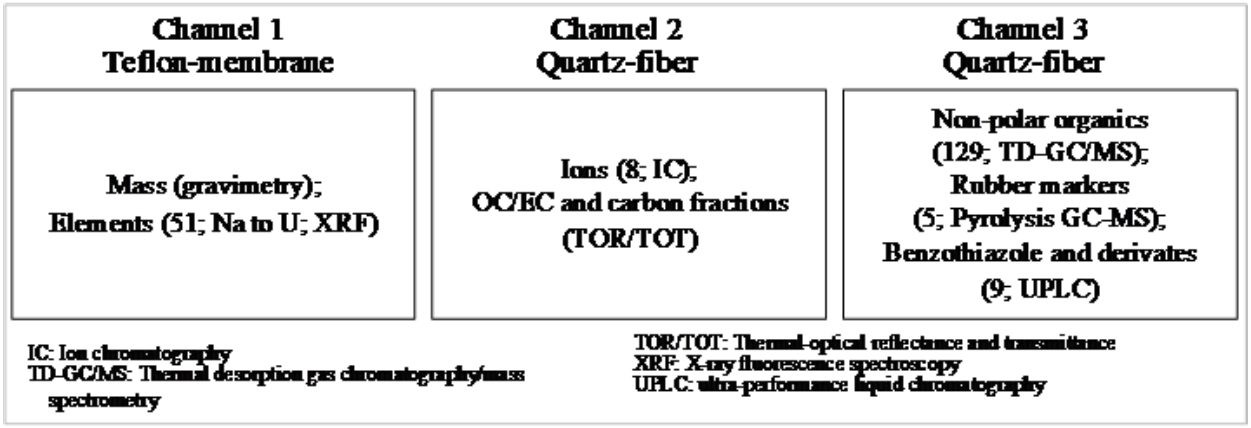

Figure 4-3: Chemical analysis of the three filter channels.

Table 4-3. Chemical analysis on ambient and source $PM_{2.5}$ and PM_{10} samples.

Measurement Method	Species	Potential Marker for
Gravimetry[1]	PM mass	
X-ray Fluorescence (XRF)[1]	Elements from sodium (Na) to uranium (U)	• Mineral dust: Al, Si, Ca, and K; • Brake wear: Cu, Sb, Ba, Fe, Zr, Mo, and Sn; • Tire wear: Zn; • Concrete road wear: Ca and S
Thermal/Optical Analysis[2]	Organic and elemental carbon (OC and EC)	• Tailpipe emissions
Ion Chromatography[2]	Water soluble ions, including chloride (Cl-), nitrate (NO_3^-), sulfate (SO_4^{2-}), ammonium (NH_4^+), sodium (Na^+), magnesium (Mg^{2+}), potassium (K^+), and calcium (Ca^{2+})	• Primary salt material: Cl^- and Na^+ • Secondary salts: NO_3^-, SO_4^{2-}, and NH_4^+ • Biomass burning: K^+
Thermal desorption GC/MS[2]	Nonpolar organics, including PAHs alkanes, cycloalkanes, hopanes, steranes, phthalates	• Tire wear: alkanes (C_{34}-C_{36}) • Tire wear: pyrene, benzo(ghi)perylene, fluoranthene, phenanthrene, and dibenzopyrenes • Motor oil emissions: hopanes and steranes
pyrolysis-GC/MS[2]	Rubber markers, including styrene, isoprene, butadiene, dipentene, and vinylcyclohexene	• NR: isoprene, dipentene • BR: butadiene, vinylcyclohexene • SBR: styrene, butadiene, vinylcyclohexene
Ultra-performance liquid chromatography (UPLC)[2]	Benzothiazole and derivatives	• Tire wear

[1]Done on Teflon filters

[2]Done on quartz-fiber filters

Dust and tire particles were analyzed for the same chemical species as roadside filter samples except that the elements for tire particles were analyzed by ICP-MS instead of XRF, because the tire particle deposits on the filter punches were not uniform and the entire filter punches need be analyzed to obtain elemental concentration.

4.3 Data Validation

Laboratory and field data are gone through quality control and quality assurance procedures to ensure data quality. Laboratory data validation evaluates the internal consistency of $PM_{2.5}$ and PM_{10} mass and chemical composition [89]. Physical consistency is tested for: 1) water soluble ions vs. elements, 2) mass closure, and 3) anion and cation balance. Field data validation includes checking flow rate of analyzers and filter samplers, automatically zero CO_2 analyzers, and comparing collocated measurements.

4.3.1 *Water Soluble Ions vs Elements*

Water soluble ions were measured by IC on quartz-fiber filter extracts while elements were measured by XRF on Teflon®-membrane filters. Most elemental concentrations are expected to be higher than corresponding ion concentrations as usually only part of element is water soluble. Several exceptions include volatile species that evaporate in the XRF vacuum or too thick particle deposits that cause the X-ray not to penetrate the particle film, resulting in underestimation in elemental concentrations.

The mass ratio of SO_4^{2-} to S is expected to equal to 3 if all S is present as water soluble SO_4^{2-}. Due to the possible existence of water-insoluble S minerals in the sample, water-soluble SO_4^{2-} should not exceed three times the S concentration within precision estimates. The U.S. EPA Quality Assurance Guidance for $PM_{2.5}$ Chemical Speciation suggests that the ratio of SO_4^{2-} over S should be within the range of 2.22–4.00 [90]. Figure 4-4a shows that the SO_4^{2-}/S ratios were close to three for most samples, with a regression slope of 2.96 and R^2 of 0.94, indicating that most of sulfur were present as soluble sulfate at the sampling sites. There were 9 samples with SO_4^{2-}/S ratio ranging 1.95-2.21, slightly lower than the U.S. EPA minimum outlier criterion of 2.22. These samples are not flagged as outliers, as roadside samples could have more insoluble sulfur minerals. Although not expected a significant contributor, organic sulfur compounds could also cause lower SO_4^{2-}/S ratios.

Figure 4-4b shows that Cl^- was higher than Cl for most samples. This is likely caused by volatile Cl species (e.g., HCl) evaporation under the XRF vacuum. As expected, Figure 4-4c and Figure 4-4d show that water soluble Ca^{2+} and K^+ were lower than elemental Ca and K, respectively for most samples, as not all Ca and K are water soluble. High correlations are observed between ions and elements, indicating consistent and good quality ion and elemental analysis.

(a) (b)

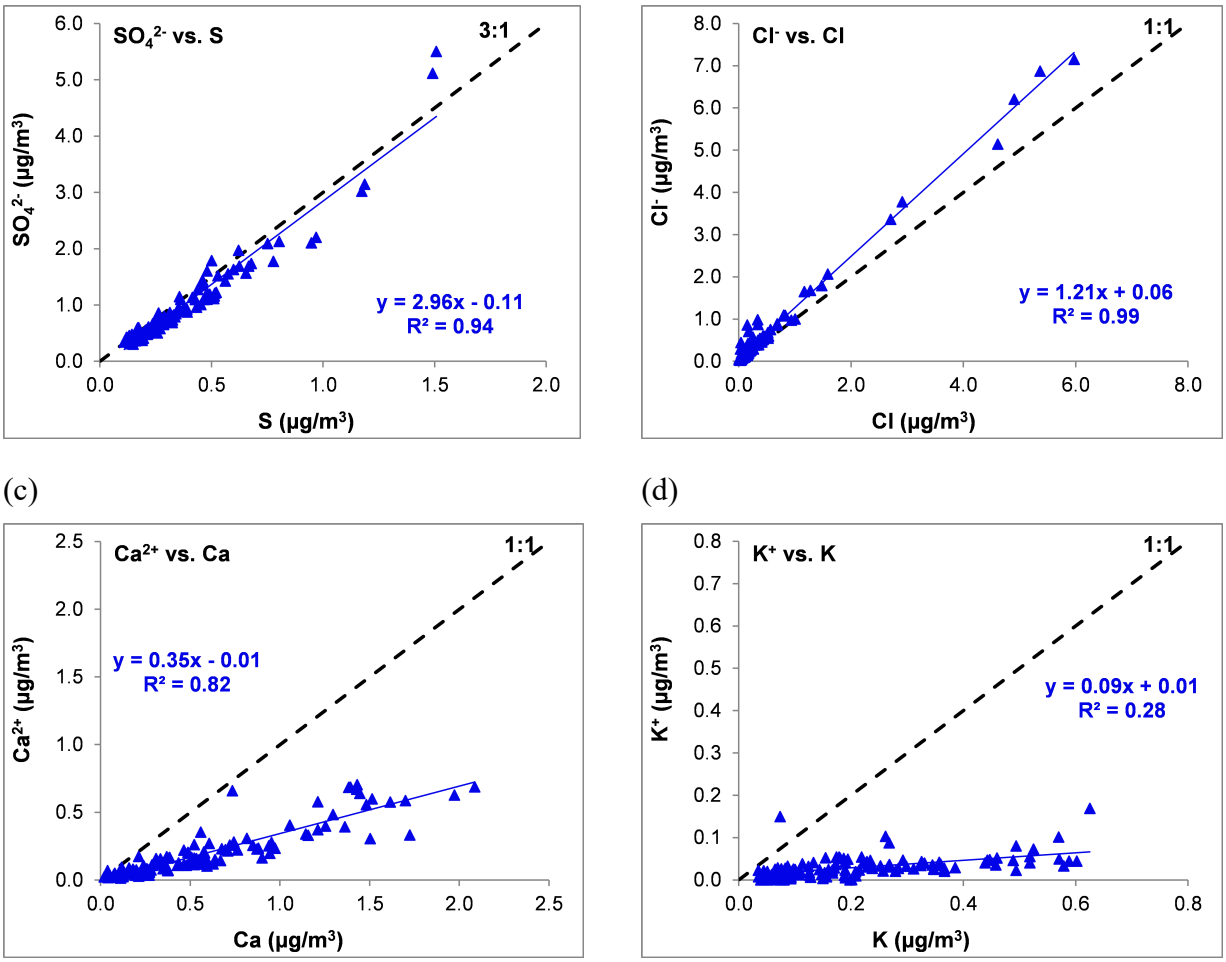

Figure 4-4: Comparison of water soluble ions versus corresponding elements for: (a) SO_4^{2-} vs. S; (b) Cl^- vs. C; (c) Ca^{2+} vs. Ca; and (d) K^+ vs. K.

4.3.2 *Mass Closure*

Mass closure, a comparison of the sum of measured species and reconstructed mass with gravimetric mass, is an indicator of the data quality of chemical analysis. It also provides information about key chemical composition and potential sources of PM [91].

Sum of measured species should be less than or equal to the corresponding gravimetric $PM_{2.5}$ and PM_{10} mass concentrations, because species such as oxygen (O) and hydrogen (H) are not measured. The U.S. EPA Quality Assurance Guidance for $PM_{2.5}$ Chemical Speciation suggests that the ratio of sum of species over gravimetric mass should be within the range of 0.60–1.32 [90]. This sum includes chemicals quantified on the Teflon-membrane and quartz-fiber filters without double counting. Measured concentrations do not account for unmeasured oxygen (O) associated with metal oxides in minerals, unmeasured anions and cations, or hydrogen (H), nitrogen (N), and O associated with organic carbon. Figure 4-5a shows that the sum of species accounts 73% of $PM_{2.5}$ and 59% of PM_{10}. It is expected that the PM_{10} sum of species is lower than that of $PM_{2.5}$ because PM_{10} contains more mineral oxides, and the O is not measured. For the 64 $PM_{2.5}$ samples, the ratio of sum of species to gravimetric mass ranged from 0.51 to 1.30,

with 5 samples having ratios less than 0.60. For the 64 PM_{10} samples, the ratio of sum of species to gravimetric mass ranged from 0.43 to 0.87, with 23 samples having ratios less than 0.60. Even though some samples have ratios less than the 0.60 guideline by U.S. EPA for ambient $PM_{2.5}$, these samples are not deemed as outliers as these are near road samples with more dust contributions, particularly for PM_{10}. A total 17 $PM_{2.5}$ samples have ratios >1.0, likely due to volatile organic species adsorbed by the quartz fiber filters and measured as OC. Field blanks were used to correct OC sampling artifacts, but these artifacts cannot always be completely corrected [92].

Mass reconstruction combines measured PM species into major chemical groups, such as ammonium (NH_4^+), sulfate (SO_4^{2-}), nitrate (NO_3^-), organic matter (OM, OC × a multiplier), EC, mineral dust, and other species without double counting [75, 91]. In this study, a multiplier of 1.2 was used to convert OC to OM because of abundant fresh vehicle exhaust emissions in the near road environment [93]. The mineral dust are estimated as 2.2×Al + 2.49×Si + 1.63×Ca + 2.42×Fe + 1.94×Ti, following the IMPROVE formula [91, 94]. Figure 4-5b compares reconstructed with gravimetric masses, with regression slopes are 0.80 and 0.81 for $PM_{2.5}$ and PM_{10}, respectively. Because the mass closure has ratios close to unity based on both sum of species and reconstructed mass, the chemical analysis of major PM constituents (i.e., gravimetric mass, ions, carbon, and elements) are of good quality.

Comparisons of reconstructed and gravimetric $PM_{2.5}$ and PM_{10} mass concentrations are also plotted in Figure 4-6, and major compositions normalized to gravimetric mass are shown in Figure 4-7. Some $PM_{2.5}$ samples had reconstructed mass higher than gravimetric mass. These are usually related to lower mass concentrations, and therefore higher analytical uncertainty. Absorption of organic gases also had larger influence on the lower concentration samples. On the other hand, the reconstructed mass for most PM_{10} samples were lower than gravimetric mass, likely due to incomplete accounting for unmeasured minerals as well as inaccurate estimate of OM from OC.

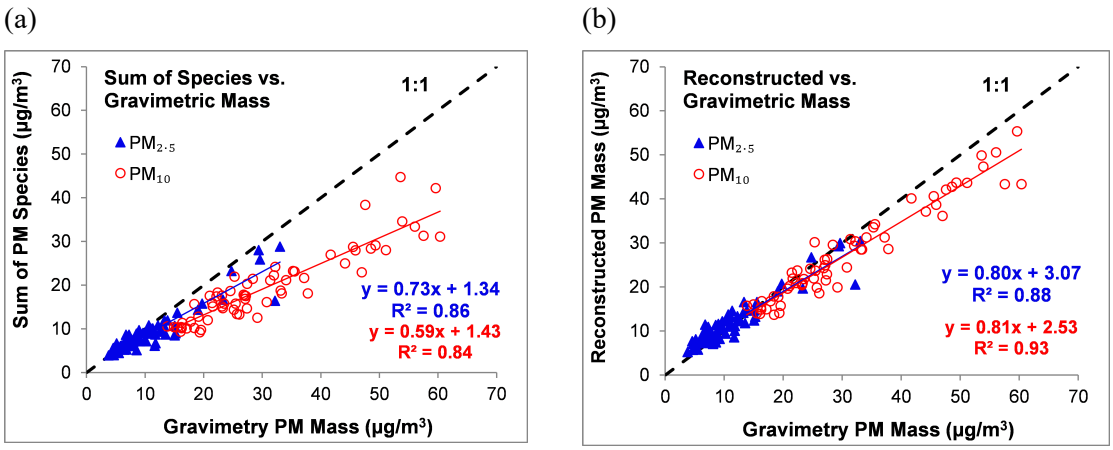

Figure 4-5: Comparison of: (a) sum of species and (b) reconstructed mass with gravimetric mass of $PM_{2.5}$ and PM_{10}.

a)

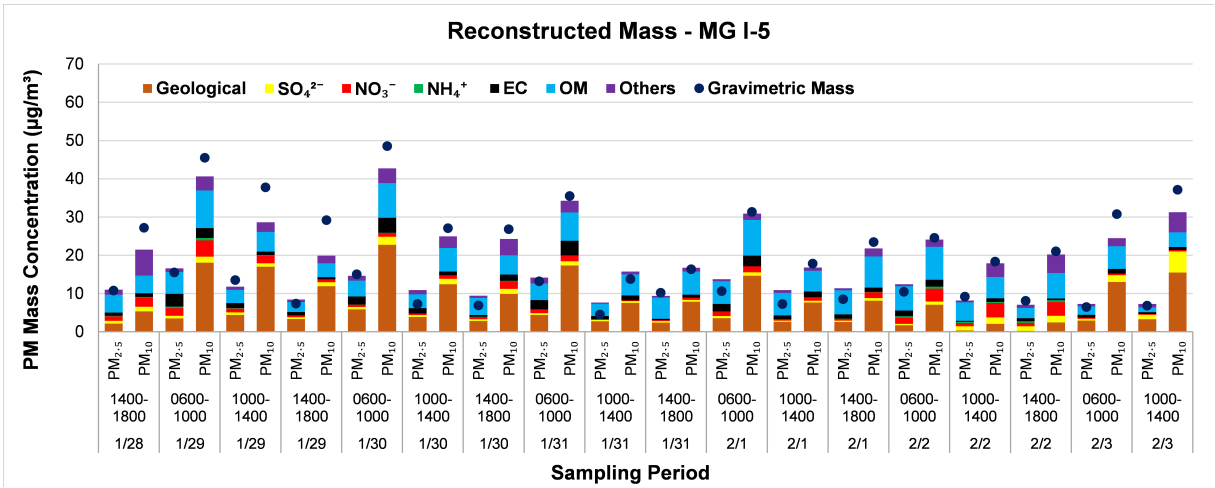
Reconstructed Mass - MG I-5
PM Mass Concentration (µg/m³)
Geological
SO4 2−
NO3 −
NH4 +
EC
OM
Others
Gravimetric Mass
Sampling Period

b)

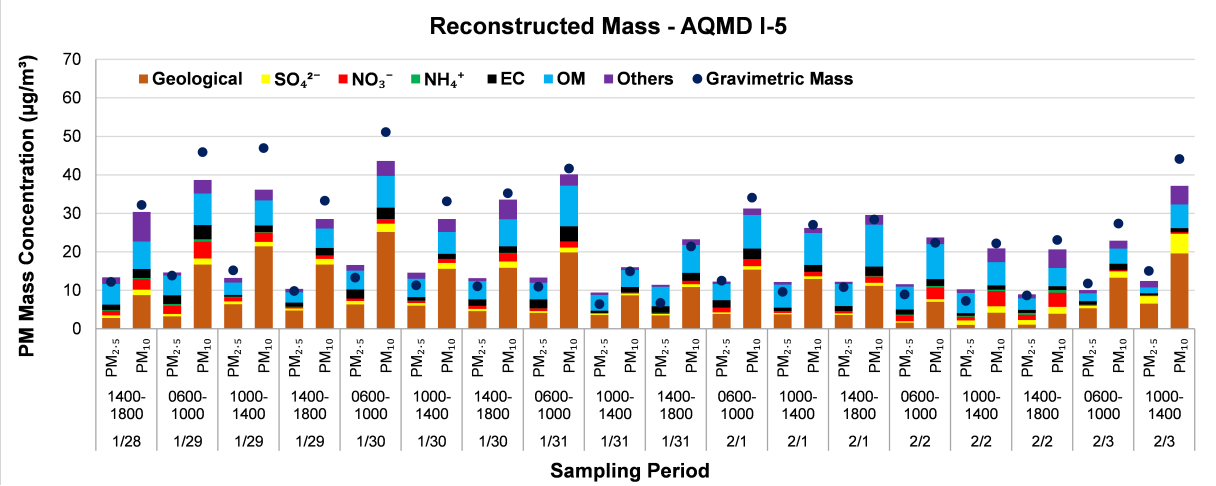
Reconstructed Mass - AQMD I-5
PM Mass Concentration (µg/m³)
Geological
SO4 2−
NO3 −
NH4 +
EC
OM
Others
Gravimetric Mass
Sampling Period

c)

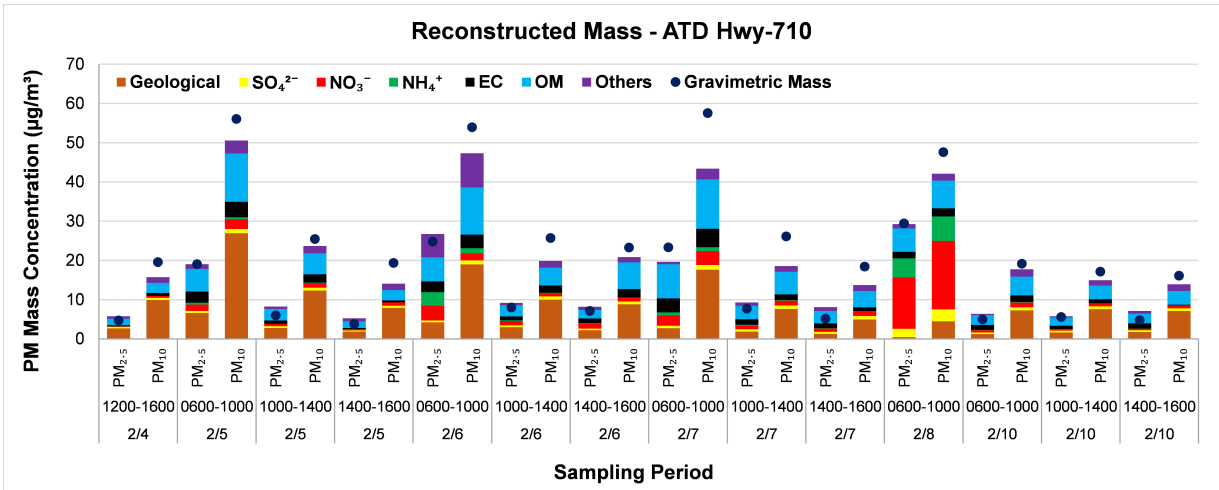
Reconstructed Mass - ATD Hwy-710
PM Mass Concentration (µg/m³)
Geological
SO4 2−
NO3 −
NH4 +
EC
OM
Others
Gravimetric Mass
Sampling Period

d)

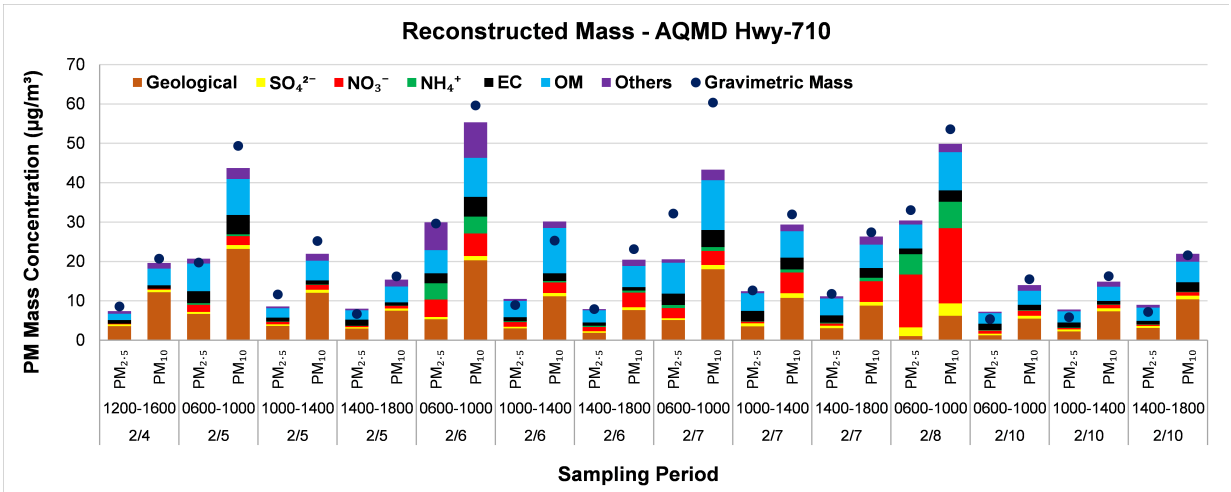

Figure 4-6: Reconstructed and gravimetric $PM_{2.5}$ and PM_{10} mass concentrations at the four sampling sites.

a)

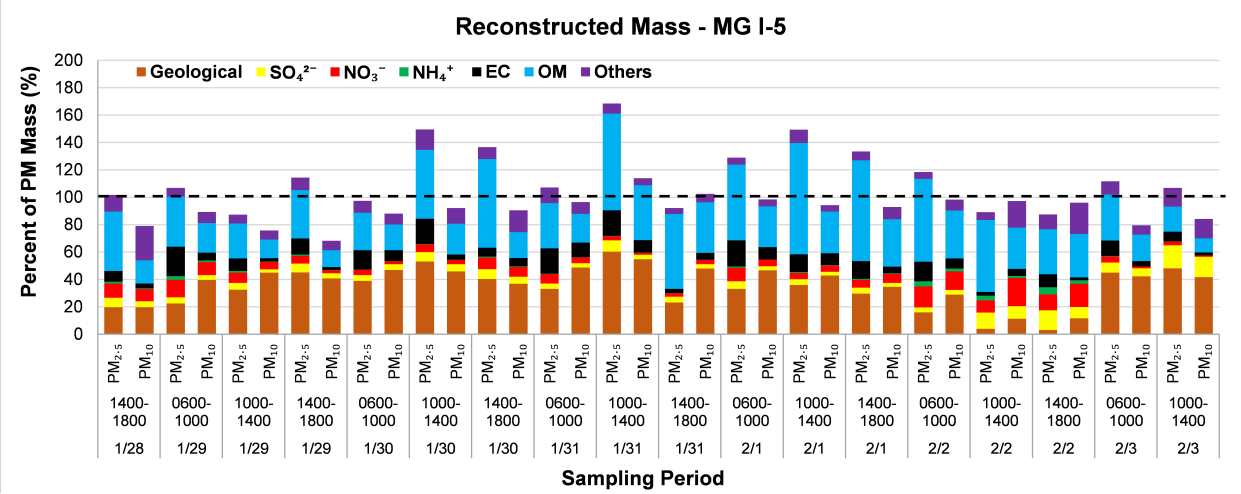

b)

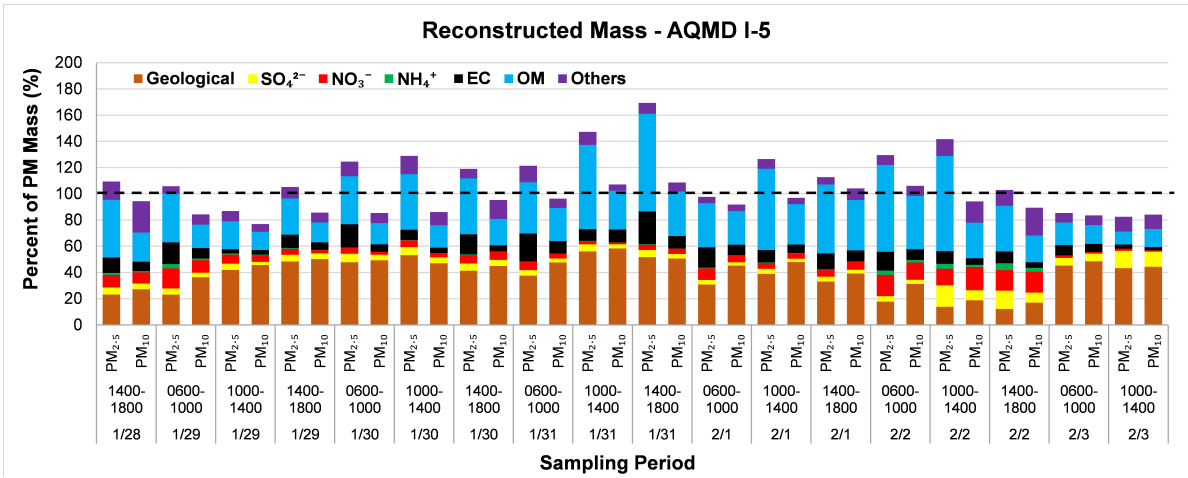

c)

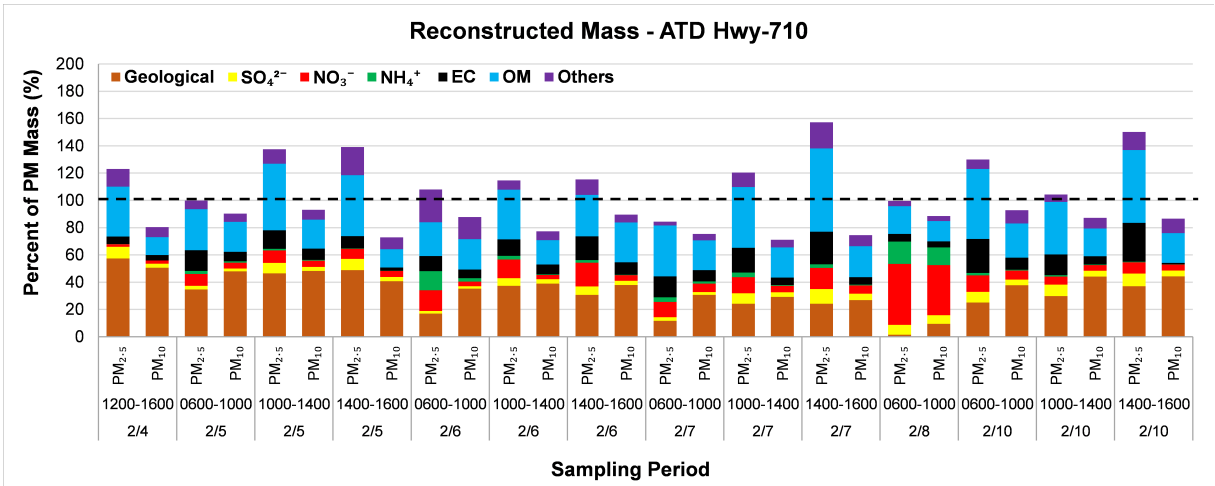

d)

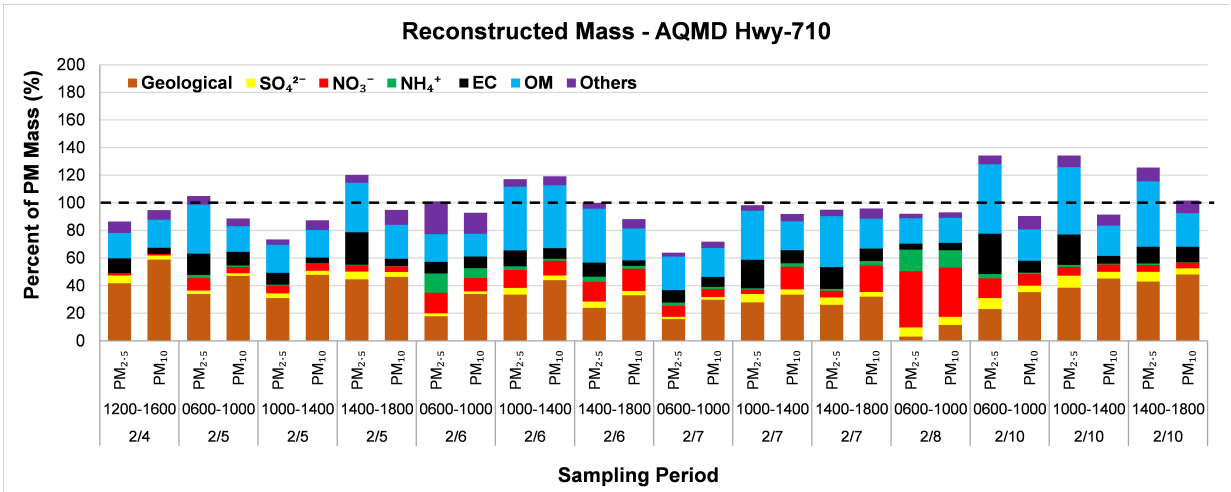

Figure 4-7: Percent of gravimetric $PM_{2.5}$ and PM_{10} mass for major compositions at the four sampling sites.

4.3.3 *Anion and Cation Balance*

The anion and cation balance compares the sum of anions (i.e., Cl^-, NO_3^-, and SO_4^{2-}) to the sum of cations (NH_4^+, Na^+, Mg^{2+}, K^+, and Ca^{2+}) in microequivalent mole concentrations (μeq/m^3), which is the product of mass concentration (in μg/m^3) divided by the atomic weight of the chemical species divided by the species' charge. Therefore:

Equation 1

$$\mu eq/m^3 for\ anions = \frac{[Cl^-]}{35.5} + \frac{[NO_3^-]}{62} + \frac{[SO_4^{2-}]}{96/2}$$

Equation 2

$$\mu eq/m^3 for\ cations = \frac{[NH_4^+]}{18} + \frac{[Na^+]}{23} + \frac{[Mg^{2+}]}{24.3/2} + \frac{[K^+]}{39.1} + \frac{[Ca^{2+}]}{40.1/2}$$

Ion balance is often used to estimate the acidity (proton loading) in atmospheric aerosols. If the sum of measured anions equals to cations, aerosols are assumed neutral; if anions exceed cations, aerosols are acidic; and if cations exceed anions, aerosols are basic [95]. Figure 4-8a shows the anion and cation balance for $PM_{2.5}$ and PM_{10} samples. When regressed over the entire concentration range, the slopes are 1.04 and 0.96, respectively, with an offset of -0.01 μeq/m^3. Figure 4-8b shows ion balance with concentrations zoomed in to 0-0.1 μeq/m^3 range, showing regression slopes of 0.92 and 0.91 for $PM_{2.5}$ and PM_{10} samples, respectively. The fact that cation concentrations are 8-9% lower than anion for samples with lower ionic concentrations indicate that these particles are slightly acidic, as the missing cation is likely dominated by proton ion H^+, which was not measured in this study. On the other hand, cations and anions are in good balance for particles with higher ionic concentrations, indicating that they are nearly neutral.

(a)

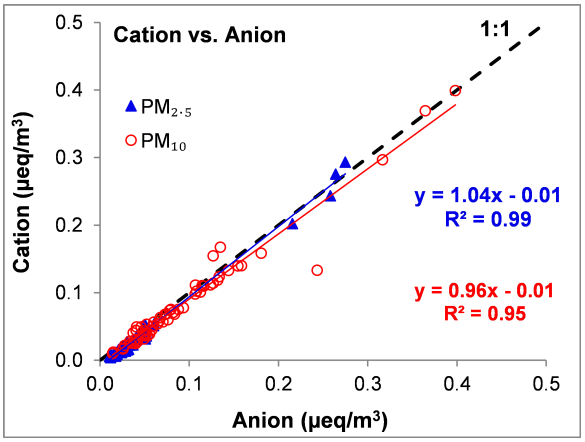

(b)

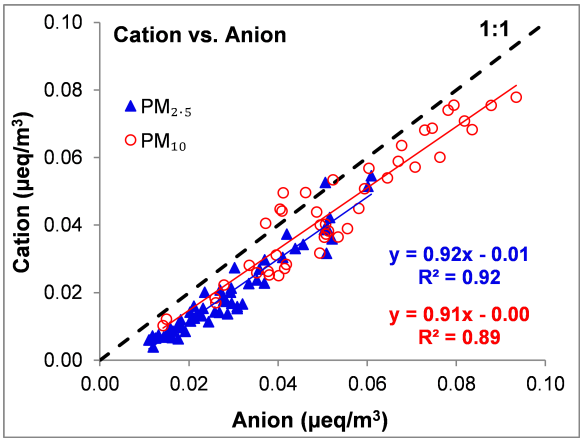

Figure 4-8: Cation versus anion balance for $PM_{2.5}$ and PM_{10} samples: (a) overall all concentration range; and (b) concentration range zoomed in at 0-0.1 μeq/m^3.

4.4 $PM_{2.5}$ and PM_{10} Concentrations and Chemical Characteristics

4.4.1 *$PM_{2.5}$ and PM_{10} Mass Concentrations*

Figure 4-9 shows collocated $PM_{2.5}$ and PM_{10} concentrations at nominal upstream and downstream sites near I-5 and Hwy 710. The average concentrations over the sampling periods are summarized in Table 4-4. At each sampling site, PM_{10} was 2-3 times of $PM_{2.5}$, with average concentrations of ~30 and 10-15 µg/m^3, respectively. The average $PM_{2.5}$ and PM_{10} concentrations at the nominal downwind sites were slightly higher than those at the nominal upwind sites, by approximately 1-4 µg/ m^3.

a)

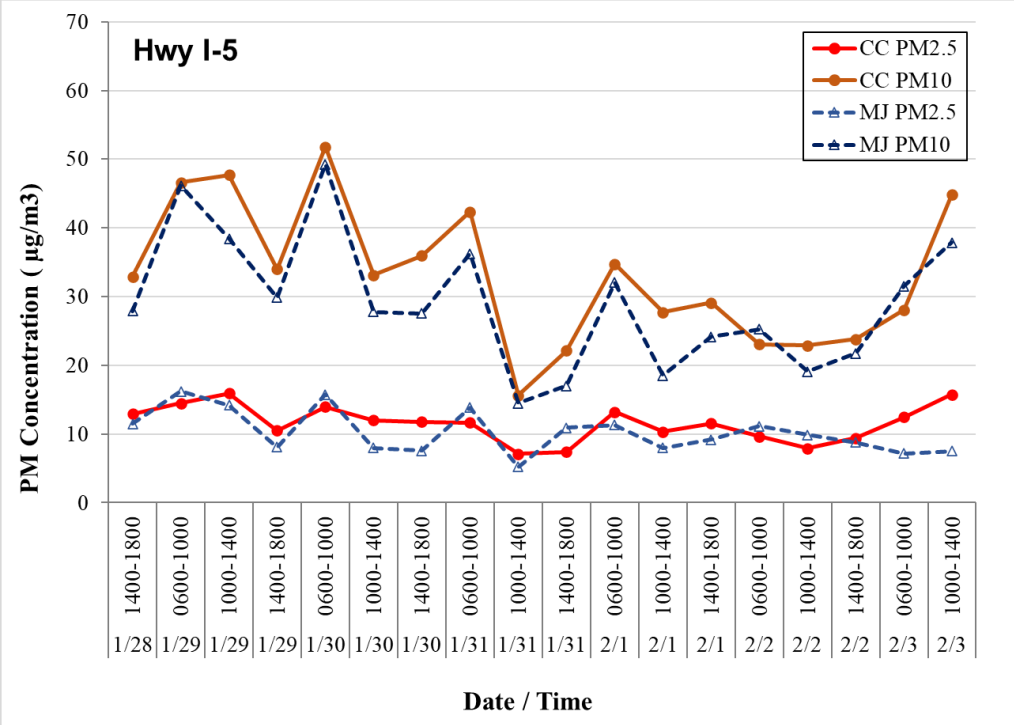

b)

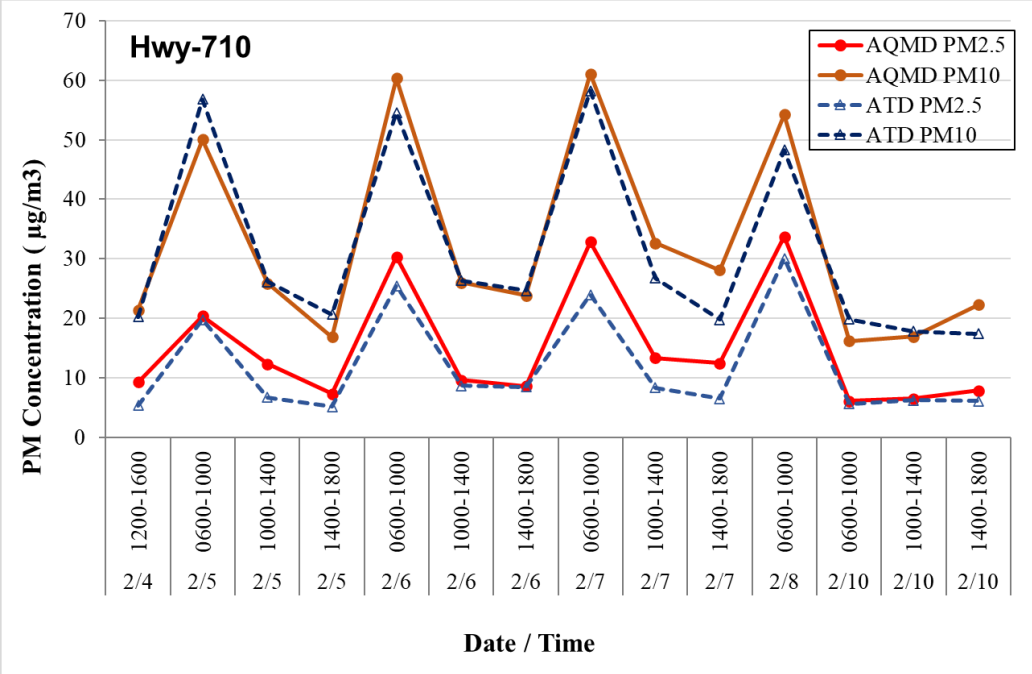

Figure 4-9: Time series of gravimetric $PM_{2.5}$ and PM_{10} concentrations at: (a) I5 and (b) Hwy 710 sites.

Table 4-4. Average $PM_{2.5}$ and PM_{10} concentrations.

Average PM Concentrations (µg/m^3)				
Site	Upwind $PM_{2.5}$	Upwind PM_{10}	Downwind $PM_{2.5}$	Downwind PM_{10}
Hwy I-5	9.56	28.47	10.88	32.49
Hwy 710	11.00	30.37	14.36	31.87

The designation upwind and downwind sites changes with wind direction. As shown in Figure 4-10, the sampling sites has relative consistent wind patterns, characterized by low speed wind in early mornings and evenings and higher speed onshore wind during day time. Approximately, the first filter sampling period (0600-1000) the AQMD sites (nominally downwind sites) were upwind of the highways, although the windspeeds were low, while the AQMD sites were downwind the highway during the second (1000-1400) and third (1400-1800) filter sampling periods. However, the daily wind direction and speed need be examined to determine the upwind and downwind designation.

Figure 4-11 shows the PM concentration differences between the nominal downwind and upwind sites. At the I-5 sampling sites, the downwind concentrations were higher than the upwind concentrations when the wind speed was > 1 m/s, except four data points. On the other hand, at the Hwy-710 sites, while all $PM_{2.5}$ differences were positive, quite a few PM_{10} data points had near zero or negative differences, which could be caused by traffic-induced wind or inhomogeneous PM_{10} concentrations.

a) b)

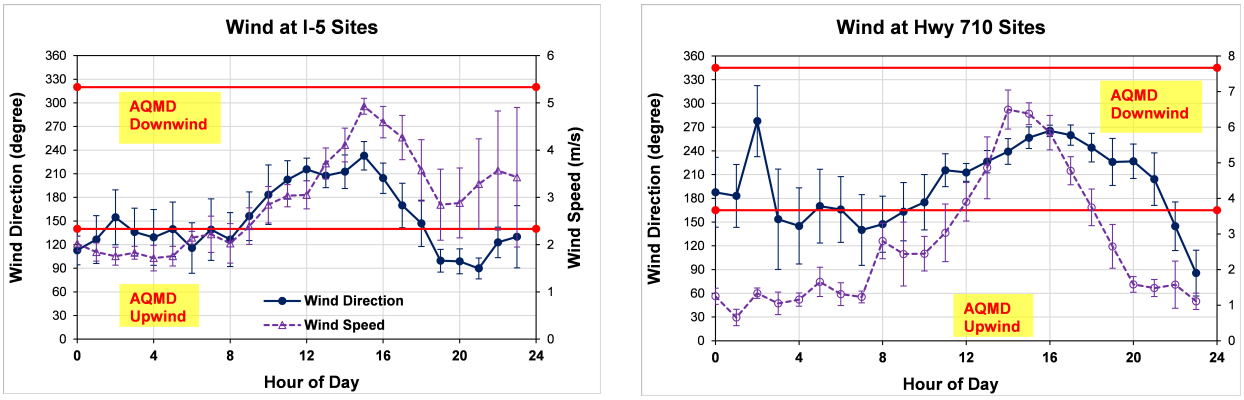

Figure 4-10: Diurnal variation of wind direction and speed at the a) I-5 and b) Hwy-710 sites averaged over the monitoring periods. The wind directions between the two horizontal red lines show approximately when the AQMD near road sites became downwind of the highways.

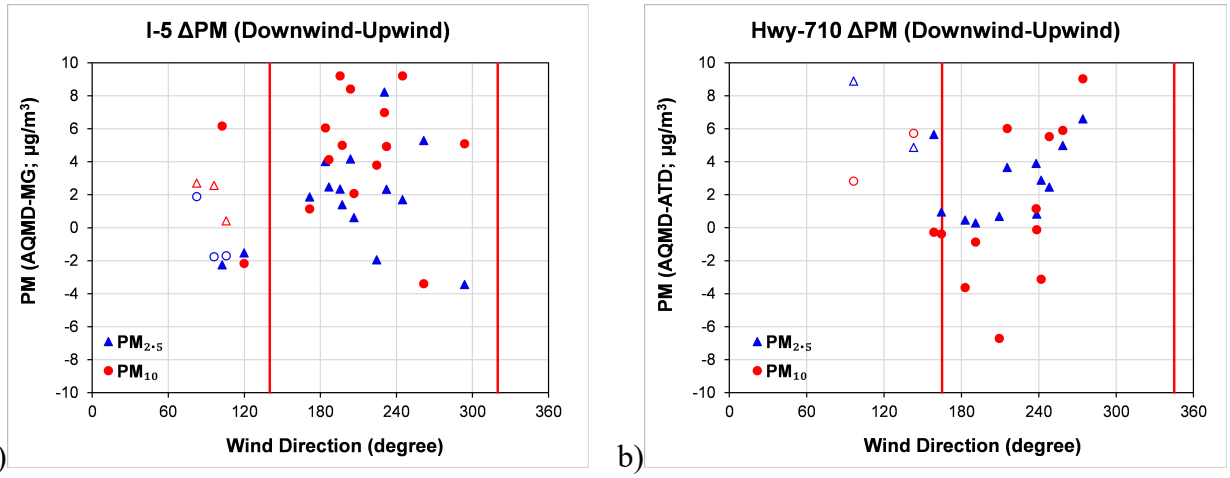

a) b)

Figure 4-11: PM concentration differences between nominal downwind (AQMD near road sites) and upwind sites at: a) I-5 and b) Hwy-710. The wind directions between the two vertical red lines show approximately when the AQMD near road sites were downwind of the highways. The solid and unfilled data symbols represent wind speed > 1 m/s or ≤1 m/s, respectively.

4.4.2 *$PM_{2.5}$ and PM_{10} Chemical Characteristics*

4.4.2.1 Major Chemical Compositions

The relative abundance of major $PM_{2.5}$ and PM_{10} chemical compositions are shown in Figure 4-12. For $PM_{2.5}$, the most abundant compositions are: OM (~30–40%), mineral dust (~25–30%), and EC (~10–15%). For PM_{10}, mineral dust (~40–45%) is the dominant composition, followed by OM (~25%), NO_3^- (~6-11%), and EC (6-8%). This difference between $PM_{2.5}$ and PM_{10} is expected as more mineral dust components in the coarse size fraction lowered the mass percent of the rest of the components.

Figure 4-13 compares major chemical composition concentrations at the four sampling sites. Due to large day-to-day concentration variations (Figure 4-6), most the differences among sites were not statically significant at $p < 0.05$. However, some patterns in the average concentrations are worth noting. For mineral dust, the concentrations at the nominal downwind sites were higher than those at the nominal upwind sites, especially for $PM_{2.5}$. EC was also higher at the downwind sites. It is also interesting to note that $PM_{2.5}$ and PM_{10} EC concentrations at the Hwy-710 sites were 26% and 19% higher than those at the I-5 sites, likely due to more diesel vehicles on Hwy-710. Sulfates are approximately the same, indicating that it is a regional air pollutant. However, nitrate and ammonium were much higher at the Hwy-710 sites than the I-5 sites. These will be further discussed in a later section.

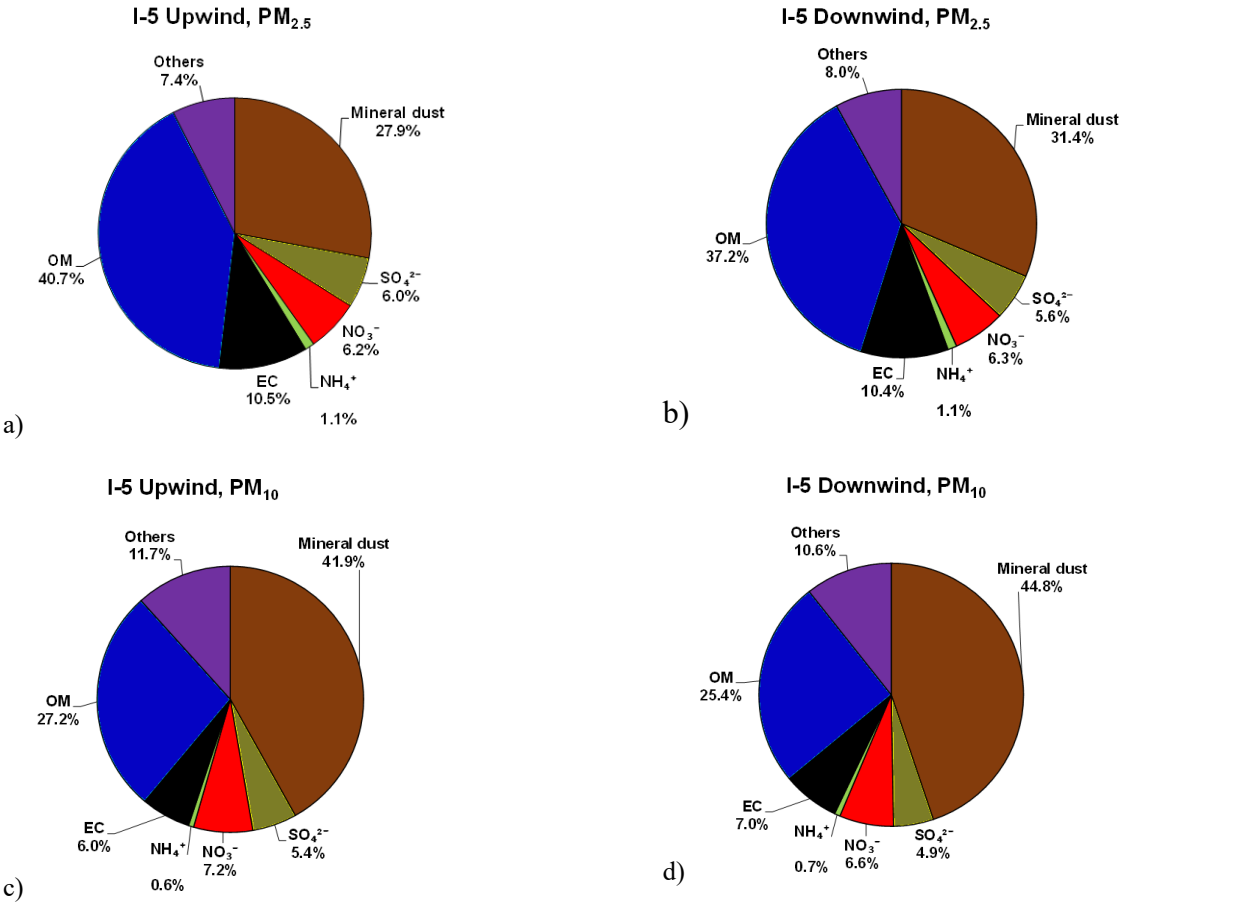

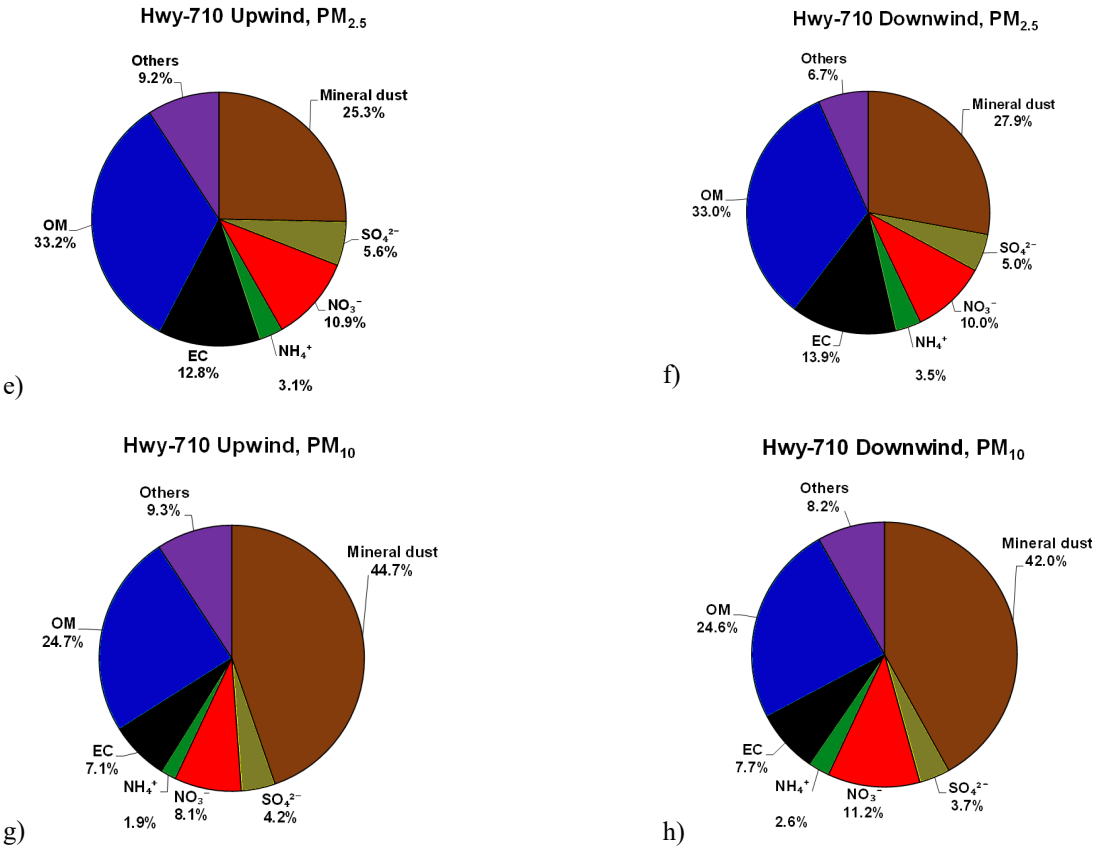

Figure 4-12: Relative abundance of major $PM_{2.5}$ and PM_{10} chemical compositions at the four sampling sites.

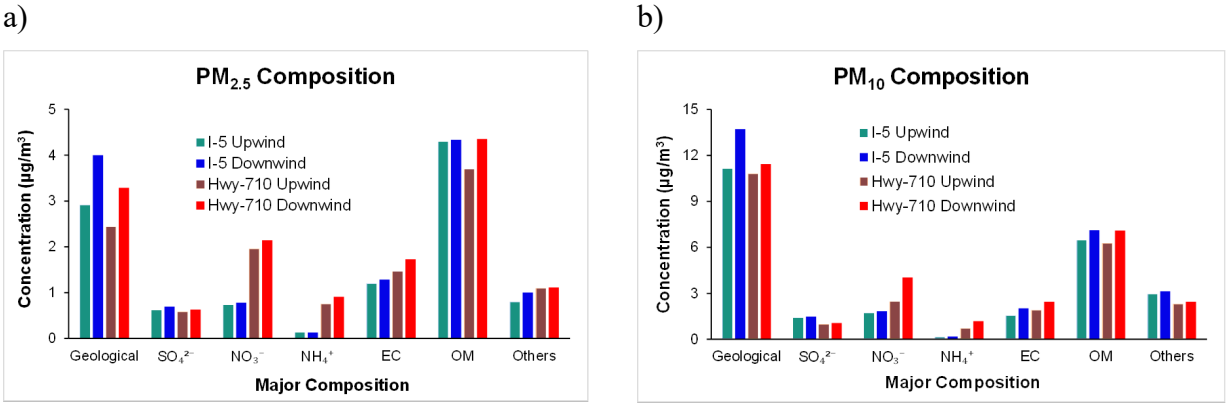

Figure 4-13: Comparison of major chemical compositions concentrations of a) $PM_{2.5}$ and b) PM_{10} at the four sampling sites.

4.4.2.2 Inorganic Ion Species

Figure 4-14 shows that the two I-5 sampling sites had similar $PM_{2.5}$ ion compositions. Except for Mg^{2+} and K^{+}, all other ions show abundances on certain sampling periods. The diversity was likely related to many aerosol sources in an urban setting of Anaheim, CA. With a few exceptions, high concentrations of NH_4^+ and NO_3^- were mostly related to higher RH and lower temperature because these conditions favor partition of NH_4NO_3 in solid phase [96].

The ion compositions are somewhat different at the Hwy-710 sites. As shown in Figure 4-15a and b, there were two high ion concentration events during the 0600–1000 sampling periods on 2/6/2020 and 2/8/2020. Both events featured very high concentrations of NH_4^+. The balancing anions were dominated by Cl^- and NO_3^- on 2/6/2020 and by NO_3^- and SO_4^{2-} on 2/8/2020, indicating potentially different inorganic ion formation pathways. Both events had relatively low ambient temperatures and high RHs with, RH reaching near 100% on 2/8/2020.

To take a more detailed look of ion composition on other sampling dates at the Hwy-710 sites, the two high concentration events were removed in Figure 4-15c and d. Compared to the I-5 sites (Figure 4-14), the Hwy-710 sites had lower concentrations of Na^+; instead, NH_4^+ was the dominant cation during most sampling periods. Compared to more diverse ion abundances at the I-5 sites, ammonium nitrate was the dominant inorganic salt, followed by sulfates at the Hwy-710 sites.

a)

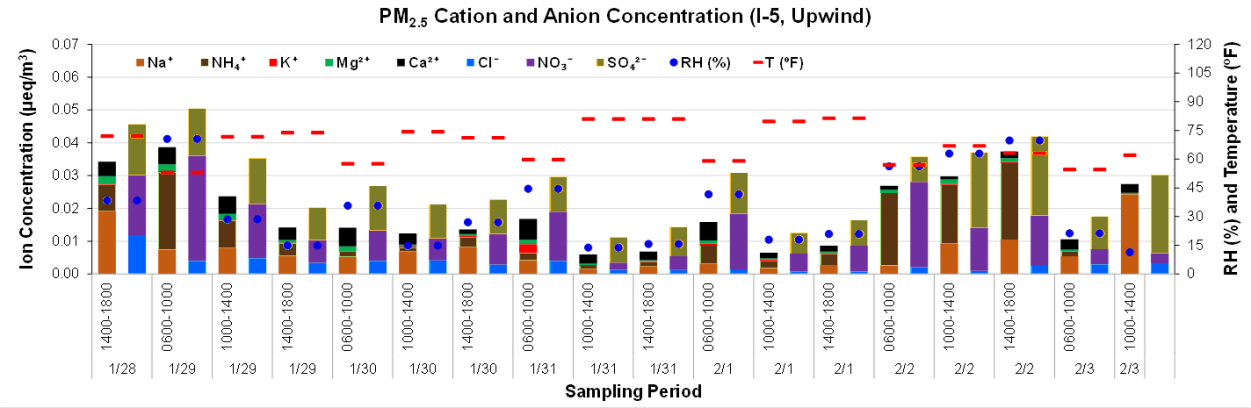

b)

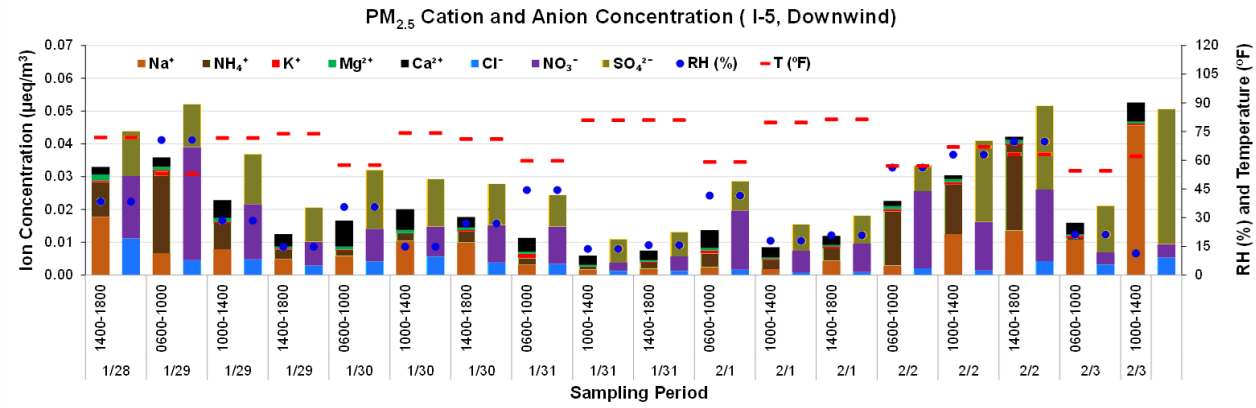

Figure 4-14: Ion concentrations at the I-5 a) upwind and b) downwind sampling sites.

a)

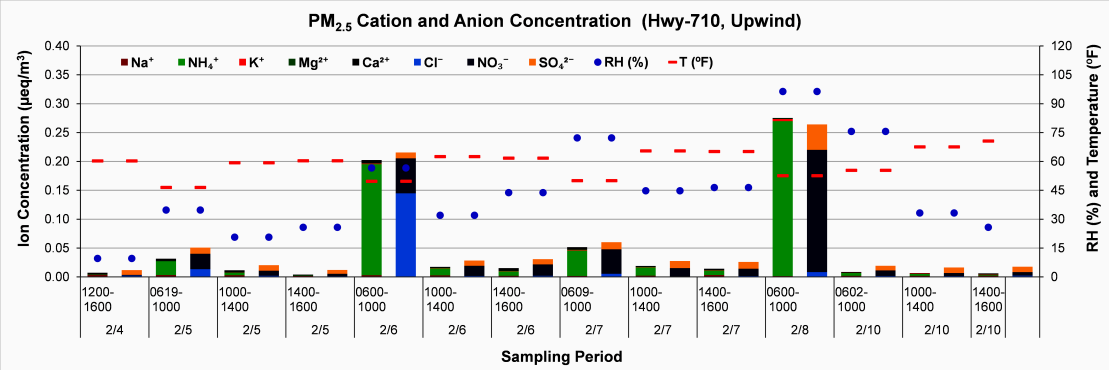
PM2.5 Cation and Anion Concentration (Hwy-710, Upwind)
Ion Concentration (µeq/m3)
RH (%) and Temperature (°F)
Na+ NH4+ K+ Mg2+ Ca2+ Cl− NO3− SO4 2− RH (%) T (°F)
1200-1600 2/4
0619-1000 2/5
1000-1400 2/5
1400-1600 2/5
0600-1000 2/6
1000-1400 2/6
1400-1600 2/6
0609-1000 2/7
1000-1400 2/7
1400-1600 2/7
0600-1000 2/8
0602-1000 2/10
1000-1400 2/10
1400-1600 2/10
Sampling Period

b)

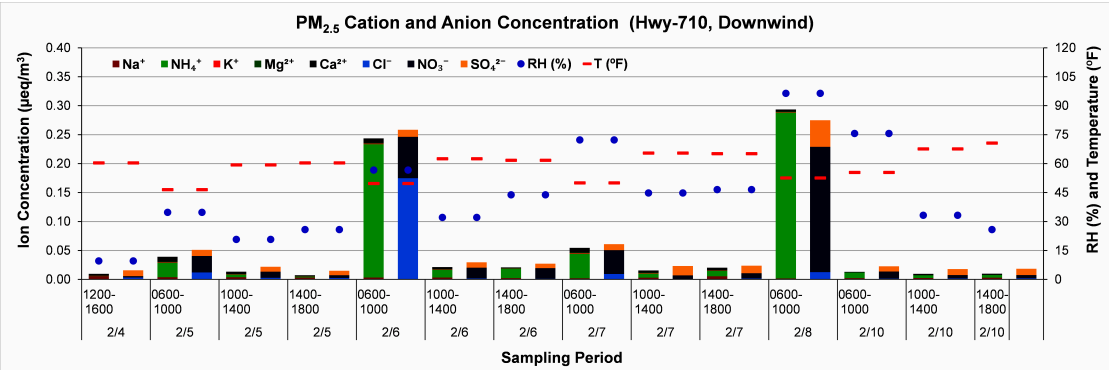
PM2.5 Cation and Anion Concentration (Hwy-710, Downwind)
Ion Concentration (µeq/m3)
RH (%) and Temperature (°F)
Na+ NH4+ K+ Mg2+ Ca2+ Cl− NO3− SO4 2− RH (%) T (°F)
1200-1600 2/4
0600-1000 2/5
1000-1400 2/5
1400-1800 2/5
0600-1000 2/6
1000-1400 2/6
1400-1800 2/6
0600-1000 2/7
1000-1400 2/7
1400-1800 2/7
0600-1000 2/8
0600-1000 2/10
1000-1400 2/10
1400-1800 2/10
Sampling Period

c)

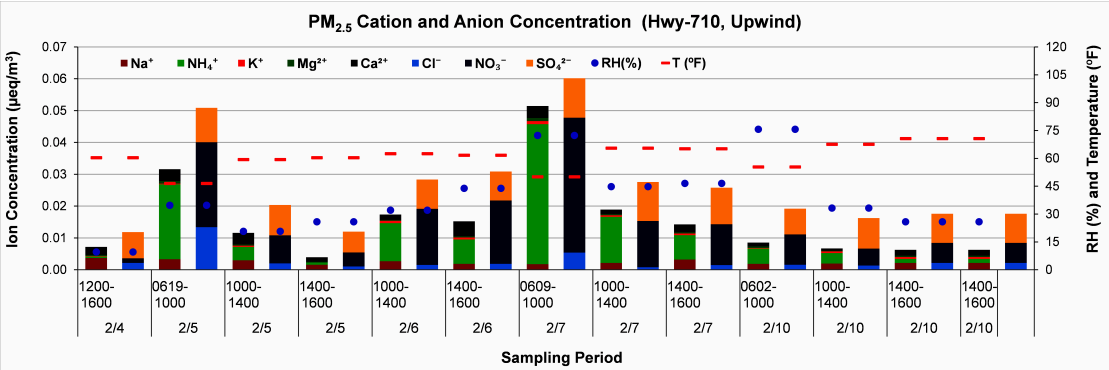
PM2.5 Cation and Anion Concentration (Hwy-710, Upwind)
Ion Concentration (µeq/m3)
RH (%) and Temperature (°F)
Na+ NH4+ K+ Mg2+ Ca2+ Cl− NO3− SO4 2− RH(%) T (°F)
1200-1600 2/4
0619-1000 2/5
1000-1400 2/5
1400-1600 2/5
1000-1400 2/6
1400-1600 2/6
0609-1000 2/7
1000-1400 2/7
1400-1600 2/7
0602-1000 2/10
1000-1400 2/10
1400-1600 2/10
1400-1600 2/10
Sampling Period

d)

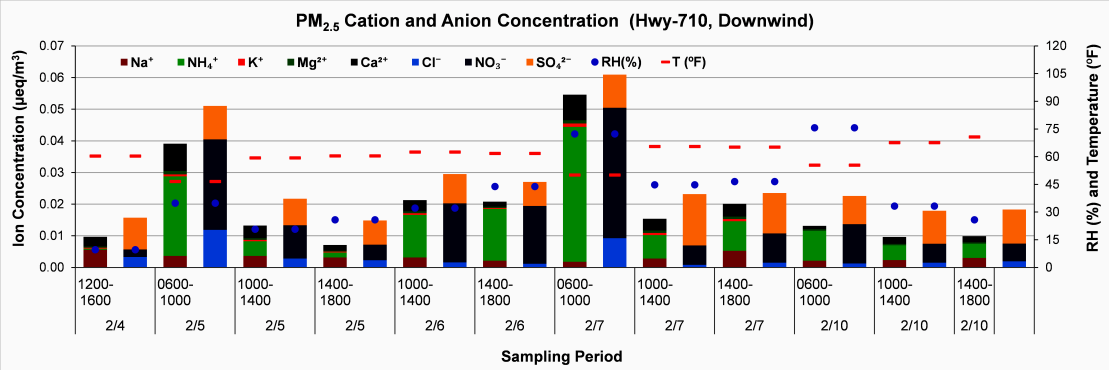

Figure 4-15: Ion concentrations at the two I-710 sampling sites: a) upwind with all data; b) downwind with all data; c) upwind without the 2/6 and 2/8 events; and d) downwind without the 2/6 and 2/8 events.

4.4.2.3 Elemental Composition: The Squared Pearson Correlations of XRF Elemental Data

XRF data obtained by DRI's PM samplers provided four-hour intervals of various element concentrations. Given that 51 element concentrations were provided in the XRF data at each location, only elements pertaining to non-exhaust PM and road dust (Si, Ca. Al, K) were prioritized. Previous research summarized by Thorpe and Harrison [3], states that elements such as Al, Ba, Ca, Cr, Cu, Fe, K, Mn, Mo, Sb, Sr, and Zn are representative of metal concentrations present in brake linings and emitted brake dust. Similarly, other metals like Si, Ti, and Zr are typically found in brake fillers, fibers, and abrasives respectively [11, 12]. These 15 elements were selected for further analysis as they are representative of key tracers for non-exhaust PM [29].

To assess statistical relationships between the selected elements, the squared Pearson correlation coefficient (R^2) was obtained through Equation 3. The value R^2, commonly referred to as the coefficient of determination explains the variability of the dependent variable, y, by the variation of the independent variable, x. Values of x_m and y_m are the averages of each respective data set. Resulting values range between 0 to 1, for a linear regression model.

Equation 3

$$R^2 = \frac{\Sigma[(x-x_m)*(y-y_m)]}{\sqrt{[\Sigma(x-x_m)^2 * \Sigma(y-y_m)^2]}}$$

To calculate R^2 values each element was individually cross examined against the remaining elements except itself. This process was replicated by only using data from the downwind locations at both Anaheim and Long Beach sites. To observe changes due to background element concentrations, another set of R^2 values were calculated by then subtracting the upwind element concentrations to the downwind concentrations.

For the Anaheim site using $PM_{2.5}$ element concentrations, strong intercorrelations are observed between Si and the elements Ca, Al, and K. This is seen in both Figure 4-16 with the downwind elements only and in Figure 4-17 which accounts for background crustal materials included in the road dust. R^2 between Fe-Ti, Fe-Cu, and Cu-Ti increase when the background concentration

is removed. Fe, Cu, and Ti are brake markers. A similar occurrence is seen between Figure 4-18 and Figure 4-19 which shows Anaheim's PM_{10} element concentrations. The downwind only Si-Ca, Si-Al, and Si-K have R^2 values of 0.94, 0.98, 0.92 respectively, which reduce to 0.79, 0.81, and 0.33 when background concentration is removed. This suggests that potassium variability is not explained by changes due to background concentrations. The background can be affected by variables such as wind direction, wind speed, and location. The opposite trend is seen with Fe for both $PM_{2.5}$ and PM_{10} R^2 values. When background is removed, Fe concentrations better correlate with variations of Zn, Ti, Cu, Ba and Zr, which are markers for brake wear particles. It should be noted PM_{10} has bigger contribution and stronger correlations for brake related elements.

The $PM_{2.5}$ element concentrations at the Long Beach site had numerous high R^2 values for elements including Fe, Si, Cu, Sr, and Zr. However, when background concentration was removed, those values decreased significantly. Figure 4-20 shows an abundance of green highlighted cells with R^2 between 0.55 and 0.92 while Figure 4-21 only shows Si-K at 0.89. A similar trend is seen between Figure 4-22 and Figure 4-23 where PM_{10} element concentrations were considered. It is important to note that the upwind location at the Long Beach site was approximately one kilometer away from the downwind location while the Anaheim upwind location was directly across the highway from the downwind location by 80 meters.

Anaheim AQMD PM2.5 Filter XRF : Element vs Element R^2

	Fe	Si	Ca	Al	K	Zn	Ti	Cu	Ba	Sb	Sr	Cr	Mn	Zr
Fe														
Si	0.54													
Ca	0.62	0.90												
Al	0.55	0.96	0.89											
K	0.42	0.72	0.67	0.69										
Zn	0.32	0.09	0.20	0.15	0.32									
Ti	0.73	0.60	0.53	0.60	0.38	0.11								
Cu	0.56	0.19	0.18	0.19	0.12	0.07	0.77							
Ba	0.07	0.09	0.02	0.10	0.01	0.03	0.26	0.21						
Sb	0.02	0.03	0.02	0.01	0.00	0.00	0.01	0.00	0.01					
Sr	0.43	0.37	0.46	0.47	0.25	0.34	0.44	0.20	0.07	0.01				
Cr	0.08	0.00	0.00	0.00	0.01	0.04	0.00	0.01	0.03	0.02	0.00			
Mn	0.53	0.18	0.24	0.27	0.26	0.63	0.42	0.38	0.06	0.01	0.58	0.03		
Zr	0.65	0.25	0.26	0.26	0.17	0.14	0.69	0.83	0.26	0.03	0.22	0.07	0.50	
Mo	0.06	0.01	0.00	0.01	0.00	0.07	0.00	0.06	0.00	0.00	0.00	0.20	0.08	0.21

Figure 4-16: Anaheim downwind $PM_{2.5}$ XRF element squared Pearson correlation

Anaheim Downwind - Upwind PM2.5 Filter XRF : Element vs Element R^2														
	Fe	Si	Ca	Al	K	Zn	Ti	Cu	Ba	Sb	Sr	Cr	Mn	Zr
Fe														
Si	0.28													
Ca	0.23	0.83												
Al	0.25	0.78	0.57											
K	0.36	0.67	0.73	0.37										
Zn	0.38	0.17	0.06	0.17	0.06									
Ti	0.87	0.17	0.16	0.17	0.28	0.29								
Cu	0.81	0.06	0.07	0.07	0.13	0.43	0.81							
Ba	0.47	0.04	0.03	0.06	0.04	0.29	0.60	0.50						
Sb	0.01	0.03	0.01	0.02	0.05	0.05	0.01	0.03	0.00					
Sr	0.01	0.13	0.13	0.19	0.04	0.03	0.00	0.00	0.00	0.00				
Cr	0.01	0.01	0.02	0.06	0.00	0.02	0.03	0.01	0.00	0.02	0.04			
Mn	0.19	0.00	0.01	0.04	0.02	0.17	0.35	0.31	0.23	0.00	0.00	0.04		
Zr	0.52	0.00	0.01	0.00	0.03	0.22	0.48	0.65	0.21	0.06	0.01	0.05	0.30	
Mo	0.02	0.13	0.09	0.21	0.09	0.04	0.03	0.00	0.01	0.02	0.00	0.02	0.05	0.14

Figure 4-17: Anaheim downwind – upwind $PM_{2.5}$ XRF filter element squared Pearson correlation

Anaheim AQMD PM10 Filter XRF : Element vs Element Correlation R^2														
	Fe	Si	Ca	Al	K	Zn	Ti	Cu	Ba	Sb	Sr	Cr	Mn	Zr
Fe														
Si	0.70													
Ca	0.77	0.94												
Al	0.66	0.98	0.91											
K	0.64	0.92	0.87	0.93										
Zn	0.47	0.36	0.42	0.31	0.42									
Ti	0.89	0.74	0.72	0.70	0.68	0.31								
Cu	0.43	0.08	0.09	0.06	0.07	0.09	0.50							
Ba	0.67	0.20	0.28	0.16	0.19	0.30	0.60	0.76						
Sb	0.00	0.03	0.04	0.05	0.05	0.02	0.00	0.07	0.02					
Sr	0.40	0.46	0.36	0.47	0.52	0.15	0.48	0.16	0.17	0.00				
Cr	0.25	0.09	0.17	0.10	0.07	0.01	0.22	0.22	0.24	0.01	0.01			
Mn	0.77	0.82	0.74	0.80	0.76	0.38	0.78	0.18	0.32	0.00	0.49	0.16		
Zr	0.39	0.05	0.07	0.03	0.05	0.08	0.44	0.95	0.75	0.14	0.13	0.24	0.17	
Mo	0.07	0.07	0.06	0.07	0.10	0.06	0.07	0.00	0.04	0.00	0.18	0.06	0.06	0.00

Figure 4-18: Anaheim downwind PM_{10} XRF element squared Pearson correlation

Anaheim Downwind - Upwind PM10 Filter XRF : Element vs Element R^2														
	Fe	Si	Ca	Al	K	Zn	Ti	Cu	Ba	Sb	Sr	Cr	Mn	Zr
Fe														
Si	0.31													
Ca	0.41	0.79												
Al	0.26	0.81	0.68											
K	0.56	0.33	0.22	0.24										
Zn	0.69	0.32	0.46	0.39	0.29									
Ti	0.90	0.27	0.30	0.21	0.49	0.70								
Cu	0.90	0.14	0.23	0.13	0.39	0.69	0.90							
Ba	0.69	0.07	0.17	0.07	0.32	0.63	0.76	0.80						
Sb	0.01	0.17	0.09	0.30	0.01	0.00	0.01	0.04	0.02					
Sr	0.53	0.22	0.23	0.12	0.27	0.38	0.43	0.46	0.28	0.00				
Cr	0.29	0.02	0.08	0.11	0.26	0.21	0.20	0.29	0.22	0.01	0.03			
Mn	0.67	0.25	0.34	0.12	0.43	0.26	0.48	0.49	0.26	0.07	0.50	0.08		
Zr	0.87	0.15	0.25	0.13	0.35	0.70	0.89	0.94	0.81	0.04	0.37	0.28	0.43	
Mo	0.01	0.03	0.01	0.00	0.01	0.01	0.01	0.06	0.00	0.02	0.00	0.25	0.00	0.04

Figure 4-19: Anaheim downwind – upwind PM_{10} XRF element squared Pearson correlation.

Long Beach AQMD PM2.5 Filter XRF : Element vs Element Correlation R^2														
	Fe	Si	Ca	Al	K	Zn	Ti	Cu	Ba	Sb	Sr	Cr	Mn	Zr
Fe														
Si	0.80													
Ca	0.78	0.92												
Al	0.84	0.88	0.79											
K	0.81	0.64	0.64	0.58										
Zn	0.57	0.44	0.47	0.42	0.73									
Ti	0.61	0.49	0.41	0.68	0.40	0.26								
Cu	0.90	0.67	0.65	0.81	0.80	0.58	0.65							
Ba	0.58	0.30	0.26	0.53	0.36	0.35	0.35	0.58						
Sb	0.42	0.29	0.31	0.27	0.60	0.33	0.54	0.47	0.07					
Sr	0.63	0.67	0.65	0.80	0.38	0.23	0.72	0.64	0.36	0.33				
Cr	0.41	0.38	0.30	0.43	0.31	0.57	0.44	0.38	0.35	0.16	0.43			
Mn	0.67	0.51	0.37	0.45	0.71	0.47	0.37	0.54	0.39	0.38	0.25	0.36		
Zr	0.75	0.63	0.45	0.72	0.54	0.31	0.73	0.68	0.42	0.35	0.56	0.45	0.72	
Mo	0.24	0.14	0.11	0.09	0.40	0.55	0.00	0.16	0.29	0.04	0.01	0.19	0.33	0.07

Figure 4-20: Long Beach downwind $PM_{2.5}$ XRF element squared Pearson correlation

Long Beach Downwind - Upwind PM2.5 Filter XRF : Element vs Element R^2														
	Fe	Si	Ca	Al	K	Zn	Ti	Cu	Ba	Sb	Sr	Cr	Mn	Zr
Fe														
Si	0.55													
Ca	0.55	0.54												
Al	0.45	0.34	0.61											
K	0.62	0.89	0.69	0.49										
Zn	0.20	0.23	0.26	0.06	0.25									
Ti	0.02	0.00	0.09	0.18	0.02	0.33								
Cu	0.34	0.31	0.17	0.18	0.25	0.01	0.14							
Ba	0.15	0.07	0.02	0.01	0.03	0.00	0.42	0.39						
Sb	0.08	0.17	0.25	0.33	0.23	0.03	0.00	0.28	0.04					
Sr	0.03	0.03	0.06	0.04	0.03	0.18	0.30	0.15	0.13	0.05				
Cr	0.32	0.33	0.37	0.22	0.41	0.32	0.13	0.10	0.01	0.09	0.09			
Mn	0.09	0.31	0.00	0.01	0.26	0.11	0.01	0.06	0.00	0.03	0.17	0.19		
Zr	0.00	0.04	0.12	0.03	0.06	0.34	0.05	0.00	0.02	0.02	0.05	0.06	0.00	
Mo	0.12	0.57	0.11	0.03	0.35	0.32	0.00	0.10	0.03	0.04	0.08	0.33	0.44	0.12

Figure 4-21: Long Beach downwind – upwind $PM_{2.5}$ XRF element squared Pearson correlation

Long Beach AQMD PM10 Filter XRF : Element vs Element Correlation R^2														
	Fe	Si	Ca	Al	K	Zn	Ti	Cu	Ba	Sb	Sr	Cr	Mn	Zr
Fe														
Si	0.86													
Ca	0.88	0.98												
Al	0.88	0.98	0.98											
K	0.89	0.96	0.94	0.92										
Zn	0.85	0.71	0.78	0.74	0.79									
Ti	0.75	0.65	0.68	0.75	0.61	0.67								
Cu	0.88	0.58	0.61	0.61	0.67	0.78	0.66							
Ba	0.61	0.29	0.30	0.30	0.36	0.47	0.46	0.79						
Sb	0.17	0.19	0.17	0.16	0.27	0.13	0.02	0.15	0.04					
Sr	0.78	0.80	0.78	0.79	0.77	0.58	0.78	0.60	0.48	0.04				
Cr	0.67	0.54	0.61	0.61	0.58	0.88	0.58	0.61	0.32	0.13	0.38			
Mn	0.84	0.84	0.88	0.85	0.86	0.81	0.73	0.65	0.37	0.20	0.78	0.67		
Zr	0.86	0.59	0.61	0.62	0.69	0.80	0.62	0.97	0.72	0.23	0.57	0.67	0.68	
Mo	0.32	0.16	0.21	0.15	0.26	0.42	0.08	0.33	0.29	0.15	0.08	0.33	0.30	0.31

Figure 4-22: Long Beach downwind PM_{10} XRF element squared Pearson correlation

Long Beach Downwind - Upwind PM10 Filter XRF : Element vs Element R^2														
	Fe	Si	Ca	Al	K	Zn	Ti	Cu	Ba	Sb	Sr	Cr	Mn	Zr
Fe														
Si	0.40													
Ca	0.64	0.38												
Al	0.34	0.70	0.35											
K	0.46	0.94	0.32	0.61										
Zn	0.42	0.74	0.43	0.64	0.62									
Ti	0.08	0.20	0.39	0.49	0.10	0.38								
Cu	0.75	0.07	0.32	0.11	0.14	0.08	0.01							
Ba	0.44	0.03	0.38	0.10	0.04	0.11	0.15	0.40						
Sb	0.15	0.31	0.27	0.26	0.30	0.33	0.17	0.01	0.05					
Sr	0.19	0.07	0.35	0.13	0.04	0.11	0.22	0.12	0.01	0.14				
Cr	0.35	0.30	0.07	0.29	0.30	0.45	0.00	0.15	0.09	0.07	0.02			
Mn	0.37	0.38	0.23	0.29	0.34	0.24	0.05	0.14	0.17	0.19	0.00	0.09		
Zr	0.50	0.01	0.16	0.02	0.04	0.05	0.00	0.76	0.31	0.04	0.03	0.12	0.07	
Mo	0.01	0.10	0.02	0.13	0.09	0.07	0.01	0.01	0.03	0.23	0.07	0.17	0.30	0.05

Figure 4-23: Long Beach downwind – upwind PM_{10} XRF element squared Pearson correlation

4.4.2.4 Distribution of Elements in Different Size Ranges

PM samples were collected by a MOUDI [97]. The MOUDI collected particles on six stages: 0.056-0.56, 0.56-1, 1-3.2, 3.2-10, 10-18, and >18 μm at a flow rate of 30 L/min. The sampling time ranged from 6 to 12.5 hours. Three sets of samples were collected near I-5 and two samples were collected near I-710. In addition, three sample sets were collected at an urban background site in Irvine, CA to compare near road and urban background environment. The main purpose of MOUDI sample, which was collected at downwind locations of the current study by Dr. Manabu's group at UCI (University of California, Irvine) and analyzed by Park at GIST (Gwangju Institute of Science and Technology) in-kind, was to better understand the effect of size speciated chemical composition on particle toxicity. The filter samples were digested by an acid solution (i.e., a mixture of HNO_3, HF, and H_3BO_3) using a microwave digestion system. The extracts were analyzed by both an Inductively Coupled Plasma – Mass Spectrometer (ICP-MS) and an Inductively Coupled Plasma – Optical Emission Spectrometer (ICP-OES). The elements by ICP-MS and ICP-OES were merged by choosing the method with the best recovery efficiency.

Figure 4-24 shows the average elemental concentration ratios between I-5, I-710, and Irvine urban sites using the concentration at the I-5 site as the reference. For most elements, the concentrations were the highest near I-5 and the lowest at the Irvine urban background site, indicating strong influence of traffic-related emissions near highways. For nominal resuspended road dust markers Al and Si in the 1-10 μm size range, the concentrations near I-5 were 2-3 times of those near I-710 and >4 times of those in Irvine. This is consistent with sampling locations. For brake wear markers Cu, Zr, and Ba, the concentrations near I-5 were 1.5–4 times of those near I-710 and 2–10 times of those in Irvine across all size ranges. For tire wear marker Zn, the concentrations near I-5 were 1.8 times of those near I-710 and 2 times of those in Irvine for the 1-10 μm size ranges.

Figure 4-25 shows the size distribution of elements in the 6 MOUDI size bins at the three sampling sites. Road dust markers Al and Si, as well as K, Ca, Ti, Fe, Mn, Rb, and Sr had higher concentrations in the size range of > 1 µm, with highest concentrations typically in the 3.2–10 or 10-18 µm size bins. The brake wear markers Cu, Zr, and Ba had the highest concentrations in the 1–3.2 or 3.2–10 µm size bins. They also had relatively high concentration in the 0.056–0.56 µm size bin, probably related to the evaporative emissions at high brake temperatures. The tire marker Zn had higher concentrations at the smaller (<1 µm) and larger (>3.2 µm) size range with the minimum in the 1–3.2 µm bin. The two modes are probably related to the hot evaporation/condensation and mechanical abrasion process, respectively. Figure 4-26 plots stacked bar charts of elements in different size ranges. Elements with higher and lower concentrations are plotted in left and right panels, respectively, for better illustration of the distributions. Similar to the data in Figure 4-25, both I-5 and I-710 samples show relative high elemental concentrations in the 3.2–10 µm size bin. Elements with lower concentrations also show higher concentrations in the 0.056–0.56 µm size bin; considering their small sizes, the number concentrations of particles containing these elements were quite high.

a)

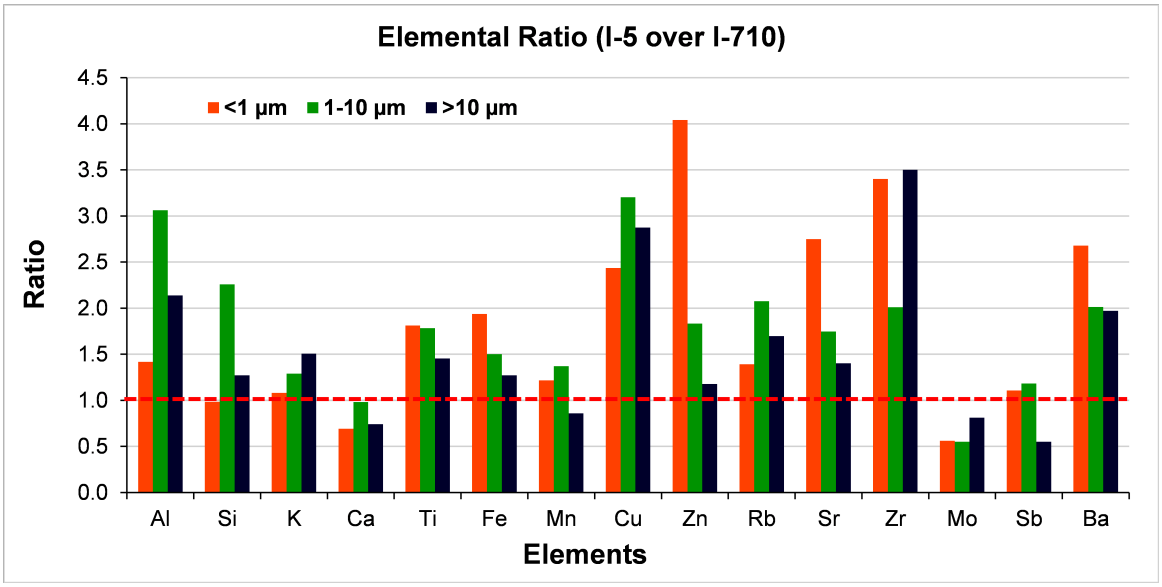

b)

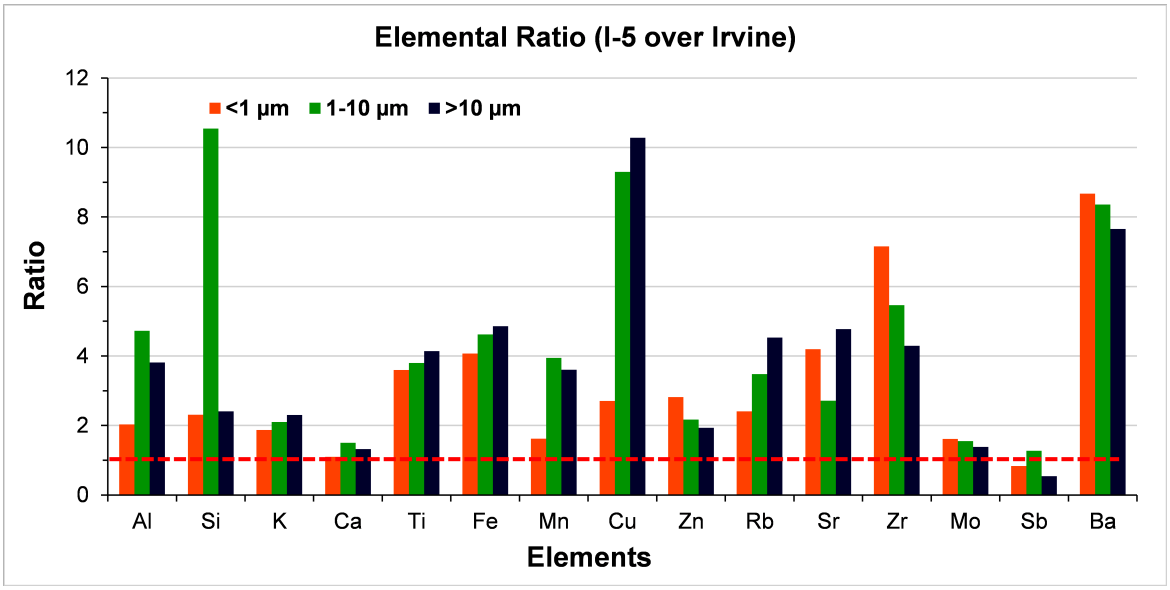

Figure 4-24: Elemental concentration ratios between: a) I-5 over I-710; and b) I-5 over Irvine, CA. The horizontal red dash lines indicate ratio of 1.

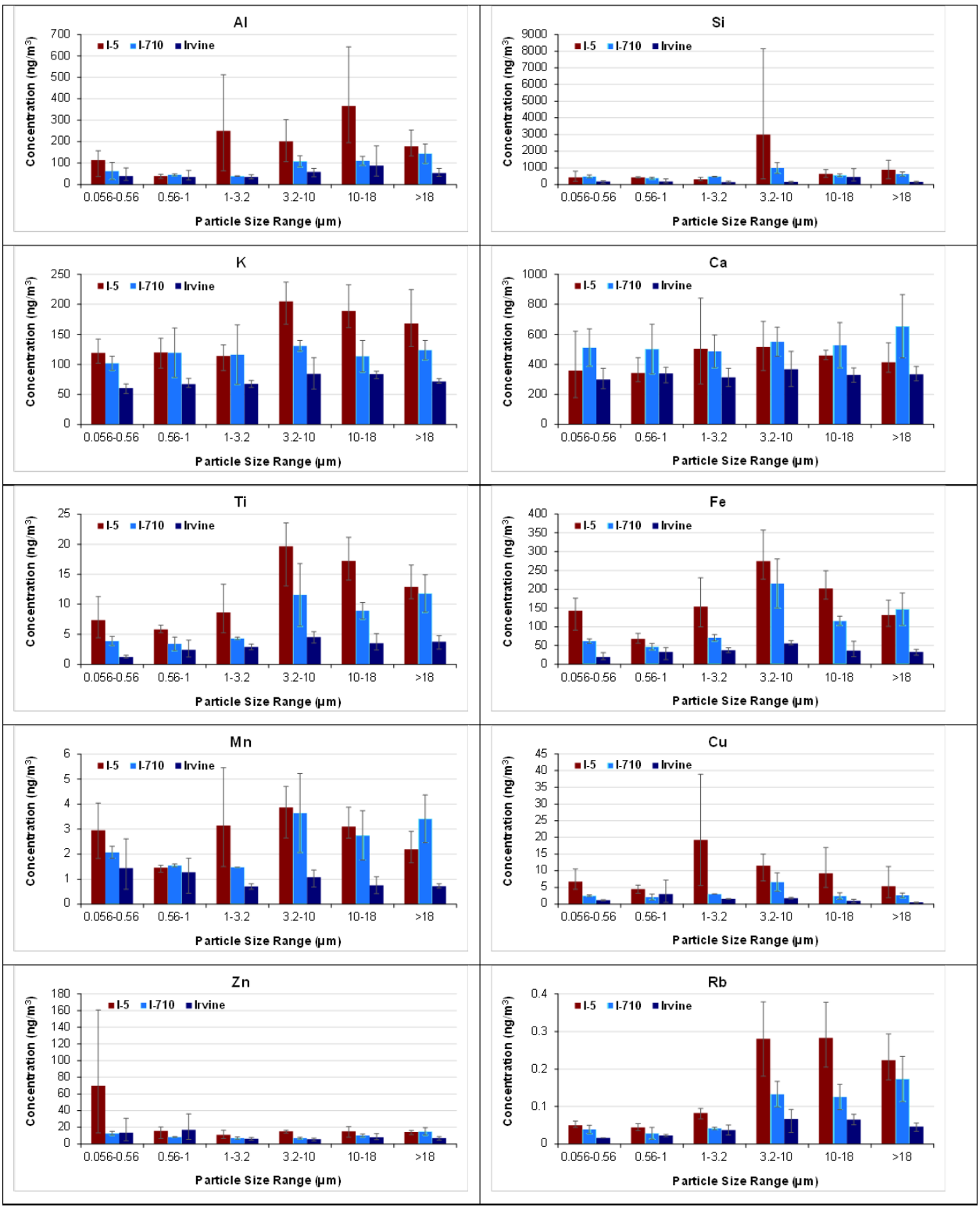
Al
Si
K
Ca
Ti
Fe
Mn
Cu
Zn
Rb
I-5
I-710
Irvine
Concentration (ng/m³)
0.056-0.56
0.56-1
1-3.2
3.2-10
10-18
>18
Particle Size Range (µm)

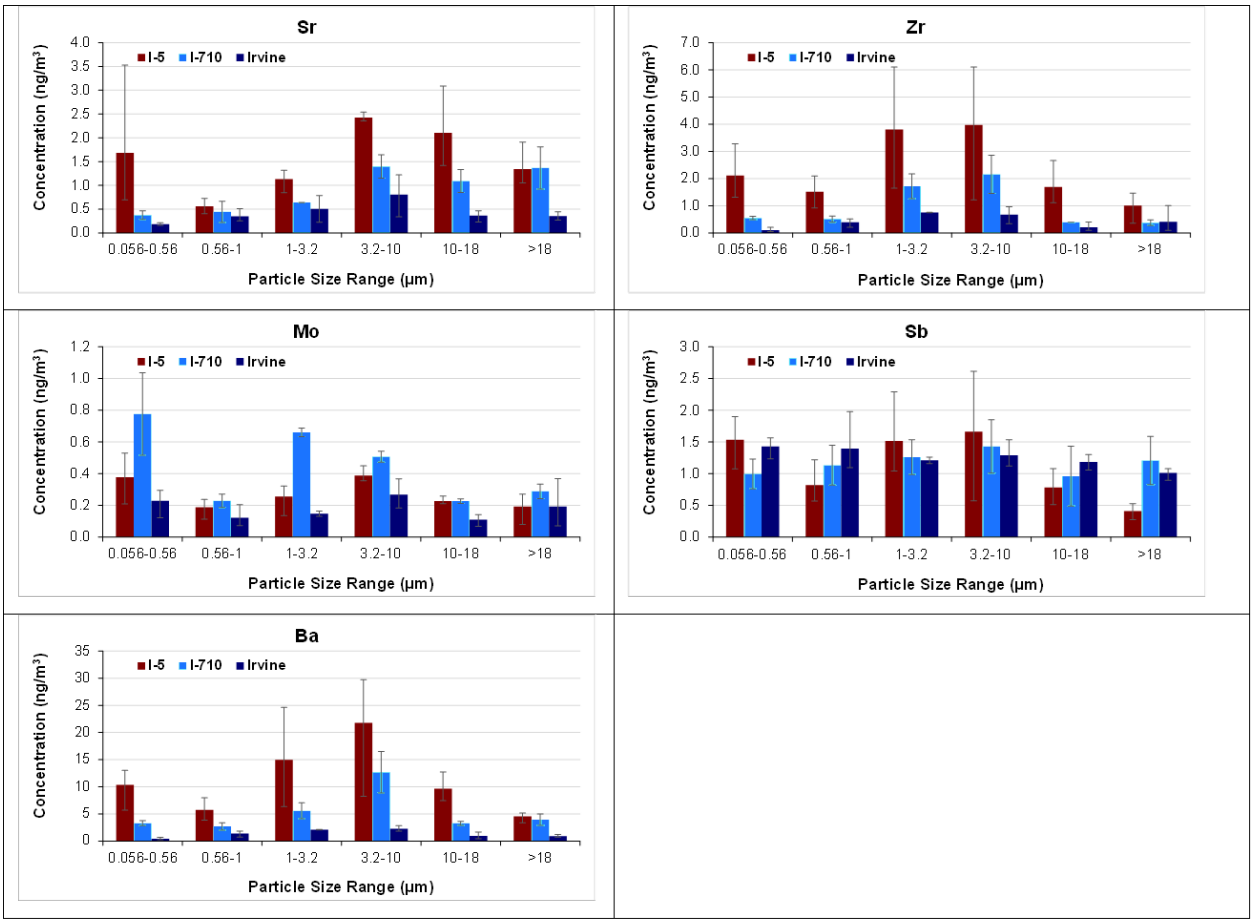

Figure 4-25: Distribution of elements in different size ranges. The bar heights and error bars indicate average and range of concentrations from multiple samples at the same site.

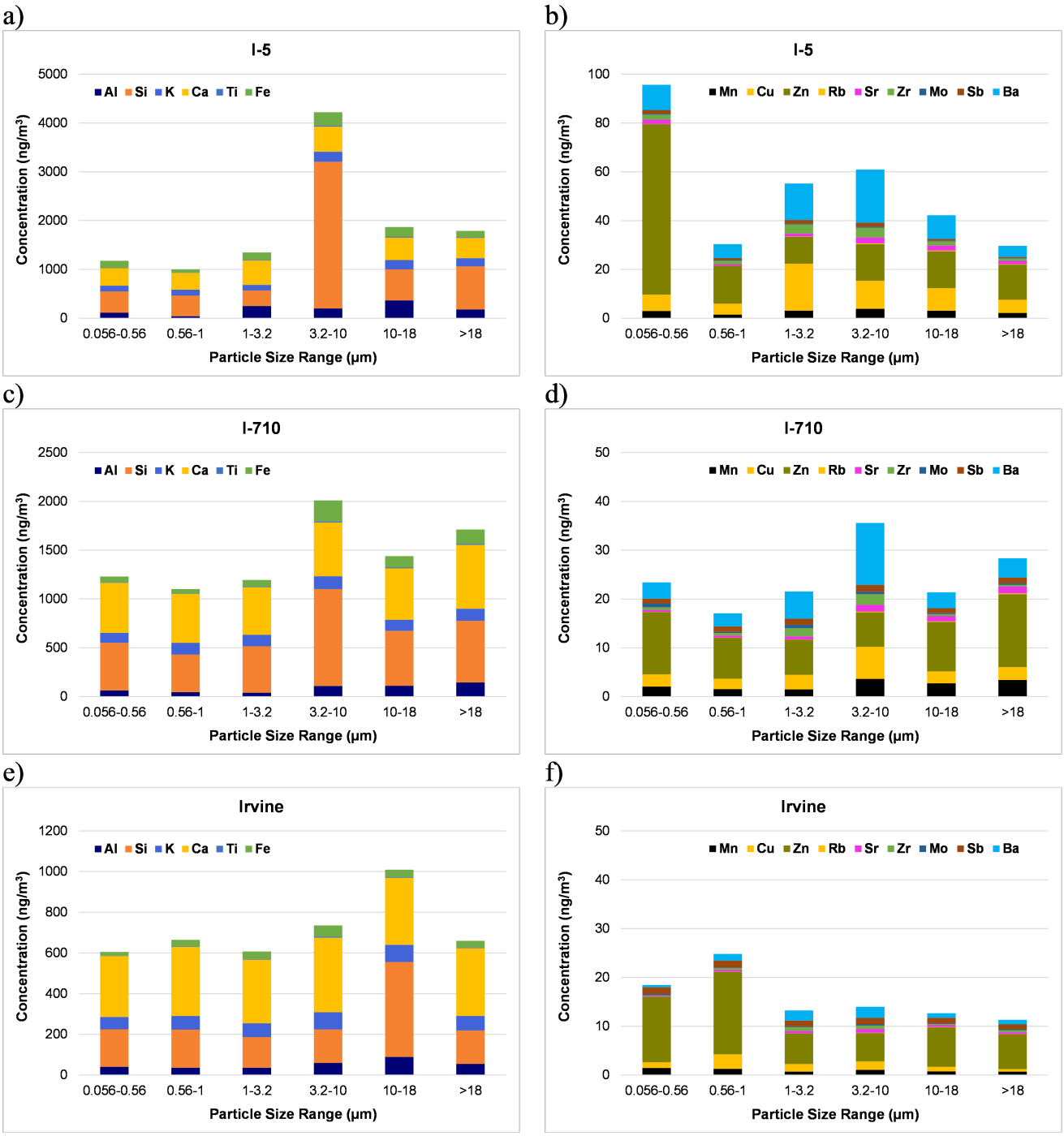

Figure 4-26: Size distribution of elemental composition. Left panels: elements with higher concentrations; and right panels: elements with lower concentrations.

4.4.2.4 Organic Composition

Table 4-5 summarizes the $PM_{2.5}$ and PM_{10} organic group concentrations at the four sampling sites. The concentrations are statistically similar ($p<0.05$) between the nominal upwind and downwind sites near each highway. The upwind/downwind differences were probably masked by the high background concentrations. Furthermore, the organic concentrations in $PM_{2.5}$ and PM_{10} size fractions are also similar, indicating that most organic species were in the $PM_{2.5}$ size fraction. However, the differences between I-5 and Hwy-710 sites are statistically significant ($p<0.05$). The concentrations of PAHs at the Hwy-710 sites were 47% higher than those at the I-5 sites. On the other hand, the I-5 sites had higher alkanes and alkenes (1.6 times), hopanes (2.3 times), steranes (1.5 times), and phthalates (6.1 times) than the Hwy-710 sites. Overall, the I-5 sites have higher measured organic concentrations than the Hwy-710 sites. These differences are likely caused by different vehicle fleet composition as well as background PM compositions. Table 4-6 summarizes the abundances of organic groups in $PM_{2.5}$ and PM_{10} samples. Again, the abundances at upwind and downwind sites are similar. Due to the higher PM_{10} mass concentrations contributed by mineral dust (Figure 4-12), the organic abundances in PM_{10} are lower than those in $PM_{2.5}$. Excluding the variable phthalate concentrations, the sums of speciated organic concentrations are 0.30-0.53% of $PM_{2.5}$ mass and 0.12-0.21% of PM_{10} mass.

Table 4-5: Average $PM_{2.5}$ and PM_{10} organic group concentrations (average ± standard deviation in ng/m^3).

Size	$PM_{2.5}$				PM_{10}			
Organics\Sites	I-5 Upwind	I-5 Downwind	Hwy-710 Upwind	Hwy-710 Downwind	I-5 Upwind	I-5 Downwind	Hwy-710 Upwind	Hwy-710 Downwind
PAHs	5.1±2.4	5.6±2.3	8.6±3.8	7.5±3.4	5.4±2.5	5.8±2.5	8.4±3.9	7.7±3.5
n-Alkanes	35.9±8.3	37.8±11.2	22.9±9.0	23.4±10.5	34.8±7.0	39.1±10.0	22.7±9.8	22.8±10.0
Hopanes	2.6±1.0	2.9±1.2	1.3±0.4	1.3±0.4	2.8±1.0	3.1±1.3	1.3±0.3	1.3±0.4
Steranes	0.7±0.3	0.8±0.3	0.5±0.2	0.5±0.3	0.7±0.2	0.8±0.3	0.5±0.3	0.5±0.3
Other alkanes/alkenes	4.2±1.1	4.9±1.2	3.3±1.4	3.0±1.0	4.5±1.1	5.0±1.3	3.0±0.9	3.0±1.1
Benzothiazole/derivates	0.9±0.3	0.9±0.3	1.1±0.3	1.2±0.5	0.9±0.3	0.9±0.2	1.1±0.3	1.2±0.4
Rubber derivates	1.8±0.6	2.1±0.5	2.1±0.9	2.3±0.9	1.9±0.4	2.1±0.4	2.2±0.8	2.2±0.8
Phthalate	911±1186	927±1061	171±61	136±46	874±1082	907±1065	149±49	138±48

Table 4-6: Abundances (mass percent) of organic groups in $PM_{2.5}$ and PM_{10} (average ± standard deviation in %).

Size	$PM_{2.5}$				PM_{10}			
Organics\Sites	I-5 Upwind	I-5 Downwind	Hwy-710 Upwind	Hwy-710 Downwind	I-5 Upwind	I-5 Downwind	Hwy-710 Upwind	Hwy-710 Downwind
PAHs	0.050±0.018	0.049±0.018	0.089±0.036	0.057±0.016	0.020±0.007	0.018±0.007	0.028±0.008	0.025±0.003
n-alkanes	0.373±0.113	0.343±0.120	0.240±0.095	0.179±0.058	0.145±0.064	0.128±0.045	0.076±0.019	0.074±0.017
Hopanes	0.027±0.011	0.027±0.012	0.015±0.007	0.010±0.004	0.012±0.007	0.010±0.005	0.005±0.001	0.004±0.001
Steranes	0.007±0.003	0.007±0.003	0.005±0.002	0.004±0.001	0.003±0.002	0.003±0.001	0.002±0.001	0.002±0.000
Other alkanes/alkenes	0.043±0.013	0.044±0.014	0.038±0.021	0.024±0.011	0.018±0.008	0.016±0.006	0.011±0.004	0.010±0.004
Benzothiazole/derivates	0.009±0.002	0.008±0.002	0.013±0.006	0.010±0.005	0.003±0.001	0.003±0.001	0.004±0.001	0.004±0.002
Rubber derivates	0.019±0.006	0.019±0.006	0.024±0.013	0.019±0.010	0.008±0.003	0.007±0.002	0.008±0.003	0.008±0.003
Phthalate	7.58±8.28	7.76±8.74	1.98±1.13	1.10±0.44	2.68±2.86	2.66±2.96	0.53±0.17	0.46±0.12

Table 4-7: PAH diagnostic ratios from this study and those in the literature.

Site\diagnostic ratio		Indeno[1,2,3-cd]pyrene/ (indeno[1,2,3-cd)pyrene + benzo[ghi]perylene)	Fluorene/ (fluorene+pyrene)	benzo[a]pyrene/ (benzo[a]pyrene+chrysene)	Pyrene/ benzo[a]pyrene
This Study	I-5	0.31±0.11	0.05±0.04	0.53±0.12	0.25±0.09
	Hwy-710	0.25±0.09	0.03±0.01	0.52±0.13	0.60±0.14
Literature	Gasoline	0.18	<0.5	0.73	~1
	Diesel	0.37	>0.5	0.5	~10

Figure 4-27 shows average PAH concentrations near the two highways. With the exception of much higher abundances of fluoranthene and pyrene at the Hwy-710 sites, both highways have similar distributions: high abundances of 4-ring (fluoranthene, pyrene, benzo[a]anthracene, and chrysene), 5-ring (benzo[b]fluoranthene, benzo[j+k]fluoranthene, benzo[e]pyrene, benzo[a]pyrene), and some 6-ring (indeno[1,2,3-cd]pyrene, dibenzo[a,h]anthracene, benzo[ghi]perylene, dibenzo[a,e]pyrene) and 7-ring (coronene) PAHs. The higher concentrations of fluoranthene and pyrene at the Hwy-710 sites is consistent with higher diesel vehicle traffic, which is known to emit more lighter molecular weight PAHs [29, 98]. The relatively high concentrations of benzo(ghi)perylene, indeno(1,2,3-cd)pyrene, and coronene are likely related to gasoline vehicle emissions [99]. Several PAH diagnostic ratios from this study are listed in Table 4-7 with comparison of those reported for gasoline and diesel vehicle emissions in the literature Ravindra et al. [98]. Due to mixed influence of gasoline and diesel vehicles in both highways, the measured diagnostic ratios are within the range of literature values for gasoline and diesel vehicles. Pyrene, benzo(ghi)perylene, fluoranthene and phenanthrene are also known to be emitted from tire wear [29]. Source apportionment is required to attribute organic concentrations to different sources.

As shown in Table 4-5, n-alkanes are significant contributors to PM organic mass and vehicle emissions are a known major source of n-alkanes [100]. Figure 4-28 shows that n-alkanes at both highways have bimodal distributions, with peaks near C23 and C29, respectively. However, the relative concentrations of these two modes are different at the two highways: I-5 had higher concentrations in the mode centered at C29 while Hwy-710 had higher concentrations centered at C23. These differences are likely caused by different gasoline and diesel fleet composition as well as ambient background concentrations.

Average concentrations of hopanes and steranes are shown in Figure 4-29 and Figure 4-30, respectively. Both sites show similar concentration distributions, with αβ-norhopane and αβ-hopane having the highest concentrations and sterane species having relative uniform concentrations. This result is consistent with the literature finding that hopane and sterane distributions are independent of fleet composition as they are derived from lubricating oil instead of gasoline or diesel fuels [29]. However, Fujita et al. [99] suggested that diesel vehicle exhaust contained higher amounts of lower molecular weight hopanes and steranes, whereas gasoline vehicle exhaust contains a more even distribution by molecular weight. Source profiles of current gasoline and diesel fleets with hopane and sterane data are needed to verify if gasoline and diesel exhaust have different distributions.

Concentration of phthalates in $PM_{2.5}$ samples are plotted in Figure 4-31. While the concentrations at the Hwy-710 sites were relatively uniform, approximately an order of magnitude higher concentrations were observed at the I-5 sites during all sampling periods of 0600-1000 as compared to other periods. The concentrations were dominated by bis(2-ethylhexyl)phthalate (DEHP) followed by di-n-octyl phthalate (DnBP). These compounds are widely used as plasticizing agents, including in rubber tire manufacturing [101]. They can also emit from the interior structures of vehicles [102] as well as facilities handling, manufacturing, or processing polyvinyl chloride (PVC) products [103]. The fact that higher concentrations of

phthalates are only present at the I-5 sites indicates that their origin are likely not from vehicle traffic. However, the extremely high ambient concentration (up to 4 µg/m^3) is an alarming sign of potential exposure risk as DEHP is designated by the U.S. EPA as a probable human carcinogen [103].

Benzothiazole and its derivatives are known markers for tire wear [29, 87]. Figure 4-32 shows that benzothiazoles are present on the filter samples, with a concentrations of 0-0.3 ng/m^3. Rubber derivatives are also tire wear markers [53, 87, 88]. Rubber pyrolysis products (Table 4-3): vinylcyclohexene (SBR, BR), dipentene (NR), styrene (SBR), isoprene (NR), and butadiene (SBR, BR) were measured above detection limits in the filter samples.

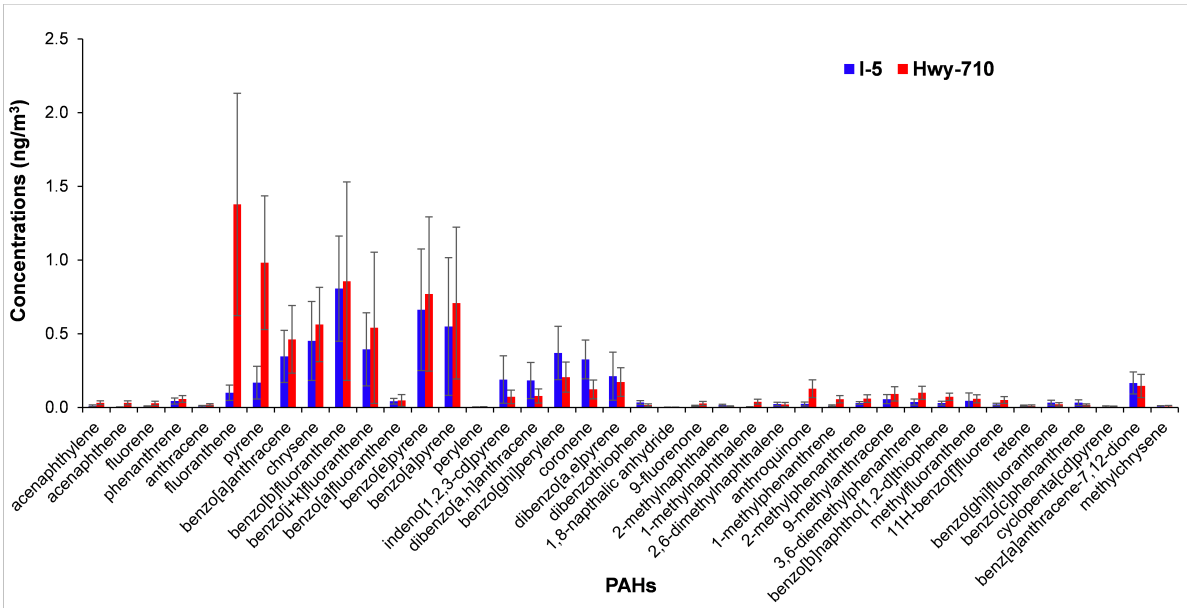

Figure 4-27: Average PAH concentrations at the I-5 and Hwy-710 sites.

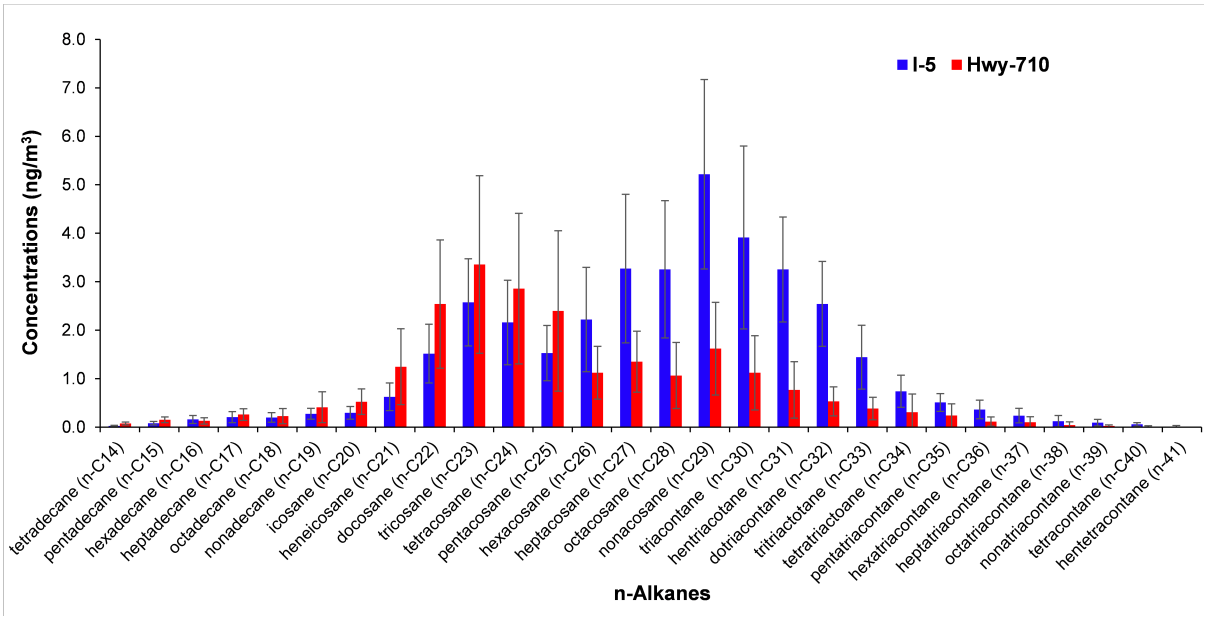

Figure 4-28: Average n-alkane concentrations at the I-5 and Hwy-710 sites.

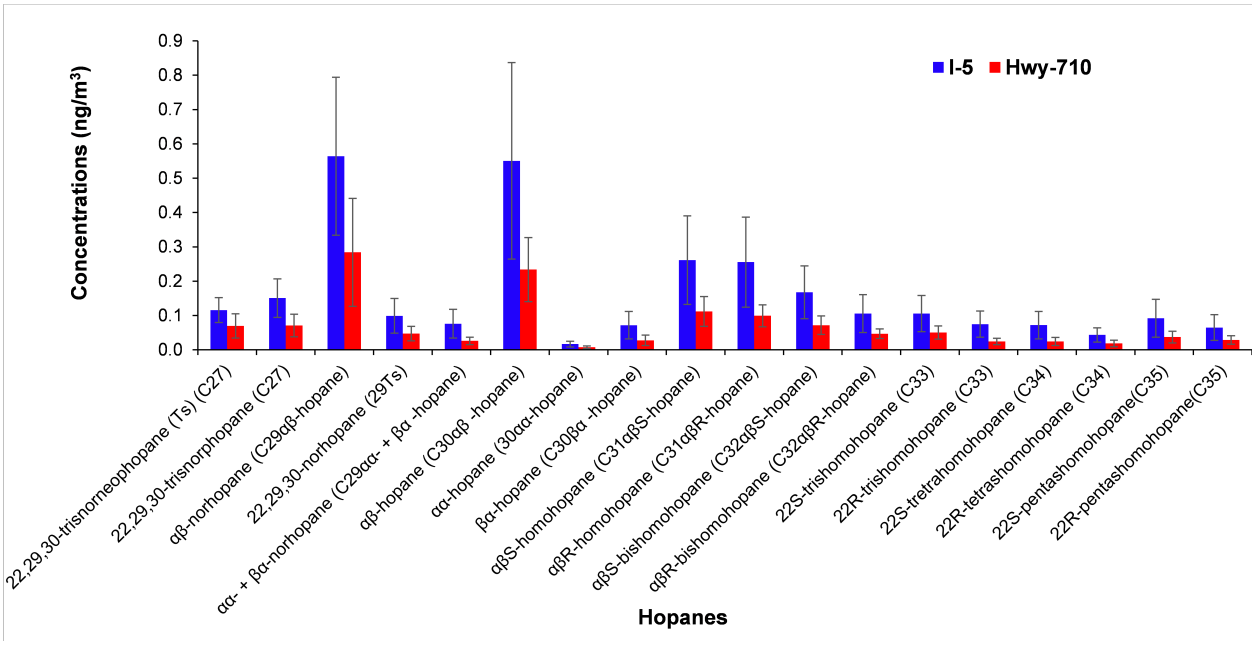

Figure 4-29: Average hopane concentrations at the I-5 and Hwy-710 sites.

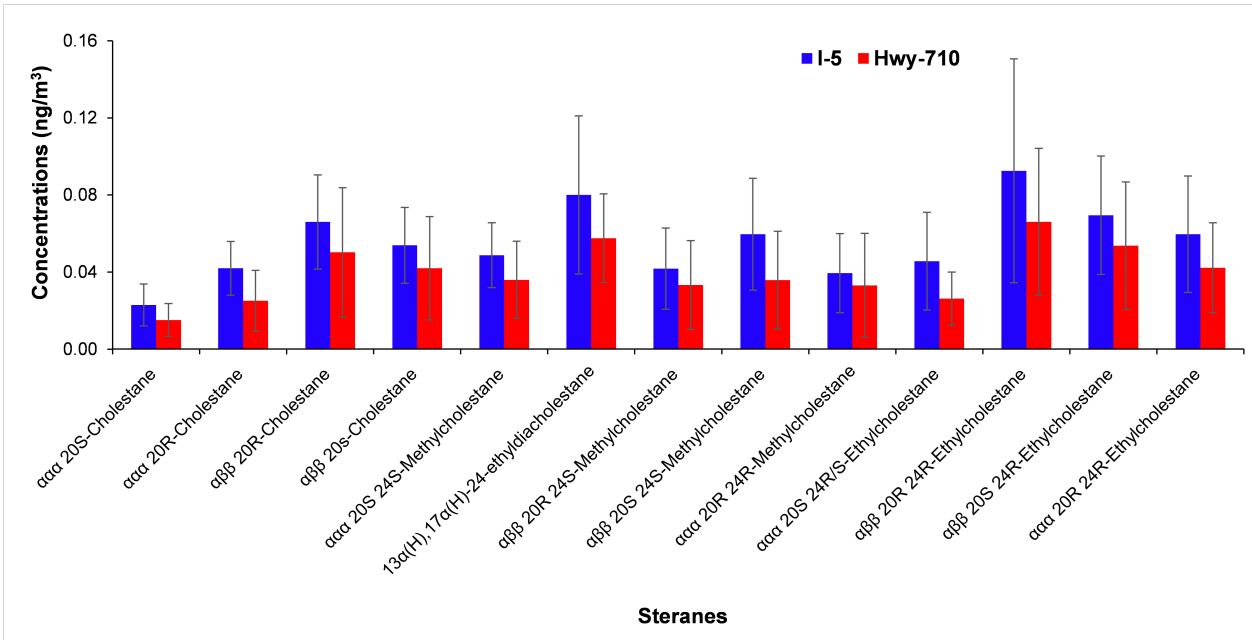

Figure 4-30: Average sterane concentrations at the I-5 and Hwy-710 sites.

a)

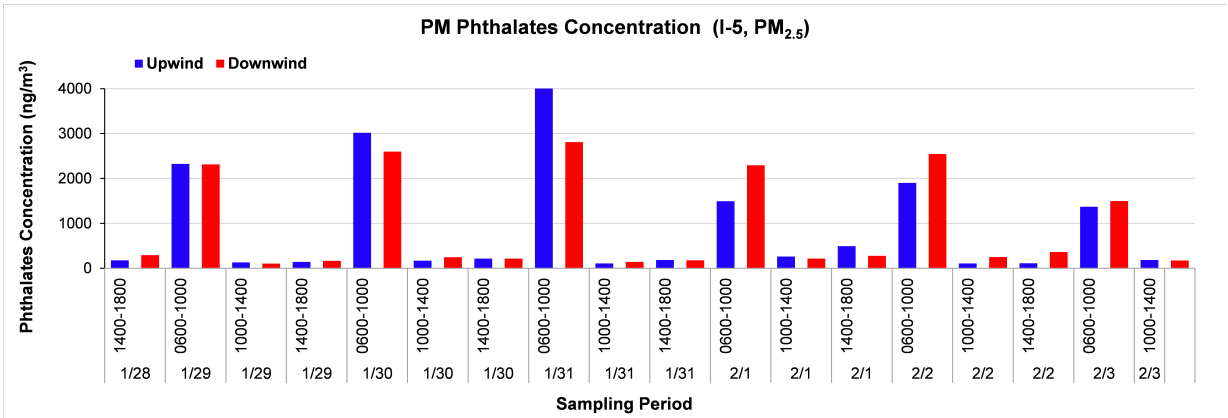

b)

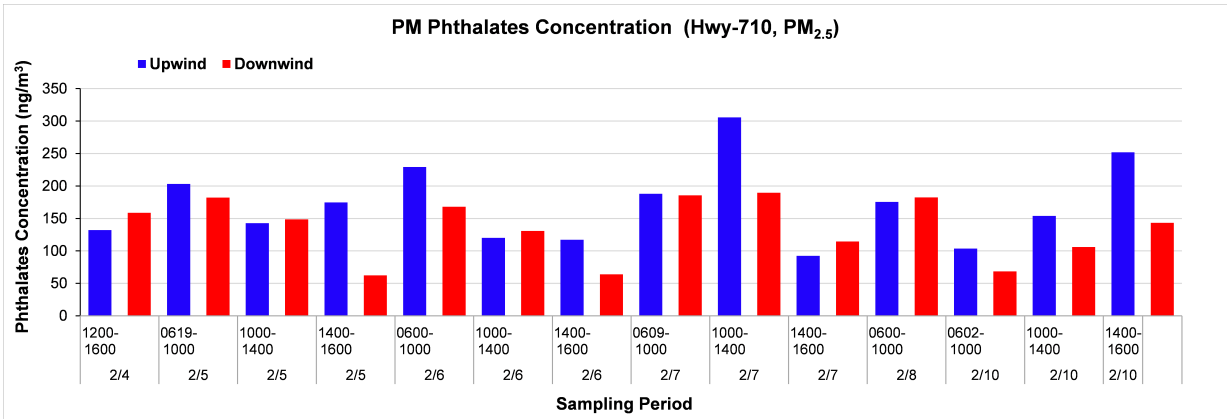

Figure 4-31: Phthalate concentrations at: a) I-5 and b) Hwy-710 sites.

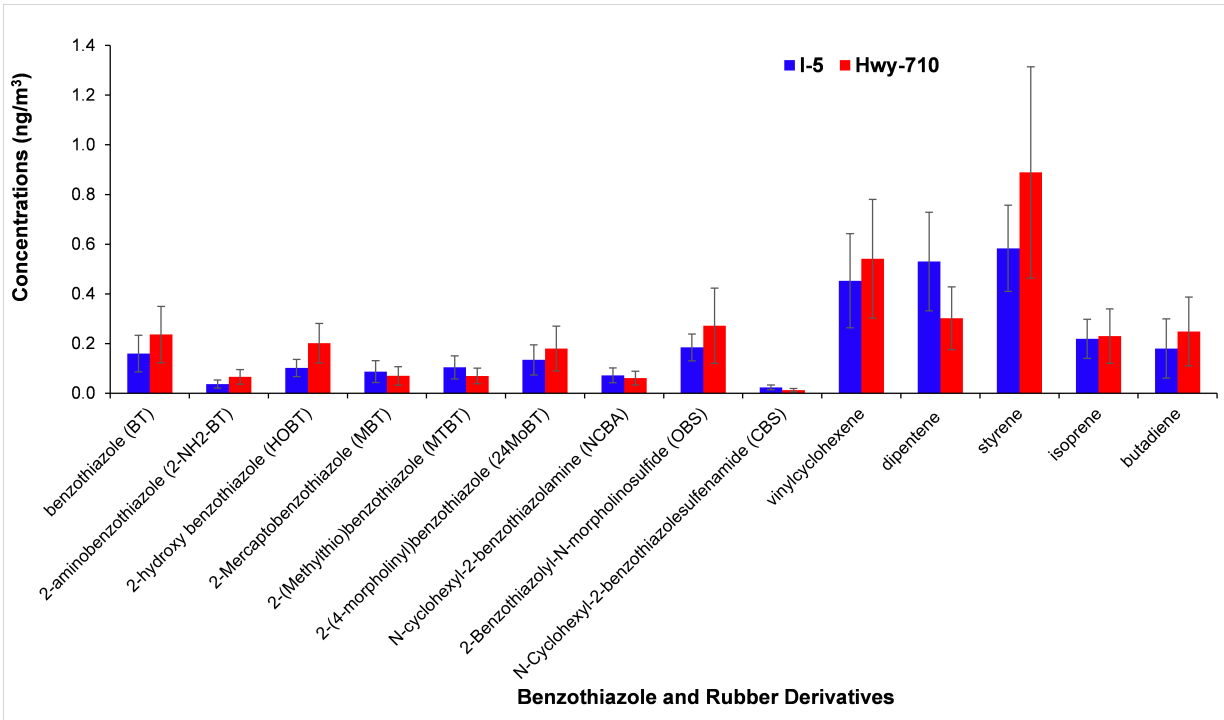

Figure 4-32: Concentrations of benzothiazole and its derivates as well as rubber derivates.

4.4.3 *Comparison of $PM_{2.5}$ vs PM_{10} ratio between lab and field measurements*

Further examination was done to crosscheck the idea of using PM mass difference between downwind and upwind location. CARB project 17RD016 found $PM_{2.5}$ brake mass emission rate and PM_{10} brake mass emission rate has a linear relationship of $y = 0.309x + 0.202$ with $R^2 = 0.95$ using controlled brake dynamometer test data. Assuming the effect of background PM concentration can be removed by subtracting upwind PM concentrations, $\Delta PM2.5_{brake}$ and $\Delta PM10_{brake}$ data were obtained from Figure 5-8 and Figure 5-9 data. Red lines in Figure 4-33 shows $y = 0.309x + 0.202$ relationship found from the brake dynamometer testing from CARB project 17RD016. Note ΔPM has both negative and positive signs depending on wind direction. Data is scattered due to uncertainties related analysis. However, at both locations the relationship between $\Delta PM2.5_{brake}$ and $\Delta PM10_{brake}$ shows good agreement with the lab results. This gives additional confidence of the source apportioned data using the near-road data.

(a)

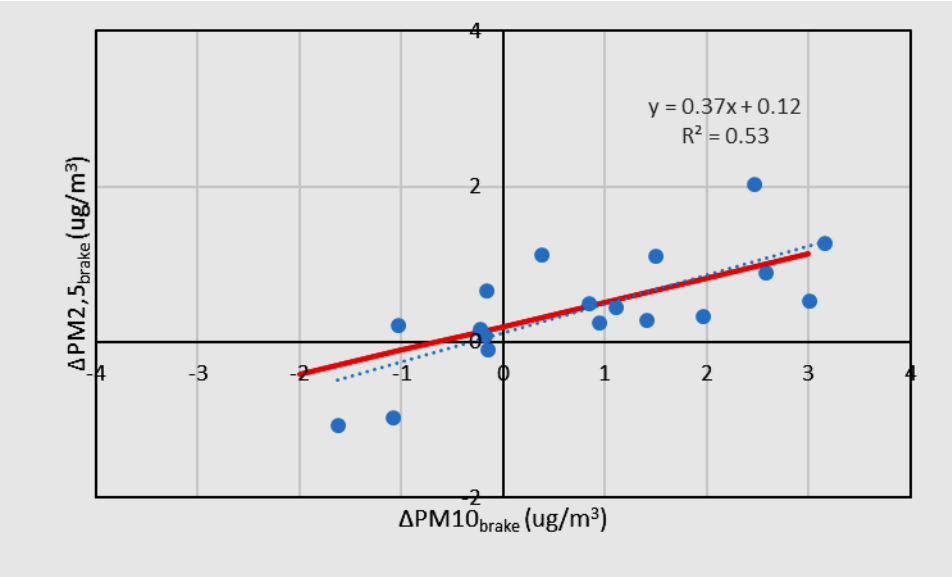

(b)

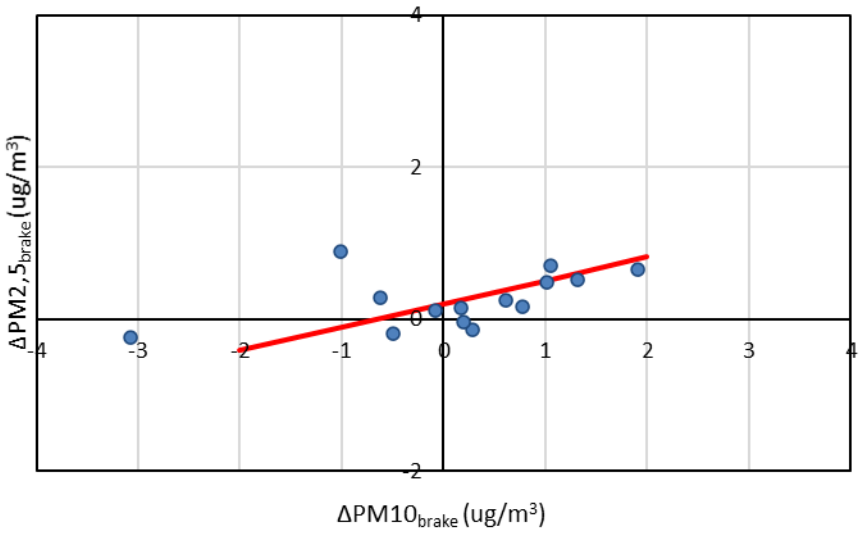

Figure 4-33 Relationship between $\Delta PM2.5_{brake}$ and $\Delta PM10_{brake}$ (a) Anaheim site (I5 site) and (b) Long Beach site (710 site)

5 Task 5: Analyze roadside data and perform source apportionment

5.1 Particle Mass and Number Distributions using HRELPI+

It is expected that less than 50% of airborne brake wear particles fall into diameter sizes smaller than 20 μm [4, 11]. Particle size may be explained by braking intensity, temperature, and brake lining materials [4, 6, 8]. Agudelo et al. [33] showed in their brake dynamometer testing funded by CARB that the mode diameter of particle number distribution is about 2 μm for LDV. Koupal et al. [31] did a follow-up lab study for HDV and reported the mode diameter of brake wear particle distribution at about 1.4 μm. For this study, real-time aerodynamic particle size distribution was measured using a Dekati HRELPI+. With this instrument, particle size distributions can range from 6 nm to 10 μm at 10 Hz sampling rate [63]. The HRELPI+ obtains measurements by charging airborne particles before passing them through a series of 13 impactor stages acting as diameter cut points and a final filter stage. This instrument was set up at the downwind locations for both the Anaheim 5-freeway and Long Beach W710 highway sites. Data collected had a time resolution of 1 second, therefore it was averaged every hour for each diameter size bin to show one hour averaged size distribution.

Figure 5-1 gives the hourly averaged number size distributions in aerodynamic diameter with peaks near the 0.01, 2.1, and 6.5 μm diameter sizes during 12 PM. This trimodal behavior did not vary significantly througout the remainder of the test day and has similar concentration magnitudes. The mode with 0.01 μm diameter is exhaust particles, while we speculate the mode with 2.1 μm is brake wear particles as the mode diameter is similar to what were reported in the dynamometer studies. It is assumed the mode with 6.5μm is resuspended road dust particles. Figure 5-2 shows hourly averaged mass distribution converted from the number distribution at the Anaheim 5-freway downwind site. The mode diameters were around 0.25 and 7 μm during 12:00. Distributions were similar for the 13:00 and 14:00.

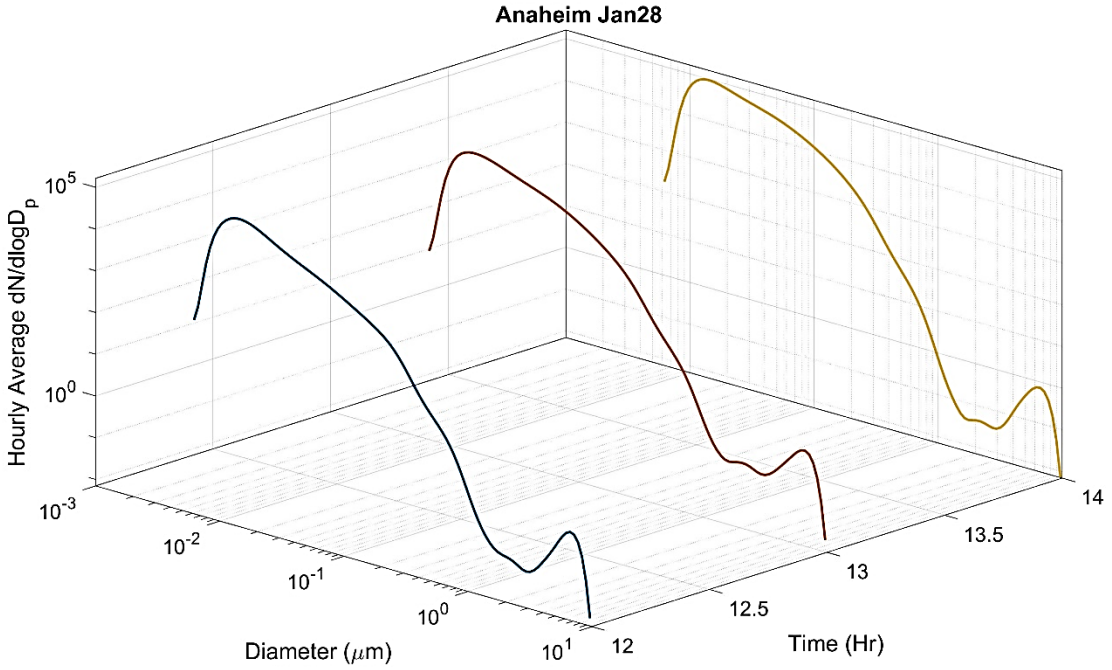

Figure 5-1: dN/dlogDp for Anaheim January 28th

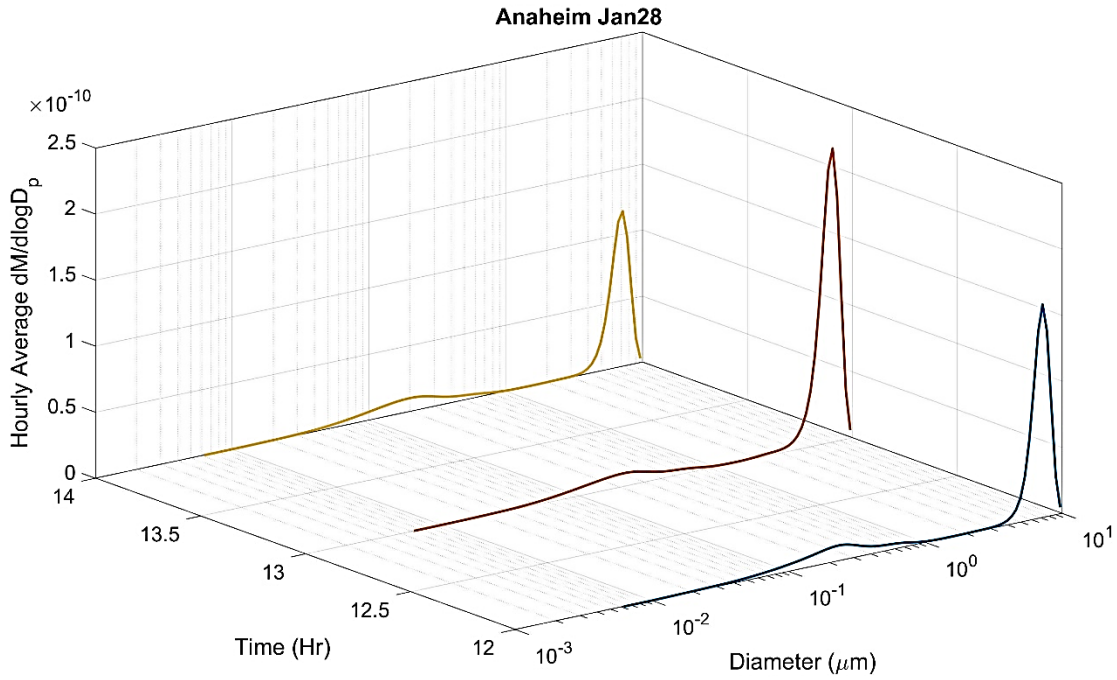

Figure 5-2: dM/dlogDp for Anaheim January 28th

The W710 highway had more heavy-duty vehicles when compared to Anaheim's 5-freeway. Data was collected between the 12:00 and 16:00 on February 6th and between the 10:00 and 18:00 on February 10th. Mass distributions appeared to be bimodal in linear scale throughout the day on February 6th seen in Figure 5-3. Whereas unimodal distributions with varying mass concentrations are seen in Figure 5-5 throughout February 10th. Both figures have large maxima at ~7 µm which is consistent to the 5-freeway mass distribution. The study by Sanders et al. [6] showed that peak mass distributions of ~6 µm are expected to be independent of brake lining types in their brake dynamometer testing. Further size speciated chemical analysis is required to better explain why mass distributions are similar between the 5-freeway made up of light duty vehicle traffic and the W710 highway with heavy-duty vehicles.

As can be seen by Figure 5-4 and Figure 5-6, the number distributions in log scale show three modes every hour with the largest in the ultrafine (<0.1 µm) particle size range. Number concentrations (dN/dlog Dp) on February 6th with magnitudes near $6.0 \cdot 10^{4}$ #/cc, $7.8 \cdot 10^{-2}$ #/cc, and 1.31 #/cc are observed at the 0.15, 2.0 and 7 µm mode diameter size respectively. February 10th number concentrations are within the same magnitude at the same diameter size locations.

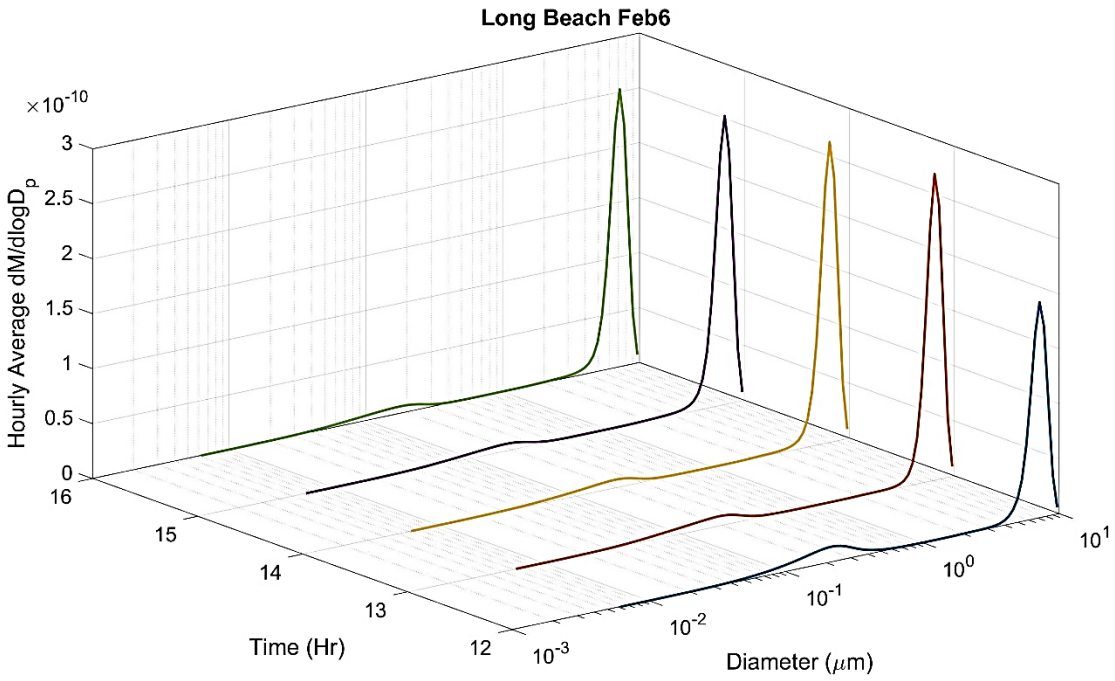

Figure 5-3: dM/dlogDp for Long Beach February 6th

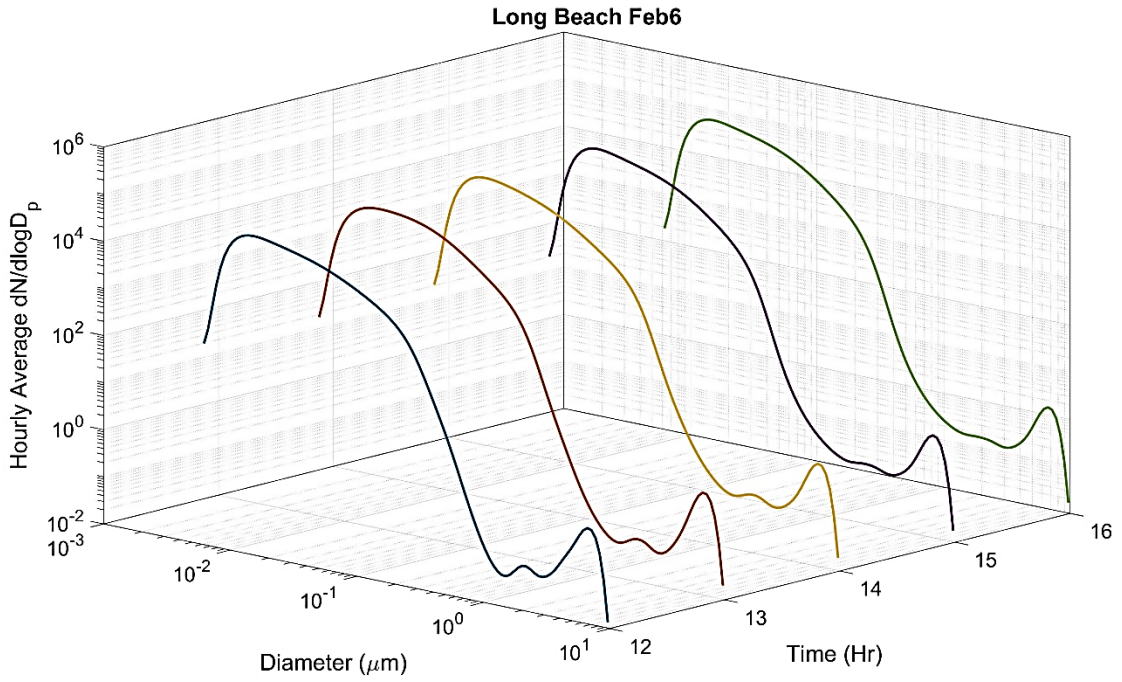

Figure 5-4: dN/dlogDp for Long Beach February 6th

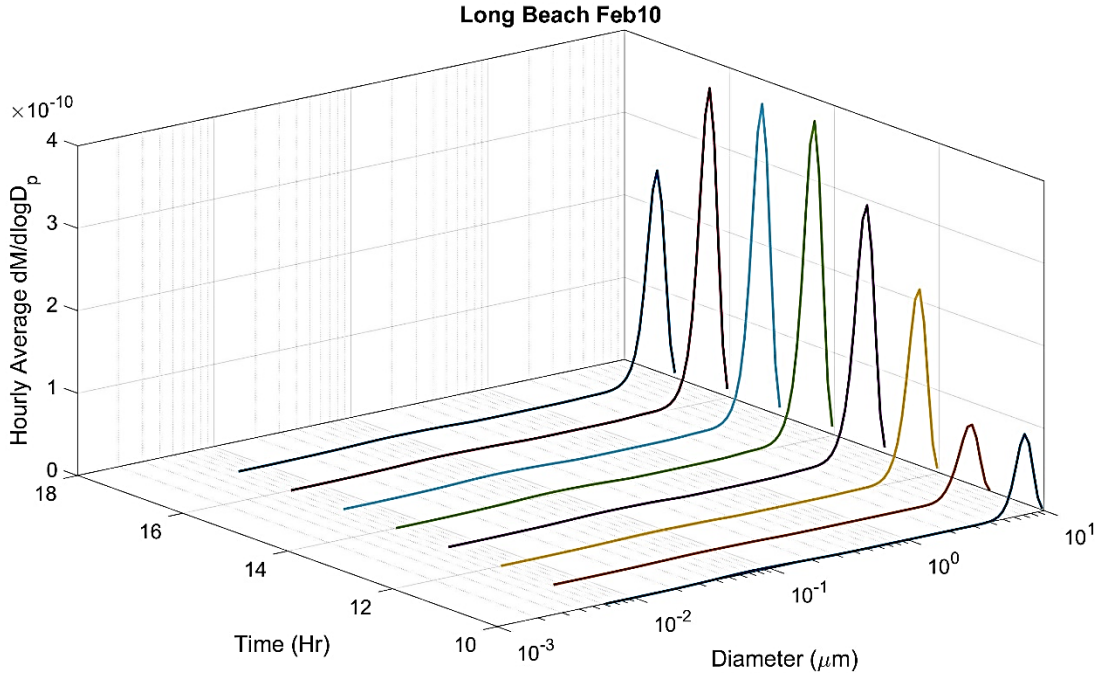

Figure 5-5: dM/dlogDp for Long Beach February 10th

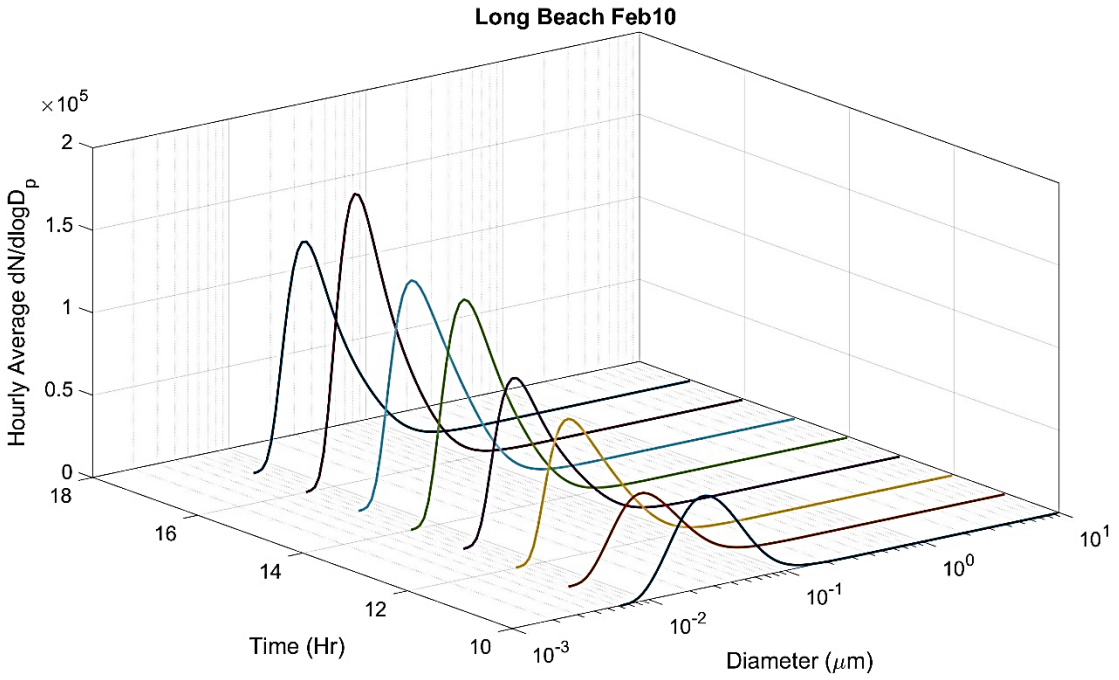

Figure 5-6: dN/dlogDp for Long Beach February 10th

5.2 Near-road PM Source Apportionment

The 2020 Brake and Tire Wear Study conducted in Los Angeles collected 64 $PM_{2.5}$ samples and 64 PM_{10} samples both in 32 pairs of upwind-downwind measurements from two near-road locations (I-5 and Hwy-710). Each of the samples were characterized for > 210 inorganic and organic species. The major sources contributing to the samples include: 1) vehicle (diesel, gasoline) exhausts, 2) brake wear, 3) tire wear, 4) road dust, and 5) urban background air. The EV-CMB model [104] was employed to quantify source-specific contributions by solving:

Equation 4

$$C_{it} = \sum_{j=1}^{J} F_{ij} S_{jt} + \varepsilon_{it}$$

where $C_{i,t}$ and ε_{it} is the measured concentration and uncertainty, respectively, of species i in PM ($PM_{2.5}$ or PM_{10}) at time t, F_{ij} is the fraction of species i in PM source profile j, and S_{jt} is the contribution of source j at time t that can be solved by minimizing χ_t^2, where:

Equation 5

$$\chi^2 = \frac{1}{I-J}\sum_{i=1}^{I}\frac{\left(C_{it} - \sum_{j=1}^{J} F_{ij}S_{jt}\right)^2}{EV_{it}}$$

where I and J indicate number of samples and sources, respectively, in the model and EV_{it} is the effective variance due to uncertainties in both measured ambient concentrations ($\sigma_{C_{ik}}$) and source profiles ($\sigma_{F_{ij}}$):

Equation 6

$$EV_{it} = \sigma_{C_{it}}^2 + \sum_{j=1}^{J} \sigma_{F_{ij}}^2 S_{jt}^2$$

Source profiles should be representative of emissions during the study and determined using the same analytical methods as the ambient samples. As recommended by Watson [105] and Chen et al. [106], sensitivity tests should be performed on selected samples to evaluate how different source profiles and combinations of EV-CMB fitting species affect source contribution estimates (SCEs). As part of a sensitivity test, the initial source profile combination is modified in subsequent trials to examine changes in the SCEs and EV-CMB performance measures. An acceptable solution requires percent mass (%mass) between 0.8 and 1.2, correlation (r^2) > 0.8, and root mean square difference between measured and fitted concentrations (i.e., chi-square: χ^2) < 4. However, r^2 should be as close to 1 as possible while χ^2 should be as small as possible. The modified pseudo-inverse normalized (MPIN) matrix indicates the most influential species (e.g., MPIN value >0.4) for each source type. For most tests, five to ten different source combinations are attempted until the best solution, in terms of EV-CMB fitting performance and MPIN matrix, is attained.

5.2.1 *Source Profiles*

Speciated $PM_{2.5}$ and PM_{10} measurements have been documented in previous sections. Source profiles assembled for this study are listed and referenced in Table 5-1. As part of this study, four dust samples were collected near the monitoring sites, resuspended in the laboratory, and sampled onto filters after a $PM_{2.5}$ or PM_{10} inlet following Chow et al. [73]'s method. Chemical analyses applied to these samples were identical to those for ambient samples. Major crustal components include Al, Si, Ca, Ti, and Fe are commonly used as markers for EV-CMB analysis [106, 107]. The crustal fraction (2.2×[Al] + 2.49×[Si] + 1.63×[Ca] + 1.94×[Ti] + 2.42×[Fe]) ranges from 20-34% in fine dust ($PM_{2.5}$) but 41–62% in coarse dust (PM_{10}). In general, fine dust also has a lower mass closure (47–61%) than coarse dust (60–92%). The best mass closure occurs for the dust PM_{10} collected from Coastal Corvette (CCDust). Composite profiles were also calculated from the four individual profiles (Table 5-1).

Brake dust were collected from laboratory experiments and analyzed for chemical composition as part of the California Regional Particulate Air Quality Study (CRPAQS, see Fitz et al. [108]).

Fe, Ba, Mn, and Cu are known markers for brake wear particles [109], and their mass fraction in the brake $PM_{2.5}$ were 20–66%, 3–13%. 0.2–0.6%, and 0.04–0.08%, respectively. CARB sponsored a brake dynamometer study in 2020, which examined 10 brake wear PM_{10} samples from three vehicles: F150, Sienna and Camry, for metal speciation using energy dispersive XRF method (ED-XRF). The 10 samples were further composited into 4 brake source profiles representing different brake pad material and positions (Table 5-1). The mass fraction of Fe, Ba, Mn, and Cu in these profiles are 11–47%, 1–11%, 0.1–0.7%, and 0.04–4.9%, respectively. Two CARB brake profiles (BRAKE-D and BRAKE-F) contain much high Cu content (4.9% and 1.7%) than observed in CRPAQS. It should be noted that Brake-D, E, F, and G (Table 5-3) were derived from PM_{10} instead of $PM_{2.5}$. To use these profiles, we assume that chemical composition of brake particles is independent of the particle size.

CRPAQS also reported two tire dust profiles, which are dominated by OC and EC, and contain high levels of Fe (18–22%), Zn (2–3%), Si (3%), Al (2–3%), Ca (2%), and Cu (1–2%). While Zn has long been used as a marker for tire wear particles [110], such high levels of crustal elements, especially Fe, in tire wear are considered unusual. As part of this study, tire wear particles were collected from a dynamometer test of Michelin and Cooper tires, resuspended (without a size cut) in the lab, and analyzed along with road dust samples. These profiles are also dominated by OC and EC (>75%). With respect to elemental composition, the two brands of tire differ the most in Si content (0.6% for Michelin versus 6% for Cooper). The Fe, Zn, Al, Ca, and Cu fractions range 0.1–0.2%, 0.5–1%, 0.04–0.2%, 0.07–0.1%, and 0.003–0.004%, respectively. Zn appears to be a consistent marker for tire wear, while other species are more variable. To use the tire profiles for $PM_{2.5}$ source apportionment, we also assume that chemical composition of tire particles is independent of the particle size.

Vehicle exhaust source profiles considered in this study are those acquired from the National Renewable Energy Laboratory Gas/Diesel Split Study [111, 112]. The Gas/Diesel Split Study measured $PM_{2.5}$ emissions from 59 light-duty (including 57 gasoline- and 2 diesel-fueled vehicles) and 30 medium- and heavy-duty diesel-fueled vehicles. The study was conducted at the Ralphs Grocery distribution center in Riverside, CA, during the summer and winter of 2001 using a “constant volume sampling system” (CVS). Profiles developed include low emitters, high emitters, and black carbon (BC) emitters for gasoline vehicles under cold and warm start conditions, as well as medium-duty and heavy-duty diesel vehicles under city and highway driving cycles. These profiles are more recent and contain full organic speciation except for alkanes. The gasoline and diesel composite profiles (GAS and DIESEL) have been successfully applied to $PM_{2.5}$ source apportionment for CRPAQS [99]. While newer profiles are preferred, after a literature review there are no diesel or gasoline exhaust profiles post the Gas/Diesel Split Study that have the species, quality, and regional specificity that suit this study. For example, speciation profiles used in CARB modeling do not contain organic species such as PAHs, hopanes and steranes, organic acids, etc. known to help separate exhaust and tire wear contributions. It is our judgement that the set of profiles used is the best available, which is further supported by the good fitting performance.

Table 5-1: Source profiles assembled for the 2020 Brake and Tire Wear Study. (Shaded entries designate profiles included in the final EV-CMB source apportionment.)

Category	Subcategory	Mnemonic	Year	Size	Description	Reference
Geological	Road Dust	MADust	2020	$PM_{2.5}$, PM_{10}	Resuspension soil dust from the Majestic (I-5 upwind) site	This study
		CCDust	2020	$PM_{2.5}$, PM_{10}	Resuspension soil dust from the Coast Corvette (I-5 downwind) site	
		ATDust	2020	$PM_{2.5}$, PM_{10}	Resuspension soil dust from the ATD (Hwy-710 upwind) site	
		AQDust	2020	$PM_{2.5}$, PM_{10}	Resuspension soil dust from the AQMD (Hwy-710 downwind) site	
		MCDust	2020	$PM_{2.5}$, PM_{10}	Composite of MADust and CCDust	
		AADust	2020	$PM_{2.5}$, PM_{10}	Composite of ATDust and AQDust	
Mobile	Brake Wear	BRAKE-1,2,3	2001	$PM_{2.5}$	Laboratory brake wear PM collected as part of the California Regional Particulate Air Quality Study (CRPAQS)	[108]
		BRAKE-C	2001	$PM_{2.5}$	Composite of Brake_1, 2, and 3	
		BRAKE-D,E,F,G*	2020	PM_{10}	Dynamometer brake wear PM collected as part of the CARB RD17016 PM10 Speciation Analysis. Brake_D: Front OES-NAO Brake_E: Front AM1-NAO Brake_F: Rear NAO Brake_G: Front AM2-LM	[13]
	Tire Wear	TIRE-1,2	2001	$PM_{2.5}$	Laboratory tire wear PM collected as part of the California Regional Particulate Air Quality Study (CRPAQS)	[108]
		COTIRE	2020	TSP	Laboratory tire dust – Cooper	This study
		MITIRE	2020	TSP	Laboratory tire dust – Michelin	
		LATIRE	2020	TSP	Composite of COTire and MITire	
	Diesel Exhaust	MDD	2001	$PM_{2.5}$	Dyno medium-dusty diesel vehicle exhausts	[99, 112]
		HDD-HW	2001	$PM_{2.5}$	Dyno heavy-dusty diesel vehicle exhausts – Highway cycle	

		HDD-HCS	2001	$PM_{2.5}$	Dyno heavy-dusty diesel vehicle exhausts – City cycle	
		DIESEL	2001	$PM_{2.5}$	Composite of medium and heavy-duty diesel vehicle exhausts	
	Gasoline Exhaust	WS-L	2001	$PM_{2.5}$	Dyno warm start - low emitters	[99, 112] [106]
		CS-L	2001	$PM_{2.5}$	Dyno cold start - low emitters	
		WS-H	2001	$PM_{2.5}$	Dyno warm start - high emitters	
		CS-H	2001	$PM_{2.5}$	Dyno cold start - high emitters	
		WS-BC	2001	$PM_{2.5}$	Dyno warm start - BC emitters	
		CS-BC	2001	$PM_{2.5}$	Dyno cold start - BC emitters	
		GAS	2001	$PM_{2.5}$	Composite of gasoline vehicle exhausts	
Secondary	Secondary Sulfate	AMSUL		$PM_{2.5}$, PM_{10}	Ammonium sulfate	[113]
	Secondary Nitrate	AMNIT		$PM_{2.5}$, PM_{10}	Ammonium nitrate	

*Only elemental compositions are available in these profiles.

Besides exhaust and non-exhaust PM, secondary nitrate and sulfate are represented by pure NH_4NO_3 (AMNIT) and $(NH_4)_2SO_4$ (AMSUL) profiles, respectively. According to previous studies, sources that may contribute to Los Angeles $PM_{2.5}$ also include sea salt, biomass burning, and industrial emissions [114]. Lacking suitable source profiles, these sources were not considered in the EV-CMB analysis, and the model may not use species that are dominated by these sources, such as sodium and chlorine ions (Na^+ and Cl^-) for sea salt and potassium (K) for biomass burning. On the other hand, important markers used include: 1) Al, Si, and Ca for road dust; 2) Fe, Mn, Cu, Ti, Sb, and Ba for brake wear; 3) Zn, OC3, and phthalates for tire wear; 4) EC and hopanes for diesel exhaust; 5) indeno[1,2,3,cd]pyrene (incdpy), benzo[g,h,i]perylene (bghipe), and corone for gasoline engine exhaust; and 7) S and NO_3^- for secondary inorganics. OC fractions (OC1-OC4) were included. Although both motor vehicle exhaust and tire wear are dominated by organic matter, they may differ significantly in their OC fractions.

5.2.2 *Sensitivity Tests*

Sensitivity tests evaluate the performance of different source profile combinations in terms of r^2, χ^2, and %MASS when applied to selected ambient PM sample(s). Usually, only one profile in each source group may be included since similar profiles result in collinearity, non-convergence, and/or negative source contributions. To create ambient PM samples that are suitable for the sensitivity test, we subtracted upwind concentrations at the I-5 site from the corresponding downwind concentrations. It is expected that the differences can be fully explained (%MASS ~ 100) by traffic-related emissions including vehicle exhaust, brake wear, tire wear, and road dust.

Since the wind direction varied from time to time, the differentiation between upwind or downwind samples for each specific period is based on the reconstructed mass of $PM_{2.5}$ or PM_{10} assuming the downwind site would have higher mass concentrations than the upwind site. However, the differences between upwind and downwind concentrations are often insignificant (i.e., below the measurement uncertainty). To maximize the signal-to-noise ratio, all the 18 samples of downwind-upwind difference were averaged to produce the chemical composition shown in Figure 5-7(a). When normalizing to the PM mass, the chemical profiles are shown in Figure 5-7(b).

Note what shown in Figure 5-7 are ambient samples, not source profiles, used in the sensitivity test. Since the onroad traffic influences both the downwind and upwind sites, the differences between the downwind and upwind measurements do not infer traffic contributions exactly. Our goal in the sensitivity analysis is to identify the optimal source profile combination for apportioning the near-road samples, rather than to quantify the traffic contributions. Corresponding samples for Hwy-710 were not created partly due to the mismatch between some upwind and downwind sampling durations and a low signal-to-noise ratio even after the averaging.

The results of sensitivity test are shown in

Table 5-2 and Table 5-3. Including any single brake profile led to poor fits (low r^2 and high χ^2) for both $PM_{2.5}$ and PM_{10}, likely due to a wide range of brake PM chemical composition within the fleet. Combing two brake profiles, BRAKE_C and BRAKE_D, improves the fitting performance substantially. The two brake profiles differ mostly in Ti and Cu content relative to Fe, with ratios of 8.8×10^{-5} and 1.2×10^{-3} in BRAKE_C and 0.34 and 0.33 in BRAKE_D, respectively.

For $PM_{2.5}$, using dust profiles generated from resuspended fine dust particles all produced %MASS well above 100 while using dust profiles generated from coarse dust particles (i.e., PM_{10}) produced much more reasonable %MASS. This is consistent with the lower mass closure in the fine dust profiles. Overall, CCDust (PM_{10}) led to the best fitting performance. Alternating different tire, gasoline exhaust, and/or diesel exhaust profiles only cause minor changes in SCEs. Trial IV and V (

Table 5-2) show the best fitting performance, while both report no significant tire contributions to $PM_{2.5}$ despite of different tire profiles. Trial V was our selected model because it uses an original (not composite) tire profile, and because of a higher Zn value (0.49) as the tire marker in the MPIN matrix.

(a)

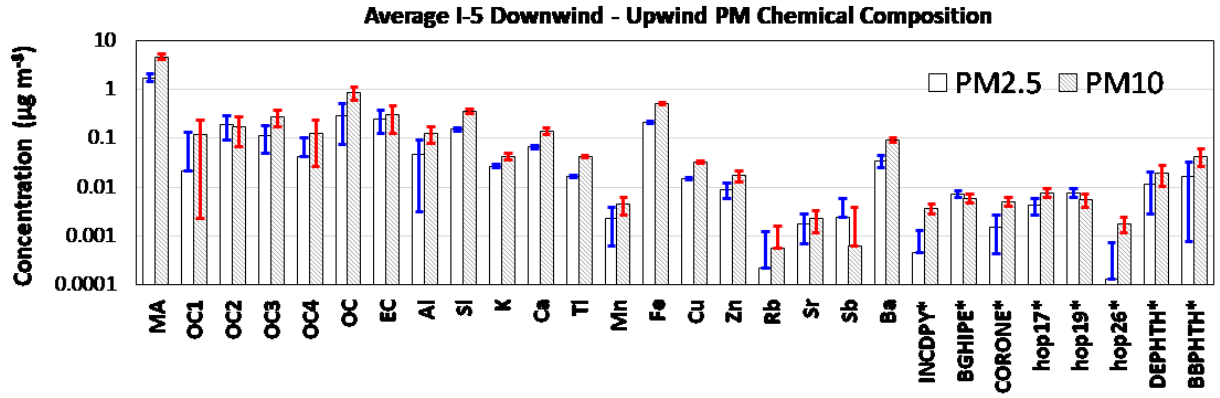

(b)

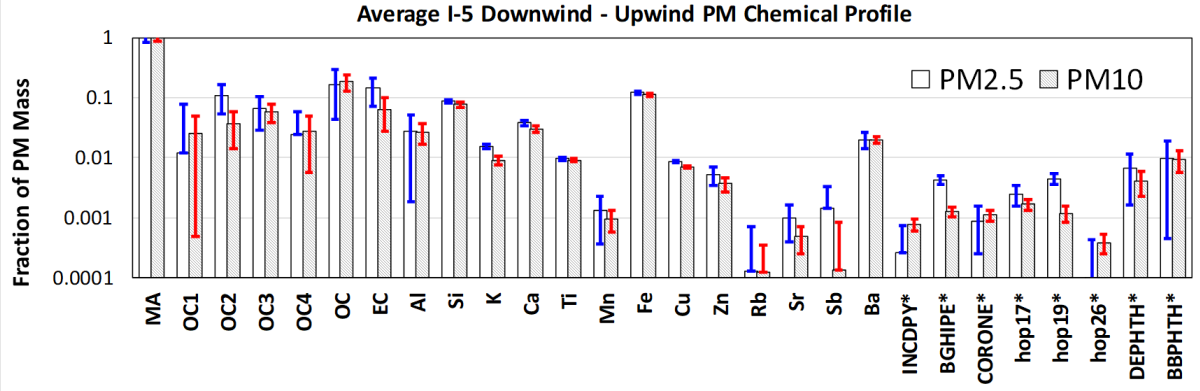

Figure 5-7: Average $PM_{2.5}$ and PM_{10} (a) chemical composition (b) chemical profiles derived from the difference of downwind and upwind measurements at the Anaheim (I-5) site. The asterix symbol indicates a multiplication of 100 in the species concentrations.

Table 5-2: EV-CMB sensitivity tests for the average "Downwind – Upwind" PM2.5 chemical composition. Source contribution estimates (SCEs ± 1σ) in µg/m^3 and performance measures (i.e., r^2, χ^2, and %MASS) are reported for each run. The profile combination in Trial V (shaded) were selected for EV-CMB modeling of all $PM_{2.5}$ samples.

		Average I-5 Downwind-Upwind $PM_{2.5}$: 1.71 ± 0.31 µg/m^3

Source	**Profile[a]**	**I**	**II**	**III**	**IV**	**V**	**VI**	**VII**
Geological	MADust (PM_{10})						**1.87 ± 0.20**	
	CCDust (PM_{10})				**1.10 ± 0.10**	**1.10 ± 0.11**		**1.12 ± 0.11**
	MADust ($PM_{2.5}$)							

	CCDust ($PM_{2.5}$)	**3.61 ± 0.27**	**2.05 ± 0.19**	**2.05 ± 0.19**				
Brake	BRAKE-3							
	BRAKE-C	**0.36± 0.11**		**0.23± 0.12**	**0.23± 0.12**	**0.23 ± 0.11**	**0.24 ± 0.12**	**0.24 ± 0.12**
	BRAKE-D		**0.73± 0.13**	**0.20± 0.09**	**0.21± 0.09**	**0.21 ± 0.09**	**0.17 ± 0.08**	**0.21 ± 0.09**
	BRAKE-E							
	BRAKE-F							
	BRAKE-G							
Tire	TIRE-1							
	COTIRE					**-0.01 ± 0.17**	**-0.16 ± 0.18**	**-0.09 ± 0.17**
	MITIRE							
	LATIRE	**-0.46 ± 0.20**	**-0.13 ± 0.18**	**-0.10 ± 0.17**	**-0.03 ± 0.17**			
Gasoline	CS-L							**0.03 ± 0.01**
	CS-H							
	CS-BC							
	GAS	**0.03 ± 0.02**	**0.03 ± 0.02**	**0.03 ± 0.02**	**0.04 ± 0.02**	**0.04 ± 0.02**	**0.03 ± 0.02**	
Diesel	MDD							
	HDD-HW							
	HDD-HCS							
	DIESEL	**0.22 ± 0.16**	**0.17 ± 0.17**	**0.16 ± 0.15**	**0.19 ± 0.15**	**0.18 ± 0.14**	**0.26 ± 0.15**	**0.30 ± 0.14**
r^2		***0.51***	***0.92***	***0.94***	***0.94***	***0.94***	***0.92***	***0.92***
χ^2		***13.00***	***1.20***	***0.73***	***0.78***	***0.78***	***0.94***	***1.12***
%MASS		***218.6***	***166.4***	***150.6***	***101.7***	***102.0***	***140.7***	***105.2***

Table 5-3: EV-CMB sensitivity tests for the average "Downwind - Upwind" PM_{10} chemical composition. Source contribution estimates (SCEs ± 1σ) in μg/m^3 and performance measures (i.e., r^2, χ^2, and %MASS) are reported for each run. The profile combination in Trial IV (shaded) were selected for EV-CMB modeling of all PM_{10} samples.

		Average I-5 Downwind-Upwind PM_{10}: 4.59 ± 0.59 μg/m^3

Source	Profile[a]	I	II	III	IV	V	VI	VII
Geological	MADust (PM_{10})	**8.21 ± 0.50**	**4.26 ± 0.47**					
	CCDust (PM_{10})			**2.58 ± 0.28**	**2.52 ± 0.30**	**2.56 ± 0.29**		
	MCDust (PM_{10})						**3.33 ± 0.79**	**3.44 ± 0.80**
Brake	BRAKE-3							
	BRAKE-C	**0.43 ± 0.19**	**0.52 ± 0.24**	**0.53± 0.25**	**0.53 ± 0.25**	**0.55 ± 0.26**	**0.51 ± 0.25**	**0.52 ± 0.25**
	BRAKE-D		**0.35 ± 0.17**	**0.43± 0.19**	**0.43 ± 0.19**	**0.44 ± 0.19**	**0.40 ± 0.18**	**0.40 ± 0.18**
	BRAKE-E							
	BRAKE-F							
	BRAKE-G							
	TIRE-1							
Tire	COTIRE				**0.18 ± 0.27**	**0.10 ± 0.26**	**0.18 ± 0.34**	**0.10 ± 0.32**
	MITIRE							
	LATIRE	**-0.53 ± 0.27**	**0.03 ± 0.26**	**0.11 ± 0.26**				
Gasoline	CS-L					**0.05 ± 0.02**		**0.05 ± 0.02**
	CS-H							
	CS-BC							
	GAS	**0.05 ± 0.03**	**0.06 ± 0.03**	**0.08 ± 0.04**	**0.08 ± 0.04**		**0.07 ± 0.04**	
	MDD							
Diesel	HDD-HW							
	HDD-HCS							
	DIESEL	**0.25 ± 0.21**	**0.17 ± 0.22**	**0.12 ± 0.22**	**0.10 ± 0.21**	**0.21 ± 0.19**	**0.10 ± 0.22**	**0.19 ± 0.19**
r^2		***0.71***	***0.93***	***0.93***	***0.93***	***0.93***	***0.89***	***0.89***
χ^2		***8.28***	***0.75***	***0.77***	***0.75***	***0.84***	***0.63***	***0.69***
%MASS		***183.3***	***117.7***	***84.0***	***84.1***	***85.1***	***100.2***	***102.1***

For PM_{10}, the same combination as $PM_{2.5}$ also produced a good fit (Trial IV in Table 5-3), though %MASS is lower (84.1). This %MASS is acceptable considering the measurement uncertainty in PM_{10} mass and absence of secondary AMSUL and AMNIT in the test. Using CS-L instead of GAS as the gasoline exhaust profile led to a similar fitting performance (Trial V). Better %MASS can be achieved by replacing CCDust with MCDust, a composite profile from CCDust and MADust, at the expense of r^2 (Trial VI and VII). The combination in Trial IV was selected mainly to be consistent with the model for $PM_{2.5}$.

The EV-CMB MPIN matrix determines the influence of each fitting species on each SCE. It is expected that the source markers cited above will have the most influence. If this is not the case, the SCEs would be in doubt. MPIN values are normalized such that they range from -1 to 1. Species with absolute MPIN values of 0.4–1 are considered influential species for a specific source. Table 5-4 (MPIN matrix for Trial V of the $PM_{2.5}$ sample in

Table 5-2) indicate that the most important BRAKE_C marker is Fe, followed by Ba while the BRAKE_D contribution is marked by Ti and Cu. For tire wear, the most influential markers are OC3 and Zn, followed by OC and diethyl phthalate (DEPHTH). Unsurprisingly, CCDust is marked by Si and Ca. Three PAH species, indeno[1,2,3,cd]pyrene (INCDPY), benzo[g,h,i]perylene (BGHIPE), and coronene (CORONE) are highlighted for the gasoline exhaust profile while EC and hop17 mark the diesel exhaust profile. The MPIN matrix meets our expectation.

Table 5-5 shows the MPIN matrix for Trial IV of the PM_{10} sample in Table 5-3. It is generally consistent with that in Table 5-4. In addition, Sb and Al are found to be associated with BRAKE_D and CCDust, respectively.

Table 5-4: MPIN matrix for the $PM_{2.5}$ Trial V sample. High MPIN values (>0.4) are marked in red and moderate values (0.2 – 0.4) are marked in yellow.

	BRAKE_C	BRAKE_D	DIESEL	GAS	COTIRE	CCDust
SPECIES[a]						
OC1	-0.03	-0.02	0.35	0.01	-0.19	0.06
OC2	-0.02	-0.01	0.19	0	-0.03	0
OC3	0.03	0.08	-0.22	0.01	1	-0.53
OC4	0	-0.01	0.26	-0.02	-0.14	0.13
OC	-0.01	0.01	0.22	0.01	0.25	-0.15
EC	-0.14	-0.07	1	-0.12	-0.27	0.02
Al	-0.01	-0.02	0.03	-0.01	-0.07	0.17
Si	-0.09	-0.05	-0.16	0.03	0.16	1

Ca	0.04	-0.07	0.25	-0.06	-0.5	0.96
Ti	-0.4	1	-0.11	-0.02	0.03	-0.03
Mn	0.09	0.22	-0.08	-0.01	0.01	-0.03
Fe	1	-0.18	-0.24	-0.05	0.01	-0.1
Cu	-0.19	0.51	-0.06	-0.01	0.03	-0.05
Zn	0.16	-0.06	-0.17	0.02	0.48	-0.25
Sb	-0.06	0.16	-0.02	0	0.01	-0.01
Ba	0.31	0.27	-0.14	-0.03	0.03	-0.12
INCDPY	0.02	0.01	-0.12	0.84	0.02	-0.05
BGHIPE	-0.02	-0.01	-0.13	1	0.02	-0.04
CORONE	-0.02	-0.01	-0.11	0.82	0.02	-0.03
hop17	0.18	0.1	0.54	0.01	-0.33	0.03
hop19	0	0	0.29	0.39	-0.18	0.04
hop26	0	0	-0.02	0.13	0	0
DEPHTH	0.01	0.01	-0.12	0.01	0.22	-0.11

Table 5-5: MPIN matrix for the PM_{10} Trial IV sample. High MPIN values (>0.4) are marked in red and moderate values (0.2 – 0.4) are marked in yellow.

	BRAKE_C	**BRAKE_D**	**DIESEL**	**GAS**	**COTIRE**	**CCDust**
SPECIES[a]						
OC1	-0.03	-0.04	0.51	0.02	-0.3	0.07
OC2	-0.03	-0.02	0.25	0.01	-0.05	0.04
OC3	0.01	0.12	-0.37	0.03	1.00	-0.23
OC4	-0.01	-0.07	0.21	-0.03	-0.22	0.3
OC	-0.03	0.01	0.14	0.02	0.33	0.05
EC	-0.14	-0.04	1.00	-0.13	-0.2	-0.07
Al	-0.06	-0.18	0.09	-0.04	-0.32	0.6
Si	-0.13	-0.27	0.04	-0.04	-0.35	1.00
Ca	-0.03	-0.16	0.1	-0.04	-0.32	0.58
Ti	-0.43	1.00	-0.09	-0.03	-0.01	0.08
Mn	0.12	0.24	-0.08	-0.03	-0.01	0.02
Fe	1.00	-0.25	-0.21	-0.08	-0.09	0.06
Cu	-0.2	0.56	-0.07	-0.01	0.06	-0.08

Zn	0.17	-0.11	-0.23	0.02	0.44	0.04
Sb	-0.13	0.28	-0.02	-0.01	-0.02	0.06
Ba	0.40	0.3	-0.16	-0.03	0.08	-0.2
INCDPY	0.02	0.02	-0.15	0.96	0.05	-0.06
BGHIPE	-0.03	-0.01	-0.13	1.00	0.03	-0.01
CORONE	-0.03	-0.01	-0.11	0.81	0.02	-0.01
hop17	0.29	0.13	0.44	0.01	-0.28	-0.06
hop19	0.01	-0.01	0.23	0.41	-0.18	0.05
hop26	-0.02	-0.02	-0.01	0.19	-0.04	0.07
DEPHTH	-0.01	0.01	-0.18	0.01	0.27	-0.01

5.2.3 *CMB Source Apportionment Results for Anaheim (I-5)*

Using the CMB model established by the sensitivity test, plus AMNIT and AMSUL to account for secondary nitrate and sulfate, respectively, Figure 5-8(a)-(b) illustrate the calculated SCEs for $PM_{2.5}$ at the I-5 downwind (Coast Corvette) and upwind (Majestic) sites. Road dust dominates most of the samples and generally contributes more at the downwind than at the upwind site. It should be noted that the road dust does not necessarily originate from the I-5 traffic, as dust from the urban background can be incorporated into the SCEs. This is also the case for other sources. Both the highest downwind and upwind dust SCEs occurred during 10–14 on 1/29/2020 and 2/3/2020. Brake wear is resolved for all samples (1–39% of $PM_{2.5}$), though the partition between BRAKE_C (low copper) and BRAKE_D (high copper) contributions varies widely from 0.7:1 to 10:1. Tire wear is absent in three samples (downwind: 10-14, 2/3/2020; upwind: 14-18, 2/2/2020 and 10-14, 2/3/2020). Gasoline contributions are minor but detectable in all samples. Diesel contributions showed up every day except 3 periods (downwind: 10-14, 1/29/10; upwind: 14-18, 1/30/2020 and 14-18, 1/31/2020) when only gasoline engine exhaust was detected. This abnormality is hard to explain but is a reminder of the uncertainty in separating diesel and gasoline contributions even with organic markers. Secondary nitrate and sulfate are also resolved for all samples, and consistent between downwind and upwind measurements (r^2 = 0.85–0.94).

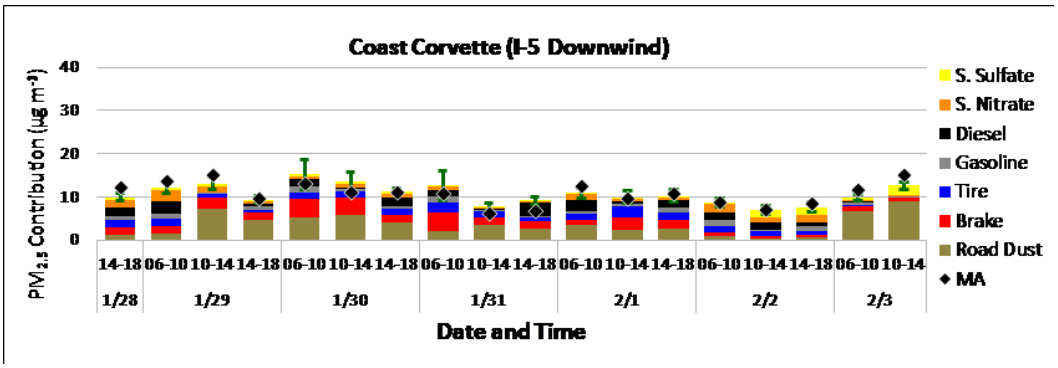
Coast Corvette (I-5 Downwind)
PM2.5 Contribution (µg m-3)
40
30
20
10
0
14-18 06-10 10-14 14-18 06-10 10-14 14-18 06-10 10-14 14-18 06-10 10-14 14-18 06-10 10-14 14-18 06-10 10-14
1/28 1/29 1/30 1/31 2/1 2/2 2/3
Date and Time
S. Sulfate
S. Nitrate
Diesel
Gasoline
Tire
Brake
Road Dust
MA

(a)

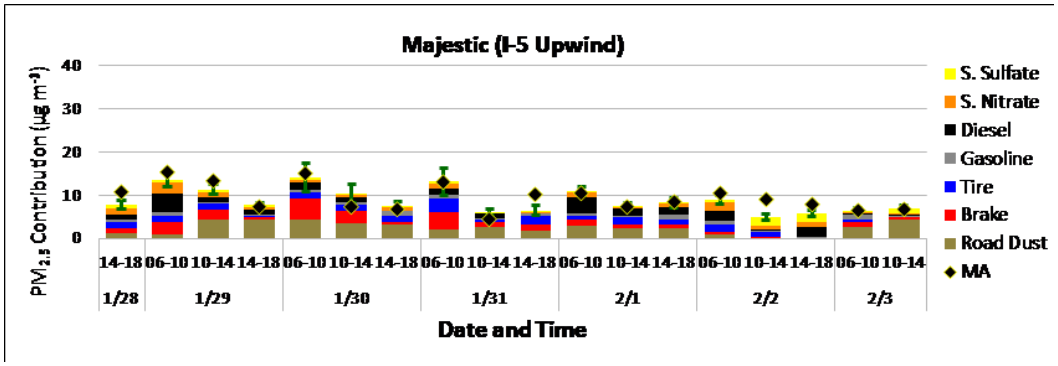
Majestic (I-5 Upwind)
PM2.5 Contribution (µg m-3)
40
30
20
10
0
14-18 06-10 10-14 14-18 06-10 10-14 14-18 06-10 10-14 14-18 06-10 10-14 14-18 06-10 10-14 14-18 06-10 10-14
1/28 1/29 1/30 1/31 2/1 2/2 2/3
Date and Time
S. Sulfate
S. Nitrate
Diesel
Gasoline
Tire
Brake
Road Dust
MA

(b)

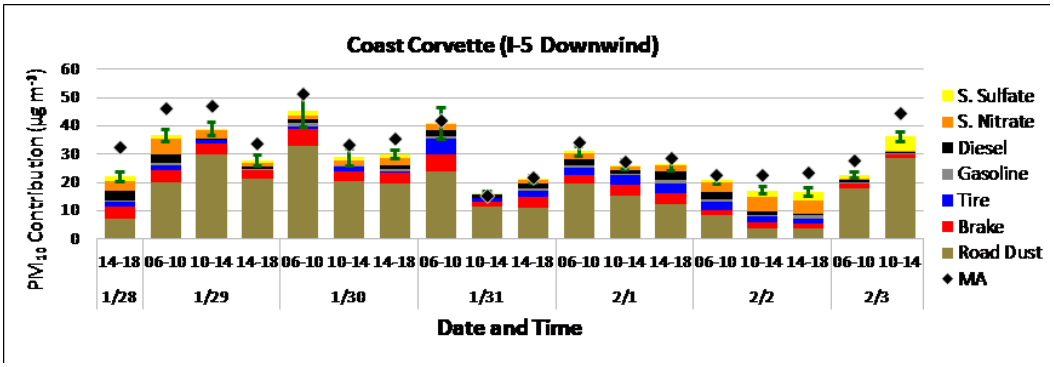
Coast Corvette (I-5 Downwind)
PM10 Contribution (µg m-3)
60
50
40
30
20
10
0
14-18 06-10 10-14 14-18 06-10 10-14 14-18 06-10 10-14 14-18 06-10 10-14 14-18 06-10 10-14 14-18 06-10 10-14
1/28 1/29 1/30 1/31 2/1 2/2 2/3
Date and Time
S. Sulfate
S. Nitrate
Diesel
Gasoline
Tire
Brake
Road Dust
MA

(c)

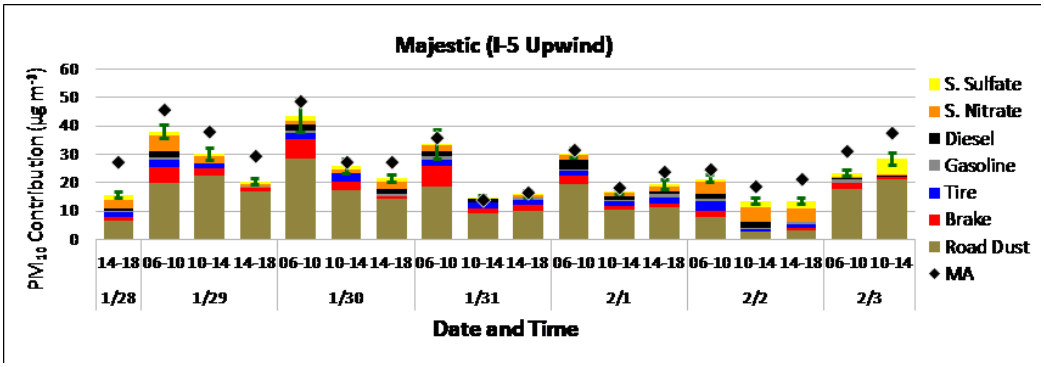

(d)

Figure 5-8: Measured PM mass (MA) and source apportionment for the (a) $PM_{2.5}$ downwind (b) $PM_{2.5}$ upwind (c) PM_{10} downwind (d) PM_{10} upwind sites in Anaheim (I-5). Error bars show the uncertainty in the total source contribution estimates.

χ^2 ranges between 0.38 and 2.7 with a median value of 0.97 for $PM_{2.5}$, and between 0.35 and 2.7 with a median value of 0.75 for PM_{10}. The fitting performance is about the same for $PM_{2.5}$ and PM_{10}. For PM_{10} source apportionment (Figure 5-8 (c)-(d)), road dust still dominates most of the time (14–76% of PM_{10}) while brake wear is resolved for all samples as well (1–20% of PM_{10}). However, there are only moderate correlations between $PM_{2.5}$ and PM_{10} SCEs, with r^2 of 0.59, 0.78, 0.35, 0.65, 0.29, 0.74, and 0.77 for road dust, brake wear, tire wear, gasoline exhaust, diesel exhaust, secondary nitrate, and secondary sulfate, respectively. This signifies uncertainties particularly for tire wear and diesel exhaust SCEs, as the current model has difficulties separating the two. When combing diesel exhaust, gasoline exhaust, and tire wear into one source, the SCE r^2 improves to ~0.7 between $PM_{2.5}$ and PM_{10}.

5.2.4 *CMB Source Apportionment Results for Long Beach (Hwy-710)*

The source apportionment for Hwy-710 downwind (AQMD) and upwind (ATD) sites using the same CMB model as that for I-5, except that the road dust profile CCDust is replaced with AQDust from locally resuspended dust. For $PM_{2.5}$, χ^2 ranges between 0.21 and 1.3 with a median value of 0.60, indicating the same or better fits compared with the I-5 case. Other road dust profiles would lower the fitting performance. Although road dust is still an important contributor to $PM_{2.5}$ (Figure 5-9 (a)-(b)), they are not as dominant on Hwy-710 as on I-5. Brake wear is resolved for all samples (1–21% of $PM_{2.5}$) while diesel exhaust and tire wear are missing in a few samples. There are 3 periods with highly elevated $PM_{2.5}$ concentrations (≥25 µg/m^3) at both downwind and upwind sites: 06-10 on 2/6, 2/7, and 2/8/2020. While the timing (06-10) is consistent with the morning rush hours, $PM_{2.5}$ concentrations measured on I-5, including those during 06-10, have all been well below 20 µg/m^3. Some of the excess $PM_{2.5}$ may be attributed to secondary ammonium nitrate, as well as other unaccounted sources such as sea salt. The Cl concentrations detected 06-10, 2/6/2020 were 4.9 and 4.6 µg/m^3 at AQMD and ATD, respectively, which are 100 times the median value of 0.04 µg/m^3 throughout the campaign.

Overall the CMB fitting performance are lower for Hwy-710 PM_{10}, with χ^2 ranging from 0.7 to 5.6 (median 2.4). This is demonstrated by larger error bars in Figure 5-9(c)-(d). PM_{10} samples generally contain higher levels of road dust than $PM_{2.5}$ and at this location, there is little downwind-upwind difference with respect to road dust contributions. Brake wear is resolved for all samples (3–16% of PM_{10}). Correlations (r^2) between $PM_{2.5}$ and PM_{10} SCEs are 0.59, 0.86, 0.33, 0.035, 0.68, 0.90, and 0.97 for road dust, brake wear, tire wear, gasoline exhaust, diesel exhaust, secondary nitrate, and secondary sulfate, respectively. The low correlation for gasoline exhaust is partly due to its low SCEs. When combing diesel exhaust, gasoline exhaust, and tire wear into one source, the SCE r^2 improves to ~0.7 between $PM_{2.5}$ and PM_{10}. PM_{10} levels during the morning rush hours (6-10) are generally 50 $\mu g/m^3$ or higher except those on 2/10/2020. Part of the PM_{10} mass may be explained by fresh and aged sea salt not included in the model, as the median Cl concentration for PM_{10} is 0.34 $\mu g/m^3$, an order of magnitude higher than that for $PM_{2.5}$. The highest Cl concentrations occurred 06-10, 2/6/2020, being 6.0 and 5.4 $\mu g/m^3$ at the downwind and upwind sites, respectively.

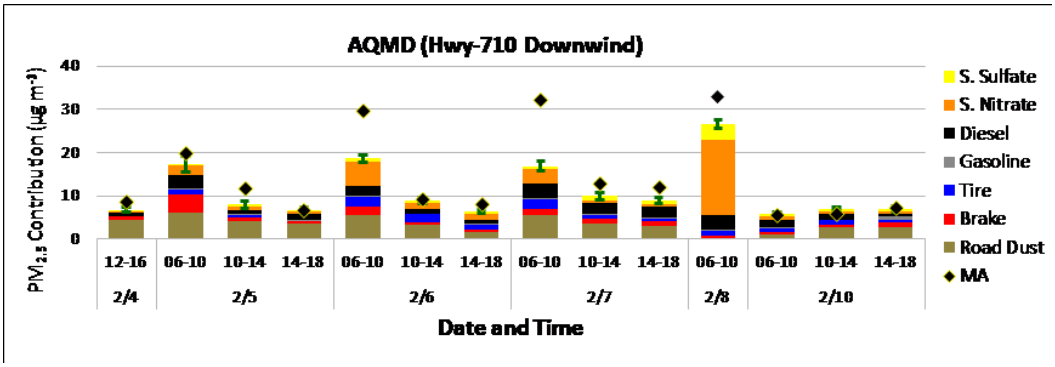

(a)

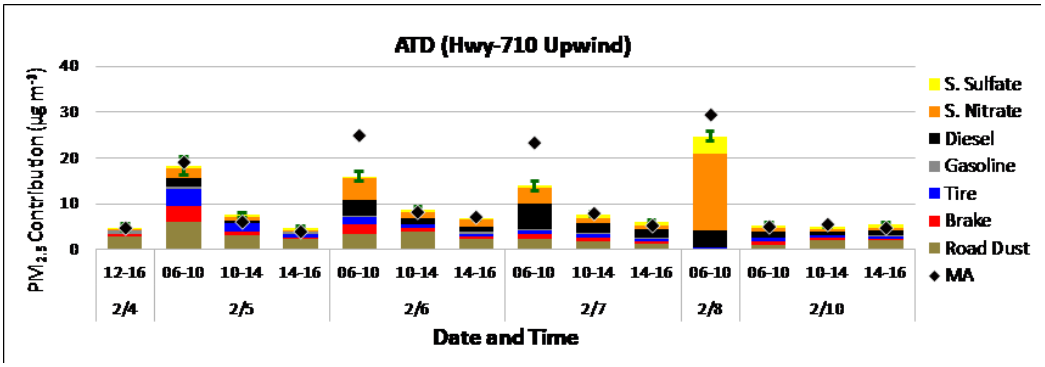

(b)

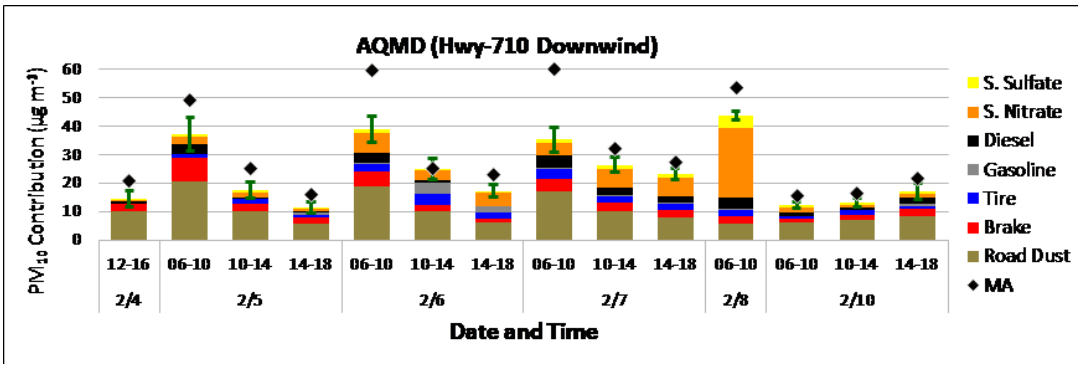

(c)

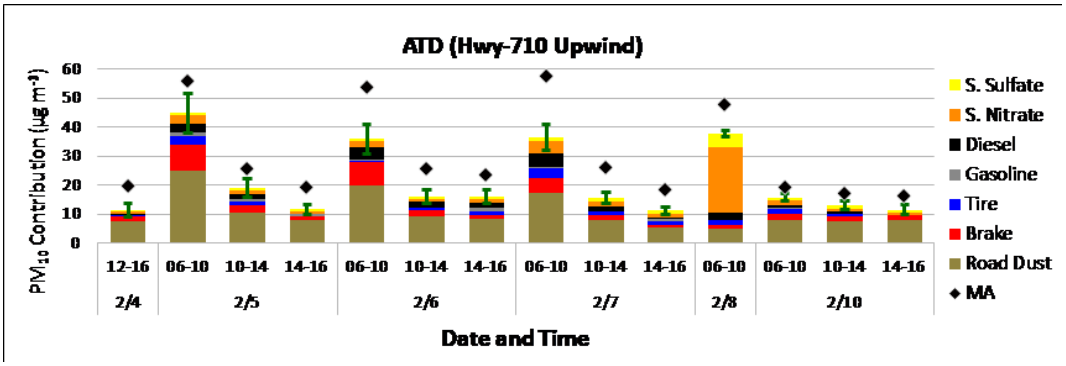

(d)

Figure 5-9: Measured PM mass (MA) and source apportionment for the (a) $PM_{2.5}$ downwind and (b) $PM_{2.5}$ upwind (c) PM_{10} downwind (d) PM_{10} upwind sites in Long Beach (Hwy-710). Error bars show the uncertainty in the total source contribution estimates.

5.2.5 *Summary of CMB Source Apportionments*

Table 5-6 compares the average source apportionment results for the I-5 (Anaheim) and Hwy-710 (Long Beach) measurements. Road dust contributes significantly higher to PM_{10} than to $PM_{2.5}$ ($p< 0.05$). The contributions of brake wear and tire wear are also higher in PM_{10}, but the differences between PM_{10} and $PM_{2.5}$ are generally not significant considering the large uncertainty in the CMB results. Brake I (Brake_C, low copper) exceeds Brake II (Brake_D, high copper) at Anaheim, but vice versa at Long Beach, likely due to different fleet compositions. The downwind-upwind differences of non-exhaust particles (road dust, brake wear, tire wear) are small, although higher values are more often found at the downwind site, especially for Anaheim. It should be noted that the designated downwind sites are not always downwind due to wind direction changes throughout a day.

For gasoline and diesel exhausts, very similar contributions are found between PM_{10} and $PM_{2.5}$ (except for gasoline exhaust at Long Beach), consistent with the dominance of fine particles in vehicle exhausts. The upwind-downwind differences are also not significant. Diesel contribution

appears to be lower at Anaheim (1.13–1.48 μg/m^3) than at Long Beach (1.75–1.92 μg/m^3) while the gasoline contribution to $PM_{2.5}$ is higher at Anaheim (0.61–0.77 μg/m^3) than at Long Beach (0.26–0.31 μg/m^3). It should be noted that brake (Brake I + Brake II) and tire wear levels in $PM_{2.5}$ are also generally higher at Anaheim than at Long Beach.

It is somewhat surprising for significantly higher contributions of secondary nitrate and secondary sulfate in PM_{10} than in $PM_{2.5}$ for both Anaheim and Long Beach (Table 5-6). Why there are substantial nitrate and sulfate in coarse particles warrants further investigations. Secondary nitrate is higher at Long Beach, while secondary sulfate appears to be relatively uniform across the Los Angeles basin.

Table 5-6: Average and standard error of source contribution estimates (SCEs in μg/m^3) for $PM_{2.5}$ and PM_{10} measured at Anaheim and Long Beach. Note "others" represent unaccounted mass.

	Anaheim (I-5)	Anaheim (I-5)	Anaheim (I-5)	Anaheim (I-5)	Long Beach (Hwy-710)	Long Beach (Hwy-710)	Long Beach (Hwy-710)	Long Beach (Hwy-710)
	Downwind (CC)	Downwind (CC)	Upwind (Majestic)	Upwind (Majestic)	Downwind (AQMD)	Downwind (AQMD)	Upwind (ATD)	Upwind (ATD)
	$PM_{2.5}$	PM_{10}	$PM_{2.5}$	PM_{10}	$PM_{2.5}$	PM_{10}	$PM_{2.5}$	PM_{10}
# of Data	18	18	18	18	14	14	14	14
Total Mass	10.9	32.5	9.6	28.5	14.4	31.9	11.0	30.4
Road Dust	3.60±0.57	17.1±1.44	2.50±0.47	14.4±1.30	3.39±0.29	10.3±1.36	2.50±0.29	10.5±1.39
Brake I	1.44±0.96	2.10±1.26	1.21±0.90	1.76±1.29	0.40±0.22	1.23±1.17	0.34±0.19	0.93±1.10
Brake II	0.54±0.36	1.18±0.61	0.34±0.31	0.68±0.55	0.74±0.34	1.81±1.39	0.55±0.33	1.97±1.63
Tire Wear	1.28±0.73	2.01±1.10	1.21±0.70	1.60±0.99	1.05±0.42	1.84±1.56	0.96±0.42	1.25±1.53
Gasoline	0.77±0.47	0.65±0.41	0.61±0.36	0.62±0.36	0.26±0.13	0.73±0.72	0.31±0.15	0.47±0.46
Diesel	1.34±0.68	1.48±0.85	1.40±0.64	1.13±0.78	1.84±0.45	1.92±1.32	1.75±0.45	1.80±1.26
S. Nitrate	0.99±0.11	2.34±0.16	0.92±0.11	2.18±0.17	2.56±0.21	4.81±0.46	2.51±0.22	3.13±0.37
S. Sulfate	0.69±0.19	1.28±0.27	0.65±0.18	1.28±0.26	0.78±0.12	1.16±0.38	0.74±0.13	1.13±0.37
Others	0.23±1.88	4.37±3.11	0.72±1.74	4.83±2.88	3.33±1.43	8.08±3.74	1.34±1.52	9.23±3.76

For the Anaheim downwind and upwind sites (Figure 5-10), road dust accounts for 26–33% and 50–53% of $PM_{2.5}$ and PM_{10} mass, respectively. The road dust fractions are higher than those often found at Los Angeles urban sites (e.g.,[114]), and likely reflect the near-road microenvironment. For $PM_{2.5}$, the non-exhaust fractions (brake + tire =~30%) exceed the exhaust fractions (diesel + gasoline =~20%), though the uncertainty in the partitioning between diesel,

gasoline, and tire wear particles should be noted. The unaccounted mass is minor (2–7%), which may be attributed to biomass burning, cooking, and industrial emissions as well as fresh and aged sea salt. For PM_{10}, the non-exhaust fractions (brake + tire) are ~15%, more than twice the exhaust fractions (diesel + gasoline) of ~6%. This indicates more enrichment of non-exhaust PM mass in coarse particles than exhaust PM mass. The fraction of unaccounted mass increases to 14–17% of PM_{10}, possibly due to fresh/aged sea salt or additional dust sources.

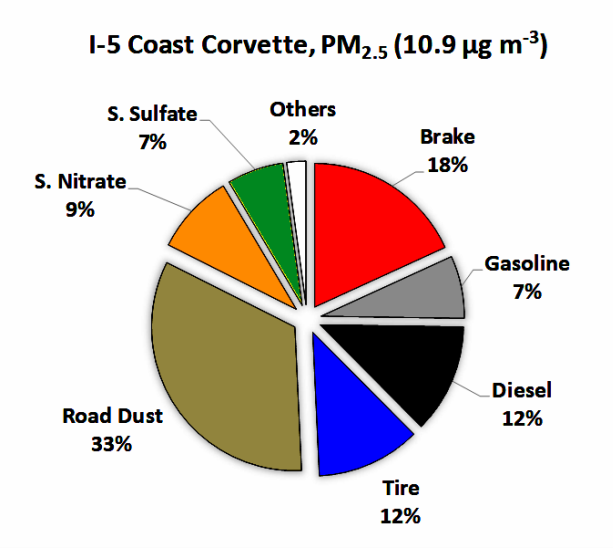

(a)

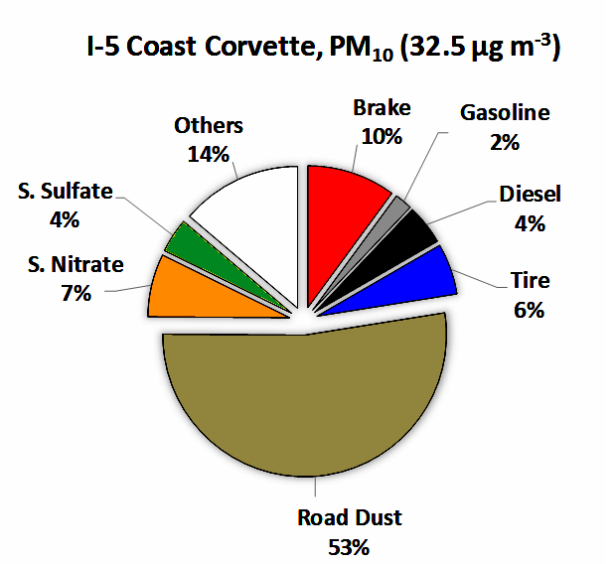

(b)

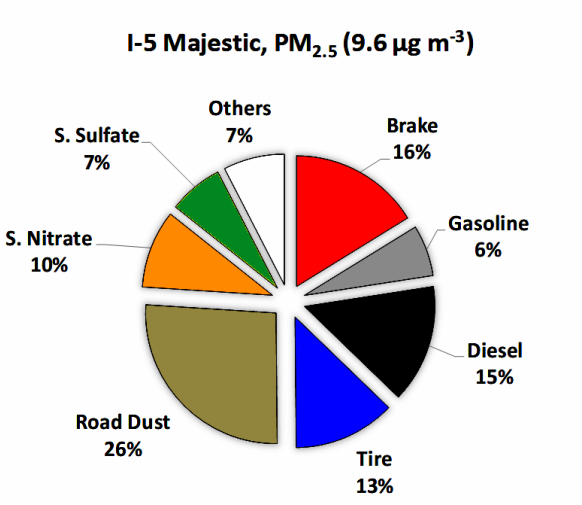

(c)

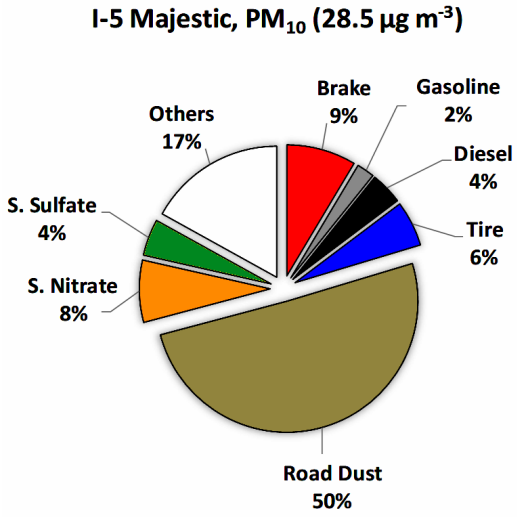

(d)

Figure 5-10: Fractions of non-exhaust and exhaust contributions to $PM_{2.5}$ and PM_{10} at the Anaheim downwind (Coast Corvette) and upwind (Majestic) sites.

For the Long Beach downwind and upwind sites, road dust fractions are lower (22–24% for $PM_{2.5}$ and 32–34% for PM_{10}, respectively), while the fractions of secondary nitrate and unidentified mass increase substantially. The large unaccounted mass during 6-10 am of a few sampling days warrants further investigations. For $PM_{2.5}$, the non-exhaust fractions (brake + tire =15–17%) are comparable with the exhaust fractions (diesel + gasoline =15–19%) on Hwy-710. For PM_{10}, the non-exhaust fractions (brake + tire) are ~14-16%, about twice the exhaust fractions (diesel + gasoline) of ~8%. This again is consistent with our findings for I-5 in Anaheim. The very similar breakdowns between upwind and downwind sites suggest a nearly equal impact of onroad traffic emissions on the downwind and upwind sites.

The aforementioned results confirm that it is not possible to quantify the traffic contributions to the downwind site by simply subtracting the upwind measurement. Our results nonetheless indicate a dominant road dust impact on near road PM, as well as relative contributions from exhaust and non-exhaust emissions. $PM_{2.5}$ non-exhaust fraction is comparable/larger than exhaust fraction, while PM_{10} non-exhaust fraction is twice as much as exhaust fraction based on results from both experiment sites. Future studies should better determine the background PM levels for a better quantification of emissions and impact from the targeted fleet.

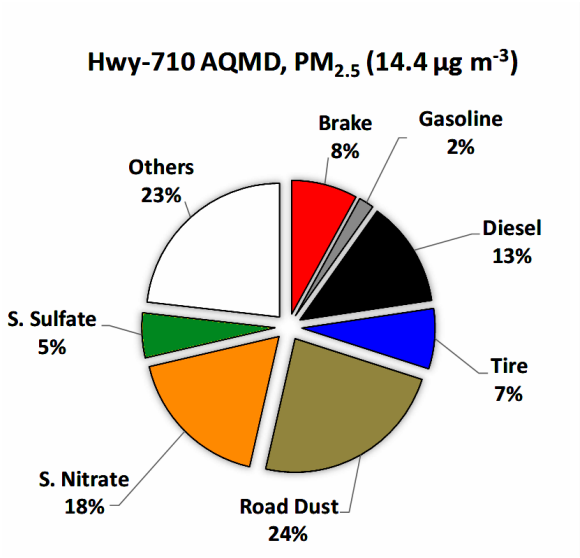

(a)

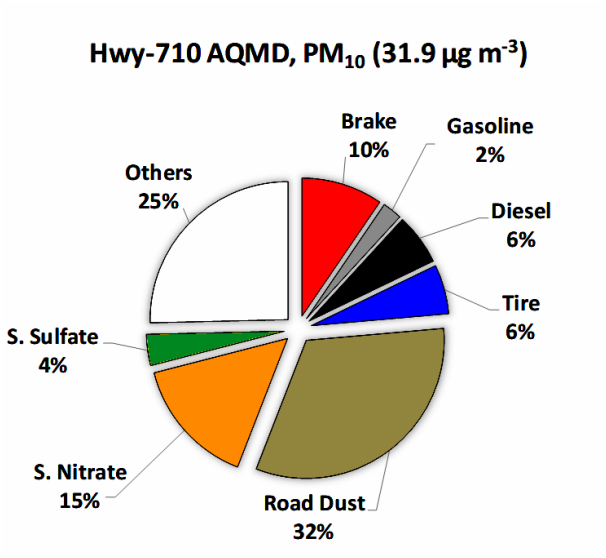

(b)

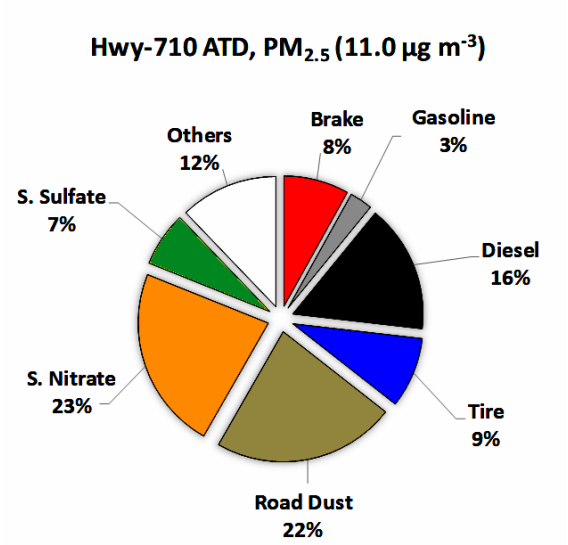

(c)

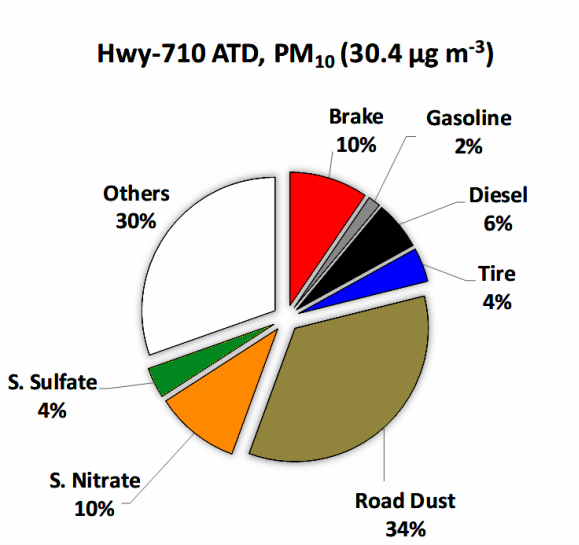

(d)

Figure 5-11: Fractions of non-exhaust and exhaust contributions to $PM_{2.5}$ and PM_{10} at the Long Beach downwind (AQM) and upwind (ATD) sites.

6 Task 6: Dispersion modeling

6.1 Anaheim Simulations

The main objective of the Anaheim simulations is to assess the impact of exhaust and non-exhaust emissions on the downwind communities. Given the uncertainties discussed in the previous chapters, our strategy is to leverage the field measurements to constrain the simulations as much as possible.

Figure 6-1 Field measurement site locations in Anaheim.

We utilized the following field measurement data from two monitoring sites as shown in Figure 6-1

- **AQMD site**: Wind direction and speed measured by the meteorological station.
- **Anaheim NR site**: Wind direction and speed at two heights (4.5m and 6.9 m) measured by two sonic Anemometers; particle size distributions (PSD) measured by EPLI at 1.5 m.

6.1.1 *Selected date and time for simulations*

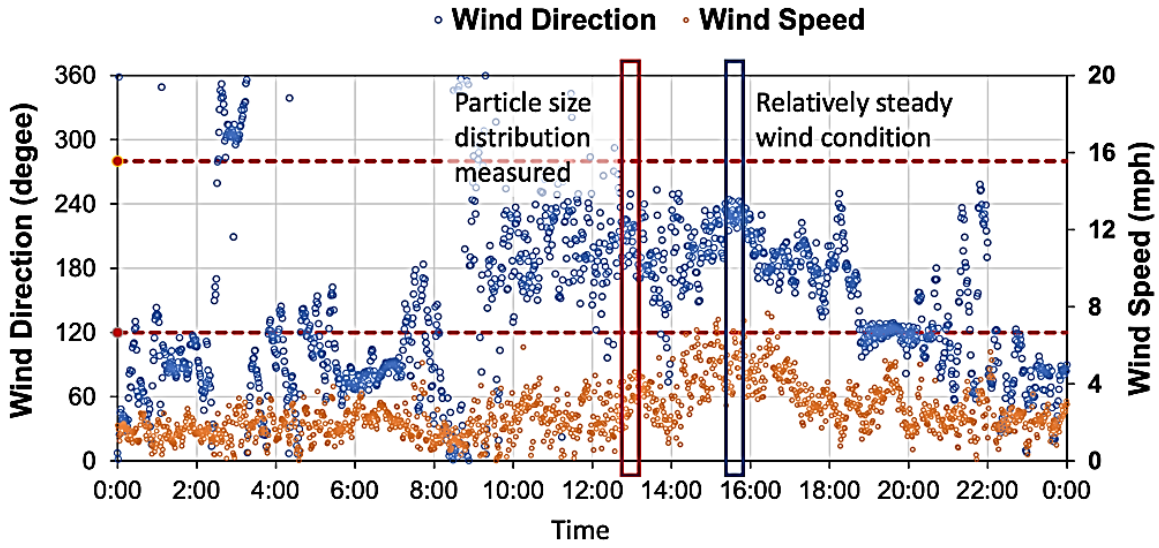

Figure 6-2: Measured wind speed and wind direction at the AQMD site on 01/28/2020

To reduce the uncertainties associated with variable wind conditions, we aimed to identify a period of time when 1) the wind speed and wind direction were relatively steady; 2) the wind direction was close to be perpendicular to the highway, blowing from Majestic Garden Hotel (MGH) to the Anaheim NR site; and 3) the wind speed was relatively high, based on the wind data collected at the AQMD site. We found that the interval around 3:45 pm on 01/28/2020, marked in Figure 6-2, fits our criteria very well. PSD measurements are not available at exactly the same time. We chose the PSD measurement at 1 pm on the same day (also marked in Figure 6-2), when the wind condition was similar to that around 3:45 pm.

6.1.2 *Method: The two-domain approach*

Ideally, our simulations would be performed on a domain similar what is shown in Figure 6-1, containing the highway emission source and both upwind and downwind communities. In reality, simulations on such a large domain are computationally prohibitive. To overcome this challenge, we came up with a two-domain approach in order to leverage field measurements data while making computational costs manageable. The domains are referred to as the Highway domain and the Community domain. We employed the Comprehensive Turbulent Aerosol Dynamics and Gas Chemistry (CTAG) model as the simulation tool.

6.1.2.1 <u>The Highway domain</u>

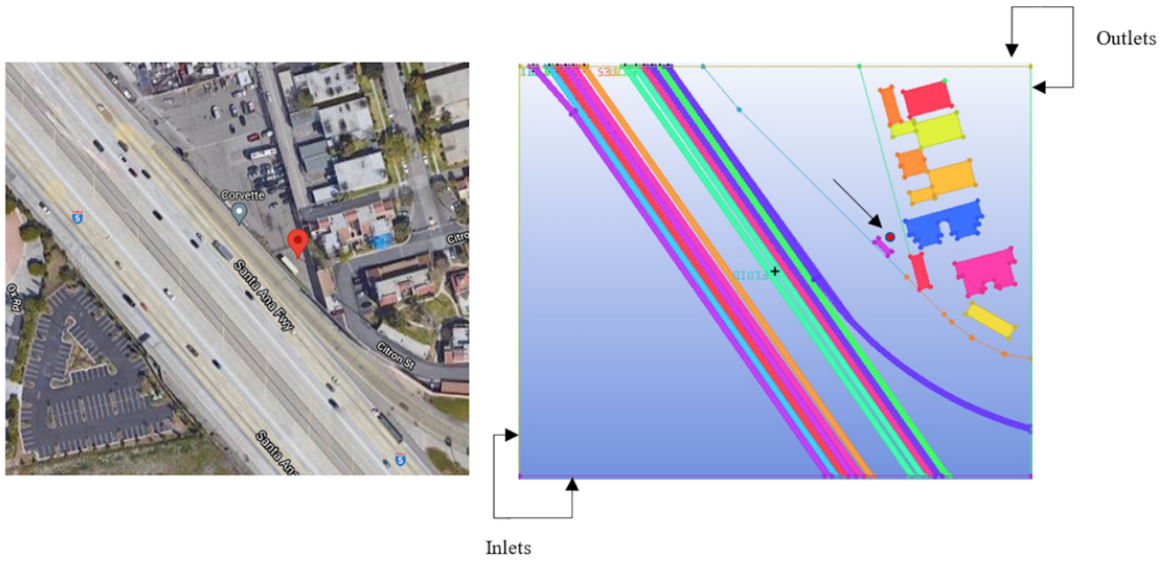

(a) (b)

Figure 6-3: Illustration of the Highway domain: a) Aerial image showing the real-world conditions; (b) Top view of the computational domain. The location of the Anaheim NR site is marked with red dots on both (a) and (b).

The Highway domain, as illustrated in Figure 6-3, consists of the highway, MGH, the Anaheim NR site. The goal of the simulations on the Highway domain is to generate velocity and concentration profiles at the Anaheim NR site, which then serve as inputs to the simulations for the Community domain.

6.1.2.1.1 Velocity profile

The inlet velocity profile applied at the inlet boundaries of the Highway domain, shown in Figure 6-3b, was determined using a reverse modeling process. We first make a log-law power profile using the following equation:

$$V_{in} = k_0 ln\left(\frac{z}{z_0}\right)$$

where k_0 and z_0 are two constants that can be estimated by the two velocity vectors measured using the anemometer at $z = 4.5\,m$ and $z = 6.9\,m$ at the Anaheim NR site. With k_0 and z_0 known, we initialize the inlet velocity profiles and conducted a simulation to see what the velocity vectors look like at the two heights. Based on the difference between the measured velocity vectors and the simulated ones at the anemometer location, we described the updated velocity profile as:

$V_{in,new} = cV_{in,old}$

where c can be conservatively found from:

$$c = \min\left(\frac{V_{meas@z=4.5\ m}}{V_{sim@z=4.5\ m}}, \frac{V_{meas@z=6.9\ m}}{V_{sim@z=6.9\ m}}\right)$$

The new velocity profile ($V_{in,new}$) acts as the inlet velocity profile for the next simulation. We continued the process until c converges and the obtained velocity vectors with the simulation are close enough to the measured ones ($c_{iter} \approx 1$). A flowchart of the process in shown in Figure 6-4.

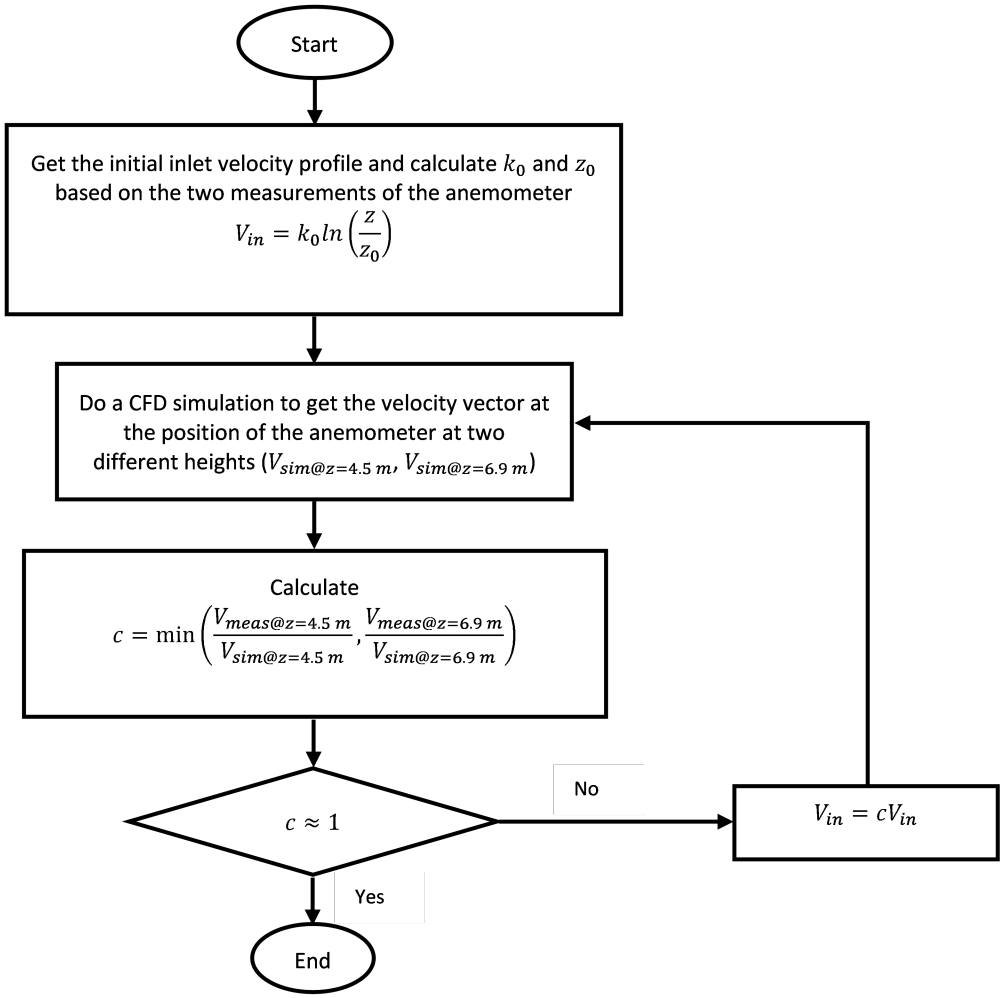

Figure 6-4: A flowchart of the implemented algorithm for determining the inlet velocity profile for the Highway domain.

This inverse modeling essentially ensures the simulations on the Highway domain captured turbulence in the urban boundary layer and from the highway without explicitly representing the urban morphology and highway source. Figure 6-5 depicts the simulated velocity profile varying with height in the computational domain at the Anaheim NR site compared to the two measured values (at 4.5 and 6.9 m). The simulated velocity profile was fitted into a regression line to be used as an input to the simulations on the Community domain. Figure 6-5 shows that the simulated velocity profile matched the measured values very well, benefited from the inverse modeling process.

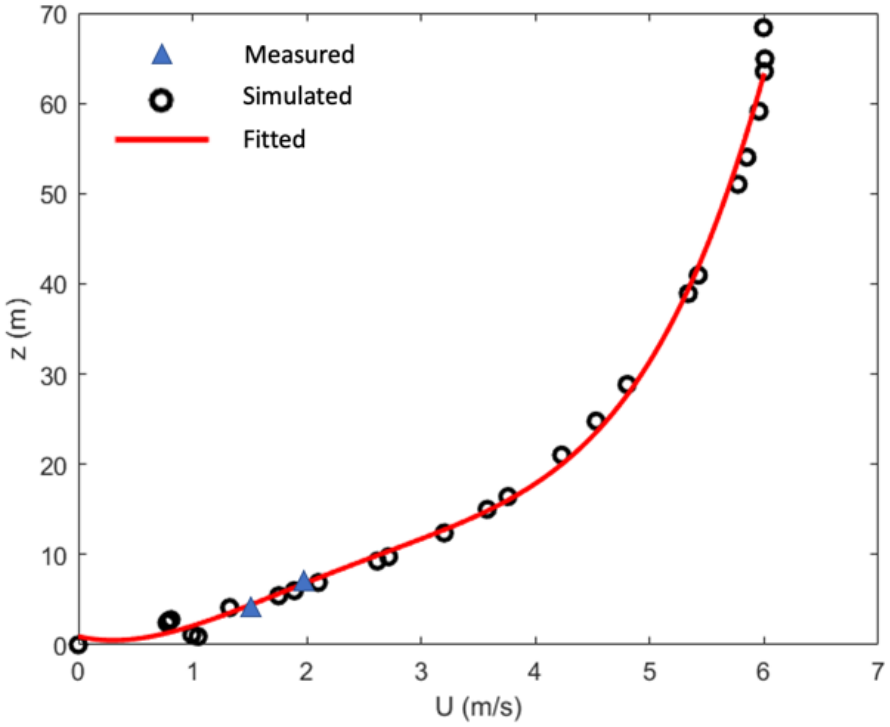

Figure 6-5: The simulated vertical profile of wind velocity in the Highway domain at the Anaheim NR site compared against the two measured values (at 4.5 and 6.9 m). The simulated velocity profile was also fitted into a regression line.

6.1.2.1.2 Particle concentration profiles

Our team has measured particle size distributions using ELPI the Anaheim NR site, which are shown in Figure 6-6a. We further discretized the PSD measured at 1 pm on 01/28/2020 into 11 size bins for our simulations. Particles in the sub-micron range are usually dominated by exhaust sources and those in the super-micron range dominated by non-exhaust sources. The inlet for the ELPI is at 1.5 m above the ground, while our simulations for the Community domain require particle concentrations over the entire domain height. We utilized the normalized vertical profile generated from the highway simulations to construct the vertical profiles of particle

concentrations. Our simulation results indicate the normalized particle concentration profiles are insensitive to particle size and deposition, due to the close vicinity to the highway source.

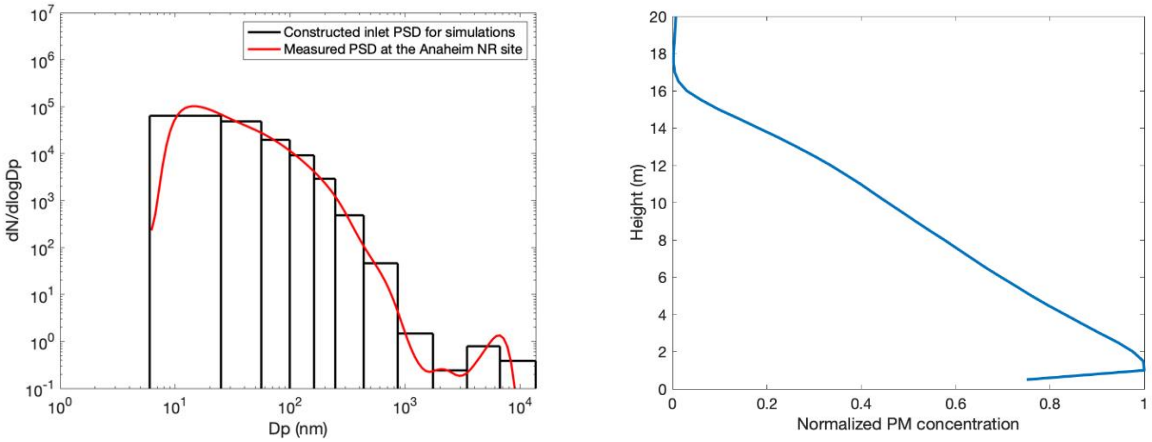

Figure 6-6 (a) Measured particle size distributions (PSD) using ELPI the Anaheim NR site and the corresponding discretized PSDs used in the simulations for the Community domain. (b) The vertical profiles of normalized particle concentrations.

6.1.2.2 The Highway domain

Figure 6-7 depicts the community domain (550 m L x 500 m W x 50 m H), where Figure 6-7a shows the real-world condition, Figure 6-7b the computational representation, and Figure 6-7c a hypothetical solid barrier (440 m in length and 6 m in height) between the highway and the community. The inlet for the Community domain is essentially a virtual wall cutting through the Anaheim NR site so that we can directly utilize the measured PSD and simulated vertical profile of normalized particle concentrations to create the inlet particle concentration profiles. As discussed in 6.1.2.1.1, we have generated the velocity profile for the inlet through an inverse modeling exercise at the Highway domain.

(a) (b)

Figure 6-7: The Community domain: (a) The real-world condition; (b) the computational domain.

6.1.2.3 The CTAG model

The CTAG model is designed to resolve the flow field including turbulent reacting flows, aerosol dynamics, and gas chemistry in complex environments. In this study, we employed the Reynolds Averaged Navier-Stokes (RANS) model to resolve the flow and turbulence. We employed the Realizable k-epsilon (k-ε) RANS model with the enhanced wall treatment for turbulence closure, and also conducted a sensitivity analysis to assess the impact of the three different types of the (k-ε) RANS models (Standard, Realizable, and RNG) on downwind pollutant concentrations. In this study, a scalar transport equation was used to model both dispersion and deposition of particles:

$$\frac{\partial \rho \widetilde{N_p(D_p)}}{\partial t} + \frac{\partial \rho \tilde{u}_i \widetilde{N_p(D_p)}}{\partial x_j} = \frac{\partial}{\partial x_j}[(D_t + D_m)\frac{\partial \widetilde{N_p(D_p)}}{\partial x_j}] + S_d(D_p)$$

where Np(Dp) is the average particle concentration of a particle size Dp. Dm is the molecular diffusivity and Dt is the turbulent diffusivity. The turbulent diffusivity dominates the molecular diffusivity. Sd(Dp) is a sink term to account for ground deposition of particles according to Seinfeld and Pandis [115].

6.1.3 *Results and Discussion*

To facilitate the discussion of the findings, we marked four planes (20 m, 75m, 195m and 375 m from the inlet, respectively), as shown in Figure 6-8, to describe the evolution of plane-averaged PSDs in the domain.

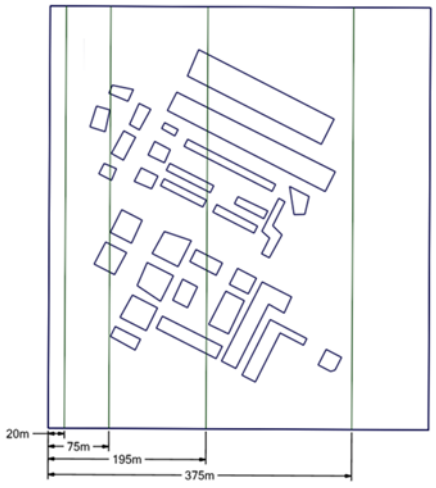

Figure 6-8: Four planes (20 m, 75 m, 195m, 375m from the inlet, respectively) to describe the evolution of particle size distributions in the domain.

Furthermore, we set up three modeling configurations, i.e., "w/o deposition, w/o wall", "w/ deposition, w/o wall" and "w/ deposition, w/wall" to examine the roles of deposition and the wall on particle concentrations.

- "w/o deposition": This scenario was created by turning off the deposition in the model.
- "w/ deposition": This scenario was created by turning on the deposition in the model.

The comparisons between "w/o deposition " and "w/ deposition" help us understand the role of dry deposition on particle concentrations and size distributions.

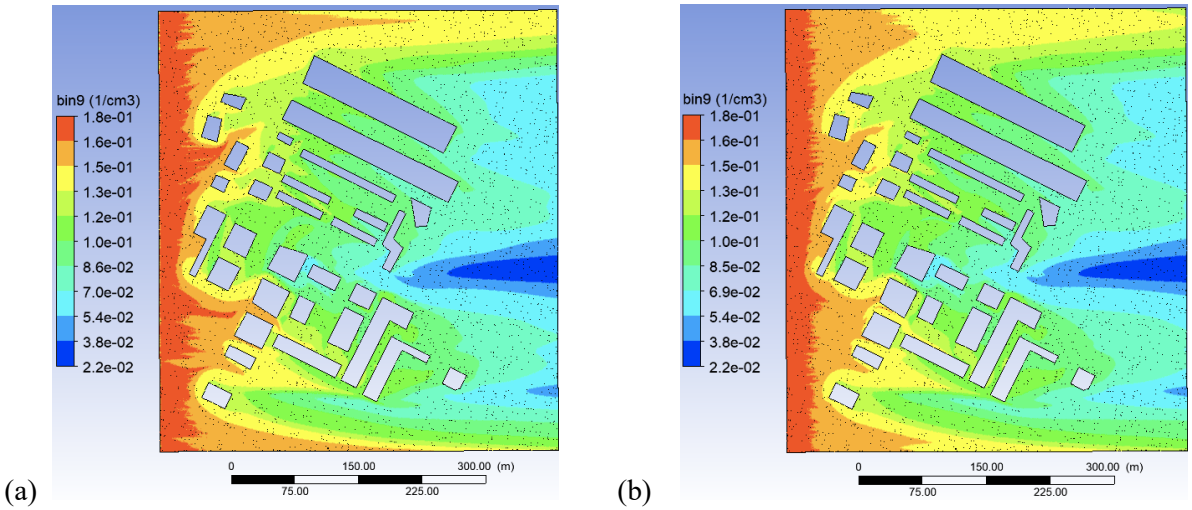

(a) (b)

Figure 6-9: Contours of particle mass concentrations (dM/dlogDp) for the size bin around 4 µm (3.44 to 6.64 µm) between (a) "w/o deposition" and (b) "w/ deposition" configurations at 1.5 m above the ground level.

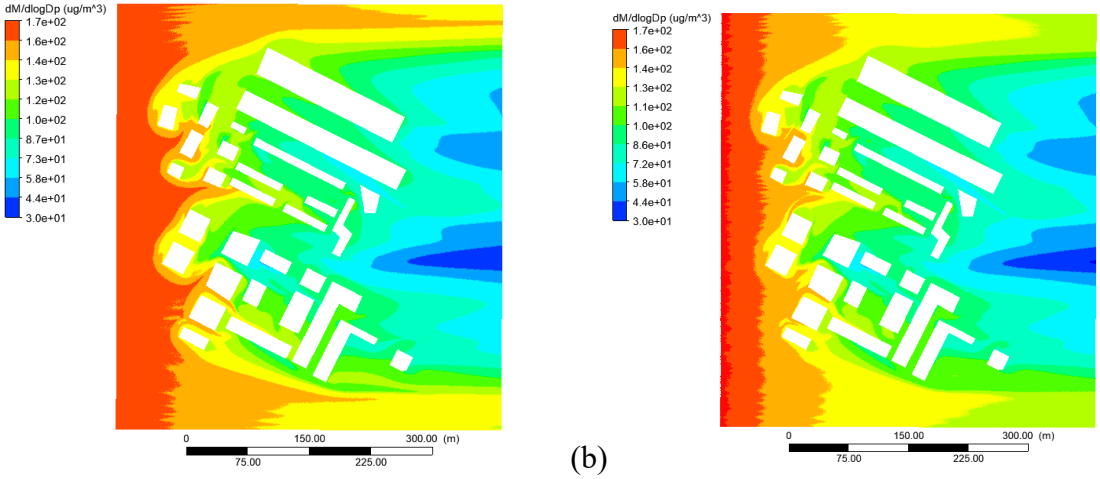

(a) (b)

Figure 6-10: Contours of particle mass concentrations (dM/dlogDp) for the size bin around 10 μm (6.64 to 13.6 μm) between (a) "w/o deposition" and (b) "w/ deposition" configurations at 1.5 m above the ground level.

Figure 6-9 compares the contours of particle concentrations (dM/dlogDp) for the size bin around 4.5 μm (3.44 to 6.64 μm) between "w/o deposition" (Figure 6-9b) and "w/ deposition" (Figure 6-7b) configurations at 1.5 m above the ground level. We chose this bin because it approximately corresponds to the peak in the mass concentrations of brake PM. Deposition is shown to reduce the concentrations for this size range, especially near the inlet where particle concentrations are relatively high compared to the rest of the domain. However, for most of the domain, the reduction due to deposition is small, estimated to be around 1 to 2% across the domain. Note that the presence of buildings in the domain has made the spatial variations considerably complex.

Figure 6-10 compares the contours of particle concentrations (dM/dlogDp) for the size bin around 10 μm (6.44 to 13.6 μm) between "w/o deposition" (Figure 6-10a) and "w/ deposition" (Figure 6-10b) configurations at 1.5 m above the ground level. This size bin approximately corresponds to the peak in the mass concentrations of road dust particles. Deposition is shown to reduce the concentrations for this size range by 5 to 7% within the Community domain, in contrast with 1-2% reduction by deposition for 4.5 μm (3.44 to 6.64 μm). The general trend is expected given the much higher deposition velocity for 10 μm particles than 4.5 μm particles.

6.1.4 *Summary*

We developed a two-domain approach to take advantage of the field measurement data to greatly reduce the uncertainties in modeling inputs while making the computational costs manageable. We constructed velocity profiles and size-resolved particle concentration profiles through simulations in the Highway domain. The dispersion and deposition of exhaust and non-exhaust particles were simulated and the effect of particle deposition was investigated in the Community domain. Our results suggest that the deposition can reduce particle mass concentrations by 1 to 2% for the size range pertain to brake PM in the downwind community and by 4-7% for the size range relevant to road dust. The implication is that near-road communities are likely exposed to non-exhaust particles from roadways, even though those particles have relatively higher deposition velocity than exhaust particles.

7 Summary and conclusions

In this study, several traffic data sources, including Caltrans PeMS, video footage processed by the ALPR, and WIM stations, at or around two study sites (i.e., Anaheim NR and I-710 NR) have been examined to explore the relationship between background mobile sources and near-road brake and tire wear emissions. Results indicate that PeMS data should be the major traffic information source given its spatio-temporal coverage (i.e., spatial proximity and temporal consistency) and data reliability. Other data sources might be useful complement to PeMS for more detailed information, e.g., vehicle type, powertrain characteristics. However, the association of information across multiple data sources is challenging due to the disparities of measurements in space, time and type.

Due to abundant coarse particles in near-road environment, PM_{10} concentrations were 2–3 times of those of $PM_{2.5}$, with $PM_{2.5}$ and PM_{10} being 10-15 and ~30 $\mu g/m^3$, respectively. However, the concentration differences between the nominal upwind and downwind sites were small, with the concentrations at the nominal downwind sites being approximately 1–4 $\mu g/ m^3$ higher.

High data quality of $PM_{2.5}$ and PM_{10} chemical speciation was demonstrated through comparison of water soluble ions and corresponding elements, gravimetric mass vs. sum of measured chemical species and reconstructed mass, and anion and cation balance. As expected from near-road environment, organic matter (OM; ~30–40%), geological materials (~25–30%), and elemental carbon (EC; ~10–15%) were the most abundant $PM_{2.5}$ compositions. Due to abundant coarse dust composition, geological materials (~40–45%) was the dominant PM_{10} composition, followed by OM (~25%), NO_3^- (~6-11%), and EC (6-8%). EC concentrations at the Hwy-710 sites were 26% and 19% higher than those at the I-5 sites for $PM_{2.5}$ and PM_{10} respectively, likely due to more diesel vehicles on Hwy-710. Anion and cation ion balance analysis indicates that particles were slightly acidic during most sampling periods when ion concentrations were relatively low, while they were nearly neutral when ion concentrations were high. Compared to more diverse ion abundances at the I-5 sites, ammonium nitrate was the dominant inorganic salt, followed by sulfates at the Hwy-710 sites. Two high NH_4^+ events were observed during the 0600–1000 sampling periods at the Hwy-710 sites, corresponding to relatively low ambient temperatures and high relative humidity. High correlations were found for elements with common sources, such as markers for brake wear (e.g., Ba and Cu) and road dust (Al and Si).

Concentrations of organic groups were higher at the I-5 sites than the Hwy-710 sites except PAHs. The distributions of PAHs at the two highways were similar, with high abundances of 4-ring, 5-ring, and some 6-ring and 7-ring PAHs. PAH concentrations near Hwy-710 were 47% higher than those near I-5; particularly, the concentrations of acenaphthene, fluoranthene and pyrene were 14.3, 13.8, and 5.8 times of those near I-5, respectively, likely due to higher diesel vehicle fractions. PM from both highways had abundant n-alkanes, with similar bimodal distributions peaking near C23 and C29, respectively, although the relative concentrations of these two modes were different near the two highways. Very high concentrations (up to 4 $\mu g/m^3$)

of phthalates were found during all sampling periods of 0600-1000 at the I-5 sites, about a factor of 10 higher than other sampling periods. These high concentration periods were not found near Hwy-710, indicating that traffic was probably not the source of high concentrations of phthalates. The sources and potential exposure risks of phthalates warrant further studies as bis(2-ethylhexyl)phthalate is designated by the U.S. EPA as a probable human carcinogen.

Based on time-integrated $PM_{2.5}$ and PM_{10} measurements with detailed speciation at the downwind and upwind of I-5 and Hwy-710, we were able to attribute the observed PM mass to non-exhaust and exhaust vehicle emissions. Road dust is shown to be the most abundant in most of samples, especially PM_{10}, which is consistent with the near-road environment. Brake and tire wear are also detectable in most of samples but with highly variable contributions from sample to sample, reflecting measurement uncertainties as well as some difficulties to separate tire wear from exhaust particles due to lack of suitable profiles and/or specific markers. In the current model, the most important markers for brake wear include Fe, Ba, Cu, and Ti, while tire wear is marked by OC3, Zn, and phthalates. Other sources that could contribute to these species warrant further investigations.

Overall, brake and tire wear contribute more to $PM_{2.5}$ than exhaust particles (diesel + gasoline) at Anaheim (29–30% vs. 19–21%) while the two are comparable at Long Beach (15–17% vs. 15–19%). For PM_{10}, the brake and tire wear contributions are 2 – 3 times the exhaust contributions. While exhaust particles are mostly fine-mode, more than 1/3 of brake and tire wear particles appear to be in the coarse mode. Brake particles measured at I-5 and Hwy-710 differ in the fine-coarse breakdown and Cu content, possibly due to different traffic composition. This study confirms the importance of non-exhaust particles in traffic-related PM emissions, even for $PM_{2.5}$. However, in the current experimental configuration, the downwind-upwind differences are too small (compared to the measurement uncertainties) to provide a direct confirmation to the source apportionment. Determining non-tailpipe emission factors from field test in urban area is very challenging and requires further study.

8 References

1. Iijima, A., et al., *Particle size and composition distribution analysis of automotive brake abrasion dusts for the evaluation of antimony sources of airborne particulate matter.* Atmospheric Environment, 2007. **41**(23): p. 4908-4919.

2. Kwak, J., S. Lee, and S. Lee, *On-road and laboratory investigations on non-exhaust ultrafine particles from the interaction between the tire and road pavement under braking conditions.* Atmospheric Environment, 2014. **97**: p. 195-205.

3. Thorpe, A. and R.M. Harrison, *Sources and properties of non-exhaust particulate matter from road traffic: a review.* Science of the total environment, 2008. **400**(1-3): p. 270-282.

4. Garg, B.D., et al., *Brake wear particulate matter emissions.* Environmental Science & Technology, 2000. **34**(21): p. 4463-4469.

5. Hagino, H., M. Oyama, and S. Sasaki, *Laboratory testing of airborne brake wear particle emissions using a dynamometer system under urban city driving cycles.* Atmospheric environment, 2016. **131**: p. 269-278.

6. Sanders, P.G., et al., *Airborne brake wear debris: size distributions, composition, and a comparison of dynamometer and vehicle tests.* Environmental science & technology, 2003. **37**(18): p. 4060-4069.

7. Wahlström, J., et al., *Airborne wear particles from passenger car disc brakes: a comparison of measurements from field tests, a disc brake assembly test stand, and a pin-on-disc machine.* Proceedings of the Institution of Mechanical Engineers, Part J: Journal of Engineering Tribology, 2010. **224**(2): p. 179-188.

8. Wahlström, J., L. Olander, and U. Olofsson, *Size, shape, and elemental composition of airborne wear particles from disc brake materials.* Tribology letters, 2010. **38**(1): p. 15-24.

9. Mosleh, M., P.J. Blau, and D. Dumitrescu, *Characteristics and morphology of wear particles from laboratory testing of disk brake materials.* Wear, 2004. **256**(11-12): p. 1128-1134.

10. Kwak, J.-h., et al., *Characterization of non-exhaust coarse and fine particles from on-road driving and laboratory measurements.* Science of the Total Environment, 2013. **458**: p. 273-282.

11. Grigoratos, T. and G. Martini, *Brake wear particle emissions: a review.* Environmental Science and Pollution Research, 2015. **22**(4): p. 2491-2504.

12. Chan, D. and G. Stachowiak, *Review of automotive brake friction materials.* Proceedings of the Institution of Mechanical Engineers, Part D: Journal of Automobile Engineering, 2004. **218**(9): p. 953-966.

13. Stanard, A., et al., *Brake and Tire Wear Emissions*, in *Final Report for project 17RD016 Prepared for the California Air Resources Board and the California Environmental Protection Agency*. 2021.

14. Österle, W., et al., *A comprehensive microscopic study of third body formation at the interface between a brake pad and brake disc during the final stage of a pin-on-disc test.* Wear, 2009. **267**(5-8): p. 781-788.

15. Österle, W., et al., *Chemical and microstructural changes induced by friction and wear of brakes.* Wear, 2001. **251**(1-12): p. 1469-1476.

16. Filip, P., Z. Weiss, and D. Rafaja, *On friction layer formation in polymer matrix composite materials for brake applications.* Wear, 2002. **252**(3-4): p. 189-198.

17. Blau, P.J. and H.M. Meyer III, *Characteristics of wear particles produced during friction tests of conventional and unconventional disc brake materials.* Wear, 2003. **255**(7-12): p. 1261-1269.

18. von Uexküll, O., et al., *Antimony in brake pads-a carcinogenic component?* Journal of Cleaner Production, 2005. **13**(1): p. 19-31.

19. Kukutschová, J., et al., *Wear performance and wear debris of semimetallic automotive brake materials.* Wear, 2010. **268**(1-2): p. 86-93.

20. Eriksson, M., F. Bergman, and S. Jacobson, *On the nature of tribological contact in automotive brakes.* Wear, 2002. **252**(1-2): p. 26-36.

21. Österle, W. and I. Urban, *Friction layers and friction films on PMC brake pads.* Wear, 2004. **257**(1-2): p. 215-226.

22. Kukutschová, J., et al., *On airborne nano/micro-sized wear particles released from low-metallic automotive brakes.* Environmental Pollution, 2011. **159**(4): p. 998-1006.

23. Dall'Osto, M., et al., *Hourly elemental concentrations in PM 2.5 aerosols sampled simultaneously at urban background and road site during SAPUSS–diurnal variations and PMF receptor modelling.* Atmospheric Chemistry and Physics, 2013. **13**(8): p. 4375-4392.

24. Johansson, C., M. Norman, and L. Burman, *Road traffic emission factors for heavy metals.* Atmospheric Environment, 2009. **43**(31): p. 4681-4688.

25. Han, S., J.-S. Youn, and Y.-W. Jung, *Characterization of PM10 and PM2.5 source profiles for resuspended road dust collected using mobile sampling methodology.* Atmospheric Environment, 2011. **45**(20): p. 3343-3351.

26. Beddows, D., et al., *Detection of brake wear aerosols by aerosol time-of-flight mass spectrometry.* Atmospheric environment, 2016. **129**: p. 167-175.

27. Gietl, J.K., et al., *Identification of brake wear particles and derivation of a quantitative tracer for brake dust at a major road.* Atmospheric Environment, 2010. **44**(2): p. 141-146.

28. Birmili, W., et al., *Trace metal concentrations and water solubility in size-fractionated atmospheric particles and influence of road traffic.* Environmental science & technology, 2006. **40**(4): p. 1144-1153.

29. Pant, P. and R.M. Harrison, *Estimation of the contribution of road traffic emissions to particulate matter concentrations from field measurements: A review.* Atmospheric Environment, 2013. **77**(0): p. 78-97.

30. Abu-Allaban, M., et al., *Tailpipe, resuspended road dust, and brake-wear emission factors from on-road vehicles.* Atmospheric Environment, 2003. **37**(37): p. 5283-5293.

31. Koupal, J., et al., *Brake Wear in Particulate Matter Emission Modeling*, in *Final Report for CalTrans Project No. 65A0703*. 2021, Eastern Research Group, Inc.

32. Agudelo, C., et al., *Design of Experiments for Effects and Interactions during Brake Emissions Testing Using High-Fidelity Computational Fluid Dynamics*. 2019, SAE Technical Paper.

33. Agudelo, C., et al., *Brake Particulate Matter Emissions Measurements for Six Light-Duty Vehicles Using Inertia Dynamometer Testing.* SAE International Journal of Advances and Current Practices in Mobility, 2020. **3**(2020-01-1637): p. 994-1019.

34. Milani, M., et al., *First evidence of tyre debris characterization at the nanoscale by focused ion beam.* Materials Characterization, 2004. **52**(4): p. 283-288.

35. Apeagyei, E., M.S. Bank, and J.D. Spengler, *Distribution of heavy metals in road dust along an urban-rural gradient in Massachusetts.* Atmospheric Environment, 2011. **45**(13): p. 2310-2323.

36. Lough, G.C., et al., *Emissions of Metals Associated with Motor Vehicle Roadways.* Environmental Science & Technology, 2005. **39**(3): p. 826-836.

37. Rogge, W.F., et al., *Sources of fine organic aerosol. 3. Road dust, tire debris, and organometallic brake lining dust: roads as sources and sinks.* Environmental Science & Technology, 1993. **27**(9): p. 1892-1904.

38. Zhang, J., et al., *Occurrence of benzothiazole and its derivates in tire wear, road dust, and roadside soil.* Chemosphere, 2018. **201**: p. 310-317.

39. Pierson, W.R. and W.W. Brachaczek, *Airborne Particulate Debris from Rubber Tires.* Rubber Chemistry and Technology, 1974. **47**(5): p. 1275-1299.

40. Kreider, M.L., et al., *Physical and chemical characterization of tire-related particles: Comparison of particles generated using different methodologies.* Science of The Total Environment, 2010. **408**(3): p. 652-659.

41. Gustafsson, M., et al., *Properties and toxicological effects of particles from the interaction between tyres, road pavement and winter traction material.* Science of The Total Environment, 2008. **393**(2â€“3): p. 226-240.

42. Mathissen, M., et al., *Investigation on the potential generation of ultrafine particles from the tire–road interface.* Atmospheric Environment, 2011. **45**(34): p. 6172-6179.

43. Cadle, S.H. and R.L. Williams, *Gas and Particle Emissions from Automobile Tires in Laboratory and Field Studies.* Journal of the Air Pollution Control Association, 1978. **28**(5): p. 502-507.

44. Gunawardana, C., et al., *Source characterisation of road dust based on chemical and mineralogical composition.* Chemosphere, 2012. **87**(2): p. 163-170.

45. Adachi, K. and Y. Tainosho, *Characterization of heavy metal particles embedded in tire dust.* Environment International, 2004. **30**(8): p. 1009-1017.

46. Harrison, R.M., et al., *Estimation of the Contributions of Brake Dust, Tire Wear, and Resuspension to Nonexhaust Traffic Particles Derived from Atmospheric Measurements.* Environmental Science & Technology, 2012. **46**(12): p. 6523-6529.

47. Amato, F., et al., *Sources and variability of inhalable road dust particles in three European cities.* Atmospheric Environment, 2011. **45**(37): p. 6777-6787.

48. Lawrence, S., et al., *Source apportionment of traffic emissions of particulate matter using tunnel measurements.* Atmospheric Environment, 2013. **77**: p. 548-557.

49. Fabretti, J.F., et al., *Elemental characterization and source identification of PM2.5 using Positive Matrix Factorization: The Malraux road tunnel, Nice, France.* Atmospheric Research, 2009. **94**(2): p. 320-329.

50. Mancilla, Y. and A. Mendoza, *A tunnel study to characterize PM2.5 emissions from gasoline-powered vehicles in Monterrey, Mexico.* Atmospheric Environment, 2012. **59**: p. 449-460.

51. Ondracek, J., et al., *Contribution of the road traffic to air pollution in the Prague city (busy speedway and suburban crossroads).* Atmospheric Environment, 2011. **45**(29): p. 5090-5100.

52. Song, F. and Y. Gao, *Size distributions of trace elements associated with ambient particular matter in the affinity of a major highway in the New Jersey-New York metropolitan area.* Atmospheric Environment, 2011. **45**(37): p. 6714-6723.

53. Panko, J.M., et al., *Measurement of airborne concentrations of tire and road wear particles in urban and rural areas of France, Japan, and the United States.* Atmospheric Environment, 2013. **72**: p. 192-199.

54. Shirmohammadi, F., et al., *Oxidative potential of on-road fine particulate matter (PM2.5) measured on major freeways of Los Angeles, CA, and a 10-year comparison with earlier roadside studies.* Atmospheric Environment, 2017. **148**: p. 102-114.

55. Bukowiecki, N., et al., *Real-World Emission Factors for Antimony and Other Brake Wear Related Trace Elements: Size-Segregated Values for Light and Heavy Duty Vehicles.* Environmental Science & Technology, 2009. **43**(21): p. 8072-8078.

56. Caltrans, *PeMs — Caltrans Performance Measurement System*. 2021, California Department of Transportation, State of California.

57. Jia, Z., et al. *The PeMS algorithms for accurate, real-time estimates of g-factors and speeds from single-loop detectors*. in *Intelligent Transportation Systems, 2001. Proceedings. 2001 IEEE*. 2001. IEEE.

58. Kwon, J., P. Varaiya, and A. Skabardonis, *Estimation of truck traffic volume from single loop detectors with lane-to-lane speed correlation.* Transportation Research Record: Journal of the Transportation Research Board, 2003(1856): p. 106-117.

59. Board, C.A.R., *Improving On-Road Vehicle Emission Estimates in Portside Environmental Justice Neighborhoods.* 2019.

60. Moosmüller, H., et al., *On-road measurement of automotive particle emissions by ultraviolet lidar and transmissometer: Instrument.* Environmental Science & Technology, 2003. **37**(21): p. 4971-4978.

61. Dreher, D.B. and R.A. Harley, *A fuel-based inventory for heavy-duty diesel truck emissions.* Journal of the Air & Waste Management Association, 1998. **48**(4): p. 352-358.

62. Bukowiecki, N., et al., *PM10 emission factors for non-exhaust particles generated by road traffic in an urban street canyon and along a freeway in Switzerland.* Atmospheric Environment, 2010. **44**(19): p. 2330-2340.

63. Keskinen, J., K. Pietarinen, and M. Lehtimäki, *Electrical low pressure impactor.* Journal of Aerosol Science, 1992. **23**(4): p. 353-360.

64. Lemmetty, M., J. Keskinen, and M. Marjamäki, *The ELPI response and data reduction II: Properties of kernels and data inversion.* Aerosol science and technology, 2005. **39**(7): p. 583-595.

65. Marjamäki, M., M. Lemmetty, and J. Keskinen, *ELPI response and data reduction I: Response functions.* Aerosol science and technology, 2005. **39**(7): p. 575-582.

66. Saari, S., et al., *Performance evaluation of the HR-ELPI+ inversion.* Aerosol Science and Technology, 2018. **52**(9): p. 1037-1047.

67. Moisio, M., *Real time size distribution measurement of combustion aerosols.* 1999.

68. Maricq, M.M., D.H. Podsiadlik, and R.E. Chase, *Size Distributions of Motor Vehicle Exhaust PM: A Comparison Between ELPI and SMPS Measurements.* Aerosol Science and Technology, 2000. **33**(3): p. 239-260.

69. Chen, M., et al., *A novel quartz crystal cascade impactor for real-time aerosol mass distribution measurement.* Aerosol Science and Technology, 2016. **50**(9): p. 971-983.

70. Asano, H., et al., *Highly Time-Resolved Atmospheric Observations Using a Continuous Fine Particulate Matter and Element Monitor.* ACS Earth and Space Chemistry, 2017. **1**(9): p. 580-590.

71. Li, Y., et al., *Monitoring and source apportionment of trace elements in PM2.5: Implications for local air quality management.* Journal of Environmental Management, 2017. **196**: p. 16-25.

72. Wang, X.L., et al., *Hong Kong Vehicle Emission Changes from 2003 to 2015 in the Shing Mun Tunnel.* Aerosol Science and Technology, 2018. **Online**.

73. Chow, J.C., et al., *A laboratory resuspension chamber to measure fugitive dust size distributions and chemical compositions.* Atmospheric Environment, 1994. **28**(21): p. 3463-3481.

74. Chow, J.C. and J.G. Watson, *Chemical analyses of particle filter deposits*, in *Aerosols Handbook : Measurement, Dosimetry, and Health Effects*, L. Ruzer and N.H. Harley, Editors. 2013, CRC Press/Taylor & Francis: New York, NY. p. 179-204.

75. Watson, J.G., et al., *Source apportionment: Principles and methods*, in *Airborne Particulate Matter: Sources, Atmospheric Processes and Health*, R.M. Harrison, Editor. 2016, Royal Society of Chemistry: London, UK. p. 72-125.

76. Watson, J.G., et al., *Filter processing and gravimetric analysis for suspended particulate matter samples.* Aerosol Science and Engineering, 2017. **1**(2): p. 193-205.

77. U.S. EPA, *QA Handbook for Air Pollution Measurement Systems - Volume II: Ambient Air Quality Monitoring Program*. 2017, U.S. Enviornmental Protection Agency, Office of Air Quality Planning and Standards, Air Quality Assessment Division: Research Triangle Park, NC.

78. U.S. EPA, *Appendix L to Part 50 - Reference method for the determination of fine particulate matter as $PM_{2.5}$ in the atmosphere.* Federal Register, 1997. **62**(138): p. 57-95.

79. Watson, J.G., J.C. Chow, and C.A. Frazier, *X-ray fluorescence analysis of ambient air samples*, in *Elemental Analysis of Airborne Particles, Vol. 1*, S. Landsberger and M. Creatchman, Editors. 1999, Gordon and Breach Science: Amsterdam, The Netherlands. p. 67-96.

80. Chow, J.C. and J.G. Watson, *Enhanced ion chromatographic speciation of water-soluble $PM_{2.5}$ to improve aerosol source apportionment.* Aerosol Science and Engineering, 2017. **1**: p. 7-24.

81. Chow, J.C., et al., *The DRI thermal/optical reflectance carbon analysis system: description, evaluation and applications in U.S. Air quality studies.* Atmospheric Environment. Part A. General Topics, 1993. **27**(8): p. 1185-1201.

82. Chow, J.C., et al., *The IMPROVE_A temperature protocol for thermal/optical carbon analysis: maintaining consistency with a long-term database.* Journal of the Air & Waste Management Association, 2007. **57**(9): p. 1014-1023.

83. Chen, L.-W.A., et al., *Multi-wavelength optical measurement to enhance thermal/optical analysis for carbonaceous aerosol.* Atmospheric Measurement Techniques, 2015. **8**: p. 451-461.

84. Ho, S.S.H., et al., *Evaluation of an in-injection port thermal desorption-gas chromatography/mass spectrometry method for analysis of non-polar organic compounds in ambient aerosol samples.* Journal of Chromatography A 2008. **1200**(2): p. 217-227.

85. Ho, S.S.H. and J.Z. Yu, *In-injection port thermal desorption and subsequent gas chromatography-mass spectrometric analysis of polycyclic aromatic hydrocarbons and n-alkanes in atmospheric aerosol samples.* Journal of Chromatography A 2004. **1059**(1-2): p. 121-129.

86. Ho, S.S.H., et al., *Precautions for in-injection port thermal desorption-gas chromatography/mass spectrometry (TD-GC/MS) as applied to aerosol filter samples.* Atmospheric Environment, 2011. **45**(7): p. 1491-1496.

87. Unice, K.M., M.L. Kreider, and J.M. Panko, *Use of a Deuterated Internal Standard with Pyrolysis-GC/MS Dimeric Marker Analysis to Quantify Tire Tread Particles in the Environment.* International Journal of Environmental Research and Public Health, 2012. **9**(11).

88. Panko, J., M. Kreider, and K. Unice, *Chapter 7 - Review of Tire Wear Emissions: A Review of Tire Emission Measurement Studies: Identification of Gaps and Future Needs*, in *Non-Exhaust Emissions*, F. Amato, Editor. 2018, Academic Press. p. 147-160.

89. Chow, J.C., et al., *Evaluation of filter-based aerosol measurements during the 1987 Southern California Air Quality Study.* Environ. Mon. Assess, 1994. **30**(1): p. 49-80.

90. U.S. EPA, *Quality Assurance Guidance Document - Quality Assurance Project Plan: $PM_{2.5}$ Chemical Speciation Sampling at Trends, NCore, Supplemental and Tribal Sites*. 2012, Ambient Air Monitoring Group, Air Quality Assessment Division, US EPA, Office of Air Quality Planning and Standards: Research Triangle Park, North Carolina.

91. Chow, J.C., et al., *Mass reconstruction methods for $PM_{2.5}$: a review.* Air Quality, Atmosphere & Health, 2015. **8**(3): p. 243-263.

92. Chow, J.C., et al., *Quantification of $PM_{2.5}$ organic carbon sampling artifacts in US networks.* Atmospheric Chemistry and Physics, 2010. **10**(12): p. 5223-5239.

93. Kleeman, M.J., J.J. Schauer, and G.R. Cass, *Size and composition distribution of fine particulate matter emitted from motor vehicles.* Environmental Science & Technology, 2000. **34**(7): p. 1132-1142.

94. Malm, W., et al., *Spatial and seasonal trends in particle concentration and optical extinction in the United States.* Journal of Geophysical research, 1994. **99**(D1): p. 1347-1370.

95. Hennigan, C.J., et al., *A critical evaluation of proxy methods used to estimate the acidity of atmospheric particles.* Atmos. Chem. Phys., 2015. **15**(5): p. 2775-2790.

96. Stelson, A.W. and J.H. Seinfeld, *Relative humidity and temperature dependence of the ammonium nitrate dissociation constant.* Atmospheric Environment (1967), 1982. **16**(5): p. 983-992.

97. Marple, V.A., K.L. Rubow, and S.M. Behm, *A Microorifice Uniform Deposit Impactor (Moudi) - Description, Calibration, and Use.* Aerosol Science and Technology, 1991. **14**(4): p. 434-446.

98. Ravindra, K., R. Sokhi, and R. Van Grieken, *Atmospheric polycyclic aromatic hydrocarbons: Source attribution, emission factors and regulation.* Atmospheric Environment, 2008. **42**(13): p. 2895-2921.

99. Fujita, E.M., et al., *Evaluations of the Chemical Mass Balance Method for Determining Contributions of Gasoline and Diesel Exhaust to Ambient Carbonaceous Aerosols*, in *Journal of the Air & Waste Management Association*. 2007, Taylor & Francis. p. 721-740.

100. Rogge, W.F., et al., *Sources of fine organic aerosol. 2. Noncatalyst and catalyst-equipped automobiles and heavy-duty diesel trucks.* Environmental Science & Technology, 1993. **27**(4): p. 636-651.

101. Chien, Y.-C., et al., *Assessment of occupational health hazards in scrap-tire shredding facilities.* Science of The Total Environment, 2003. **309**(1): p. 35-46.

102. Bu, Z., et al., *Phthalates in Chinese vehicular environments: Source emissions, concentrations, and human exposure.* Indoor Air, 2021. **n/a**(n/a).

103. Miao, Y., et al., *Lifetime cancer risk assessment for inhalation exposure to di(2-ethylhexyl) phthalate (DEHP).* Environmental Science and Pollution Research, 2017. **24**(1): p. 312-320.

104. Watson, J.G., J.A. Cooper, and J.J. Huntzicker, *The effective variance weighting for least squares calculations applied to the mass balance receptor model.* Atmospheric Environment (1967), 1984. **18**(7): p. 1347-1355.

105. Watson, J.G., *Protocol for Applying and Validating the CMB Model for PM2.5 and VOC*. 2004, U.S. Environmental Protection Agency: Research Triangle Park, NC.

106. Chen, L.-W.A., et al., *Wintertime particulate pollution episodes in an urban valley of the Western US: a case study.* Atmospheric Chemistry and Physics, 2012. **12**(21): p. 10051-10064.

107. Chen, L.-W.A., et al., *Chemical mass balance source apportionment for combined PM2.5 measurements from U.S. non-urban and urban long-term networks☆.* Atmospheric Environment, 2010. **44**(38): p. 4908-4918.

108. Fitz, D.C., Judith C.; Zielinka, Babara, *Development of a Gas and Particulate Matter Organic Speciation Profile Database*. 2004, California Air Resources Board: Sacramento, CA.

109. Ondráček, J., et al., *Contribution of the road traffic to air pollution in the Prague city (busy speedway and suburban crossroads).* Atmospheric Environment, 2011. **45**(29): p. 5090-5100.

110. Harrison, R.M., et al., *Estimation of the Contributions of Brake Dust, Tire Wear, and Resuspension to Nonexhaust Traffic Particles Derived from Atmospheric Measurements.* Environmental Science & Technology, 2012. **46**(12): p. 6523-6529.

111. Fujita, E.M., et al., *Evaluations of the Chemical Mass Balance Method for Determining Contributions of Gasoline and Diesel Exhaust to Ambient Carbonaceous Aerosols.* Journal of the Air & Waste Management Association, 2007. **57**(6): p. 721-740.

112. Fujita, E.M., et al., *Variations in Speciated Emissions from Spark-Ignition and Compression-Ignition Motor Vehicles in California's South Coast Air Basin.* Journal of the Air & Waste Management Association, 2007. **57**(6): p. 705-720.

113. Watson, J.G., et al., *Chemical Mass Balance Source Apportionment of PM10during the Southern California Air Quality Study.* Aerosol Science and Technology, 1994. **21**(1): p. 1-36.

114. Hasheminassab, S., et al., *Long-term source apportionment of ambient fine particulate matter (PM 2.5) in the Los Angeles Basin: A focus on emissions reduction from vehicular sources.* Environmental Pollution, 2014. **193**: p. 54-64.

115. Seinfeld, J. and S. Pandis, *Atmospheric Chemistry and Physics. 1997.* New York, 2008.

116. Harrison, R.M., A.M. Jones, and R. Barrowcliffe, *Field study of the influence of meteorological factors and traffic volumes upon suspended particle mass at urban roadside sites of differing geometries.* Atmospheric Environment, 2004. **38**(37): p. 6361-6369.

117. Wang, J.M., et al., *Near-road air pollutant measurements: accounting for inter-site variability using emission factors.* Environmental science & technology, 2018. **52**(16): p. 9495-9504.

Appendix A: Chemical Mass Balance Source Profiles

PNO	Mnemonic	SIZE	K+	K+U	NO3-	NO3-U	OC1	OC1U	OC2	OC2U	OC3	OC3U	OC4	OC4U	EC1	EC1U	EC2	EC2U	EC3	EC3U	POC	POCU	OC	OCU	EC
20013	Brake_1	PM2.5	0.00033	0.00005	0.00000	0.00046	0.05398	0.00478	0.02276	0.00287	0.06414	0.00600	0.02512	0.00361	0.00938	0.00338	0.01445	0.00207	0.00869	0.00265	0.00006	0.00067	0.16607	0.01139	0.03246
20014	Brake_2	PM2.5	0.00027	0.00003	0.00062	0.00019	0.01963	0.00174	0.02509	0.00307	0.07567	0.00657	0.02036	0.00285	0.01171	0.00090	0.01697	0.00233	0.01302	0.00396	0.00005	0.00027	0.14080	0.00978	0.04166
20015	Brake_3	PM2.5	0.00314	0.00023	0.00110	0.00016	0.01773	0.00157	0.01540	0.00189	0.06072	0.00527	0.06211	0.00863	0.07991	0.00597	0.02827	0.00386	0.00564	0.00171	0.00000	0.00021	0.15596	0.01220	0.11382
20016	Brake_C	PM2.5	0.00125	0.00164	0.00057	0.00055	0.03045	0.02041	0.02108	0.00506	0.06684	0.00783	0.03587	0.02285	0.03366	0.04007	0.01990	0.00736	0.00912	0.00371	0.00004	0.00043	0.15427	0.01272	0.06264
ARB1	Brake_D	PM10																							
ARB2	Brake_E	PM10																							
ARB3	Brake_F	PM10																							
ARB4	Brake_G	PM10																							
20017	Tire_1	PM2.5	0.00271	0.00027	0.01643	0.00212	0.12925	0.01181	0.08657	0.01105	0.20442	0.02013	0.07980	0.01173	0.06504	0.02329	0.04330	0.00643	0.01378	0.00427	0.00034	0.00252	0.50038	0.03659	0.12177
20018	Tire_2	PM2.5	0.00366	0.00049	0.02234	0.00425	0.14834	0.01527	0.22169	0.02970	0.61421	0.06371	0.14819	0.02308	0.12465	0.04507	0.14962	0.02228	0.00000	0.00173	0.00030	0.00557	1.13274	0.09850	0.27397
25346	WS-L	PM2.5	0.00110	0.00073	0.03212	0.01702	0.19522	0.19406	0.16631	0.03654	0.23437	0.09011	0.11142	0.03673	0.14665	0.06558	0.18015	0.16097	0.00792	0.00494	0.00853	0.00849	0.71584	0.26229	0.32621
25347	CS-L	PM2.5	0.00098	0.00063	0.01857	0.01172	0.15857	0.14201	0.16649	0.03150	0.16480	0.04900	0.08066	0.01817	0.15386	0.03912	0.11874	0.08489	0.00551	0.00303	0.00219	0.00266	0.57270	0.13559	0.27590
25348	WS-H	PM2.5	0.00098	0.00131	0.00759	0.00929	0.48691	0.27152	0.12247	0.06331	0.13346	0.08451	0.06879	0.03980	0.07915	0.05612	0.11183	0.11882	0.00561	0.00429	0.02787	0.05211	0.83949	0.32462	0.16867
25349	CS-H	PM2.5	0.00038	0.00035	0.00485	0.00405	0.40785	0.22825	0.13453	0.07484	0.08876	0.02678	0.05879	0.02050	0.08976	0.05237	0.06491	0.05147	0.00397	0.00305	0.01081	0.01710	0.70074	0.21502	0.14784
25350	WS-BC	PM2.5	0.00036	0.00009	0.02207	0.01611	0.07793	0.08474	0.08486	0.04795	0.11353	0.03081	0.07871	0.03388	0.20774	0.08889	0.18095	0.17329	0.00334	0.00339	0.00205	0.00488	0.35709	0.18291	0.38997
25351	CS-BC	PM2.5	0.00040	0.00020	0.01407	0.00955	0.13575	0.08841	0.07380	0.02629	0.06317	0.01312	0.04134	0.00667	0.15490	0.05497	0.27477	0.14642	0.00209	0.00146	0.02639	0.02864	0.34045	0.08704	0.40532
25352	MDD-MIX	PM2.5	0.00185	0.00078	0.00362	0.00705	0.25566	0.09574	0.21996	0.10517	0.26885	0.11163	0.17548	0.09093	0.23664	0.07531	0.51141	0.07351	0.00835	0.00634	0.00062	0.00176	0.92056	0.39516	0.75573
25353	HHDD-HW	PM2.5	0.00154	0.00015	0.00119	0.00238	0.21570	0.09525	0.11314	0.03852	0.19881	0.06746	0.08482	0.03434	0.28968	0.06091	0.48064	0.19344	0.00457	0.00304	0.00022	0.00148	0.61268	0.23565	0.77466
25354	HHDD-HCS	PM2.5	0.00136	0.00058	0.00000	0.00080	0.16895	0.01907	0.08068	0.00891	0.12333	0.02153	0.05370	0.00660	0.24723	0.05227	0.56250	0.05625	0.00023	0.00038	0.00022	0.00121	0.42687	0.05128	0.80989
25355	HHDD-MIX	PM2.5	0.00145	0.00040	0.00059	0.00168	0.19233	0.06782	0.09691	0.03116	0.16107	0.06146	0.06926	0.02830	0.26846	0.04750	0.52157	0.13573	0.00240	0.00306	0.00022	0.00095	0.51978	0.18652	0.79228
25356	DIESEL	PM2.5	0.00155	0.00053	0.00135	0.00383	0.20816	0.07616	0.12767	0.06294	0.18801	0.07289	0.09581	0.05461	0.26050	0.05994	0.51903	0.12689	0.00389	0.00384	0.00032	0.00138	0.61997	0.21715	0.78314
25357	GAS	PM2.5	0.00070	0.00068	0.01655	0.01211	0.24370	0.18195	0.12474	0.04988	0.13301	0.06082	0.07328	0.02851	0.13868	0.06143	0.15522	0.12997	0.00474	0.00353	0.01297	0.02560	0.58772	0.20124	0.28565
Copper1	COTIRE1	TSP					0.00007	0.00000	0.04876	0.00001	0.42867	0.00002	0.02743	0.00001	0.05600	0.00001	0.18831	0.00002	0.00067	0.00000	0.00916	0.00001	0.51409	0.00003	0.23582
Copper2	COTIRE2	TSP					0.00008	0.00000	0.04647	0.00001	0.35330	0.00002	0.01278	0.00002	0.06665	0.00001	0.12773	0.00003	0.00000	0.00000	0.18948	0.00001	0.60211	0.00004	0.19438
Michelin1	MITIRE1	TSP	0.00002	0.00001	0.00025	0.00009	0.00000	0.00000	0.07890	0.00001	0.49254	0.00002	0.03634	0.00002	0.10956	0.00001	0.29825	0.00003	0.00000	0.00000	0.00000	0.00002	0.60779	0.00004	0.40782
Michelin2	MITIRE2	TSP	0.00002	0.00001	0.00019	0.00007	0.00004	0.00000	0.07881	0.00001	0.47160	0.00003	0.01553	0.00002	0.11335	0.00001	0.26122	0.00003	0.00000	0.00000	0.00000	0.00002	0.56598	0.00004	0.37457
Copper	COTIRE	TSP					0.00008	0.00000	0.04762	0.00162	0.39099	0.05329	0.02010	0.01036	0.06133	0.00754	0.15802	0.04284	0.00033	0.00047	0.09932	0.12751	0.55810	0.06224	0.21510
Michelin	MITIRE	TSP	0.00002	0.00001	0.00022	0.00008	0.00002	0.00002	0.07886	0.00007	0.48207	0.01480	0.02593	0.01471	0.11145	0.00267	0.27974	0.02619	0.00000	0.00000	0.00000	0.00002	0.58688	0.02956	0.39119
MiCo	TIRE	TSP					0.00005	0.00004	0.06324	0.01806	0.43653	0.06153	0.02302	0.01092	0.08639	0.02931	0.21888	0.07602	0.00017	0.00033	0.04966	0.09331	0.57249	0.04311	0.30315
RESQ2485	AQ Dust	PM2.5	0.00198	0.00017	0.00295	0.00033	0.00608	0.00046	0.02961	0.00230	0.09156	0.01155	0.06946	0.01171	0.01860	0.01174	0.02062	0.00898	0.00000	0.00002	0.00755	0.00062	0.20425	0.01536	0.03168
RESQ2489	MA Dust	PM2.5	0.00103	0.00012	0.00283	0.00055	0.00932	0.00083	0.02811	0.00255	0.11300	0.01519	0.03743	0.00657	0.04906	0.03105	0.03838	0.01682	0.00000	0.00005	0.01269	0.00126	0.20056	0.01772	0.07475
RESQ2493	CC Dust	PM2.5	0.00088	0.00008	0.00165	0.00028	0.00570	0.00043	0.01209	0.00096	0.06238	0.00792	0.03033	0.00514	0.01662	0.01049	0.01413	0.00617	0.00000	0.00003	0.00151	0.00032	0.11201	0.00856	0.02923
RESQ2497	AT Dust	PM2.5	0.00044	0.00006	0.00179	0.00036	0.00044	0.00011	0.00981	0.00083	0.06726	0.00869	0.03141	0.00538	0.02540	0.01605	0.02077	0.00908	0.00000	0.00004	0.00000	0.00041	0.10892	0.00874	0.04618
RESQ2520	Dust	PM2.5	0.00108	0.00065	0.00231	0.00068	0.00539	0.00367	0.01990	0.01040	0.08355	0.02342	0.04216	0.01847	0.02742	0.01917	0.02348	0.01100	0.00000	0.00004	0.00544	0.00583	0.15644	0.05312	0.04546
RESQ2540	MCDust	PM2.5	0.00095	0.00011	0.00224	0.00083	0.00751	0.00256	0.02010	0.01133	0.08769	0.03579	0.03388	0.00590	0.03284	0.02318	0.02625	0.01715	0.00000	0.00004	0.00710	0.00791	0.15628	0.06262	0.05199
RESQ2560	AADust	PM2.5	0.00121	0.00110	0.00237	0.00082	0.00326	0.00398	0.01971	0.01401	0.07941	0.01718	0.05043	0.02691	0.02200	0.01406	0.02070	0.00903	0.00000	0.00003	0.00377	0.00534	0.15659	0.06741	0.03893
RESQ2487	AQDust	PM10	0.00217	0.00018	0.00281	0.00031	0.00270	0.00021	0.02627	0.00200	0.08212	0.01030	0.04713	0.00792	0.02320	0.01464	0.00809	0.00354	0.00000	0.00002	0.01302	0.00098	0.17124	0.01264	0.01827
RESQ2491	MADust	PM10	0.00102	0.00011	0.00162	0.00044	0.00488	0.00041	0.01081	0.00094	0.04587	0.00602	0.02364	0.00409	0.01531	0.00968	0.01327	0.00587	0.00000	0.00005	0.02166	0.00182	0.10686	0.00881	0.00691
RESQ2495	CCDust	PM10	0.00110	0.00010	0.00094	0.00025	0.00135	0.00013	0.01322	0.00103	0.07830	0.00987	0.05167	0.00871	0.02279	0.01439	0.01059	0.00464	0.00000	0.00003	0.01340	0.00103	0.15793	0.01185	0.01999
RESQ2499	ATDust	PM10	0.00034	0.00005	0.00268	0.00035	0.00312	0.00025	0.01461	0.00115	0.08350	0.01056	0.04929	0.00832	0.02875	0.01815	0.03423	0.01490	0.00000	0.00003	0.02258	0.00172	0.17311	0.01309	0.04040
RESQ2510	Dust	PM10	0.00116	0.00076	0.00201	0.00089	0.00302	0.00145	0.01623	0.00688	0.07245	0.01785	0.04293	0.01299	0.02251	0.01453	0.01654	0.01198	0.00000	0.00003	0.01766	0.00516	0.15229	0.03103	0.02139
RESQ2530	MCDust	PM10	0.00106	0.00010	0.00128	0.00048	0.00312	0.00249	0.01201	0.00170	0.06208	0.02293	0.03765	0.01982	0.01905	0.01226	0.01193	0.00529	0.00000	0.00004	0.01753	0.00584	0.13239	0.03611	0.01345
RESQ2550	AADust	PM10	0.00126	0.00130	0.00275	0.00033	0.00291	0.00030	0.02044	0.00824	0.08281	0.01043	0.04821	0.00812	0.02598	0.01649	0.02116	0.01848	0.00000	0.00003	0.01780	0.00676	0.17218	0.01287	0.02933

PNO	Mnemonic	SIZE	ECU	Al	AlU	Si	SiU	S	SU	Cl	ClU	K	KU	Ca	CaU	Ti	TiU	V	VU	Mn	MnU	Fe	FeU	Co	CoU
20013	Brake_1	PM2.5	0.00499	0.00050	0.00010	0.00432	0.00033	0.00761	0.00055	0.00020	0.00021	0.00041	0.00005	0.00140	0.00012	0.00012	0.00402	0.00000	0.00170	0.00467	0.00045	0.65766	0.04666	0.00000	0.00973
20014	Brake_2	PM2.5	0.00498	0.00060	0.00007	0.00434	0.00032	0.00539	0.00039	0.00032	0.00005	0.00052	0.00005	0.00129	0.00010	0.00001	0.00340	0.00000	0.00144	0.00579	0.00049	0.59290	0.04195	0.00064	0.00877
20015	Brake_3	PM2.5	0.00823	0.00667	0.00049	0.01937	0.00138	0.02352	0.00167	0.00000	0.00052	0.00455	0.00034	0.03420	0.00242	0.00000	0.01556	0.00000	0.00614	0.00181	0.00020	0.19954	0.01412	0.00018	0.00295
20016	Brake_C	PM2.5	0.04456	0.00259	0.00354	0.00934	0.00868	0.01217	0.00989	0.00017	0.00033	0.00182	0.00236	0.01230	0.01897	0.00004	0.00948	0.00117	0.00377	0.00409	0.00205	0.48337	0.24792	0.00027	0.00775
ARB1	Brake_D	PM10		0.00000	0.00734	0.01127	0.00238	0.02326	0.00980			0.01369	0.00463	0.00936	0.00445	0.04820	0.02245	0.00000	0.00009	0.00744	0.00997	0.15062	0.02798	0.00026	0.00023
ARB2	Brake_E	PM10		0.00749	0.00734	0.01106	0.00425	0.02786	0.00664			0.00912	0.00942	0.01328	0.00613	0.04121	0.03952	0.00020	0.00019	0.00187	0.00012	0.20914	0.01997	0.00023	0.00020
ARB3	Brake_F	PM10		0.00000	0.00734	0.00942	0.00807	0.02263	0.01048			0.01290	0.00178	0.02218	0.02766	0.06098	0.00324	0.00000	0.00100	0.00077	0.00009	0.11414	0.01052	0.00022	0.00002
ARB4	Brake_G	PM10		0.00000	0.00734	0.00521	0.00006	0.00330	0.00003			0.00000	0.00100	0.00000	0.00100	0.00078	0.00001	0.00011	0.00015	0.00422	0.00075	0.46595	0.02513	0.00138	0.00020
20017	Tire_1	PM2.5	0.02517	0.02721	0.00212	0.02993	0.00232	0.01907	0.00144	0.00133	0.00027	0.00557	0.00046	0.01600	0.00122	0.00206	0.00059	0.00000	0.00072	0.00106	0.00013	0.18321	0.01355	0.00000	0.00273
20018	Tire_2	PM2.5	0.05237	0.02380	0.00226	0.02904	0.00270	0.01939	0.00172	0.00063	0.00120	0.00632	0.00073	0.01745	0.00159	0.00241	0.00396	0.00002	0.00162	0.00090	0.00018	0.22076	0.01898	0.00031	0.00331
25346	WS-L	PM2.5	0.18850	0.00183	0.00059	0.04276	0.01121	0.04319	0.03678	0.00297	0.00317	0.00106	0.00069	0.00765	0.00403	0.00005	0.00076	0.00000	0.00500	0.00010	0.00006	0.00681	0.00433	0.00000	0.01000
25347	CS-L	PM2.5	0.12170	0.00162	0.00081	0.03697	0.00980	0.03833	0.02871	0.00467	0.00550	0.00096	0.00072	0.00736	0.00397	0.00005	0.00038	0.00000	0.00500	0.00004	0.00003	0.00630	0.00551	0.00000	0.01000
25348	WS-H	PM2.5	0.12452	0.00094	0.00124	0.05087	0.07358	0.00926	0.00929	0.00061	0.00042	0.00034	0.00036	0.00742	0.00553	0.00002	0.00078	0.00000	0.00500	0.00003	0.00005	0.00307	0.00265	0.00000	0.01000
25349	CS-H	PM2.5	0.07321	0.00049	0.00026	0.03556	0.04536	0.01403	0.02035	0.00183	0.00283	0.00042	0.00043	0.00583	0.00384	0.00002	0.00036	0.00000	0.00500	0.00003	0.00003	0.00290	0.00289	0.00000	0.01000
25350	WS-BC	PM2.5	0.15073	0.00082	0.00073	0.07576	0.04460	0.02037	0.01381	0.00126	0.00033	0.00042	0.00017	0.01625	0.03319	0.00000	0.00064	0.00000	0.00500	0.00002	0.00004	0.00435	0.00237	0.00000	0.01000
25351	CS-BC	PM2.5	0.14315	0.00074	0.00031	0.04534	0.02149	0.03484	0.02859	0.00361	0.00215	0.00028	0.00015	0.00270	0.00130	0.00005	0.00028	0.00000	0.00500	0.00003	0.00002	0.00193	0.00056	0.00000	0.01000
25352	MDD-MIX	PM2.5	0.08315	0.00265	0.00302	0.01202	0.00696	0.03274	0.02017	0.00151	0.00060	0.00142	0.00161	0.00764	0.00491	0.00016	0.00127	0.00000	0.00500	0.00000	0.00009	0.00646	0.00574	0.00000	0.01000
25353	HHDD-HW	PM2.5	0.25732	0.00140	0.00122	0.01198	0.00120	0.01011	0.00483	0.00027	0.00025	0.00084	0.00069	0.00737	0.00219	0.00021	0.00090	0.00000	0.00500	0.00003	0.00006	0.00454	0.00064	0.00000	0.01000
25354	HHDD-HCS	PM2.5	0.08099	0.00141	0.00062	0.01209	0.00136	0.00765	0.00165	0.00078	0.00038	0.00114	0.00012	0.00632	0.00063	0.00009	0.00076	0.00000	0.00500	0.00001	0.00006	0.00868	0.00449	0.00000	0.01000
25355	HHDD-MIX	PM2.5	0.17285	0.00140	0.00089	0.01203	0.00120	0.00888	0.00359	0.00052	0.00039	0.00099	0.00049	0.00685	0.00158	0.00015	0.00059	0.00000	0.00500	0.00002	0.00004	0.00661	0.00370	0.00000	0.01000
25356	DIESEL	PM2.5	0.14858	0.00172	0.00171	0.01203	0.00365	0.01484	0.01197	0.00077	0.00053	0.00110	0.00091	0.00705	0.00282	0.00015	0.00091	0.00000	0.00500	0.00001	0.00007	0.00657	0.00410	0.00000	0.01000
25357	GAS	PM2.5	0.13364	0.00107	0.00074	0.04788	0.04112	0.02667	0.02478	0.00249	0.00298	0.00058	0.00047	0.00787	0.01403	0.00003	0.00057	0.00000	0.00500	0.00004	0.00004	0.00423	0.00342	0.00000	0.01000
Copper1	COTIRE1	TSP	0.00002	0.00171	0.00012	0.06113	0.00177	0.00000	0.01000	0.00000	0.00100	0.00038	0.00007	0.00111	0.00015	0.00010	0.00001	0.00000	0.00000	0.00002	0.00000	0.00122	0.00003	0.00000	0.00000
Copper2	COTIRE2	TSP	0.00003	0.00177	0.00012	0.06016	0.00174	0.00000	0.01000	0.00000	0.00100	0.00043	0.00008	0.00122	0.00016	0.00011	0.00001	0.00000	0.00000	0.00001	0.00000	0.00118	0.00003	0.00000	0.00000
Michelin1	MITIRE1	TSP	0.00003	0.00044	0.00004	0.00590	0.00019	0.00000	0.01000	0.00000	0.00100	0.00034	0.00006	0.00070	0.00013	0.00006	0.00000	0.00000	0.00000	0.00001	0.00000	0.00206	0.00005	0.00000	0.00000
Michelin2	MITIRE2	TSP	0.00003	0.00045	0.00004	0.00615	0.00020	0.00000	0.01000	0.00000	0.00100	0.00042	0.00007	0.00077	0.00013	0.00006	0.00000	0.00000	0.00000	0.00001	0.00000	0.00208	0.00005	0.00000	0.00000
Copper	COTIRE	TSP	0.02930	0.00174	0.00012	0.06065	0.00175	0.00000	0.01000	0.00000	0.00100	0.00040	0.00007	0.00116	0.00016	0.00010	0.00001	0.00000	0.00000	0.00001	0.00000	0.00120	0.00003	0.00000	0.00000
Michelin	MITIRE	TSP	0.02351	0.00044	0.00004	0.00603	0.00019	0.00000	0.01000	0.00000	0.00100	0.00038	0.00007	0.00074	0.00013	0.00006	0.00000	0.00000	0.00000	0.00001	0.00000	0.00207	0.00005	0.00000	0.00000
MiCo	TIRE	TSP	0.10396	0.00109	0.00075	0.03334	0.03154	0.00000	0.01000	0.00000	0.00100	0.00039	0.00007	0.00095	0.00025	0.00008	0.00003	0.00000	0.00000	0.00001	0.00000	0.00164	0.00050	0.00000	0.00000
RESQ2485	AQ Dust	PM2.5	0.00247	0.01441	0.00196	0.05643	0.00419	0.00125	0.00010	0.00045	0.00005	0.00481	0.00036	0.02861	0.00213	0.00238	0.00018	0.00000	0.00000	0.00050	0.00007	0.02176	0.00163	0.00014	0.00002
RESQ2489	MA Dust	PM2.5	0.00676	0.01197	0.00384	0.04723	0.00413	0.00134	0.00014	0.00022	0.00008	0.00419	0.00037	0.00940	0.00086	0.00129	0.00013	0.00007	0.00001	0.00026	0.00014	0.01642	0.00150	0.00013	0.00004
RESQ2493	CC Dust	PM2.5	0.00234	0.02285	0.00254	0.07361	0.00554	0.00427	0.00032	0.00073	0.00007	0.00864	0.00065	0.02706	0.00204	0.00244	0.00019	0.00001	0.00000	0.00034	0.00007	0.02353	0.00178	0.00014	0.00002
RESQ2497	AT Dust	PM2.5	0.00381	0.01889	0.00293	0.05270	0.00416	0.00286	0.00023	0.00024	0.00005	0.00563	0.00045	0.00843	0.00069	0.00279	0.00022	0.00000	0.00000	0.00034	0.00010	0.02324	0.00186	0.00008	0.00003
RESQ2520	Dust	PM2.5	0.02091	0.01703	0.00483	0.05749	0.01139	0.00243	0.00143	0.00041	0.00024	0.00582	0.00197	0.01837	0.01095	0.00223	0.00065	0.00002	0.00003	0.00036	0.00010	0.02124	0.00330	0.00012	0.00003
RESQ2540	MCDust	PM2.5	0.03218	0.01741	0.00770	0.06042	0.01865	0.00280	0.00207	0.00047	0.00036	0.00642	0.00315	0.01823	0.01249	0.00187	0.00081	0.00004	0.00004	0.00030	0.00011	0.01997	0.00503	0.00013	0.00004
RESQ2560	AADust	PM2.5	0.01026	0.01665	0.00317	0.05456	0.00417	0.00206	0.00113	0.00034	0.00015	0.00522	0.00058	0.01852	0.01427	0.00258	0.00029	0.00000	0.00000	0.00042	0.00011	0.02250	0.00174	0.00011	0.00004
RESQ2487	AQDust	PM10	0.00145	0.02658	0.00232	0.08825	0.00643	0.00248	0.00018	0.00077	0.00006	0.00790	0.00058	0.05478	0.00399	0.00341	0.00025	0.00003	0.00000	0.00086	0.00008	0.03848	0.00281	0.00017	0.00002
RESQ2491	MADust	PM10	0.00122	0.02595	0.00350	0.09186	0.00740	0.00294	0.00024	0.00044	0.00007	0.00852	0.00069	0.02262	0.00184	0.00410	0.00033	0.00000	0.00001	0.00069	0.00012	0.03469	0.00282	0.00011	0.00003
RESQ2495	CCDust	PM10	0.00163	0.04383	0.00363	0.13467	0.00996	0.00775	0.00058	0.00122	0.00010	0.01555	0.00115	0.04851	0.00359	0.00412	0.00031	0.00000	0.00000	0.00087	0.00009	0.04148	0.00307	0.00023	0.00003
RESQ2499	ATDust	PM10	0.00316	0.04575	0.00385	0.12319	0.00919	0.00646	0.00048	0.00043	0.00005	0.01346	0.00100	0.01659	0.00125	0.00479	0.00036	0.00012	0.00001	0.00083	0.00009	0.05022	0.00375	0.00022	0.00003
RESQ2510	Dust	PM10	0.01393	0.03553	0.01072	0.10949	0.02298	0.00491	0.00260	0.00071	0.00038	0.01136	0.00374	0.03562	0.01883	0.00410	0.00056	0.00004	0.00005	0.00081	0.00009	0.04122	0.00661	0.00018	0.00005
RESQ2530	MCDust	PM10	0.00924	0.03489	0.01264	0.11327	0.03028	0.00535	0.00340	0.00083	0.00056	0.01204	0.00497	0.03557	0.01830	0.00411	0.00032	0.00000	0.00000	0.00078	0.00012	0.03809	0.00480	0.00017	0.00009
RESQ2550	AADust	PM10	0.01565	0.03617	0.01355	0.10572	0.02471	0.00447	0.00281	0.00060	0.00024	0.01068	0.00393	0.03568	0.02700	0.00410	0.00097	0.00007	0.00006	0.00085	0.00008	0.04435	0.00831	0.00019	0.00003

PNO	Mnemonic	SIZE	Ni	NiU	Cu	CuU	Zn	ZnU	As	AsU	Se	SeU	Br	BrU	Rb	RbU	Sr	SrU	Sb	SbU	Ba	BaU	Pb	PbU	FLUORA
20013	Brake_1	PM2.5	0.00000	0.00021	0.00078	0.00006	0.00017	0.00002	0.00000	0.00009	0.00000	0.00002	0.00000	0.00003	0.00007	0.00001	0.00182	0.00013	0.00010	0.00041	0.03393	0.00249	0.00047	0.00004	0.00001
20014	Brake_2	PM2.5	0.00000	0.00019	0.00049	0.00004	0.00019	0.00001	0.00000	0.00014	0.00001	0.00000	0.00001	0.00002	0.00015	0.00001	0.00088	0.00006	0.00000	0.00022	0.02897	0.00208	0.00091	0.00007	0.00001
20015	Brake_3	PM2.5	0.00000	0.00007	0.00042	0.00003	0.01389	0.00098	0.00000	0.00003	0.00002	0.00000	0.00001	0.00002	0.00007	0.00001	0.00202	0.00014	0.00004	0.00017	0.13481	0.00955	0.00016	0.00002	0.00001
20016	Brake_C	PM2.5	0.00000	0.00017	0.00057	0.00019	0.00475	0.00792	0.00000	0.00010	0.00001	0.00001	0.00000	0.00002	0.00010	0.00004	0.00157	0.00060	0.00005	0.00029	0.06590	0.05973	0.00051	0.00038	0.00001
ARB1	Brake_D	PM10	0.00014	0.00015	0.04888	0.05071	0.00000	0.00100																	
ARB2	Brake_E	PM10	0.00005	0.00004	0.00060	0.00025	0.00293	0.00472																	
ARB3	Brake_F	PM10	0.00012	0.00005	0.01717	0.01402	0.00000	0.00100																	
ARB4	Brake_G	PM10	0.00004	0.00005	0.00035	0.00003	0.00000	0.00100																	
20017	Tire_1	PM2.5	0.00000	0.00011	0.01034	0.00077	0.03363	0.00249	0.00000	0.00016	0.00000	0.00008	0.00015	0.00003	0.00001	0.00007	0.01075	0.00080	0.00090	0.00122	0.00000	0.00430	0.00026	0.00008	0.00019
20018	Tire_2	PM2.5	0.00000	0.00018	0.01889	0.00163	0.01829	0.00158	0.00000	0.00036	0.00000	0.00019	0.00023	0.00008	0.00000	0.00016	0.01511	0.00131	0.00000	0.00279	0.00000	0.01005	0.00031	0.00055	0.00037
25346	WS-L	PM2.5	0.00019	0.00008	0.00053	0.00018	0.00432	0.00212	0.00000	0.00007	0.00000	0.00004	0.00064	0.00048	0.00003	0.00003	0.00002	0.00003	0.00000	0.01000	0.00362	0.00346	0.00039	0.00029	0.00353
25347	CS-L	PM2.5	0.00017	0.00012	0.00054	0.00029	0.00475	0.00278	0.00000	0.00003	0.00001	0.00002	0.00076	0.00066	0.00000	0.00002	0.00001	0.00002	0.00000	0.01000	0.00151	0.00130	0.00030	0.00027	0.00180
25348	WS-H	PM2.5	0.00004	0.00003	0.00063	0.00094	0.00462	0.00343	0.00001	0.00007	0.00000	0.00004	0.00005	0.00008	0.00000	0.00003	0.00001	0.00003	0.00000	0.01000	0.00263	0.00471	0.00035	0.00036	0.00531
25349	CS-H	PM2.5	0.00003	0.00002	0.00052	0.00059	0.00434	0.00367	0.00000	0.00003	0.00000	0.00002	0.00010	0.00016	0.00000	0.00001	0.00001	0.00002	0.00000	0.01000	0.00047	0.00091	0.00025	0.00024	0.00116
25350	WS-BC	PM2.5	0.00005	0.00003	0.00065	0.00059	0.00522	0.00704	0.00000	0.00006	0.00000	0.00003	0.00024	0.00018	0.00000	0.00003	0.00001	0.00003	0.00000	0.01000	0.00240	0.00187	0.00013	0.00009	0.00212
25351	CS-BC	PM2.5	0.00004	0.00002	0.00026	0.00014	0.00276	0.00341	0.00000	0.00003	0.00000	0.00001	0.00046	0.00039	0.00000	0.00002	0.00001	0.00001	0.00000	0.01000	0.00040	0.00072	0.00013	0.00004	0.00126
25352	MDD-MIX	PM2.5	0.00000	0.00005	0.00004	0.00006	0.00314	0.00124	0.00001	0.00011	0.00003	0.00006	0.00175	0.00142	0.00001	0.00006	0.00003	0.00006	0.00000	0.01000	0.00576	0.00432	0.00001	0.00017	0.00062
25353	HHDD-HW	PM2.5	0.00000	0.00004	0.00017	0.00003	0.00373	0.00037	0.00001	0.00008	0.00003	0.00004	0.00001	0.00004	0.00001	0.00003	0.00002	0.00004	0.00000	0.01000	0.00072	0.00230	0.00007	0.00012	0.00166
25354	HHDD-HCS	PM2.5	0.00002	0.00003	0.00022	0.00009	0.00424	0.00093	0.00000	0.00006	0.00001	0.00003	0.00003	0.00003	0.00000	0.00003	0.00004	0.00003	0.00000	0.01000	0.00280	0.00188	0.00015	0.00010	0.00154
25355	HHDD-MIX	PM2.5	0.00001	0.00002	0.00020	0.00007	0.00398	0.00070	0.00000	0.00005	0.00002	0.00003	0.00002	0.00003	0.00001	0.00002	0.00003	0.00003	0.00000	0.01000	0.00176	0.00149	0.00011	0.00008	0.00160
25356	DIESEL	PM2.5	0.00001	0.00004	0.00016	0.00008	0.00377	0.00087	0.00000	0.00008	0.00002	0.00004	0.00045	0.00086	0.00001	0.00004	0.00003	0.00004	0.00000	0.01000	0.00276	0.00272	0.00009	0.00012	0.00135
25357	GAS	PM2.5	0.00009	0.00007	0.00052	0.00054	0.00433	0.00406	0.00000	0.00005	0.00000	0.00003	0.00038	0.00038	0.00001	0.00002	0.00001	0.00002	0.00000	0.01000	0.00184	0.00260	0.00026	0.00024	0.00253
Copper1	COTIRE1	TSP	0.00000	0.00000	0.00003	0.00000	0.00975	0.00015	0.00000	0.00000	0.00000	0.00000	0.00000	0.00100	0.00000	0.00000	0.00001	0.00000	0.00001	0.00000	0.00006	0.00000	0.00001	0.00000	0.00000
Copper2	COTIRE2	TSP	0.00000	0.00000	0.00003	0.00000	0.00949	0.00014	0.00000	0.00000	0.00000	0.00000	0.00000	0.00100	0.00000	0.00000	0.00001	0.00000	0.00001	0.00000	0.00006	0.00000	0.00001	0.00000	0.00000
Michelin1	MITIRE1	TSP	0.00000	0.00000	0.00004	0.00000	0.00497	0.00007	0.00000	0.00000	0.00000	0.00000	0.00000	0.00100	0.00000	0.00000	0.00000	0.00000	0.00001	0.00000	0.00004	0.00000	0.00000	0.00000	0.00000
Michelin2	MITIRE2	TSP	0.00000	0.00000	0.00004	0.00000	0.00496	0.00007	0.00000	0.00000	0.00000	0.00000	0.00000	0.00100	0.00000	0.00000	0.00000	0.00000	0.00001	0.00000	0.00004	0.00000	0.00000	0.00000	0.00000
Copper	COTIRE	TSP	0.00000	0.00000	0.00003	0.00000	0.00962	0.00018	0.00000	0.00000	0.00000	0.00000	0.00000	0.00100	0.00000	0.00000	0.00001	0.00000	0.00001	0.00000	0.00006	0.00000	0.00001	0.00000	0.00000
Michelin	MITIRE	TSP	0.00000	0.00000	0.00004	0.00000	0.00496	0.00007	0.00000	0.00000	0.00000	0.00000	0.00000	0.00100	0.00000	0.00000	0.00000	0.00000	0.00001	0.00000	0.00004	0.00000	0.00000	0.00000	0.00000
MiCo	TIRE	TSP	0.00000	0.00000	0.00003	0.00000	0.00729	0.00269	0.00000	0.00000	0.00000	0.00000	0.00000	0.00100	0.00000	0.00000	0.00000	0.00000	0.00001	0.00000	0.00005	0.00001	0.00000	0.00000	0.00000
RESQ2485	AQ Dust	PM2.5	0.00008	0.00001	0.00028	0.00003	0.00447	0.00033	0.00000	0.00003	0.00000	0.00004	0.00006	0.00004	0.00002	0.00004	0.00015	0.00003	0.00005	0.00012	0.00019	0.00038	0.00000	0.00008	0.00000
RESQ2489	MA Dust	PM2.5	0.00011	0.00002	0.00072	0.00008	0.00128	0.00013	0.00006	0.00006	0.00008	0.00009	0.00000	0.00010	0.00013	0.00009	0.00028	0.00008	0.00055	0.00028	0.00041	0.00086	0.00008	0.00018	0.00000
RESQ2493	CC Dust	PM2.5	0.00011	0.00001	0.00102	0.00008	0.00140	0.00011	0.00000	0.00003	0.00007	0.00004	0.00006	0.00005	0.00007	0.00004	0.00033	0.00004	0.00044	0.00014	0.00123	0.00044	0.00022	0.00009	0.00003
RESQ2497	AT Dust	PM2.5	0.00014	0.00002	0.00011	0.00003	0.00116	0.00011	0.00007	0.00004	0.00010	0.00006	0.00008	0.00007	0.00004	0.00006	0.00004	0.00005	0.00018	0.00019	0.00000	0.00058	0.00021	0.00012	0.00000
RESQ2520	Dust	PM2.5	0.00011	0.00002	0.00053	0.00042	0.00208	0.00160	0.00003	0.00004	0.00006	0.00006	0.00005	0.00007	0.00006	0.00006	0.00020	0.00013	0.00031	0.00023	0.00046	0.00060	0.00013	0.00013	0.00001
RESQ2540	MCDust	PM2.5	0.00011	0.00002	0.00087	0.00022	0.00134	0.00012	0.00003	0.00005	0.00008	0.00007	0.00003	0.00008	0.00010	0.00007	0.00030	0.00006	0.00050	0.00022	0.00082	0.00069	0.00015	0.00014	0.00002
RESQ2560	AADust	PM2.5	0.00011	0.00004	0.00020	0.00012	0.00282	0.00234	0.00004	0.00005	0.00005	0.00007	0.00007	0.00006	0.00003	0.00005	0.00010	0.00008	0.00012	0.00016	0.00009	0.00049	0.00010	0.00015	0.00000
RESQ2487	AQDust	PM10	0.00005	0.00001	0.00066	0.00005	0.00724	0.00053	0.00000	0.00002	0.00000	0.00003	0.00000	0.00003	0.00006	0.00003	0.00032	0.00003	0.00001	0.00009	0.00045	0.00029	0.00022	0.00006	0.00000
RESQ2491	MADust	PM10	0.00015	0.00002	0.00169	0.00014	0.00260	0.00022	0.00042	0.00006	0.00003	0.00007	0.00000	0.00008	0.00000	0.00007	0.00059	0.00007	0.00089	0.00022	0.00038	0.00065	0.00028	0.00014	0.00004
RESQ2495	CCDust	PM10	0.00008	0.00001	0.00190	0.00014	0.00224	0.00017	0.00002	0.00002	0.00000	0.00004	0.00004	0.00004	0.00005	0.00004	0.00066	0.00006	0.00034	0.00012	0.00323	0.00044	0.00018	0.00008	0.00000
RESQ2499	ATDust	PM10	0.00004	0.00001	0.00048	0.00004	0.00229	0.00017	0.00000	0.00003	0.00012	0.00004	0.00005	0.00005	0.00003	0.00004	0.00022	0.00004	0.00000	0.00013	0.00172	0.00042	0.00036	0.00009	0.00000
RESQ2510	Dust	PM10	0.00008	0.00005	0.00118	0.00072	0.00359	0.00244	0.00011	0.00021	0.00004	0.00005	0.00002	0.00005	0.00003	0.00005	0.00045	0.00021	0.00031	0.00042	0.00145	0.00134	0.00026	0.00010	0.00001
RESQ2530	MCDust	PM10	0.00012	0.00006	0.00180	0.00015	0.00242	0.00025	0.00022	0.00029	0.00002	0.00005	0.00002	0.00006	0.00002	0.00005	0.00063	0.00007	0.00062	0.00039	0.00180	0.00201	0.00023	0.00011	0.00002
RESQ2550	AADust	PM10	0.00005	0.00001	0.00057	0.00013	0.00477	0.00350	0.00000	0.00002	0.00006	0.00008	0.00002	0.00004	0.00004	0.00004	0.00027	0.00007	0.00001	0.00011	0.00109	0.00090	0.00029	0.00010	0.00000

PNO	Mnemonic	SIZE	FLUORAU	PYRENE	PYRENEU	BAPYRN	BAPYRNU	BEPYRN	BEPYRNU	INCDPY	INCDPYU	BGHIPE	BGHIPEU	CORONE	CORONEU	RETENE	RETENEU	hop17	hop17U	hop19	hop19U	hop25	hop25U	hop26	hop26U
20013	Brake_1	PM2.5	0.00001	0.00002	0.00001	0.00001	0.00002	0.00000	0.00001	0.00000	0.00002	0.00000	0.00002	0.00000	0.00001	0.00000	0.00001	0.00007	0.00004	0.00001	0.00001	0.00000	0.00001	0.00000	0.00001
20014	Brake_2	PM2.5	0.00001	0.00001	0.00000	0.00000	0.00001	0.00000	0.00000	0.00000	0.00001	0.00000	0.00001	0.00000	0.00000	0.00000	0.00000	0.00020	0.00011	0.00003	0.00001	0.00000	0.00000	0.00000	0.00000
20015	Brake_3	PM2.5	0.00000	0.00001	0.00000	0.00000	0.00001	0.00001	0.00000	0.00001	0.00001	0.00000	0.00001	0.00000	0.00000	0.00000	0.00000	0.00005	0.00003	0.00002	0.00001	0.00000	0.00000	0.00000	0.00000
20016	Brake_C	PM2.5	0.00001	0.00001	0.00000	0.00000	0.00001	0.00000	0.00000	0.00001	0.00001	0.00000	0.00002	0.00000	0.00000	0.00000	0.00001	0.00010	0.00008	0.00002	0.00001	0.00000	0.00000	0.00000	0.00000
ARB1	Brake_D	PM10																							
ARB2	Brake_E	PM10																							
ARB3	Brake_F	PM10																							
ARB4	Brake_G	PM10																							
20017	Tire_1	PM2.5	0.00006	0.00047	0.00005	0.00000	0.00010	0.00000	0.00003	0.00000	0.00008	0.00014	0.00011	########	0.00010	0.00000	0.00004	0.00299	0.00162	0.00037	0.00013	0.00000	0.00006	0.00000	0.00006
20018	Tire_2	PM2.5	0.00012	0.00129	0.00013	0.00000	0.00019	0.00000	0.00006	0.00004	0.00016	0.00026	0.00021	0.00000	0.00006	0.00000	0.00008	0.00678	0.00368	0.00231	0.00072	0.00000	0.00006	0.00027	0.00033
25346	WS-L	PM2.5	0.00424	0.00420	0.00547	0.00006	0.00008	0.00019	0.00005	0.00056	0.00046	0.00144	0.00099	0.00119	0.00089	0.00007	0.00011	0.00002	0.00006	0.00000	0.00000	0.00000	0.00001	0.00000	0.00002
25347	CS-L	PM2.5	0.00206	0.00226	0.00301	0.00011	0.00011	0.00020	0.00011	0.00050	0.00031	0.00134	0.00078	0.00102	0.00066	0.00004	0.00004	0.00003	0.00005	0.00000	0.00000	0.00001	0.00001	0.00001	0.00002
25348	WS-H	PM2.5	0.00563	0.00612	0.00633	0.00010	0.00011	0.00013	0.00009	0.00009	0.00009	0.00022	0.00025	0.00029	0.00023	0.00001	0.00002	0.00031	0.00055	0.00132	0.00150	0.00003	0.00008	0.00004	0.00010
25349	CS-H	PM2.5	0.00209	0.00121	0.00216	0.00013	0.00012	0.00014	0.00012	0.00016	0.00010	0.00045	0.00031	0.00045	0.00049	0.00000	0.00000	0.00042	0.00032	0.00069	0.00087	0.00005	0.00005	0.00008	0.00007
25350	WS-BC	PM2.5	0.00047	0.00237	0.00181	0.00017	0.00025	0.00016	0.00017	0.00037	0.00035	0.00128	0.00153	0.00130	0.00188	0.00013	0.00030	0.00007	0.00006	0.00045	0.00078	0.00000	0.00001	0.00001	0.00002
25351	CS-BC	PM2.5	0.00053	0.00106	0.00032	0.00023	0.00013	0.00020	0.00007	0.00037	0.00012	0.00093	0.00013	0.00076	0.00020	0.00000	0.00001	0.00003	0.00005	0.00021	0.00037	0.00000	0.00000	0.00001	0.00001
25352	MDD-MIX	PM2.5	0.00010	0.00093	0.00024	0.00000	0.00002	0.00000	0.00001	0.00000	0.00002	0.00000	0.00002	0.00000	0.00001	0.00000	0.00001	0.00002	0.00002	0.00005	0.00006	0.00000	0.00002	0.00000	0.00002
25353	HHDD-HW	PM2.5	0.00110	0.00177	0.00114	0.00001	0.00002	0.00001	0.00002	0.00000	0.00001	0.00000	0.00002	0.00000	0.00001	0.00000	0.00001	0.00013	0.00008	0.00006	0.00003	0.00000	0.00001	0.00000	0.00001
25354	HHDD-HCS	PM2.5	0.00103	0.00179	0.00108	0.00002	0.00004	0.00001	0.00001	0.00000	0.00001	0.00000	0.00001	0.00000	0.00000	0.00001	0.00001	0.00017	0.00009	0.00008	0.00004	0.00000	0.00000	0.00000	0.00000
25355	HHDD-MIX	PM2.5	0.00099	0.00178	0.00103	0.00002	0.00003	0.00001	0.00001	0.00000	0.00001	0.00000	0.00001	0.00000	0.00000	0.00000	0.00001	0.00015	0.00008	0.00007	0.00004	0.00000	0.00000	0.00000	0.00000
25356	DIESEL	PM2.5	0.00090	0.00157	0.00095	0.00001	0.00003	0.00001	0.00001	0.00000	0.00001	0.00000	0.00002	0.00000	0.00000	0.00000	0.00001	0.00012	0.00008	0.00006	0.00005	0.00000	0.00001	0.00000	0.00001
25357	GAS	PM2.5	0.00313	0.00287	0.00381	0.00013	0.00014	0.00017	0.00011	0.00034	0.00028	0.00094	0.00083	0.00084	0.00092	0.00004	0.00013	0.00015	0.00026	0.00045	0.00079	0.00002	0.00004	0.00002	0.00005
Copper1	COTIRE1	TSP	0.00000	0.00000	0.00000	0.00000	0.00000	0.00000	0.00000	0.00000	0.00000	0.00000	0.00000	0.00000	0.00000	0.00000	0.00000	0.00000	0.00000	0.00000	0.00000	0.00000	0.00000	0.00000	0.00000
Copper2	COTIRE2	TSP	0.00000	0.00000	0.00000	0.00000	0.00000	0.00000	0.00000	0.00000	0.00000	0.00000	0.00000	0.00000	0.00000	0.00000	0.00000	0.00000	0.00000	0.00000	0.00000	0.00000	0.00000	0.00000	0.00000
Michelin1	MITIRE1	TSP	0.00000	0.00000	0.00000	0.00000	0.00000	0.00000	0.00000	0.00000	0.00000	0.00000	0.00000	0.00000	0.00000	0.00000	0.00000	0.00000	0.00000	0.00000	0.00000	0.00000	0.00000	0.00000	0.00000
Michelin2	MITIRE2	TSP	0.00000	0.00000	0.00000	0.00000	0.00000	0.00000	0.00000	0.00000	0.00000	0.00000	0.00000	0.00000	0.00000	0.00000	0.00000	0.00000	0.00000	0.00000	0.00000	0.00000	0.00000	0.00000	0.00000
Copper	COTIRE	TSP	0.00000	0.00000	0.00000	0.00000	0.00000	0.00000	0.00000	0.00000	0.00000	0.00000	0.00000	0.00000	0.00000	0.00000	0.00000	0.00000	0.00000	0.00000	0.00000	0.00000	0.00000	0.00000	0.00000
Michelin	MITIRE	TSP	0.00000	0.00000	0.00000	0.00000	0.00000	0.00000	0.00000	0.00000	0.00000	0.00000	0.00000	0.00000	0.00000	0.00000	0.00000	0.00000	0.00000	0.00000	0.00000	0.00000	0.00000	0.00000	0.00000
MiCo	TIRE	TSP	0.00000	0.00000	0.00000	0.00000	0.00000	0.00000	0.00000	0.00000	0.00000	0.00000	0.00000	0.00000	0.00000	0.00000	0.00000	0.00000	0.00000	0.00000	0.00000	0.00000	0.00000	0.00000	0.00000
RESQ2485	AQ Dust	PM2.5	0.00000	0.00000	0.00000	0.00000	0.00000	0.00000	0.00000	0.00000	0.00000	0.00000	0.00000	0.00000	0.00000	0.00000	0.00000	0.00000	0.00000	0.00000	0.00000	0.00000	0.00000	0.00000	0.00000
RESQ2489	MA Dust	PM2.5	0.00000	0.00000	0.00000	0.00000	0.00000	0.00000	0.00000	0.00000	0.00000	0.00000	0.00000	0.00000	0.00000	0.00000	0.00000	0.00000	0.00000	0.00000	0.00000	0.00000	0.00000	0.00000	0.00000
RESQ2493	CC Dust	PM2.5	0.00000	0.00001	0.00000	0.00000	0.00000	0.00000	0.00000	0.00000	0.00000	0.00000	0.00000	0.00000	0.00000	0.00000	0.00000	0.00000	0.00000	0.00001	0.00000	0.00000	0.00000	0.00000	0.00000
RESQ2497	AT Dust	PM2.5	0.00000	0.00000	0.00000	0.00000	0.00000	0.00000	0.00000	0.00000	0.00000	0.00000	0.00000	0.00000	0.00000	0.00000	0.00000	0.00001	0.00000	0.00000	0.00000	0.00000	0.00000	0.00000	0.00000
RESQ2520	Dust	PM2.5	0.00002	0.00000	0.00001	0.00000	0.00000	0.00000	0.00000	0.00000	0.00000	0.00000	0.00000	0.00000	0.00000	0.00000	0.00000	0.00000	0.00000	0.00000	0.00000	0.00000	0.00000	0.00000	0.00000
RESQ2540	MCDust	PM2.5	0.00002	0.00001	0.00001	0.00000	0.00000	0.00000	0.00000	0.00000	0.00000	0.00000	0.00000	0.00000	0.00000	0.00000	0.00000	0.00000	0.00000	0.00000	0.00000	0.00000	0.00000	0.00000	0.00000
RESQ2560	AADust	PM2.5	0.00000	0.00000	0.00000	0.00000	0.00000	0.00000	0.00000	0.00000	0.00000	0.00000	0.00000	0.00000	0.00000	0.00000	0.00000	0.00000	0.00001	0.00000	0.00000	0.00000	0.00000	0.00000	0.00000
RESQ2487	AQDust	PM10	0.00000	0.00000	0.00000	0.00000	0.00000	0.00000	0.00000	0.00000	0.00000	0.00000	0.00000	0.00000	0.00000	0.00000	0.00000	0.00000	0.00000	0.00000	0.00000	0.00000	0.00000	0.00000	0.00000
RESQ2491	MADust	PM10	0.00000	0.00002	0.00000	0.00000	0.00000	0.00001	0.00000	0.00000	0.00000	0.00000	0.00000	0.00000	0.00000	0.00000	0.00000	0.00000	0.00000	0.00001	0.00000	0.00000	0.00000	0.00000	0.00000
RESQ2495	CCDust	PM10	0.00000	0.00000	0.00000	0.00000	0.00000	0.00000	0.00000	0.00000	0.00000	0.00000	0.00000	0.00000	0.00000	0.00000	0.00000	0.00000	0.00000	0.00000	0.00000	0.00000	0.00000	0.00000	0.00000
RESQ2499	ATDust	PM10	0.00000	0.00000	0.00000	0.00001	0.00000	0.00000	0.00000	0.00000	0.00000	0.00000	0.00000	0.00000	0.00000	0.00000	0.00000	0.00001	0.00000	0.00000	0.00000	0.00000	0.00000	0.00000	0.00000
RESQ2510	Dust	PM10	0.00002	0.00000	0.00001	0.00000	0.00000	0.00000	0.00000	0.00000	0.00000	0.00000	0.00000	0.00000	0.00000	0.00000	0.00000	0.00000	0.00000	0.00000	0.00000	0.00000	0.00000	0.00000	0.00000
RESQ2530	MCDust	PM10	0.00003	0.00001	0.00001	0.00000	0.00000	0.00001	0.00000	0.00000	0.00000	0.00000	0.00000	0.00000	0.00000	0.00000	0.00000	0.00000	0.00000	0.00000	0.00000	0.00000	0.00000	0.00000	0.00000
RESQ2550	AADust	PM10	0.00000	0.00000	0.00000	0.00001	0.00001	0.00000	0.00000	0.00000	0.00000	0.00000	0.00000	0.00000	0.00000	0.00000	0.00000	0.00000	0.00001	0.00000	0.00000	0.00000	0.00000	0.00000	0.00000

PNO	Mnemonic	SIZE	prist	pristU	phytan	phytanU	DMPHTH	DMPHTHU	DEPHTH	DEPHTHU	DBPHTH	DBPHTHU	BBPHTH	BBPHTHU	BEPHTH	BEPHTHU	DOPHTH	DOPHTHU	BT	BTU	VLCYHE	VLCYHEU	DPTE	DPTEU	STYR	STYRU	ISOP	ISOPU	BUTD	BUTDU
20013	Brake_1	PM2.5	0.00190	0.00037	0.00053	0.00008	0.00000	0.00010	0.00000	0.00010	0.00000	0.00010	0.00000	0.00010	0.00000	0.00010	0.00000	0.00010	0.00000	0.00010	0.00000	0.00010	0.00000	0.00010	0.00000	0.00010	0.00000	0.00010	0.00000	0.00010
20014	Brake_2	PM2.5	0.00076	0.00015	0.00020	0.00003	0.00000	0.00010	0.00000	0.00010	0.00000	0.00010	0.00000	0.00010	0.00000	0.00010	0.00000	0.00010	0.00000	0.00010	0.00000	0.00010	0.00000	0.00010	0.00000	0.00010	0.00000	0.00010	0.00000	0.00010
20015	Brake_3	PM2.5	0.00068	0.00013	0.00014	0.00002	0.00000	0.00010	0.00000	0.00010	0.00000	0.00010	0.00000	0.00010	0.00000	0.00010	0.00000	0.00010	0.00000	0.00010	0.00000	0.00010	0.00000	0.00010	0.00000	0.00010	0.00000	0.00010	0.00000	0.00010
20016	Brake_C	PM2.5	0.00111	0.00068	0.00029	0.00021	0.00000	0.00010	0.00000	0.00010	0.00000	0.00010	0.00000	0.00010	0.00000	0.00010	0.00000	0.00010	0.00000	0.00010	0.00000	0.00010	0.00000	0.00010	0.00000	0.00010	0.00000	0.00010	0.00000	0.00010
ARB1	Brake_D	PM10																												
ARB2	Brake_E	PM10																												
ARB3	Brake_F	PM10																												
ARB4	Brake_G	PM10																												
20017	Tire_1	PM2.5	0.00618	0.00122	0.00395	0.00059	0.00000	0.00010	0.00000	0.00010	0.00000	0.00010	0.00000	0.00010	0.00000	0.00010	0.00000	0.00010	0.00000	0.00010	0.00000	0.00010	0.00000	0.00010	0.00000	0.00010	0.00000	0.00010	0.00000	0.00010
20018	Tire_2	PM2.5	0.01278	0.00257	0.00441	0.00072	0.00000	0.00010	0.00000	0.00010	0.00000	0.00010	0.00000	0.00010	0.00000	0.00010	0.00000	0.00010	0.00000	0.00010	0.00000	0.00010	0.00000	0.00010	0.00000	0.00010	0.00000	0.00010	0.00000	0.00010
25346	WS-L	PM2.5	0.00000	0.00010	0.00000	0.00010	0.00000	0.00010	0.00000	0.00010	0.00000	0.00010	0.00000	0.00010	0.00000	0.00010	0.00000	0.00010	0.00000	0.00010	0.00000	0.00010	0.00000	0.00010	0.00000	0.00010	0.00000	0.00010	0.00000	0.00010
25347	CS-L	PM2.5	0.00000	0.00010	0.00000	0.00010	0.00000	0.00010	0.00000	0.00010	0.00000	0.00010	0.00000	0.00010	0.00000	0.00010	0.00000	0.00010	0.00000	0.00010	0.00000	0.00010	0.00000	0.00010	0.00000	0.00010	0.00000	0.00010	0.00000	0.00010
25348	WS-H	PM2.5	0.00002	0.00002	0.00078	0.00081	0.00000	0.00010	0.00000	0.00010	0.00000	0.00010	0.00000	0.00010	0.00000	0.00010	0.00000	0.00010	0.00000	0.00010	0.00000	0.00010	0.00000	0.00010	0.00000	0.00010	0.00000	0.00010	0.00000	0.00010
25349	CS-H	PM2.5	0.00001	0.00002	0.00001	0.00003	0.00000	0.00010	0.00000	0.00010	0.00000	0.00010	0.00000	0.00010	0.00000	0.00010	0.00000	0.00010	0.00000	0.00010	0.00000	0.00010	0.00000	0.00010	0.00000	0.00010	0.00000	0.00010	0.00000	0.00010
25350	WS-BC	PM2.5	0.00008	0.00011	0.00000	0.00004	0.00000	0.00010	0.00000	0.00010	0.00000	0.00010	0.00000	0.00010	0.00000	0.00010	0.00000	0.00010	0.00000	0.00010	0.00000	0.00010	0.00000	0.00010	0.00000	0.00010	0.00000	0.00010	0.00000	0.00010
25351	CS-BC	PM2.5	0.00008	0.00002	0.00004	0.00006	0.00000	0.00010	0.00000	0.00010	0.00000	0.00010	0.00000	0.00010	0.00000	0.00010	0.00000	0.00010	0.00000	0.00010	0.00000	0.00010	0.00000	0.00010	0.00000	0.00010	0.00000	0.00010	0.00000	0.00010
25352	MDD-MIX	PM2.5	0.00002	0.00005	0.00244	0.00130	0.00000	0.00010	0.00000	0.00010	0.00000	0.00010	0.00000	0.00010	0.00000	0.00010	0.00000	0.00010	0.00000	0.00010	0.00000	0.00010	0.00000	0.00010	0.00000	0.00010	0.00000	0.00010	0.00000	0.00010
25353	HHDD-HW	PM2.5	0.00000	0.00001	0.00056	0.00010	0.00000	0.00010	0.00000	0.00010	0.00000	0.00010	0.00000	0.00010	0.00000	0.00010	0.00000	0.00010	0.00000	0.00010	0.00000	0.00010	0.00000	0.00010	0.00000	0.00010	0.00000	0.00010	0.00000	0.00010
25354	HHDD-HCS	PM2.5	0.00030	0.00020	0.00041	0.00008	0.00000	0.00010	0.00000	0.00010	0.00000	0.00010	0.00000	0.00010	0.00000	0.00010	0.00000	0.00010	0.00000	0.00010	0.00000	0.00010	0.00000	0.00010	0.00000	0.00010	0.00000	0.00010	0.00000	0.00010
25355	HHDD-MIX	PM2.5	0.00015	0.00021	0.00049	0.00009	0.00000	0.00010	0.00000	0.00010	0.00000	0.00010	0.00000	0.00010	0.00000	0.00010	0.00000	0.00010	0.00000	0.00010	0.00000	0.00010	0.00000	0.00010	0.00000	0.00010	0.00000	0.00010	0.00000	0.00010
25356	DIESEL	PM2.5	0.00012	0.00015	0.00097	0.00098	0.00000	0.00010	0.00000	0.00010	0.00000	0.00010	0.00000	0.00010	0.00000	0.00010	0.00000	0.00010	0.00000	0.00010	0.00000	0.00010	0.00000	0.00010	0.00000	0.00010	0.00000	0.00010	0.00000	0.00010
25357	GAS	PM2.5	0.00003	0.00008	0.00014	0.00034	0.00000	0.00010	0.00000	0.00010	0.00000	0.00010	0.00000	0.00010	0.00000	0.00010	0.00000	0.00010	0.00000	0.00010	0.00000	0.00010	0.00000	0.00010	0.00000	0.00010	0.00000	0.00010	0.00000	0.00010
Copper1	COTIRE1	TSP	0.00000	0.00000	0.00000	0.00000	0.00001	0.00000	0.00001	0.00000	0.00005	0.00000	0.00005	0.00000	0.00141	0.00007	0.00032	0.00002	0.00000	0.00000	0.00000	0.00000	0.00001	0.00000	0.00001	0.00000	0.00000	0.00000	0.00000	0.00000
Copper2	COTIRE2	TSP	0.00000	0.00000	0.00000	0.00000	0.00010	0.00001	0.00017	0.00001	0.00061	0.00003	0.00058	0.00003	0.00631	0.00032	0.00430	0.00022	0.00000	0.00000	0.00002	0.00000	0.00002	0.00000	0.00003	0.00000	0.00001	0.00000	0.00001	0.00000
Michelin1	MITIRE1	TSP	0.00000	0.00000	0.00000	0.00000	0.00001	0.00000	0.00002	0.00000	0.00007	0.00000	0.00006	0.00000	0.00083	0.00004	0.00057	0.00003	0.00000	0.00000	0.00000	0.00000	0.00000	0.00000	0.00000	0.00000	0.00000	0.00000	0.00000	0.00000
Michelin2	MITIRE2	TSP	0.00000	0.00000	0.00000	0.00000	0.00002	0.00000	0.00002	0.00000	0.00009	0.00000	0.00007	0.00000	0.01863	0.00093	0.00847	0.00042	0.00000	0.00000	0.00001	0.00000	0.00000	0.00000	0.00001	0.00000	0.00000	0.00000	0.00000	0.00000
Copper	COTIRE	TSP	0.00000	0.00000	0.00000	0.00000	0.00006	0.00007	0.00009	0.00011	0.00033	0.00039	0.00031	0.00037	0.00386	0.00346	0.00231	0.00282	0.00000	0.00000	0.00001	0.00002	0.00001	0.00001	0.00002	0.00002	0.00000	0.00000	0.00000	0.00000
Michelin	MITIRE	TSP	0.00000	0.00000	0.00000	0.00000	0.00002	0.00000	0.00002	0.00000	0.00008	0.00002	0.00006	0.00001	0.00973	0.01259	0.00452	0.00559	0.00000	0.00000	0.00000	0.00000	0.00000	0.00000	0.00001	0.00000	0.00000	0.00000	0.00000	0.00000
MiCo	TIRE	TSP	0.00000	0.00000	0.00000	0.00000	0.00004	0.00004	0.00005	0.00008	0.00020	0.00027	0.00019	0.00026	0.00679	0.00827	0.00342	0.00383	0.00000	0.00000	0.00001	0.00001	0.00001	0.00001	0.00001	0.00001	0.00000	0.00000	0.00000	0.00000
RESQ2485	AQ Dust	PM2.5	0.00000	0.00000	0.00000	0.00000	0.00105	0.00006	0.00081	0.00005	0.00579	0.00032	0.00478	0.00026	1.43721	0.07876	0.81168	0.04448	0.00008	0.00000	0.00049	0.00003	0.00023	0.00001	0.00053	0.00003	0.00026	0.00001	0.00016	0.00001
RESQ2489	MA Dust	PM2.5	0.00000	0.00000	0.00000	0.00000	0.00138	0.00011	0.00145	0.00011	0.00602	0.00043	0.00474	0.00034	1.34834	0.09634	0.76478	0.05464	0.00007	0.00001	0.00028	0.00002	0.00012	0.00001	0.00034	0.00002	0.00012	0.00001	0.00009	0.00001
RESQ2493	CC Dust	PM2.5	0.00001	0.00000	0.00000	0.00000	0.00003	0.00001	0.00002	0.00000	0.00009	0.00001	0.00011	0.00001	0.00180	0.00010	0.00070	0.00004	0.00001	0.00000	0.00001	0.00000	0.00001	0.00000	0.00001	0.00000	0.00000	0.00000	0.00001	0.00000
RESQ2497	AT Dust	PM2.5	0.00001	0.00000	0.00002	0.00000	0.00001	0.00001	0.00002	0.00001	0.00008	0.00001	0.00005	0.00001	0.00150	0.00009	0.00041	0.00003	0.00000	0.00000	0.00000	0.00000	0.00001	0.00000	0.00001	0.00000	0.00000	0.00000	0.00000	0.00000
RESQ2520	Dust	PM2.5	0.00001	0.00001	0.00000	0.00001	0.00062	0.00070	0.00058	0.00069	0.00299	0.00336	0.00242	0.00270	0.69721	0.80398	0.39439	0.45517	0.00004	0.00004	0.00020	0.00023	0.00009	0.00011	0.00022	0.00026	0.00010	0.00012	0.00007	0.00008
RESQ2540	MCDust	PM2.5	0.00001	0.00001	0.00000	0.00000	0.00070	0.00096	0.00074	0.00101	0.00305	0.00419	0.00242	0.00328	0.67507	0.95215	0.38274	0.54029	0.00004	0.00005	0.00015	0.00019	0.00006	0.00008	0.00018	0.00023	0.00006	0.00008	0.00005	0.00006
RESQ2560	AADust	PM2.5	0.00000	0.00001	0.00001	0.00001	0.00053	0.00073	0.00042	0.00056	0.00293	0.00403	0.00241	0.00334	0.71936	1.01520	0.40605	0.57366	0.00004	0.00005	0.00025	0.00034	0.00012	0.00016	0.00027	0.00037	0.00013	0.00018	0.00008	0.00011
RESQ2487	AQDust	PM10	0.00000	0.00000	0.00000	0.00000	0.00069	0.00004	0.00045	0.00003	0.00238	0.00013	0.00196	0.00011	0.39849	0.02108	0.24653	0.01304	0.00002	0.00000	0.00011	0.00001	0.00005	0.00000	0.00011	0.00001	0.00004	0.00000	0.00002	0.00000
RESQ2491	MADust	PM10	0.00002	0.00000	0.00000	0.00000	0.00003	0.00001	0.00003	0.00001	0.00010	0.00001	0.00013	0.00001	0.00316	0.00020	0.00088	0.00006	0.00001	0.00000	0.00002	0.00000	0.00002	0.00000	0.00003	0.00000	0.00001	0.00000	0.00001	0.00000
RESQ2495	CCDust	PM10	0.00001	0.00000	0.00000	0.00000	0.00001	0.00000	0.00001	0.00000	0.00004	0.00000	0.00003	0.00000	0.00093	0.00005	0.00019	0.00001	0.00000	0.00000	0.00000	0.00000	0.00000	0.00000	0.00000	0.00000	0.00000	0.00000	0.00000	0.00000
RESQ2499	ATDust	PM10	0.00001	0.00000	0.00001	0.00000	0.00001	0.00001	0.00001	0.00000	0.00003	0.00000	0.00003	0.00000	0.00127	0.00007	0.00017	0.00001	0.00000	0.00000	0.00000	0.00000	0.00000	0.00000	0.00001	0.00000	0.00000	0.00000	0.00000	0.00000
RESQ2510	Dust	PM10	0.00001	0.00001	0.00000	0.00001	0.00018	0.00034	0.00012	0.00022	0.00064	0.00116	0.00054	0.00095	0.10096	0.19836	0.06194	0.12306	0.00001	0.00001	0.00003	0.00005	0.00002	0.00002	0.00004	0.00005	0.00001	0.00002	0.00001	0.00001
RESQ2530	MCDust	PM10	0.00001	0.00001	0.00000	0.00000	0.00002	0.00002	0.00002	0.00001	0.00007	0.00004	0.00008	0.00007	0.00205	0.00158	0.00054	0.00048	0.00000	0.00000	0.00001	0.00001	0.00001	0.00001	0.00001	0.00002	0.00000	0.00000	0.00001	0.00001
RESQ2550	AADust	PM10	0.00000	0.00000	0.00001	0.00001	0.00035	0.00048	0.00023	0.00031	0.00121	0.00166	0.00099	0.00136	0.19988	0.28088	0.12335	0.17420	0.00001	0.00001	0.00006	0.00008	0.00003	0.00003	0.00006	0.00007	0.00002	0.00002	0.00001	0.00001

Appendix B: Data Samples from California PeMS

This appendix presents some sample data files obtained from PeMS for traffic analysis.

I-5 North upstream VDS (#1205452)

1	5 Minutes	Lane 1 Truck Fl	Lane 1 Truck Pr	Lane 2 Truck Fl	Lane 2 Truck Pr	Lane 3 Truck Fl	Lane 3 Truck Pr	Lane 4 Truck Fl	Lane 4 Truck Pr	# Lane Points	% Observed
2	1/28/2020 0:00	0	0.00	0	0.00	6	12.80	6	18.20	4	0.00
3	1/28/2020 0:05	0	0.00	0	0.00	4	8.20	6	15.00	4	0.00
4	1/28/2020 0:10	0	0.00	0	0.00	5	11.90	6	16.20	4	0.00
5	1/28/2020 0:15	0	0.00	0	0.00	5	11.40	7	21.90	4	0.00
6	1/28/2020 0:20	0	0.00	0	0.00	6	14.30	8	27.60	4	0.00
7	1/28/2020 0:25	0	0.00	0	0.00	1	2.80	6	21.40	4	0.00
8	1/28/2020 0:30	0	0.00	0	0.00	3	7.00	9	28.10	4	0.00
9	1/28/2020 0:35	0	0.00	0	0.00	3	7.30	9	30.00	4	0.00
10	1/28/2020 0:40	0	0.00	0	0.00	7	20.00	8	23.50	4	0.00
11	1/28/2020 0:45	0	0.00	0	0.00	3	10.00	5	20.00	4	0.00
12	1/28/2020 0:50	0	0.00	0	0.00	6	18.20	5	21.70	4	0.00
13	1/28/2020 0:55	0	0.00	0	0.00	1	3.30	5	22.70	4	0.00
14	1/28/2020 1:00	0	0.00	0	0.00	1	3.70	4	19.00	4	0.00
15	1/28/2020 1:05	0	0.00	0	0.00	2	7.10	4	19.00	4	0.00
16	1/28/2020 1:10	0	0.00	0	0.00	1	3.20	5	21.70	4	0.00
17	1/28/2020 1:15	0	0.00	0	0.00	0	0.00	3	15.80	4	0.00
18	1/28/2020 1:20	0	0.00	0	0.00	2	7.10	5	23.80	4	0.00
19	1/28/2020 1:25	0	0.00	0	0.00	2	7.70	4	20.00	4	0.00
20	1/28/2020 1:30	0	0.00	0	0.00	0	0.00	3	16.70	4	0.00
21	1/28/2020 1:35	0	0.00	0	0.00	1	4.30	1	5.90	4	0.00
22	1/28/2020 1:40	0	0.00	0	0.00	1	5.60	3	15.80	4	0.00
23	1/28/2020 1:45	0	0.00	0	0.00	0	0.00	3	20.00	4	0.00
24	1/28/2020 1:50	0	0.00	0	0.00	1	5.60	2	13.30	4	0.00
25	1/28/2020 1:55	0	0.00	0	0.00	1	5.60	2	16.70	4	0.00
26	1/28/2020 2:00	0	0.00	0	0.00	2	10.50	2	16.70	4	0.00
27	1/28/2020 2:05	0	0.00	0	0.00	1	4.80	3	15.00	4	0.00
28	1/28/2020 2:10	0	0.00	0	0.00	2	10.00	1	7.10	4	0.00
29	1/28/2020 2:15	0	0.00	0	0.00	1	4.20	2	15.40	4	0.00
30	1/28/2020 2:20	0	0.00	0	0.00	1	5.00	2	14.30	4	0.00

I-710 North upstream VDS (#717962)

1	5 Minutes	Lane 1 Truck Fl	Lane 1 Truck Pr	Lane 2 Truck Fl	Lane 2 Truck Pr	Lane 3 Truck Fl	Lane 3 Truck Pr	Lane 4 Truck Fl	Lane 4 Truck Pr	# Lane Points	% Observed
2	2/4/2020 0:00	0	0.00	0	0.00	2	5.60	3	10.00	4	0.00
3	2/4/2020 0:05	0	0.00	0	0.00	2	5.60	3	10.30	4	0.00
4	2/4/2020 0:10	0	0.00	0	0.00	2	5.60	3	10.30	4	0.00
5	2/4/2020 0:15	0	0.00	0	0.00	2	5.90	3	10.70	4	0.00
6	2/4/2020 0:20	0	0.00	0	0.00	1	3.00	2	7.40	4	0.00
7	2/4/2020 0:25	0	0.00	0	0.00	1	3.20	2	7.70	4	0.00
8	2/4/2020 0:30	0	0.00	0	0.00	1	3.30	2	8.30	4	0.00
9	2/4/2020 0:35	0	0.00	0	0.00	1	3.40	2	8.30	4	0.00
10	2/4/2020 0:40	0	0.00	0	0.00	1	3.60	2	8.70	4	0.00
11	2/4/2020 0:45	0	0.00	0	0.00	1	3.60	2	8.70	4	0.00
12	2/4/2020 0:50	0	0.00	0	0.00	1	3.80	2	9.50	4	0.00
13	2/4/2020 0:55	0	0.00	0	0.00	1	4.00	2	10.00	4	0.00
14	2/4/2020 1:00	0	0.00	0	0.00	1	4.20	2	10.00	4	0.00
15	2/4/2020 1:05	0	0.00	0	0.00	1	4.20	2	10.50	4	0.00
16	2/4/2020 1:10	0	0.00	0	0.00	1	4.30	2	10.50	4	0.00
17	2/4/2020 1:15	0	0.00	0	0.00	1	4.30	2	10.50	4	0.00
18	2/4/2020 1:20	0	0.00	0	0.00	1	4.50	2	11.10	4	0.00
19	2/4/2020 1:25	0	0.00	0	0.00	1	4.80	2	11.80	4	0.00
20	2/4/2020 1:30	0	0.00	0	0.00	1	4.80	1	5.90	4	0.00
21	2/4/2020 1:35	0	0.00	0	0.00	1	4.80	1	5.90	4	0.00
22	2/4/2020 1:40	0	0.00	0	0.00	1	4.80	1	5.90	4	0.00
23	2/4/2020 1:45	0	0.00	0	0.00	1	5.00	1	5.90	4	0.00
24	2/4/2020 1:50	0	0.00	0	0.00	1	5.00	1	6.30	4	0.00
25	2/4/2020 1:55	0	0.00	0	0.00	1	5.30	1	6.30	4	0.00
26	2/4/2020 2:00	0	0.00	0	0.00	1	5.60	1	6.70	4	0.00

Appendix C: Data Samples Processed with ALPR Software

This appendix presents some sample data files processed by CARB's engineers with ALPR software.

I-5 North Study Site

Datetime	Matching Region	Veh Type	Model Yea	Fuel Type	Notes
1/28/20 11:47 AM	CA	LDV	2014	G	Back
1/28/20 11:47 AM	CA	MDV	2002	G	Back
1/28/20 11:47 AM	CA	LDV	2012	B	Back
1/28/20 11:47 AM	CA	LDV	2013	G	Back
1/28/20 11:47 AM	CA	LDV	2013	G	Back
1/28/20 11:47 AM					Back
1/28/20 11:47 AM	CA	LDV	2017	G	Back
1/28/20 11:47 AM					Back
1/28/20 11:47 AM	CA	LDV	2017	F	Back
1/28/20 11:47 AM	CA	LDV	2018	G	Back
1/28/20 11:47 AM	CA	MDV	2017	F	Back
1/28/20 11:48 AM					Back
1/28/20 11:48 AM	CA	LDV	2007	G	Back
1/28/20 11:48 AM	CA	LDV	2013	G	Back
1/28/20 11:48 AM	CA	LDV	2017	G	Back
1/28/20 11:48 AM	CA	LDV	2011	G	Back
1/28/20 11:48 AM	CA	LDV	2006	G	Back
1/28/20 11:48 AM	CA	LDV	2007	G	Back
1/28/20 11:48 AM					Back
1/28/20 11:49 AM	CA	LDV	2004	G	Back
1/28/20 11:49 AM	CA	LDV	2013	G	Back
1/28/20 11:49 AM	CA	LDV	2017	B	Back

I-710 North Study Site

Datetime	Matching Regi	Veh Type	Model Year	Fuel Type	Notes
2/4/20 12:18 PM					17255
2/4/20 12:18 PM					17255
2/4/20 12:18 PM					17255
2/4/20 12:18 PM	CA	LDV	2015	G	17255
2/4/20 12:18 PM	CA	LDV	2018	G	17255
2/4/20 12:18 PM	CA	LDV	2010	G	17255
2/4/20 12:18 PM	CA	Trailer	2017		17255
2/4/20 12:18 PM	CA	LDV	2013	B	17255
2/4/20 12:18 PM	CA	LDV	2008	G	17255
2/4/20 12:18 PM	CA	LDV	2017	G	17255
2/4/20 12:18 PM	CA	LDV	2009	G	17255
2/4/20 12:18 PM	CA	LDV	2015	G	17255
2/4/20 12:18 PM	CA	LDV	2001	G	17255
2/4/20 12:18 PM	CA	LDV	2011	G	17255
2/4/20 12:18 PM	CA	LDV	2018	G	17255
2/4/20 12:18 PM					17255
2/4/20 12:18 PM	CA	LDV	2002	G	17255

Appendix D: WIM Data Samples

This appendix presents some sample data files related to the weigh-in-motion stations.

Data sample from Station #80 that is associated with the I-5 North Study Site (01/28/2020 ~ 02/03/2020)

28 Tues	11,291	9,166	436	218	5,030	924	56	487	3,566	97	75	10	8	121	699
29 Wed	11,706	6,596	164	304	4,643	868	62	448	2,933	94	89	14	78	128	2,045
30 Thurs	12,193	6,618	152	283	4,706	878	66	485	3,104	108	76	8	29	124	2,326
31 Fri	12,366	6,427	185	293	4,748	820	70	491	2,930	98	64	6	46	110	2,690
	58,845	35,208	1,107	1,366	23,855	4,286	333	2,321	15,578	491	341	44	181	575	9,474
Total	314,276	209,473	11,728	7,531	145,824	21,485	1,850	11,386	74,451	1,843	1,646	196	742	3,100	44,222

Classification — Number of Vehicles — Saturday, February 01, 2020 12:00AM

Day	Total	Weighed	OverWt	4	5	6	7	8	9	10	11	12	13	14	15
1 Sat	8,110	2,989	52	338	3,274	330	71	266	817	4	31	1	14	84	2,880
2 Sun	3,415	1,915	17	81	1,704	90	8	40	378	3	7	1	1	37	1,065
	11,525	4,904	69	419	4,978	420	79	306	1,195	7	38	2	15	121	3,945
3 Mon	10,542	9,923	569	238	5,170	849	49	466	3,374	62	40	4	2	98	190

Data sample from Station #60 that is associated with the I-710 North Study Site (2/4/2020 ~ 2/10/2020)

Classification | Number of Vehicles | Saturday, February 01, 2020 12:00AM

Day	Total	Weighed	OverWt	4	5	6	7	8	9	10	11	12	13	14	15
1 Sat	0	0	0	0	0	0	0	0	0	0	0	0	0	0	0
2 Sun	0	0	0	0	0	0	0	0	0	0	0	0	0	0	0
	0	0	0	0	0	0	0	0	0	0	0	0	0	0	0
3 Mon	0	0	0	0	0	0	0	0	0	0	0	0	0	0	0
4 Tues	0	0	0	0	0	0	0	0	0	0	0	0	0	0	0
5 Wed	0	0	0	0	0	0	0	0	0	0	0	0	0	0	0
6 Thurs	2,730	1,836	58	57	804	310	2	60	1,179	27	33	3	0	37	218
7 Fri	17,295	13,243	453	186	4,175	2,236	29	342	8,697	371	211	23	5	201	819
8 Sat	5,810	4,319	83	100	2,191	570	12	114	2,017	38	254	4	1	151	358
9 Sun	2,284	1,736	56	122	982	138	2	36	707	10	8	0	0	130	149
	28,119	21,134	650	465	8,152	3,254	45	552	12,600	446	506	30	6	519	1,544

	Total	Weighed	OverWt	4	5	6	7	8	9	10	11	12	13	14	15
10 Mon	17,561	16,724	804	165	2,995	1,912	22	336	11,044	440	214	9	5	199	220
11 Tues	19,717	18,674	1,010	186	3,080	2,073	41	361	12,676	568	252	7	5	215	253

Appendix E: Toxicity measurement

Professor Manabu Shraiwa's group from UCI co-located their samplers at downwind locations during the field test of this project and post-analyzed toxicity of PM measured near highway 5 and 710. Briefly, environmentally persistent free radicals (EPFRs), such as quinones, were 36 ± 14 pmol m^{-3}, two times higher at near highway locations compared to a background location EPFRs concentrations correlated well with CO, NOx, EC and OC indicating its relationship with tailpipe emissions. EPFRs were also well correlated with Fe and Cu suggesting stabilization of EPFRs by non-tailpipe emissions. ROS formation and DTT activity showed different trends between two locations indicating complex interplay among various PM redox-active chemical components. The study was published and details can be found at the following journal citation: Environmentally Persistent Free Radicals, Reactive Oxygen Species Generation, and Oxidative Potential of Highway $PM_{2.5}$, *ACS Earth Space Chem. 2021, 5, 1865−1875.*

Appendix F: Issues with Background Subtraction: Downwind – Upwind

PM samples collected at near-road measurement sites include PM from both the traffic on the road and background. As such it is necessary to separate contribution of background PM concentrations to determine emission factors from near road measurement. Figure A-1 shows the difference in PM mass concentrations between downwind and upwind locations based on gravimetric filter samples. The PM data was taken from Figure 4-9. The ΔPM concentrations are very small and sometimes PM mass concentrations at upwind location show larger values compared to that at downwind location.

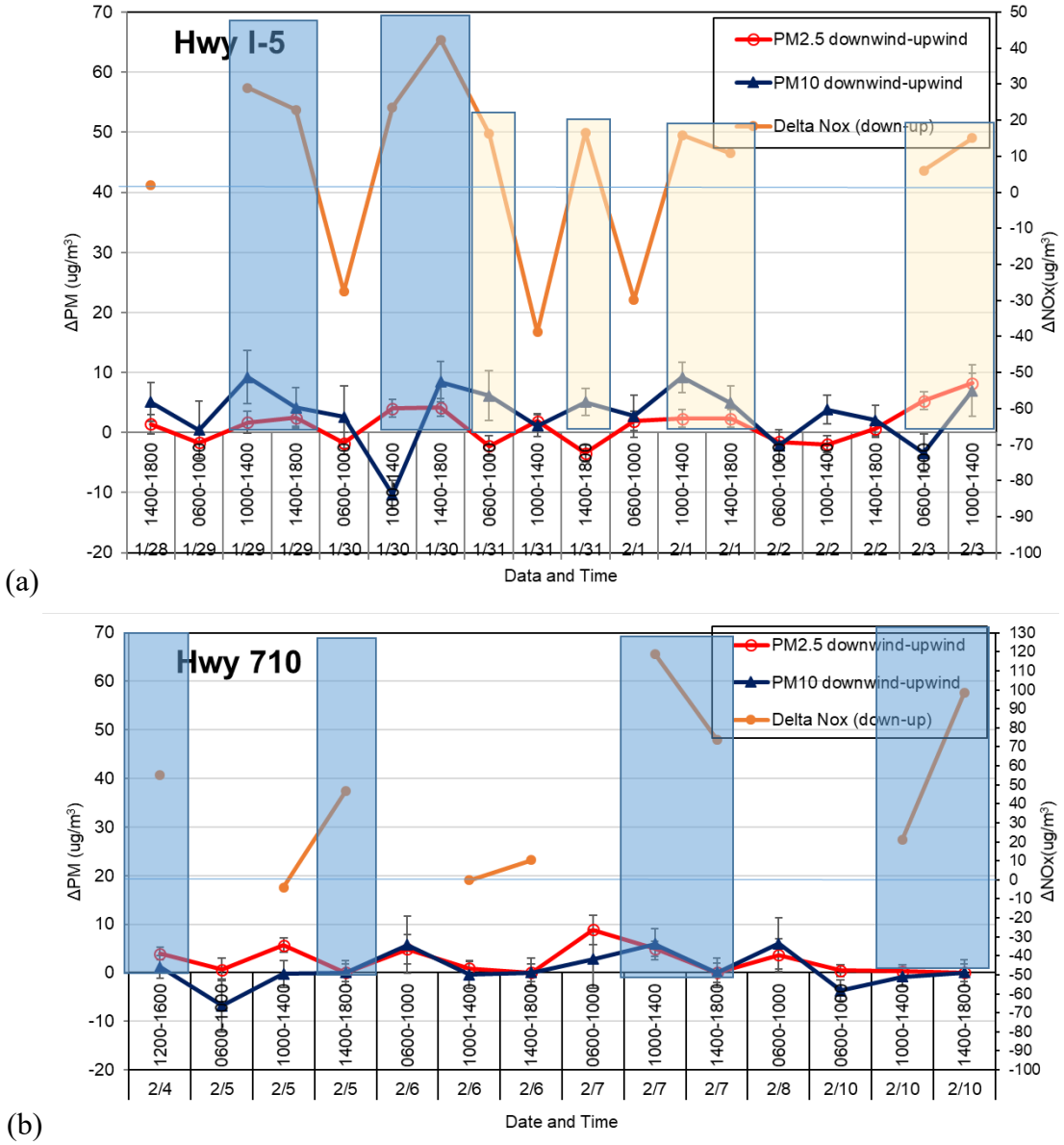

Figure A-1: ΔPM (Downwind-Upwind) (a) Anaheim site (b) Long beach site

ΔNOx is obtained by subtracting 4 hour averaged upwind NOx concentrations from 4 hour averaged downwind NOx concentrations. Data points in blue shaded area are when ΔNOx is larger than 20 µg/m^3. This criteria was proposed by Bukowiecki et al. [55] to filter the data for strong signal to noise ratio. Sampling periods with ΔNOx larger than 20 µg/m^3 may indicate the effect of advection is strong compared to the effect of vehicle induced turbulence and diffusion for the transport of both aerosol and gas. On the other hand, sampling periods with ΔNOx larger than 20 µg/m^3 may indicate the effect of advection is not strong compared to the effect of vehicle

induced turbulence and diffusion for the transport of both aerosol and gas. For the latter case, separating the contribution of background PM from total PM mass concentration is expected to be very difficult. As shown in Figure A-1, applying the criteria of ΔNOx being larger than 20 $\mu g/m^3$ reduces the number of valid data points - when cross wind is significant - substantially. Data points shaded in orange box show qualitatively adequate data that can be included for further analysis to determine emission factors of non-tailpipe emissions. As these quality data points are too few, we conducted the following analysis in this appendix without filtering the data based on ΔNOx concentration.

Harrison et al. [116] studied the influence of meteorological factors and traffic volumes upon suspended particle mass at urban roadside sites of differing geometries. They recognized subtraction of PM mass measured at urban background from PM mass measured at near road location is not as simple as they had initially thought. Figure A-2 shows comparison of upwind and downwind PM and NOx mass concentrations following Harrison et al. [116]'s approach to understand how to better separate or subtract background PM concentrations. For comparison, nearest urban background locations (AQMD Compton site for Long Beach (or highway 710) and AQMD Pampas Land site for Anaheim (or highway 5) location) were also used as another upwind location to understand how close or different the concentrations are compared to our upwind locations just across the highway. There was no significant difference in NOx concentration between urban background site (Compton) and our upwind (ATD location at Long Beach site) for 4 hour averaged data as shown in Figure 6-2b. There was a little difference in NOx concentration between the nearest upwind urban background location (Pampas Lane) and our upwind site (Majestic hotel) just across highway at the Anaheim site. It appears the nearest urban background location (Pampas lane) in upwind direction shows lower background concentrations compared to those measured at our upwind location (Majestic hotel) just across the highway for Anaheim location. For more discussion, please read latest papers from Greg Evans' group from the University of Toronto on the subtlety and difficulty of subtracting background signals. Figure A-2 shows the difference in concentrations between upwind and downwind locations are much smaller for PM compared to NOx. That is because NOx emissions are primarily from the roadway while PM has much higher background contribution.

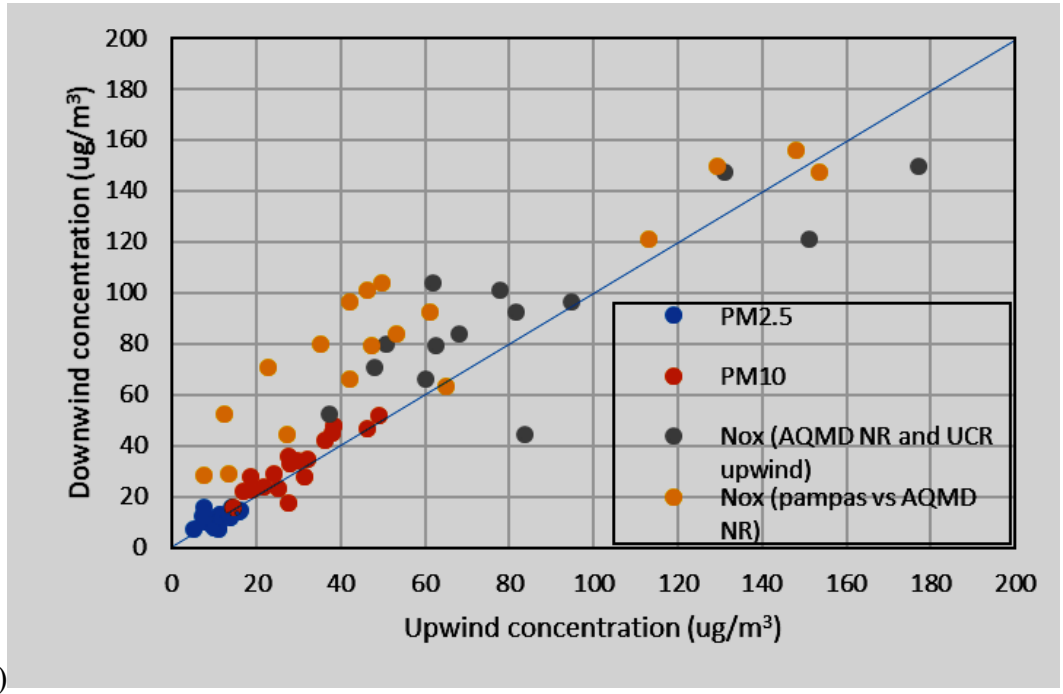

(a)

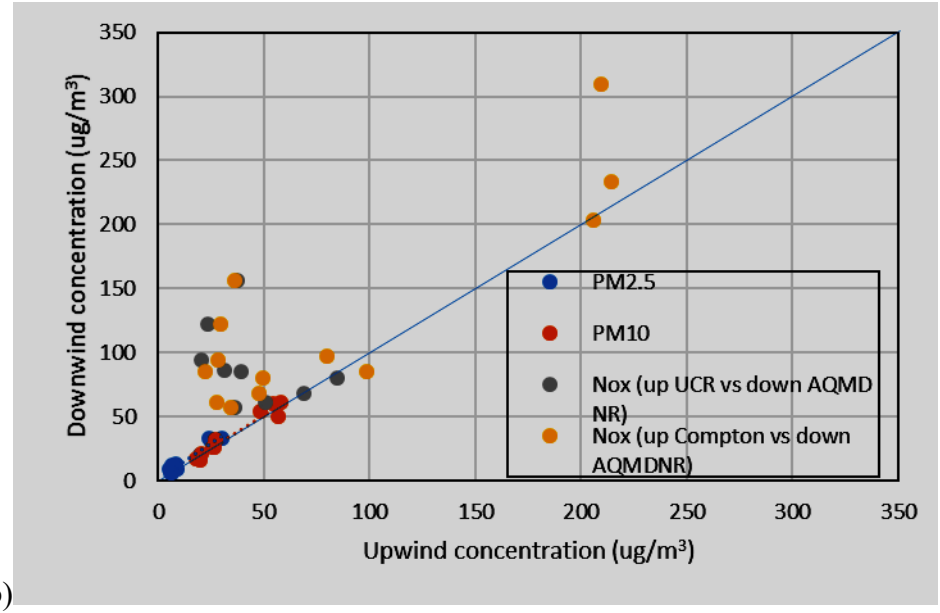

(b)

Figure A-2: Relationship between upwind (background) and downwind PM and NOx concentrations at (a) Anaheim site (b) Long Beach site

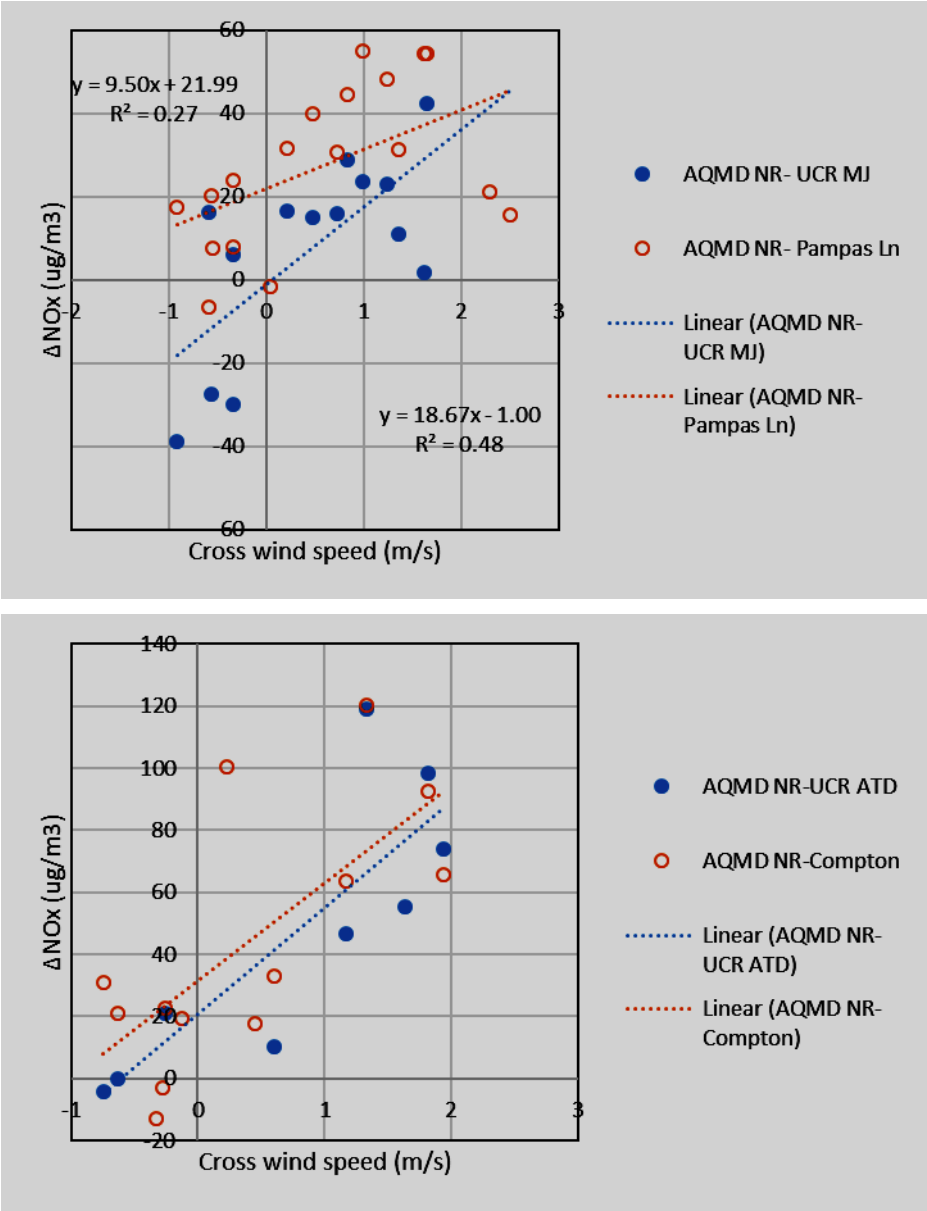

Figure A-3: Delta NOx vs cross wind speed. Delta NOx is downwind concentration – upwind concentration. Cross wind speed was measured at downwind AQMD NR sites (a) Anaheim location (b) Long Beach location

To understand the effect of cross wind on the transport of pollutants, ΔNOx was plotted against the cross wind speed. Figure A-3 shows two cases: one with the upwind location right across the highway and the other nearest AQMD urban background site at least a mile away from the highway into residential area. Interestingly when trend lines were obtained between ΔNOx and cross wind, the trendline with upwind location right across the street pass through origin while the trendline with urban background location has y-intercept. Wang et al. [117] pointed out one of the disadvantages of using far located urban background is asynchronous PM concentrations

compared to the measurement site. It was interesting that even for the urban background relatively close to the measurement site also showed some offset compared to the upwind location nearby the road. Figure A-3 supports that our upwind site measurement has advantages compared to urban background site measurement in upwind direction (Pampas ln).

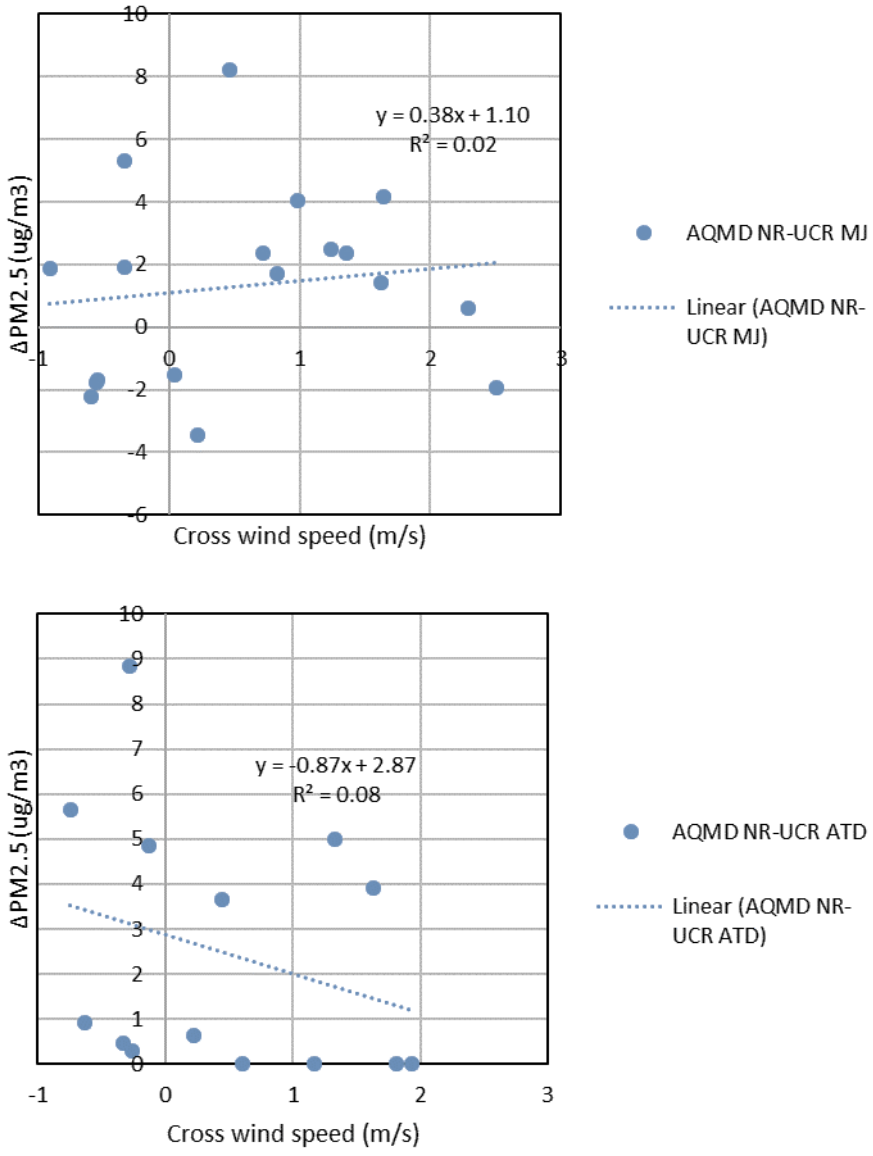

Figure A-4: Delta $PM_{2.5}$ vs cross wind speed Delta PM is downwind concentration – upwind concentration. Cross wind speed was measured at downwind AQMD NR sites (a) Anaheim location (b) Long Beach location

Next, crosswind speed was plotted against ΔPM concentration in Figure A-4. The PM data in Figure A-4 is much more scattered compared to the NOx data in Figure A-3 again due to larger contribution of background concentrations in PM. The correlation coefficient (R^2) is much smaller than that of ΔNOx. The figure shows there is a weak positive correlation between cross wind speed and $\Delta PM_{2.5}$ in the Anaheim location. The center of the data is in the first quadrant for both locations. On the other hand negative correlation was found for the Long Beach location.

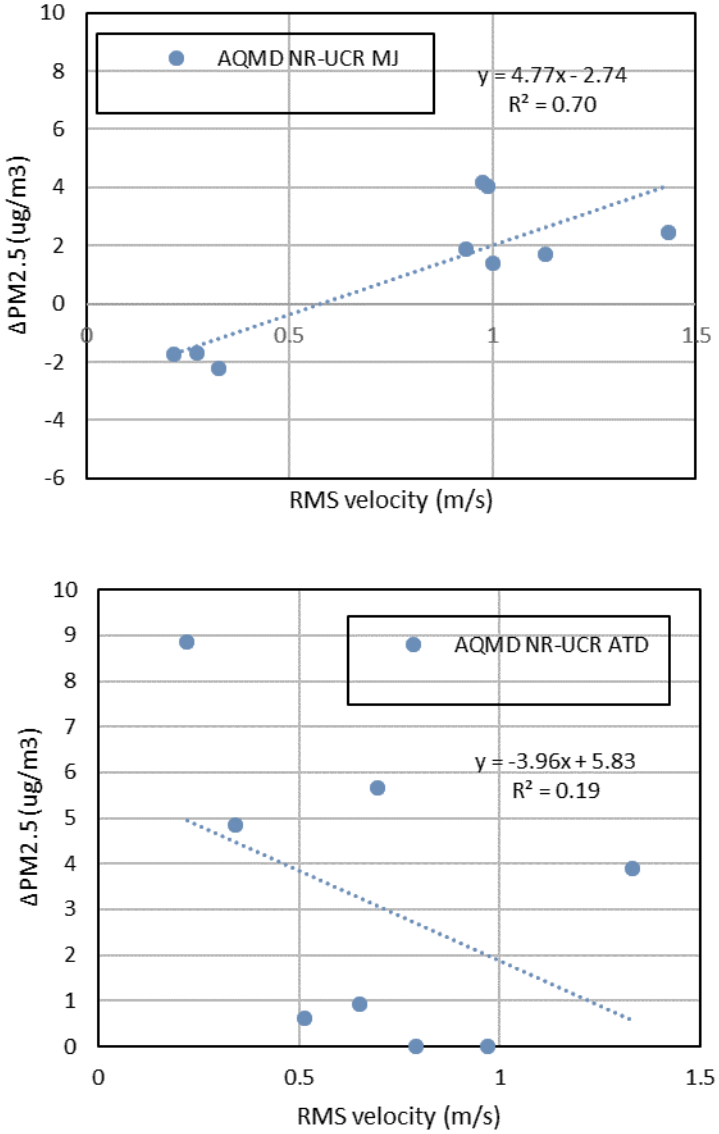

Figure A-5: Delta $PM_{2.5}$ vs RMS wind velocity at 6.9m of the downwind site.

When $\Delta PM_{2.5}$ is plotted against RMS velocity measured at the downwind location the correlation improved significantly in the Anaheim location. This indicates the transport of pollutants from roadways to the downwind location in the very near road is affected by turbulence and much less by wind direction. However, in the Long Beach location where both downwind and upwind locations are much further away compared to Anaheim location, RMS measured at downwind location did not have positive correlation with $\Delta PM_{2.5}$.

Figure A-6a shows relationship between mean wind velocity and RMS velocity determined from the sonic data measured at 6.9m height of the Anaheim downwind location. It shows a linear relationship with R^2 =0.76. Figure A-6b shows the relationship between RMS velocity and mean velocity in the Long Beach location. Turbulent intensity at the downwind location ranged from 50 to 100% at the Anaheim location while it ranged from 30 to high 50% in the Long Beach location reflecting much further distance of the measurement locations from the road way as shown in Figure A-8.

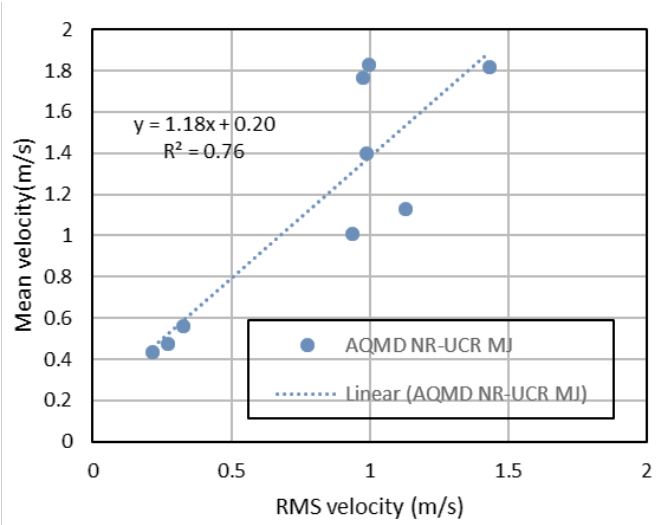

(a)

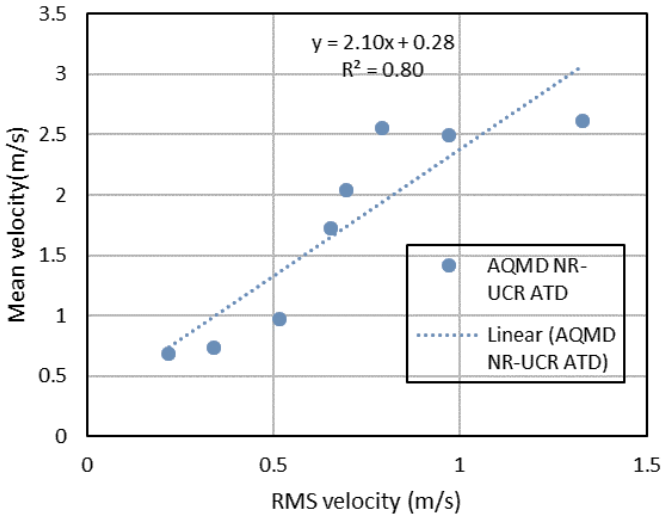

(b)

Figure A-6: Relationship between mean velocity and RMS velocity (a) Anaheim (b) Long Beach

(a)

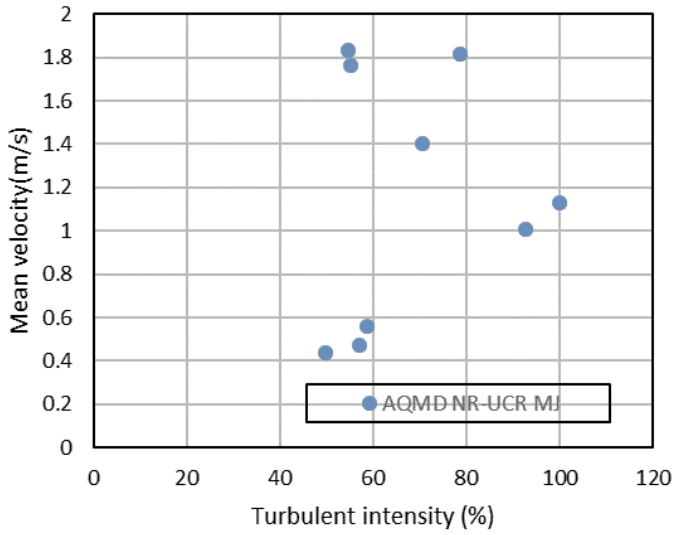

(b)

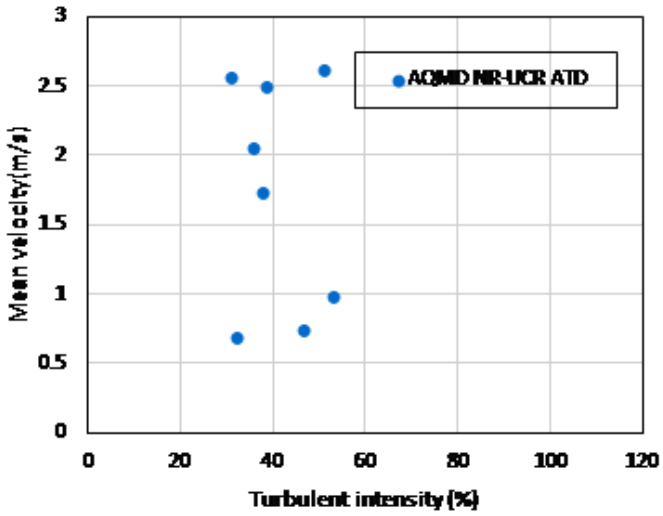

Figure A-7: Relationship between mean velocity and Turbulent Intensity, RMS velocity (a) Anaheim (b) Long Beach

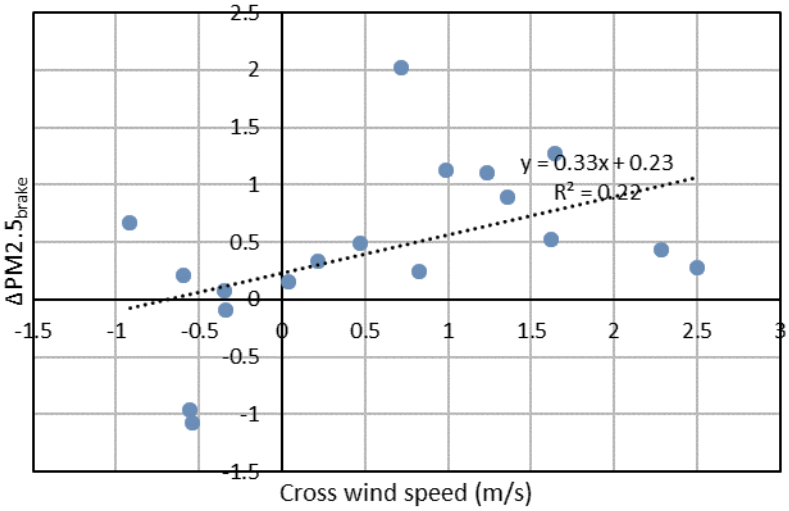

(a)

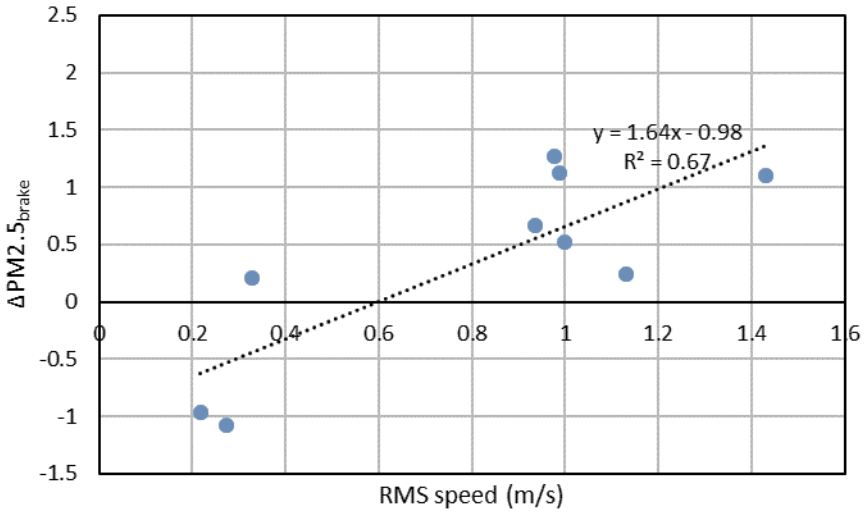

(b)

Figure A-8: Relationship between $\Delta PM2.5_{brake}$, cross wind speed and RMS speed in the Anaheim location (a) $\Delta PM2.5_{brake}$ vs cross wind speed (b) $\Delta PM2.5_{brake}$ vs RMS speed

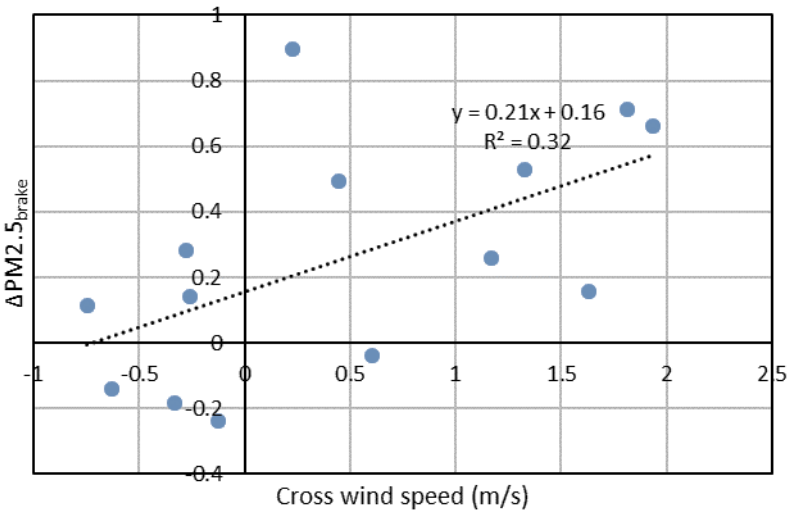

(a)

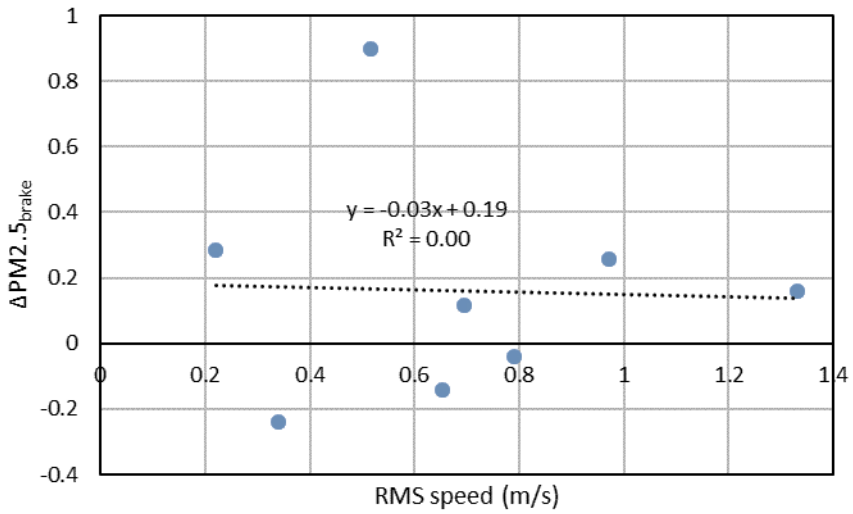

(b)

Figure A-9: Relationship between $\Delta PM2.5_{brake}$, cross wind speed and RMS speed in the Long Beach location (a) $\Delta PM2.5_{brake}$ vs cross wind speed (b) $\Delta PM2.5_{brake}$ vs RMS speed

Figure A-8 shows RMS speed has a better correlation than cross wind speed with $\Delta PM2.5_{brake}$ in Anaheim location. On the other hand, Figure A-9 shows cross wind speed has a better correlation than RMS speed with $\Delta PM2.5_{brake}$ in the Long Beach location. Anaheim measurement location was very close to the road and so the dispersion was better correlated with the RMS speed measurement at the downwind location. On the other hand, the downwind location in the Long Beach location is further away and no longer reflects the fluctuation of the flow in the road and so found no correlation with $\Delta PM2.5_{brake}$.

Appendix G: Calculation of dilution factors and Emission factors for PM2.5 & PM10

This section outlines the process used to calculate dilution factors and emission factors for $PM_{2.5}$ and PM_{10} using data measured on site during the field campaign as well as data from other resources such as PeMS Data Source and the CARB's EMFAC database. The method and equations were obtained from the works of Bukowiecki et al. [55]. Their work uses NOx concentrations from upwind and downwind sites to determine the dilution factor. This dilution factor is then used to find emission factors for PM by linear regression analysis.

Dilution

Atmospheric dilution factors were calculated using background corrected NOx concentrations (ΔNOx), number of heavy duty vehicles (n_{HDV}), number of light duty vehicles (n_{LDV}), and NOx

emission factors ($EF_{NOx,LDV}$ & $EF_{NOx,HDV}$) from EMFAC shown in equation **Error! Not a valid bookmark self-reference.**.

Equation 7

$$d = \frac{EF_{NOx,LDV} \cdot n_{LDV} + EF_{NOx,HDV} \cdot n_{HDV}}{\Delta NOx}$$

EF_{NOx} was extracted from EMFAC for light and heavy-duty vehicles separately at the corresponding average vehicle speed measured by PeMS. ΔNOx values in μg/m^3 were obtained by taking the difference between downwind and upwind NOx measurements. Four sets of dilution values were obtained at each testing site which are detailed in Table A-1. The first set of dilution values were obtained using ΔNOx values between the downwind location (AQMD near road site) and an upwind location, while the second set used ΔNOx values between the AQMD near road location and the nearest upwind AQMD urban background locations namely AQMD background site located at Pampas Ln in Anaheim, CA and AQMD background site located at Compton, CA. Both dilution 1 and dilution 2 contained an hourly and a four-hour average set. In addition, to establish strong dilution factors, only values with ΔNOx > 20 μg/m^3 were considered as recommended by Bukowiecki et al. [55].

Table A-1: Background corrected NOx concentration descriptions at each testing site.

	Anaheim	**Long Beach**
Dilution 1 (hourly & 4-hr avg)	ΔNOx (AQMD NR – Majestic Hotel)	ΔNOx (AQMD NR – ATD)
Dilution 2 (hourly & 4-hr avg)	ΔNOx (AQMD NR – Background Pampas Ln)	ΔNOx (AQMD NR – Background Compton)

The number of heavy duty and light duty vehicles (veh/hr) were obtained from Caltrans PeMS Data Source at each testing site. For each bound, namely south and north bound, PeMS data of upstream and downstream monitoring stations were averaged. The averaged north and south bound traffic counts were summed to represent total vehicle number on the road in both directions. Lastly, CARB's EMFAC database was used to quantify NOx emission factors (g/veh/mi) for LDV & HDV as a function of vehicle speed (mi/hr). PeMS recorded vehicle speed at each location was averaged to obtain 1 hour time resolutions. Polynomial interpolation was performed to obtain NOx emission factors at each average vehicle speeds for Anaheim and Long Beach seperately.

Emission Factors

Following the dilution calculation, PM emission factors were calculated by linear regression as shown by equation **Error! Not a valid bookmark self-reference.** which used the known ΔPM concentration (C_x) where x means species (PM, NOx, CO). The species in this regression is PM for our application, number of light and heavy-duty vehicles (n_{LDV} & n_{HDV}), and dilution factors (d).

Equation 8

$$C_{x,local\ traffic} = EF_{x,LDV} \cdot \left(\frac{n_{LDV}}{d}\right) + EF_{x,HDV} \cdot \left(\frac{n_{HDV}}{d}\right) + C$$

The ΔPM concentrations were calculated similarly to ΔNOx values where the downwind concentration was subtracted by the upwind and background concentration separately. This summary is detailed in Table A-2.

Table A-2: Summary of PM concentrations used for linear regression calculations.

	Anaheim	**Long Beach**
ΔPM2.5 DRI's Gravimetric filter	AQMD NR downwind filter– Majestic Hotel filter	AQMD NR downwind filter – ATD filter
ΔPM2.5 UCR Horiba PX-375	AQMD NR downwind PX – Majestic Hotel PX	AQMD NR downwind PX – ATD PX
ΔPM2.5 PX-375 – Pampas Ln	AQMD NR downwind PX – AQMD Pampas Lane background	No data
ΔPM10 DRI's Gravimetric filter	AQMD NR downwind filter– Majestic Hotel filter	AQMD NR downwind filter – ATD filter

Each linear regression analysis performed used a combination of PM concentration and dilution factor sets which matched by location and time. For example, when hourly $\Delta PM_{2.5}$(UCR) was used as the concentration, hourly dilution 1 was used as the dilution variable. The number of heavy duty and light duty vehicles were calculated as hourly and 4-hour avg values depending on the concentration and dilution time set used.

Additionally, an average fleet emission factor, not distinguishing light-duty and heavy-duty vehicle emissions, was also calculated using another regression **Error! Not a valid bookmark self-reference.** where n_{total} is the sum of heavy and light duty vehicles.

Equation 9

$$C_{x,local\ traffic} = EF_{x,fleet} \cdot \left(\frac{n_{total\ vehicle}}{d}\right) + C$$

The linear regression analysis results are shown in Table A-3 and Table A-4 for the Anaheim and Long Beach testing sites respectively. Figure A-1 to Figure A-4 show emission factors for each combination of dilution and concentration sets used in the regression analysis. Only the emission factors with corresponding p-values less than 0.05 were significant and are boxed in each figure. For the Anaheim test site, these emission factors have values of 0.16 g/veh/mi and 0.36 g/veh/mi for LDV, 1.43 g/veh/mi and 3.26 g/veh/mi for HDV, and 0.15 g/veh/mi and 0.45 g/veh/mi for total fleet for two different sets of data to determine dilution ratio. For the Long Beach test site, the emission factor was 0.32 g/veh/mi for total fleet. The uncertainty was too large for LDV and HDV emission factors for the Long Beach sites. The uncertainty of the analysis comes from multiple aspects. First, percentage of brake PM from total PM mass is constant. Second, dilution ratios for NOx, exhaust PM and non-tailpipe PM are the same at the measurement location. Third dilution ratios of from north bound and south bound traffic are the same. All of the above assumption may have contributed to the uncertainty.

As these emission factors are for $PM_{2.5}$ and PM_{10}, the percentage of brake PM from the source apportionment was applied to these values. For the Anaheim location 18% of the total mass are assumed as brake PM for $PM_{2.5}$. For Long Beach location 8% of the total mass are assumed as brake $PM_{2.5}$. following results in Figure 5-10 and Figure 5-11. These translate to 16.9 mg/veh/km to 38.0 mg/veh/km for brake $PM_{2.5}$ for LDV and 151.1 mg/veh/km and 344.4 mg/km for brake $PM_{2.5}$ HDV in the Anaheim location. For Long Beach location it was 15.9 mg/veh/km for the total fleet brake $PM_{2.5}$. These emission factors are also much higher than previously reported in Abu-Allaban et al. [30]. We do not believe the emission factor of brake particles obtained following Bukowiecki et al. [55]'s method is accurate from this study.

Table A-3: Linear regression results for Emission factors of LDV, HDV, and total fleet at the Anaheim testing site.

	Regression using n_LDV & n_HDV							Regression using n_total			
	R square	EF_LDV	standard err	p-value	EF_HDV	standard err	p-value	R square	EF_total	standard err	p-value
ΔPM2.5 (filter) * dilution 1 4 hr-avg	0.00	0.00	0.12	0.98	0.16	2.38	0.96	0.00	0.00	0.08	0.99
ΔPM2.5 (UCR- Pampas)* dilution 2 Hourly	0.28	0.16	0.05	0.00	1.43	0.52	0.01	0.15	0.13	0.05	0.01
ΔPM2.5 (UCR) * dilution 1 Hourly	0.67	0.36	0.07	0.00	3.26	0.92	0.00	0.45	0.28	0.08	0.00
ΔPM2.5 (UCR)* dilution 1 4 hr-avg	0.90	0.46	0.16	0.21	5.59	3.24	0.33	0.64	0.38	0.20	0.20
ΔPM10 (filter) * dilution 1 4 hr-avg	0.93	-0.13	0.04	0.17	-1.00	0.72	0.40	0.83	-0.12	0.04	0.09

Table A-4: Linear regression results for Emission factors of LDV, HDV, and total fleet at the Long Beach testing site.

	Regression using n_LDV & n_HDV							Regression using n_total			
	R square	EF_LDV	standard err	p-value	EF_HDV	standard err	p-value	R square	EF_total	standard err	p-value
ΔPM2.5 (UCR)* dilution 1 hourly	0.13	0.37	0.26	0.18	0.08	0.92	0.93	0.12	0.36	0.25	0.17
ΔPM2.5 (UCR)* dilution 1 4 hr-avg	0.90	0.31	0.12	0.12	0.24	0.50	0.68	0.90	0.32	0.06	0.01
ΔPM2.5 (filter) * dilution 1 4 hr-avg	0.45	0.15	0.11	0.27	0.33	0.46	0.52	0.40	0.11	0.06	0.18
ΔPM10 (filter) * dilution 1 4hr-avg	0.62	-0.36	0.24	0.23	-2.22	1.04	0.12	0.01	0.04	0.23	0.88

Figure A-1: Emission factors for LDV and HDV results from linear regression analysis at the Anaheim site.

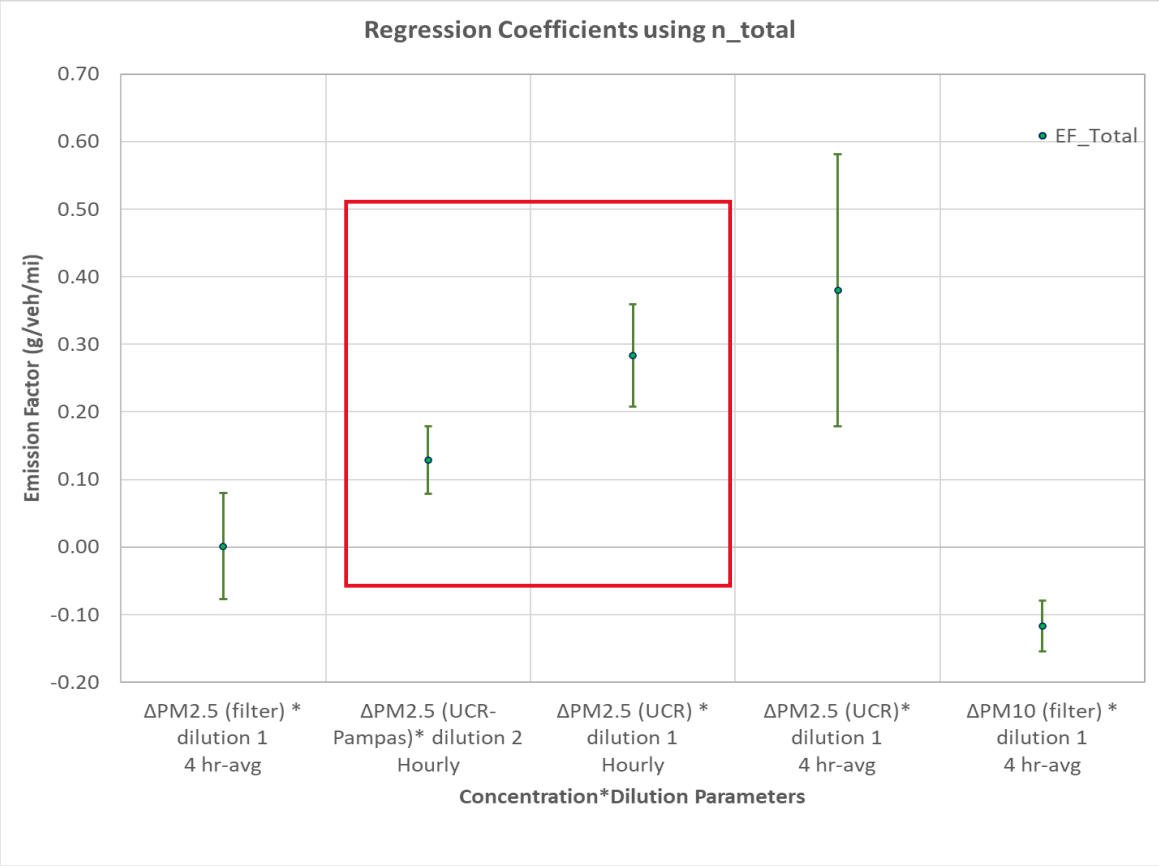

Figure A-2: Emission factors for total fleet results from linear regression analysis at the Anaheim site.

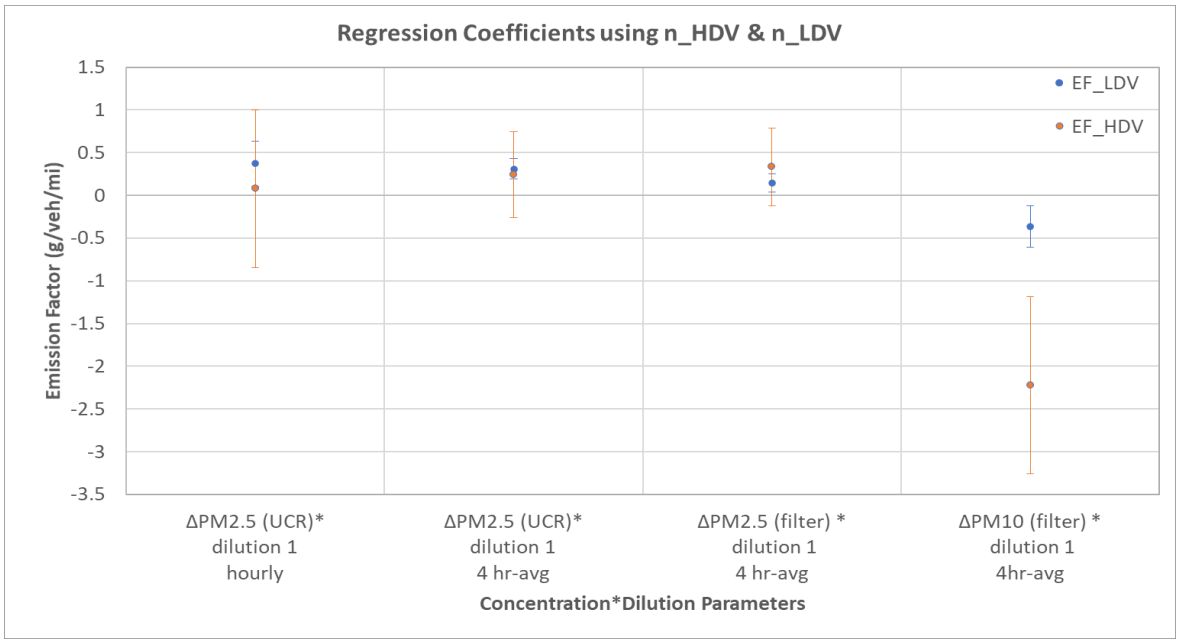

Figure A-3: Emission factors for LDV and HDV results from linear regression analysis at the Long Beach site.

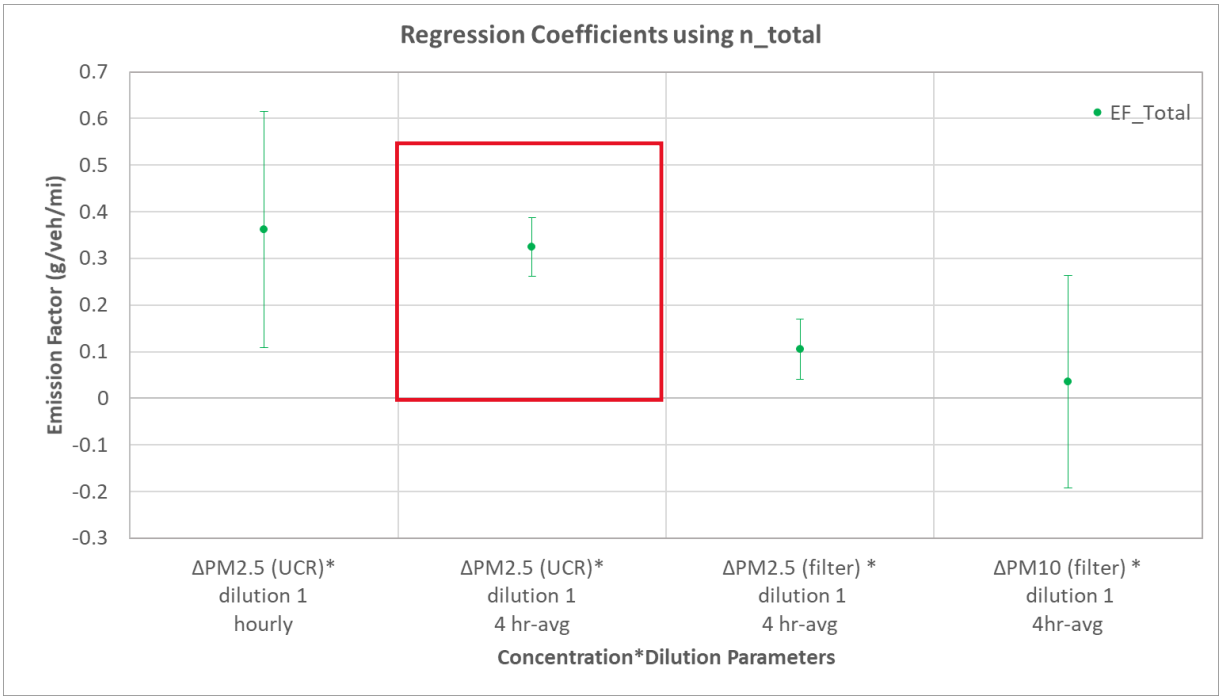

Figure A-4: Emission factors for total fleet results from linear regression analysis at the Long Beach site.